Università degli Studi di Napoli Federico II
Ph.D. Program in
Information Technology and Electrical Engineering
XXXV Cycle

Thesis for the Degree of Doctor of Philosophy

Distributed Control of Cyber-Physical Energy Systems: Towards the Energy Transition

by
Bianca Caiazzo

Advisor: Prof. Stefania Santini

Co-advisor: Prof. Amedeo Andreotti

Scuola Politecnica e delle Scienze di Base
Dipartimento di Ingegneria Elettrica e delle Tecnologie dell'Informazione

I am indebted to my father for living, but to my teacher for living well.

Alexander the Great

Distributed Control of Cyber-Physical Energy Systems: Towards the Energy Transition

Ph.D. Thesis presented
for the fulfillment of the Degree of Doctor of Philosophy
in Information Technology and Electrical Engineering
by

Bianca Caiazzo

January 2023

Approved as to style and content by

____

Prof. Stefania Santini, Advisor

____

Prof. Amedeo Andreotti, Co-advisor

Università degli Studi di Napoli Federico II
Ph.D. Program in Information Technology and Electrical Engineering
XXXV cycle - Chairman: Prof. Stefano Russo

http://itee.dieti.unina.it

Candidate's declaration

I hereby declare that this thesis submitted to obtain the academic degree of Philosophiæ Doctor (Ph.D.) in Information Technology and Electrical Engineering is my own unaided work, that I have not used other than the sources indicated, and that all direct and indirect sources are acknowledged as references.
Parts of this dissertation have been published in international journals and/or conference articles (see list of the author's publications at the end of the thesis).

Napoli, March 9, 2023

Bianca Caiazzo

Abstract

Recent advances in Information and Communication Technologies, along with the deployment of small-scale distributed generation sources, led to the current energy transition, mainly devoted to decarbonisation of energy sector and net zero greenhouse gas emissions. Microgrids (MGs) represent the conceptualization of this transition, where the combination of physical plants with novel bi-directional measurement and control loops entails the vision of MGs as cyber-physical energy systems in a networked control perspective. Hence, distributed control and multi-agent systems theory are the key enabling tools for MGs optimization and management.

However, the spread of distributed smart nodes within this modern power systems, endowed with sensing/actuation, control and communication capabilities, poses novel issues that cannot be neglected in control design phase to guarantee effective, resilient and reliable MGs operations. From one side, different communication constraints arise due to the large amount of connected devices, such as: *i*) communication time-delays in information sharing process; *ii*) need of sampled-data formulation of distributed controllers to facilitate their implementation in digital control platform; *iii*) limited communication bandwidth with the need to avoid communication resources waste. Besides, some fundamental control requirements are expected to be satisfied in MGs operations, namely: *iv*) short convergence time to timely accommodate their fast changing operating conditions; *v*) resilience to unknown model mismatches, large disturbances/uncertainties affecting the entire MGs dynamics. The purpose of the thesis is to answer these research questions by designing suitable distributed control protocols aiming at improving the MGs working operating conditions, thus promoting the current green energy revolution.

Keywords: Microgrids, Distributed Control, Multi-Agent Systems, Cyber-Physical Energy Systems, Time-delay Systems.

Sintesi in lingua italiana

I recenti progressi tecnologici, insieme all'ampia diffusione di unità di generazione di energia distribuita di piccola taglia, hanno condotto all'attuale transizione energetica, principalmente devota alla decarbonizzazione del settore energetico e alla riduzione a zero delle emissioni di gas serra. Le Microgrids (MGs), intese come microreti intelligenti, rappresentano la concettualizzazione di questa transizione grazie alla loro intrinseca combinazione di impianti fisici, sistemi di monitoraggio smart e flussi di comunicazione bidirezionali. In tale prospettiva, emerge il concetto di sistemi energetici cyberfisici. Pertanto, algoritmi di controllo distribuito e teoria di sistemi multi-agente saranno il cuore della tesi.
Tuttavia, la diffusione di agenti intelligenti dotati di capacità computazionale, di comunicazione e di controllo, nei moderni sistemi energetici pone nuove sfide nella fase di progettazione degli algoritmi di controllo, necessarie da considerare per garantire condizioni operative più affidabili, efficienti e resilienti. Da un lato, emergono diversi vincoli di comunicazione: *i*) ritardi di comunicazione durante l'interazione tra agenti; *ii*) necessità di implementazione degli algoritmi di controllo su piattaforme digitali; *iii*) larghezza di banda di comunicazione limitata con conseguente necessità di evitare lo spreco di risorse di comunicazione. Inoltre, è richiesto il soddisfacimento di requisiti di controllo cruciali in tali applicazioni, come ad esempio: *iv*) adattamento tempestivo a condizioni operative fortemente variabili; *v*) resilienza a disturbi e incertezze ignote, nonchè a dinamiche molto complesse che influenzano l'intera dinamica della rete. La tesi intende rispondere a queste sfide aperte attraverso la progettazione di algoritmi di controllo distribuito appropriati volti a migliorare le condizioni operative delle nuove reti intelligenti, contribuendo a promuovere l'attuale rivoluzione 'verde'.

Parole chiave: Microgrids, Controllo Distribuito, Sistemi Multi-Agente, Sistemi Cyberfisici Energetici, Teoria di Sistemi con ritardo.

Contents

Acknowledgements

I am grateful to Tel Aviv University and, in particular, to the School of Electrical Engineering for the hospitality during my period abroad. Thanks to Prof. Emilia Fridman for her supervision, encouragement and inspiring experience.

I wish to acknowledge my great debt to Prof. Stefano Russo, our ITEE PhD program Chairman, who worked a lot and with great efforts by spending his time to help us and to create an inspiring professional environment.

Heartfelt thanks to Stefania, my supervisor, for her guidance during my PhD program. She was an example of great women and scientist for me. Of the friends and colleagues with whom I have worked on problems directly pertinent to this thesis, it is a pleasure to acknowledge Alberto, who was the first person who believed in me and helped me to never give up. My special thanks also to all members of DaisyLab, as they are my second family.

Naples, Italy
January 2023

Bianca Caiazzo

List of Acronyms

The following acronyms are used throughout the thesis.

PC	Primary Control
SC	Secondary Control
TC	Tertiary Control
ISS	Input-to-State Stability
LMIs	Linear Matrix Inequalities
UB	Ultimate Bound
UUB	Uniform Ultimately Bounded
LPV	Linear Parameter-Varying
LTI	Linear Time-Invariant
DGs	Distributed Generations
ESSs	Energy Storage Systems
MASs	Multi-Agent Systems
NCS	Networked Control System

ODEs	Ordinary Differential Equations
TDSs	Time-Delay Systems
RFDE	Retarded Functional Differential Equation
PID	Proportional-Integral-Derivative
PIR	Proportional-Integral-Retarded
PI	Proportional-Integral
PD	Proportional-Derivative
CPS	Cyber-Physical System
DETM	Dynamic Event-Triggered Mechanism
DET	Dynamic Event-Triggered
ETC	Event-Triggered Control
ET	Event-Triggered
0-GES	Globally Exponentially Stable in absence of an input
CPES	Cyber-Physical Energy System
MG	Microgrid
DERs	Distributed Energy Resources
SG	Smart Grid
CERTS	Consortium for Electric Reliability Technology Solutions
ET	Event-Triggered
PV	Photovoltaic

WTs	Wind Turbines
CHP	Combined Heat and Power
PCC	Point of Common Coupling
RTU	Remote Terminal Units
DNO	Distribution Network Operator
HAN	Home Area Network
DMPC	Distributed Model Predictive Control
BAN	Business Area Network
IAN	Industrial Area Network
CANs	Costumer Area Networks
NANs	Neighborhood Area Networks
WANs	Wide Area Networks
AANs	Access Area Networks
WiMAX	Worldwide Interoperability for Microwave Access
WPANs	Wireless Personal Area Networks
GSM	Global System for Mobile communications
IS-95	Interim Standard 95
UMTS	Universal Mobile Telecommunications System
GPRS	General Packet Radio Service
LTE	Long Term Evolution

LANs	Local Area Networks
MANs	Metropolitan Area Networks
PLC	Power Line Communication
SGIRM	Smart Grid Interoperability Reference Model
TLS	Transport Layer Security
EPRI	Electric Power Research Institute
EU	European Union
CEER	Council of European Energy Regulators
NRAs	National Energy Regulators
NRAs	National Regulatory Authorities
ISGAN	International Smart Grid Action Network
ETP	European Technology Platform
SPM	Smart Polygeneration Microgrid
DSO	Distributed System Operators
QoS	Quality of Service
MV	Medium Voltage
A.S.SE.M SpA	Azienda San SEverino Marche SpA
AEEG	Autorità per l'Energia Elettrica e il Gas
AMI	Advanced Metering Infrastructure
FLISR	Fault Location, Isolation and System Restoration

SoC	State of Charge
EMS	Energy Management System
RESs	Renewable Energy Sources
ICT	Information and Communication Technologies
IoE	Internet of Energy
DSMC	Distributed Sliding Mode Controller
SMC	Sliding Mode Controller
NN	Neural Network
ANN	Artificial Neural Network
NZS	NonZero-Sum

List of Figures

List of Tables

Notation

The following notation is used within the thesis

$0_{n\times m}$ Null matrix of $n \times m$ dimensions

$\dot{x}(t)$, $\ddot{x}(t)$ The first and the second derivatives of x with respect to time t

$\lambda_{max}(P)$, $\lambda_{min}(P)$ The maximum and the minimum eigenvalue of $P = P^{\top} \in \mathbb{R}^{n\times n}$

$\mathbb{C}$ The set of complex numbers

$\mathbb{N}$ The set of natural numbers

$\mathbb{R}$ The set of real numbers

$\mathbb{R}^n$ The Euclidean space with the norm $|\cdot|$

$\mathbb{R}^{n\times m}$ The space of real $n \times m$ matrices with the induced norm $|\cdot|$

$\mathbb{R}_+$ The set of nonnegative real numbers

$\mathbb{Z}$ The set of integers

$\mathbb{Z}_+$ The set of nonnegative integers

$C[a,b], C([a,b],\mathbb{R}^n)$ The space of continuous functions $\phi : [a,b] \to \mathbb{R}^n$ with norm $\|\phi\|_C = \max_{\theta\in[a,b]} |\phi(\theta)|$

$col\{a,b\}$ Column vector $[a^\top b^\top]^\top$

I Identity Matrix

I_n Identity matrix of dimension n

$L_2[0,\infty)$ The space of functions $\phi : \mathbb{R}_+ \to \mathbb{R}^n$ with the norm $\|\phi\|_{L_2} = [\int_o^\infty |\phi(\theta)|^2 \, d\theta]^{\frac{1}{2}}$

$L_\infty(a,b)$ The space of essentially bounded functions $\phi : (a,b) \to \mathbb{R}^n$ with the norm $\|\phi\|_\infty = esssup_{\theta\in(a,b)}|\phi(\theta)|$

$M^\top$ Transpose matrix of M

$P > 0$ ($P \geq 0$) The symmetrix matrix P is positive (semi-positive) definite

$W[a,b]$ The space of absolutely continuous functions $\phi : [a,b] \to \mathbb{R}^n$ with $\frac{d\phi}{d\theta} \in L_2(a,b)$ and with the norm $\|\phi\|_W = \|\phi\|_C + \|\frac{d\phi}{d\theta}\|_{L_2}$

$x_t : [-h,0] \to \mathbb{R}^n$ $x_t(\theta) = x(t+\theta), \theta \in [-h,0]$

j Imaginary unit with $j^2 = -1$

Chapter 1

Introduction

Driven by the desire of moving to a low-carbon energy future, the next generation of power systems, referred as Smart Grid (SG), is approaching and a novel operating philosophy is entailed, where monitoring, communication, coordination and control become key tasks for a more efficient use of energy. This green transition is underway in complete harmony with the governance and management of energy sector across Europe, which has recently confirmed and enriched its commitment towards full decarbonization through the European Union (EU) Green Deal and Fit for 55 package [16]. These policies aim at turning the EU into the first *climate-neutral continent* by 2050 by acting, among different sectors, also on the energy one. Note that, *climate neutrality* by 2050 means achieving net zero greenhouse gas emissions for EU countries as a whole, mainly by cutting emissions, investing in green technologies and protecting the natural environment [17]. Along this line, the EU conveys a clear message to increase the usage of Renewable Energy Sources (RESs) to achieve the aforementioned objectives, along with the exploitation of the novel Information and Communication Technologies (ICT) to improve control, efficiency, reliability and safety of the novel smart power grids. Therefore, according to Horizon Europe 2021-2027, SG refers to a self-healing-capable grid able to provide reliable, energy-efficient and high-quality power via the incorporation of advanced two-way communication and the integration of RESs, which can be smaller, more environmentally and distributed over loads centers, thus making these new systems more flexible with respect to con-

ventional power network [18].
As elementary units of SG, Microgrid (MG) is a promising paradigm towards the decarbonisation of energy systems due to the integration of both renewable and conventional Distributed Generations (DGs) and Energy Storage Systems (ESSs), able to supply local loads in small geographic areas, while mitigating environmental concerns. Furthermore, the presence of DGs into the network transforms distribution networks from *passive* to *active* with a bidirectional power flow, which need to incorporate flexible and intelligent control with distributed intelligent systems [19]. The combination of these physical plants with novel measurement and control loops let the MG to be investigated as Cyber-Physical System (CPS) (or, in the specific case, Cyber-Physical Energy System (CPES)) in a Networked Control System (NCS) perspective, where several spatially distributed systems coexist together with a communication between sensors, actuators and controllers enabled through a shared band limited digital communication network.
Generally, a MG operates in *grid-connected* mode, meaning that voltage and frequency dynamics of the involved entities are dominated by the main grid. Conversely, when critical events or outages occur, it can switch to *islanded* mode to remain the power supply by itself, while both voltage/frequency stability and power balance among DGs and loads have to be preserved via proper control strategies. It results that the design of control loops is a more critical tasks in the latter operational mode and needs further investigation as the MG works autonomously as an independent entity. A hierarchical control architecture is commonly employed for MG control purposes, which consists of three layers, namely: Primary Control (PC), usually based on communication-free droop-control method at the local level in order to ensure active and reactive power sharing among DGs; Secondary Control (SC), whose aim is to compensate voltage and frequency deviations induced by PC; Tertiary Control (TC), which deals with the optimal power flow management between the MG and the main grid by virtue of economic aspects [2, 20, 21].
The thesis mainly focuses on the SC layer of the hierarchical control architecture, which represents the more critical level to guarantee nominal working conditions in islanded MG operations. At this level, control schemes can be typically categorized into three main classes, namely centralized,

decentralized and distributed [7, 22]. Traditional centralized control approaches rely on a central controller which globally commands on the gathered system wide information and requires complex communication networks adversely affecting system flexibility and configurability. Moreover, reliability issues arise by posing 'single-point of failure', meaning that, by the failure of the central controller, the whole control system fails down [8]. Although decentralized control methods exploit DGs local measurements, they are far from involving communication among DGs, thus experiencing instability and low efficiency of the system.
Conversely, distributed control, which will be the thesis core, has been recently regarded as the superior alternative to the previous approaches since the distributed structure of the communication network, along with cooperative control protocols distributed over DGs, allow overcoming the need of the central controller and, hence, the control system does not fail down subsequent to outage of a single unit [8]. It results a higher reliability, flexibility and scalability of the entire electrical network [22].
In this perspective, a MG can be considered as a Multi-Agent Systems (MASs), where each component is modeled as a dynamical system able to reach a desired coordinated behavior at the global level by using only its neighboring information to locally control its state variables [23, 24]. Based on these considerations, the SC of MG can be recast as a leader-tracking problem of MASs where, by exploiting consensus and synchronization theory, the objective is to ensure that voltage and frequency magnitudes of DGs track their respective desired set-points, both in nominal and troublesome operating conditions (e.g., in correspondence of reference variations, loads changing and plug-and-play phenomena). In this theoretical framework, distributed control strategies, properly enabled via communication networks, strongly impact on the MG performance, as well as on the coordination of DGs involved into the electrical grid, which interact among them in the cyber space by exploiting their on-board smart devices. From one side, by endowing all the electronically interfaced Distributed Energy Resources (DERs) with sensing/actuation, control and communication capabilities, the MG working scenarios result to be more effective, resilient and reliable, with an improvement in the overall control performance. On the other hand, the widely usage of smart connected devices along with the large employment of ICT lead to several communication impairments

that cannot be neglected in the control design phase in order to ensure good performance, while preventing instability phenomena [9].
Among different communication constraints, communication time-delay is one of the universal phenomena arising in MASs and, hence, in MG since it straightly comes from the communication networks during data acquisition and data transmission processes. The presence of communication time-delay is usually addressed in the technical literature under the restrictive assumption that delay is unique and constant [25, 26], which results to be unrealistic in practical applications. Indeed, when treating with wireless/wired communication networks, each communication link connecting a pair of nodes is affected by variable time-delays depending on actual conditions of the communication channel. Hence, to ensure that delays are properly counteracted by a suitable control strategy, it is required that control inputs have to be computed on the basis of outdated information depending on a time-varying communication delays. Moreover, although some works in technical literature model communication time-delays as time-varying function, they do not povide delay-dependent gain tuning rule, meaning that no stability margin with respect to communication latencies can be guaranteed by existing controllers [27, 28].
Furthermore, it is worth noting that in practical applications the control accuracy is crucial and usually it could be required to ensure a convergence towards the nominal set-points a finite-time interval. This is particularly important in MG control due to the presence of highly variable loads requiring for nominal operating conditions. From control viewpoint, while there exist several finite-time control protocols in the technical literature aiming at solving voltage/frequency regulation problem in islanded MG [29, 30], only few attempts are devoted to the design of distributed strategies able to cope simultaneously with time-varying communication delays and finite-time control requirements without either providing delay-dependent stability criteria or a gain-tuning mechanism [23, 31].
Another fundamental control requirement in distributed SC of islanded MG is to consider the presence of unknown model mismatches, external disturbances and uncertainties arising from the MG modeling phase, as well as from all the involved complex phenomena such as topological changes, unbalanced and nonlinear loads, high-frequency pulse-width voltage modulation and transition between modes of operation [8, 32]. In this non-trivial

scenario, most of the distributed control strategies consider only the presence of bounded uncertainties acting on DGs dynamics and, to manage them, they usually design adaptive methods based on Artificial Neural Network (ANN) [33], backstepping [34] and fuzzy technique [35], which result in high computational complexity, thus making difficult their implementation in real-time applications. Moreover, these adaptive control strategies are able to ensure the solely Uniform Ultimately Bounded (UUB) stability.

Besides the aforementioned issues, as in MASs and, hence, in MG applications, the intelligent nodes are spatially distributed over a monitoring area and controlled by exploiting software running on digital computers, the hypothesis of continuous interaction among agents results to be unrealistic, while it would be relevant to formulate control strategies in sampled-data fashion [36, 12]. In addition, the communication network bandwidth sometimes may also be restricted and it would be desirable to design control strategies aiming at ensuring a more efficient use of the communication infrastructure, while avoiding waste of communication resources [9]. Therefore, from the literature overview, the design of distributed control laws aiming at reducing the communication and computation burden is one of the crucial issue that requires further investigation [9].

Based on the above considerations, from the literature overview on distributed SC of inverter-based islanded MG, the following main challenges arise:

1. Designing of finite-time distributed cooperative control strategies able to cope with time-varying communication delays, as well as providing delay-dependent stability conditions with a gain-tuning rule;

2. Designing of a distributed cooperative control strategy which does not require any knowledge about global MG information, such as communication graph topology, system dynamics and/or bound of external disturbances, thus counteracting any kind of unmodeled dynamics/unknown uncertainties/unbounded disturbances;

3. Designing of distributed cooperative sampled-data controllers able to reduce communication network workload and save its limited resources, without compromising MG control performance.

The aim of the thesis is to address and solve these challenges by introducing different control strategies. Specifically, challenge 1 is tackled in a twofold way. Firstly, without considering convergence time requirement and with the aim to counteract the solely presence of heterogeneous communication time-varying delays, a fully-distributed Proportional-Integral (PI) control strategy is introduced to solve leader-tracking problem in general high-order MASs in the presence of multiple time-varying communication delays depending on the specific communication channel conditions. Delay-dependent stability conditions guaranteeing the exponential convergence of the synchronization error trajectories are derived by exploiting Lyapunov-Krasovskii theory along with Halanay inequality, thus resulting in Linear Matrix Inequalities (LMIs) whose solution allows finding delay margin guaranteeing stability. Then, a robust finite-time networked-based controller is also introduced to solve secondary voltage regulation problem in islanded MG with the aim of counteracting the presence of time-varying communication delays, while guaranteeing a finite-time convergence. Finite-time stability conditions are analytically provided in terms of LMIs by leveraging again Lyapunov-Krasovskii method, which involve gain-tuning rule, as well as the the maximum tolerable delays. Extensive simulation results, carried out on the well-known benchmark IEEE 14-bus test system, confirm the analytical derivation and reveal both the effectiveness and the robustness of the controller in ensuring voltage restoration in finite-time in spite of the effects of time-varuing communication delays.
To address challenge 2, a novel distributed Proportional-Integral-Derivative (PID)-like control strategy is designed to solve secondary voltage recovery problem, which embeds self-tuning adaptive mechanisms. Specifically, the design is performed in a fully distributed fashion, meaning that no knowledge about MG global information is required, thus allowing to embed any kind on unmodeled dynamics, unbounded and completely-unknown disturbances. By exploiting the solely information flow in the communication network from NCS perspective, the updating control laws are derived by leveraging Lyapunov theory combined with Barbalat lemma, thus proving the asymptotic MG voltage synchronization in different highly varying operating conditions, as well as the boundedness of the involved adaptive signals. Most notably, compared with existing adaptive mechanisms employed for MG SC purposes, the proposed distributed controller involves a

reduced computational burden and network communication resources savings, according to the metric in [37], thus being more performing from an implementation perspective.

Furthermore, three different communication resources saving-oriented control strategies are introduced to address challenge 3. Specifically, firstly, with the aim of moving from a continuous to a periodic inter-agent interaction, two distributed cooperative control strategies are proposed to ensure a preliminary reduction of the amount of sent control signals used for stabilization purposes. Then, a further reduction of the communication network workload is achieved via a distributed sampled-data Dynamic Event-Triggered Mechanism (DETM) used to solve again voltage recovery control problem in islanded MG. In this latter case, the analytical derivation, carried out by leveraging Lyapunov-Krasovskii method, leads to stability conditions in the form of LMIs, whose solution allows finding both sampling period and DETM parameters preserving the MG stability.

Finally, although the book core relies on distributed control strategies employed at SC level of the hierarchical MG control architecture, a first attempt to analyse the behaviour of a single power converter is provided in the last part of the thesis. Specifically, since a flyback power converter can be modeled as a delayed switched affine system [38, 39], a novel time-dependent switching is proposed to stabilize delayed affine systems by exploiting the constructive time-delay approach to periodic averaging [40]. This latter is herein extended to systems with fast-varying piecewise-continuous coefficients and non-small delays, whose Input-to-State Stability (ISS) is analytically proven by leveraging Lyapunov-Krasovskii theory. This theoretical derivation leads to feasible stability conditions expressed as LMIs, whose solution allows evaluating upper bounds both on non-small delays and small parameters $\epsilon > 0$ involved into the time-dependent switching rule preserving the ISS.

1.1 Thesis Outline

The thesis is structured as follows.

- In Chapter 2 the emerging green transition towards SG and MG paradigm is introduced by highlighting both the main differences with respect to conventional power systems and the enabling technologies. Moreover, the European and the Italian frameworks are briefly discussed.

- In Chapter 3 the three-layer hierarchical architecture, commonly employed for MG control, is fristly described. Then, by focusing on SC layer with distributed control approaches, some useful concepts and definition in the general context of MASs are provided so to finally get into the MG model in a CPES perspective.

- Chapter 4 presents the open challenges, arising in distributed control of MASs and addressed through the thesis. In particular, the problems are tailored for MG application, so to highlight the motivations and contributions of the thesis.

- Chapter 5 is devoted to the design of distributed control strategies aiming at guaranteeing resilience with respect to communication time delays. Firstly, the exponential leader-tracking consensus control problem for general MASs in the presence of multiple communication time-delays is addressed and solved via a fully distributed PI control strategies, while the stability analysis is derived by exploiting Lyapunov-Krasovskii method along with Halanay inequality. These latter lead to feasible LMIs exponential stability conditions, while exemplary numerical simulations confirm the effectiveness of the approach. Then, taking into account both the presence of communication latencies and convergence-time requirement, the secondary voltage regulation problem in inverter-based islanded MG is also addressed through the chapter via a novel distributed networked-based controllers able to counteract both the presence of communication delays and natural deviations induced by PC. Here, delay-dependent stability conditions are derived by leveraging again Lyapunov-Krasovskii method, thus resulting in LMIs whose solution provides the control gain tuning and the maximum tolerable delay. Numerical simulations, carried out on IEEE 14-bus test system, confirm the theoretical derivation, both in nominal and troublesome MG working conditions. Note that, the content of this chapter has been presented in [41, 42].

- Chapter 6 presents the design of a distributed SC strategy for voltage regulation problem in isladend MG in an uncertain and completely unknown environment. In particular, a distributed adaptive PID-like controller is suggested to counteract unknown uncertainties arising from external disturbances and parameters mismatches, while recovering the desired voltage set-point. The adaptive mechanisms are derived by leveraging Lyapunov theory, while the asymptotic stability of the entire network is proven by using Barbalat lemma. Detailed numerical simulations confirm the effectiveness of the proposed controller in ensuring voltage regulation also in non-trivial scenarios involving reference/loads variations and plug-and-play phenomena. Note that, the content of this chapter is in the ongoing work [43].

- In Chapter 7 preliminary results towards a periodic and sampled-data control are presented. Specifically, firstly a distributed sampled-data PID controller is introduced to solve voltage recovery problem in MG, whose derivative actions are approximated via finite-difference approximation, thus resulting in a delayed controller able to achieve a significant reduction of the communication burden without compromise MG performance. The theoretical derivation, carried out by leveraging Lyapunov-Krasovskii theory, leads to LMIs-based exponential stability conditions depending on the sampling period, while its effectiveness is numerically proven via exemplary numerical simulations. Moreover, the leader-tracking problem in a general delayed MASs under periodic time-varying communication networks is also addressed in this chapter via a fully distributed delayed control strategy without requiring the connectivity of the network for all the time interval, thus implying a periodic control action properly activated by a time-dependent switching rule. This latter is derived by exploiting time-delay approach to periodic averaging, while it is proven that the switching mechanism preserve the ISS of the entire network. Lyapunov-Krasovskii theory, also in this case, leads to LMIs stability conditions, whose solution allows finding upper bounds on state and input delays, as well as on small parameter affecting the variation speed of the communication graph. Note that, the content of this chapter can be found in [14, 44].

- Chapter 8 tackles the secondary voltage recovery problem in islanded MG with the aim of further reducing communication frequency among DGs, while maintaining desired performance and saving communication network workload. To solve the problem, distributed sampled-data controller presented in previous Chapter 7 is enriched with a DETM embedding Zeno-freeness property, which avoids waste of communication resources via an aperiodic control action. By leveraging Lyapunov-Krasovskii theory, exponential stability conditions are derived in the form of LMIs, whose solution allows finding maximum sampling period and DETM parameters preserving the stability. The IEEE 14-bus test system is employed to corroborate the effectiveness of the proposed controller. The content of this chapter is in the ongoing work [45].

- Chapter 9 deals with the extension of the constructive time-delay approach to periodic averaging presented in [40, 46] to the class of systems with fast-varying piecewise-continuous coefficients and non-small delays, whose ISS is analytically proven by employing Lyapunov-Krasovskii theory. This latter leads to feasible LMIs stability conditions, whose solution allows evaluating upper bounds on small parameter $\epsilon > 0$ and non-small delays preserving the ISS. Then, these theoretical results are further applied for the stabilization of delayed affine systems by time-dependent switching. Exemplary numerical simulations, involving the stabilization of a single delayed flyback power converter, confirm the effectiveness of the theoretical results. Note that, the content of this chapter can be found in [47].

- In Chapter 10 conclusions are drawn.

Chapter 2

Towards the energy transition: the Smart Grids era

As has long been expected, the nature of the utility market is changing. Conventional power systems are essentially centralized fossil fuel-based energy systems, which have a low efficiency and cause pollution to the environment. This means that in conventional energy systems there is a huge amount energy left behind in the process of electricity generation, which implies a substantial waste of limited natural resources and emits lots of carbon dioxide (CO_2) into the air [48]. Besides, the reliability of traditional electric grid is ensured mainly by having excessive power capacity in the whole system, with one-way power plants to consumers [48]. Therefore, during the last few decades, these traditional power plants have been facing some major challenges, such as long-distance transmission, carbon emission, environment pollution and energy crisis [49]. In this perspective, modern society requires power systems to be endowed with several features, such as high reliability, scalability, security and interoperability, while being a cost-effective solution [18].
According to Horizon Europe $2021-2027$ [50], SG will be the next generation of electric power system as it is recognized as a self-healing-capable grid, which constitutes an intelligent infrastructure in smart cities able to provide reliable, energy-efficient and high-quality power, while improving the standard of living and maintaining a sustainable environment. These future electric grids are envisioned to be environment friendly, sophisti-

Table 2.1. Comparison between conventional and Smart Grids [15].

	Conventional Grid	**Smart Grid**
System Topology	Radial topology (electricity generated from the power plant, transmitted via transmission lines and distributed at the distribution level).	Decentralized topology (electricity generated and transmitted in multiple ways at the transmission and distribution levels).
Communication	Single way, not real time.	Bi-directional real-time way.
Disturbance rehabilitate	Manual and the protection of assets from faults is the main priority.	Self-healing, prevents rapid deterioration, and minimizes effect.
Power flow control	Limited.	Fully automated.
Consumers engagement	No participation.	Extensive participation and option of being a prosumer.
Metering	Electromechanical, not real time.	Digital and real time.
Realiability	Susceptible to failure and outage.	Autometed; pro-active protection and prevention; power quality is the main concern.

cated and capable of bi-directional power flow via their ability in enhancing the integration of RESs, along with the exploitation of recent advances in ICT. Specifically, in order to revolutionize the conventional electrical power systems with efficient way of delivering, managing, and integrating green and renewable energy technologies, the Energy Internet (also called Internet of Energy (IoE) or SG 2.0) is introduced by integrating these physical plants with ICT. The aim of this innovative approach is to ensure a connection of each electric component within the network at any time. On the other hand, the integration of RESs through SG helps mitigate the emission of carbon particulate and greenhouse gases, thus facilitating both climate change mitigation and climate change adaptation. Table 2.1 shows a comparison between conventional electric grids and modern SG in order to highlight their main differences, while Figure 2.1 offers a conceptualization of modern SG.

As elementary units of SG, MG is a promising paradigm towards the decarbonisation of energy systems due to the integration of renewable DGs and ESSs, able to supply local loads in small geographic areas, while mitigating environmental concerns. A schematic representation of MG is provided in Figure 2.2. Since it is able to connect/disconnect from the utility grid

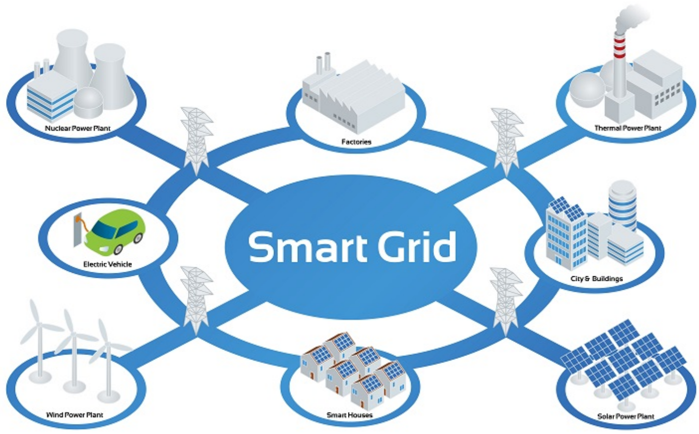

Figure 2.1. The power systems transition: Smart Grids conceptualization.

and operate into two operational modes (i.e., grid-connected and islanded modes), MG can not only serve its internal loads and its neighborhood communities by islanding itself from the main grid in emergency situations, but also offer grid flexibility to promote the injection of low-cost clean energy with stability and sustainability [51]. Thanks to the interconnection of electric-coupled physical systems and communication-coupled cyber systems, MG can be considered as a CPES where, in order to enhance flexibility and reliability of the entire system, networked and distributed control theory needs to be exploited, along with MASs framework and peer-to-peer communications [52]. This chapter presents an introduction to MG concept and aims at presenting some practical and useful information for MG successful integration in order to better understand the coming electrical revolution.

2.1 The role of Distributed Generation in future energy systems

According to the technical literature, DGs play a crucial rule in future energy systems due to their ability in providing energy storage and de-

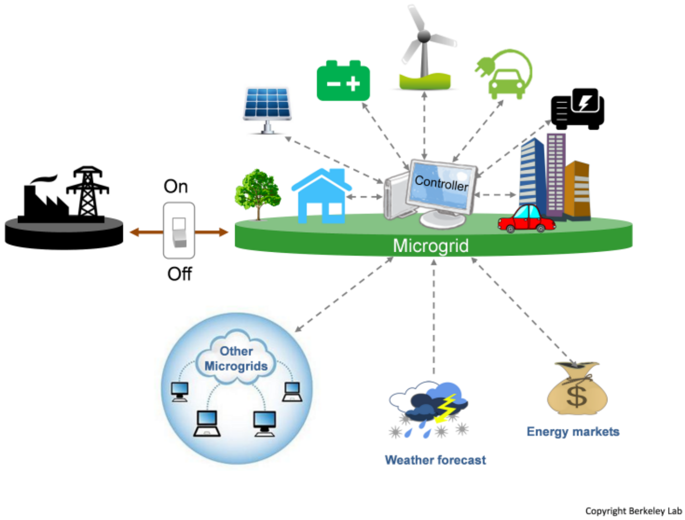

Figure 2.2. Elementary unit of Smart Grid: the Microgrid.

mand response. The development of ICT in the fields of DERs, as well as the deployment of power electronic devices, has given rise the power generation economy towards smaller scale [53]. In DGs, integrated small non-conventional energy resources can be used to supply loads in their neighborhood, which implies that generation units must be installed in distribution systems. This technology enhances system security, reliability, efficiency and power quality, while decreasing operating cost and minimizing the environmental impact. Moreover, since DGs generally are small scaled (1 $[kW]$ to 50 $[MW]$) systems, which produce electricity close to customers, a lower capital is also required to build such small-sized-based power plants [20].

RESs are key components of DGs infrastructure since they can be integrated to any system at desired scales. Although there is a wide variety of RESs that could be integrated for installing DGs plant, the wind and solar power plant are most suitable resources among others. Therefore, these latter energy sources dominate DERs type in any MG infrastructure, according to Global Status Report of REN21 [2].

Based on these considerations, the drawbacks of centralized generation can be eliminated via the flexibility and resiliency of DGs, whose higher benefits can be achieved by improving MG infrastructures. Although a precise and unique definition of DGs does not exist in the technical literature, it is possible to highlight the universally accepted attributed of DGs [19]:

- they are not centrally planned by power utility, nor centrally dispatched;
- they are normally smaller than 50 $[MW]$;
- the power sources or DGs are usually connected to the distribution systems, which are typically of voltages 230/415 $[V]$ up to 145 $[kV]$.

Furthermore, the benefits that straightly come from their introduction can be summarized as below:

- most of the countries in the world are looking for non-conventional and renewable sources as an alternative to conventional generation to timely supply the rapid load growth in order to mitigate the depletion of fossil fuel reserve;
- the usage of DERs would help to generate eco-friendly clean power with much lesser environmental impact, as it is the main goal of all countries, which are preferring renewable sources over fossil fuel in order to cut down greenhouse gas (carbon and nitrogenous by-products) emissions, while counteracting climate change and global warming;
- DGs allow increase the overall energy efficiency by creating cogeneration, trigeneration or CHP plants for utilising the waste heat for industrial/domestic/commercial applications;
- since DGs are geographically widespread and usually located close to loads, it is easier to find sites for them, along with their lower construction time and capital investment; the physical proximity allows also to reduce transmission and distribution losses;
- the power quality and reliability result improved due to the capability of DERs to operate both in stand-alone and grid-connected modes, thus increasing the whole generation;

- the introduction of DGs into the distribution system leads to transition from passive distribution network, with unidirectional electricity transportation, to active distribution network, with bidirectional power flows in the network.

Since active distribution network idea is crucial to capture the strength points of modern smart energy systems, a more detailed explanation will be given in the next section.

2.2 Active Distribution Networks

When DGs are not included into distribution networks, these latter are defined as *passive*, since the electrical power is supplied by the national grid system to the customers embedded in the distribution networks, and the power flow is *unidirectional*. As opposite, these latter become *active* when DGs are involved into the distribution networks, thus leading to *bidirectional* power flow. In particular, the penetration of DGs may bring to situations where the generated power exceeds the load request. In this case, this surplus can be exported from distribution to transmission/sub-transmission system. However, in order to guarantee safe and economical operations, active distribution networks require proper control, supervision and communication systems, which leads to SG and MG concepts. As anticipated above, SG idea is associated with the exhaustive use of ICT in the power grid, which enables the information sharing among different electrical entities involved in the network, each of them equipped with smart devices, thus leading to the possibility to implement suitable control strategies and network optimization techniques. In doing so, MG framework derives from combination of active distribution networks endowed with DGs, ESSs and local loads, collectively managed in order to guarantee the achievement of different objectives, namely [42]: *i*) ensure nominal working operating conditions; *ii*) increase the hosting capacity of renewable power generators; *iii*) improve the energy security and reliability; *iv*) offer flexibility services to the grid. Therefore, the MG is able to import/export energy to the grid by monitoring and controlling active and reactive power, which is the key feature of active distribution network.

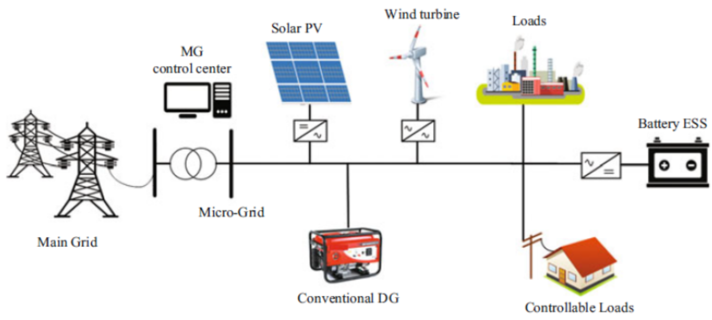

Figure 2.3. Microgrid structure and components [1].

2.3 Microgrid Architecture

The concept of MG was firstly introduced by the USA Consortium for Electric Reliability Technology Solutions (CERTS) to minimize the cost and increase the power quality effectively all around the world [1]. According to U.S. Department of Energy Microgrid Exchange Group, a MG can be defined as follows: *"A microgrid is a group of interconnected loads and distributed energy resources within clearly defined electrical boundaries that acts as a single controllable entity with respect to the grid. A Microgrid can connect and disconnect from the grid to enable both grid-connected and islanded-modes of operation."*. All the components involved into the conventional network are basically involved also into the MG, but in a more compact structure since the generation units are located in the neighborhood of the loads, meaning that power transmission losses are minimized with respect to the exisisting transmission system. It follows that MG can be considered as scaled-down version of the existing networks, where sophisticated monitoring and control strategies are embedded so to make the whole system smart and efficiently manageable and optimizable. The presence of ESSs is another crucial feature of MG, which are able to mitigate the unavoidable intermittent nature of RESs, whose widespread is facilitated into modern MG.

DERs, such as solar Photovoltaic (PV) units, Wind Turbines (WTs), Combined Heat and Power (CHP) modules, along with controllable loads, such as electric vehicles, can be included into modern smart MG due to

their advantages in reducing carbon emission, enhancing energy efficiency, improvement of power quality and reliability and mitigation of line losses. Since MG is part of distribution systems, it is connected to the utility grid at the Point of Common Coupling (PCC) via power electronic-based switchgear (see Figure 2.3). Although the two MG operational modes will be better detailed in the sequel, it is important to clarify that when the MG is disconnected from the main grid, it is particularly important to ensure the success of its operations, especially via the usage of ESSs devices. Moreover, if faults occur into the main grid, MG should be able to switch in islanded mode, thus guaranteeing a higher reliability and resilience of the local distribution network.
DGs, whose generated power range is $4 - 10000$ $[KW]$, consist of rotating type and inverter type generating devices. The former are used, for instance, for IC engines, gas turbines, microalternator, whereas the inverter type are employed for PV, WTs and fuel cells. However, in both cases, power electronic converters are required for their interface [54]. These latter are also required for the interface of ESSs, which can involve, e.g., batteries, flywheels, super-capacitors and superconducting magnetic energy storage. A MG control system with an intelligence level is required to guarantee safe operations in different modes, which can be implemented in centralized or distributed fashion.
Therefore, it is possible to conclude that the basic building and interconnected blocks in MG are as follows:

1. different kind of power generation sources, including renewable ones;

2. different loads with several consumption profiles;

3. network intelligence, including all the devices required for monitor and control the system.

Figure 2.4 highlights how these blocks are connected among them. The first link refers to the bi-directional energy flow from power plants to consumers, while the second ones is based on communication channels among different electrical entities in the MG, whose data are gathered and exploited for control purposes by using different sensors and actuators.

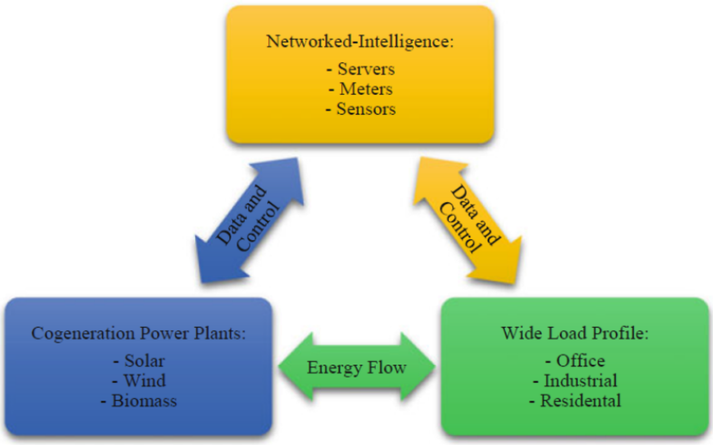

Figure 2.4. Building blocks of microgrids [2].

2.3.1 Operational Modes

Based on the PCC and its capability to work both autonomously and connected to the utility/main grid, MG can operate in two different modes, i.e., grid connected and islanded modes [2].
In grid connected mode, the MG behaviour, in terms of voltage and frequency dynamics, is dominated by the main grid and in this case the load demand can be met all the time. Therefore, on the basis of the load request of the main grid, MG will either supply or absorb power by acting as a controllable load or controllable source. Moreover, it is worth noting that in grid-connected mode any disturbance in the MG can be neglected in frequency regulation process due to the limited capacity of the MG with respect to the utility grid [1]. Summarizing, the grid-connected mode is characterized by the following two key points [54]:

- the frequency and voltage magnitude are controlled by the main grid;
- DGs are able to supply loads all the time.

If unplanned faults or disturbances, as well as some planned actions, such as maintenance operations, arise in the main grid, MG switches to islanded or stand-alone mode and starts to operate autonomously. This key feature is crucial to ensure higher power quality and voltage/frequency control. However, in this situation suitable control strategies are needed in order to guarantee frequency and voltage regulation, as well as to maintain the required power quality. Therefore, in islanded mode MG control becomes a more challenging task and, unlike previous, the following characteristics can be summarized [54]:

- DGs are equipped with control devices in order to guarantee frequency and voltage magnitude regulation;
- the MG supplies active and reactive power to the load.

2.3.2 The Energy Management System

In order to guarantee a proper management of the several entities involved into the MG, an effective Energy Management System (EMS) has to be involved into the MG to deal with monitoring and control tasks with the aim to enable appropriate actions in time steps near to real time. EMS provides a decision support system which, by considering operational constraints and system conditions (e.g., load consumption, electricity market price, generation capability and stored energy), determines how exchanging energy with the main grid, while counteracting critical conditions of contingencies. Therefore, the following functionalities are provided by EMS:

- monitoring of the MG in different operating conditions;
- analysis of the MG conditions;
- ability to counteract possible threats;
- enabling quick decisions in critical situations;
- performing control actions.

As it is possible to observe in Figure 2.5, EMS consists of three different modules, each of them associated with three different tasks: *i*) monitoring module; *ii*) decision making module; *iii*) control module. In the sequel, a briefly explanation about the tasks of each module of EMS will be presented.

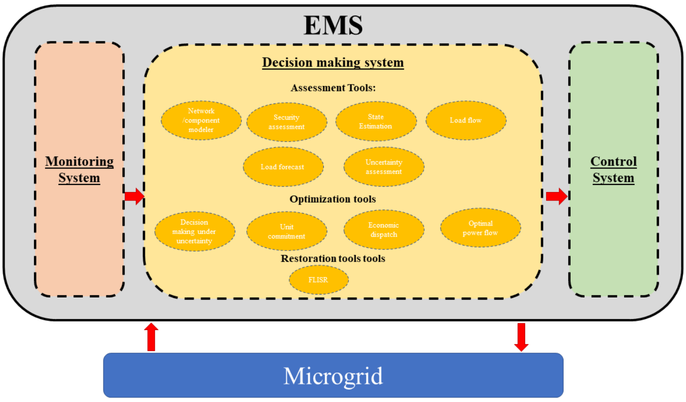

Figure 2.5. General scheme of Energy Management System in Microgrid.

The monitoring system deals with the data gathering task by exploiting meters and sensors in order to provide a real-time picture of the MG. These collected information cover: the status and performance of switches, lines and trasformer; the output power of DGs; the output power of ESSs along with their State of Charge (SoC); the status of reactors and capacitors of the network, and so on [1]. Then, by exploiting the communication infrastructure, Remote Terminal Units (RTU) send these collected data to EMS.

Based on the priority and the complexity of the operations to be performed, control system module in EMS is able to control the MG via automatic or manual control actions. Clearly, if no remote access to the components exists, the manual control is the unique option and the system operator calls the plant operator to perform the required control action.

The focus of the EMS is the decision making system, which tackles the assessment, optimization and restoration of the MG by exploiting different tools. For instance, assessment tools provide the operator a clear vision about the MG conditions in the current working scenario. Examples of assessment tools can be, e.g., network and component modeler, security assessment tools, load forecast and estimation, load flow, uncertainty assessment and so on.

Since different resources optimization strategies can be applied to supply load request, several optimization tools are embedded into the decision-making system of EMS, each of them facing with different economical and technical objectives. Optimization tools can be: *i*) unit committment which, by considering economic objectives and technical features of DGs and ESSs, schedules the online generation units in the operation horizon; *ii*) economic dispatch which, through the exploitation of fast linear models, finds the optimal output power of the active DGs; *iii*) optimal power flow, which solves the power flow computation by taking into account different objectives, e.g., loss minimization, cost reduction, profit maximization, while at the same time allows to embed network constraints; *iv*) decision making under uncertainty, which includes different techniques related to stochastic programming, robust optimization, information gap theory and so on. Finally, restoration tools are also included into the decision making system so to deal with the Fault Location, Isolation and System Restoration (FLISR) task. Note that, the identification of faults location, along with their respective isolation, are crucial tasks in MG, which can be performed automatically or manually depending on the smartness level of meters and switches into the network.

2.4 Communication in Microgrids

As a cluster of DGs, ESSs and local loads, physically interconnected via power transmission lines, MG has to satisfy different control objectives in terms of active and reactive power flow and frequency/voltage regulation, along with the management of the energy market, while at the same time providing additional ancillary services. To deal with these latter control objectives, by exploiting the use of several sensors, it is required to create an Advanced Metering Infrastructure (AMI) into the MG, which enables the data gathering in order to timely counteract faults or emergency events by implementing correct protection actions. To ensure the achievement of above-mentioned control requirements, different control architectures can be implemented into the MG, able to operate in centralized, decentralized or distributed fashion. Usually, the control architecture of MG follows a three-layer hierarchical structure, which will be deeply detailed in the next chapter. However, these considerations suggest that information sharing among different entities involved into the MG at different levels is required in order to ensure the fulfillment of control requirements, while

maintaining nominal operating conditions. Although the requirements of the communication infrastructure depend on the control architecture, it is worth mentioning that the information exchange occurs both among smart controllers embedded into DGs, but also among external operators as Distribution Network Operator (DNO), thus leading to the need to exploit different communication technologies at different MG levels.
Therefore, based on the coverage and functions, the following three main area networks are identified in the MG communication infrastructure [1]:

- *Costumer Area Networks (CANs)*: these networks are related to the first step of the communication process since they refer to the information exchange among consumers and MG. Home Area Network (HAN), Business Area Network (BAN) and Industrial Area Network (IAN) are possible CANs depending on the consumption profile, which provide data in terms of voltage, current, power and frequency values by usually using wired or wireless technologies; this kind of network provides a low bandwidth and two-way communication links in order to accomplish demand side management tasks;

- *Neighborhood Area Networks (NANs)*: these networks provide two-way communication among MG controllers and customer concentrators or gateway, meaning that the data collected in CANs are sent to MG controllers to implement required actions; in distributed architectures DGs controllers exchange information each other so to achieve different control objectives;

- *Wide Area Networks (WANs)* or *Access Area Networks (AANs)*: they are two-way communication systems used for long distances; indeed these communication networks enable information sharing between the MG and the utility grid, as well as between the MG and external operators as DNO, or other MGs. Thereore, herein high capacity and high bandwidth are required in order to deal with the huge amount of data and longer distances, especially for real-time response and safe operations.

Finally, Figure 2.6 summarizes the general communication infrastructure in MG by clearly differentiating CANs, NANs and WANs levels, whose main features, crucial for the choice of the most suitable communication technology to be adopt, are detailed in Table 2.2.

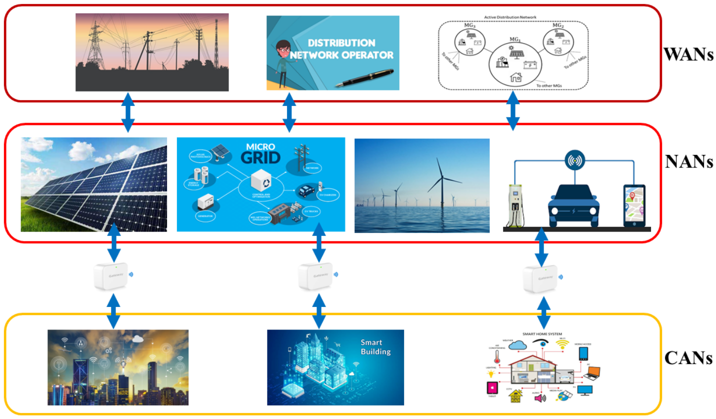

Figure 2.6. Microgrid Communication Infrastructure.

Table 2.2. Main features of different area networks: CANs, NANs and WANs.

Area Network	Data rate	Range	Bandwidth	Latency	Traffic
CAN	Low bit rate $1-30$ $[kbps]$	Tens of meters	Low	$2-15$ $[s]$	Periodic
NAN	$10-100$ $[kbps]$	Hundreds of meters	Medium	10 $[ms]$ to 2 $[s]$	Periodic
WAN	High bit rate (Hundreds of $Mbps$ to few $Gbps$)	Tens of kilometers	Wide	Few $[ms]$ to 1 $[s]$	Random

2.4.1 Wireless Technologies

The main advantages of wireless technologies rely on their ability in avoiding physical connections, their low operation costs along with a higher flexibility in expanding the network, while offering easy installation of remote units. Wireless technologies used in MG application are, e.g., WLAN, Worldwide Interoperability for Microwave Access (WiMAX), Zigbee, cellular mobile networks, and Bluetooth, which will be briefly detailed in the sequel [1].

1. WLAN: by using wireless distribution method, this technology is able to cover a limited area of some hundreds of meters, such as homes,

schools and office building, where it provides rubust and high-speed communication links among different devices. WLAN are based on IEEE 802.11 standards family including the IEEE 802.11a/b/g/n, which operate in the industrial, scientific and medical radio-frequency bands that include 2.4 and 5 GHz frequency bands. However, the main drawbacks of this technology are the missing roaming and authentication features, as well as the limited range that it can cover. WLAN is used in MG for faults protection, monitoring and control of DERs, thus improving the reliability of the power system;

2. WiMAX: it is able to support both fixed and mobile broadband wireless access in order to deliver a connection to a network; it is a long-range system based on the IEEE standard 802.16e series, whose aim is to ensure worldwide interoperability for microwave access. It is very useful to apply this kind of communication technology in MG application due to its benefit in providing long-distance coverage and high data rates. Some applications could be: the real-time data gathering from household meters; real-time pricing and energy consumptions of customers so to ensure the achievement of economic objectives; realt-ime monitoring and control for detection of power outage;

3. ZigBee: it is a low-cost, low-power, wireless mesh network standard mainly used for control and monitoring purposes. It is based on IEEE 802.15.4 standard for low-rate Wireless Personal Area Networks (WPANs). This technology is able to reduce the average consumption of current since its devices have low latency; although the coverage area usually ranges from $10 - 100$ $[m]$, longer distances can be reached by using mesh network of intermediate devices. Compared with other WPANs (e.g., Bluetooth or Wi-Fi), Zigbee results to be simpler and less expensive. Zegbee cannot be applied in MG critical location due to its low memort and low processing capacity, but it could be a suitable solution in HAN;

4. Cellular mobile networks: they include Global System for Mobile communications (GSM), Interim Standard 95 (IS-95), CDMA2000, Universal Mobile Telecommunications System (UMTS) and General Packet Radio Service (GPRS), which is an extension of GSM, and are

essentially based on 2G and 3G technologies. Among them, GPRS is recognized as the most efficient ones with variable throughput and latency times depending on the number of the users sharing the service at the same time and it is very appropriate in MG application since it does not require constant transmission rate;

5. Long Term Evolution (LTE): it is able to provide high-speed communication and data transfer with scalable bandwidth by using 4G wireless broadband technology, while at the same time managing with fast moving mobiles and supporting multicast and broadcast streams. The downlink peak and uplink peak rates are about 300 $[Mbps]$ and 75 $[Mbps]$, with a latency less than 5 $[ms]$. LTE technology, as well as its next generation LTE-Advanced, are widely used in MG and SG thanks to their benefits in high peak data rates and scalable bandwidth, along with their low-cost for upgrading the existing 3G networks;

6. Bluetooth: it is used for information sharing process among devices located at short distances; in MG applications it could be used for local monitoring tasks in a coverage area of $10 - 100$ $[m]$. However, it is worth noting that bluetooth may interfere with IEEE 802.11 based WLAN, thus providing weak security with respect to other standards.

Note that, other kind of wireless technologies can be found in MG applications, such as microwave technology, which is able to cover long-distances up to 60 $[km]$, thus offering the possibility to be applied in external communication channels, e.g., among MG controllers and DNO or other MG.

2.4.2 Wired Technologies

Now, some wired technologies commonly used in modern MG will be discussed.

1. Power Line Communication (PLC): since it was able to support conventional power distribution services, such as remote metering, load control and teleprotection among electrical substation, this technology has been always used in electric power system. However, its

disadvantages rely on the very limited data rate and small coverage area: indeed, to achieve higher data rates it is require to reduce the cover range. Besides, since power distribution systems are originally designed for $50 - 60$ $[Hz]$ transmissions, noise, attenuation and distortion problems can affect PLC based communication, with the possibility to cause inappropriate operations for controlled devices. However, it can be found in HAN since no dedicated communication networks installation is required and the smaller distances in HAN can be successfully managed.

2. Optical fiber communication: it can be installed in areas with high electromagnetic interference and its advantages are: *i*) low loss; *ii*) high data-carrying capacity; *iii*) large coverage area with a high volume of data. Moreover, different from other kind of electrical transmission lines, fiber cables are not affected by crosstalk interference, even in the case of long distances. In MG application, it could be used in WANs to enable real-time communication among the MG and external agents, such as DNO or other MG, so to optimize the high installation costs by exploiting their full transmission capacity;

3. Ethernet: they are based on IEEE 802.3 standard for Local Area Networks (LANs) and Metropolitan Area Networks (MANs); Data rates of $1-100$ $[Gbps]$ can be achieved and installation process is very easy and low-cost; therefore, it is commonly used in any computerized equipment. Moreover, it supports security and cryptography features; its usage has been extended to SCADA systems, whose application in MG field is related to monitoring and control tasks of electric power generation, storage resources, energy distribution and other ancillary services, which are enables via point-to-point or point-to-multipoint communications as channels among DGs and their respective controllers.

2.4.3 MG Communication Standards

In order to enable the integration of power systems with ICT and move towards the framework of CPES, while guaranteeing the fulfillment of interconnectivity and interoperability objectives, the communication infrastructure in MG has to follow international standards, especially concerned with security issues in modern power systems. The most common standards applied in MG are listed as follows [1]:

- **IEEE Std. 2030**: This standard integrates three different domains, i.e., the power systems, its respective communication and information technologies in a unified vision so to establish the relation and the suitable integration, along with the proper data flow among them. In doing so, this standard brings to appropriate guidelines towards the achievement of SG/MG interoperability from these three domains, thus representing the so-called Smart Grid Interoperability Reference Model (SGIRM). This latter, by also providing specifications about design tables, data flows, logical connection, communication channels and digital information management, leads to a unified framework where the interoperability criteria among the three different domains can be easily caught.

- **IEEE Std. 1547.3**: this standard promotes the interoperability of distributed resources (fuel cells, PV, WTs, microturbines, other DGs and also ESSs) involved in the power systems by providing guidelines related to monitoring, information exchange and control tasks in order to support interaction among distributed resources controllers and other stakeholder entities.

- **NISTIR 7628-1**: it provides cybersecurity-oriented guidelines in SG applications that has to be considered in the designing of effective cybersecurity strategies. By using this standard specifications, it is possible to evaluate and identify a specific risk, as well as define the appropriate security requirements.

- **IEC 62351**: it was developed by the IEC Technical Committee, Working Group 15 with the aim of defining different security objectives, such as authentication of data transfer through digital signatures, prevention of eavesdropping, prevention of playback/spoofing and intrusion detection. It applies the existing security protocols, such as Transport Layer Security (TLS), widely used in different industrial application fields.

- **IEC 61850**: it specifies the structure of the data, the naming conventions for data, how execute testing procedure and how control different devices in the power system.

- **IEC 60870**: it was developed by IEC Technical Committee 57, Working Group 03 to provides specifications for power system monitoring, control and communication for telecontrol, teleprotection and telecommunication operations in the power system. It includes different configurations and covers also asynchronous data transmission, thus defining requirements on coding, formatting and synchronization of variable data frames satisfying integrity requirements.

- **IEC 61968**: different standards are herein involved related to information exchanges among electrical distribution system entities, which are developed by the IEC Technical Commitee 57 Working Group 14. The aim of this standard is to facilitate the integration of middleware services and interface adapters based on events in loosely coupled and heterogeneous environments in order to ensure non-real time data message transactions.

2.4.4 Looking Forwards Interoperability, Scalability and Security Requirements

Since a unique solution for communication infrastructure in MG does not still exists, multiple communication technologies may be used in different MG levels, thus bringing to interoperability issues among different parts. As disclosed in Figure 2.7, *Interoperability* of SG can be defined as the ability of diverse systems to work together, use the compatible parts, exchange information or equipment from each other, and work cooperatively to perform tasks [55]. Based on this definition, it is clear that specific and unique communication rules have to be specified in MG field. This issue is addressed by the above mentioned international standards IEEE Std-2030, IEEE Std-1547.3, and IEC 61850 (see [1] and references therein), which provide the best practices for achieving SG interoperability and DGs interoperability, thus offering the possibility to achieve a universal communication infrastructure where multiple and heterogeneous communication technologies are employed.

Another crucial feature that should be guaranteed in MG communication infrastructure is the *scalability* property, which refers to the possibility to accommodate multiple devices and services into the power systems, as well

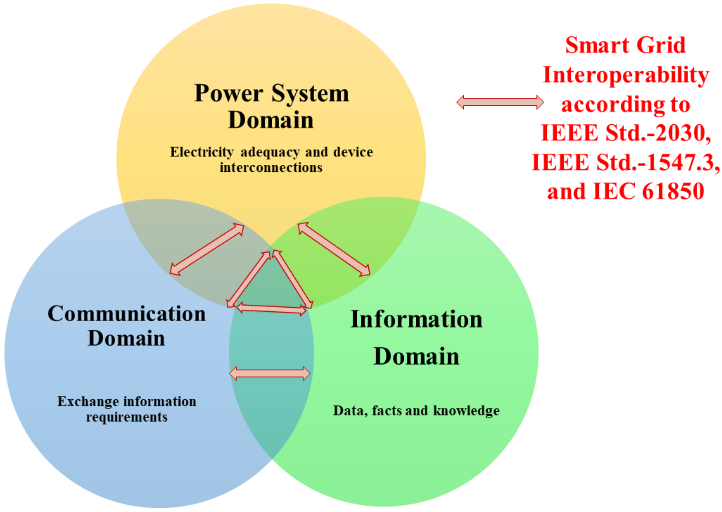

Figure 2.7. Smart Grid Interoperability concept [3].

as an increasing number of end-user interactions [55].
Finally, according to the Electric Power Research Institute (EPRI), the last but not the least communication requirement facing the SG/MG development is related to *cybersecurity* of systems [55], particularly crucial especially when considering private information about users, like power usage patterns and energy prices, thus leading also the possibility to disrupt appropriate operations of the power systems. Technical literature interested on cybersecurity issues proposes different solutions towards privacy protection, encryption and authentication algorithms, as well as intrusion detection.

2.5 Smart Metering Technology in Microgrids

Smart meters are an other important milestone in the design of modern SG and MG since they can be exploited in order to obtain users energy consumption information, which can be useful not only for remote data collection of suppliers, but also for improving monitoring and control actions via their integration into the EMS. According to the technical literature [1], traditional electricity meters involve electromechanical electricity meters and electronic meters, which have some drawbacks, namely:

- the meters readings have to be periodically manually checked by several inspectors;
- no updated measurements of consumption data are available, meaning that the billing process results to be expensive and time-consuming as it is based on energy consumption forecasts;
- customers energy saving is hindered since it is difficult to find new hourly-based tariffs;
- problems about the development of meter software applications along with the implementation of supportive network infrastructures.

It results that, by using traditional meters, although the customer is able to know its own electricity consumption profile, the statics of consumption cannot be changed till the customer changes its consumption habit.

The development of novel ICT has completely changed electricity meters, leading to the so-called *smart meters*. Compared to traditional meters, which require manual measurements and readings, these devices meant to be *smart*, i.e., equipped with communication capability. According to the European Commission (2012/148/EU), a smart meter device is defined as *"an electronic system that can measure energy consumption, adding more information than a conventional meter, and can transmit and receive data using a form of electronic communication"* [1]. Therefore, these novel devices endow the electricity meter with a communication and a control infrastructure, with the possibility to collect real-time information about different electrical variables (such as energy consumption data, voltage, etc.) and communicate them to service provider, along with the execution of proper control actions (remotely or locally). It follows that the usage of these new smart devices is crucial for monitoring and control of all the electrical entities involved into the MG, thus supporting DGs and ESSs, which are essential for MG operations. Moreover, they enable a direct communication among energy providers and customers via the bidirectional information flow. By providing information about energy consumption along the day, smart meters would be key devices towards a secure, affordable and sustainable energy supply since these information

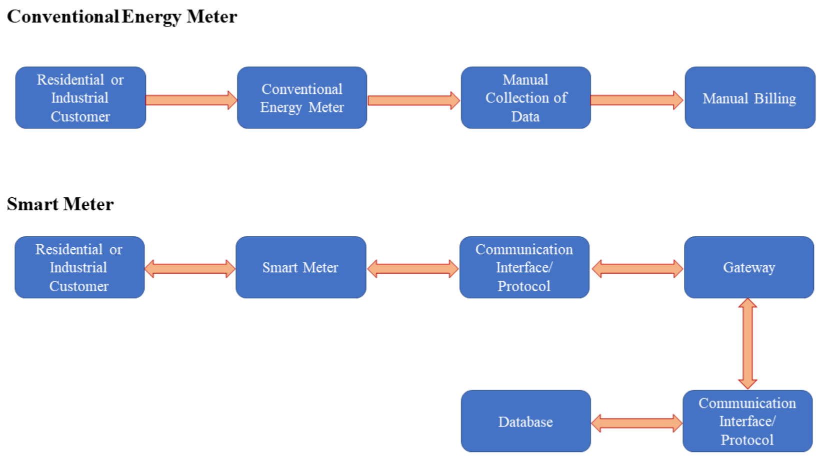

Figure 2.8. Comparison between conventional electricity meters and smart meters operations [4].

can be used by providers to make suitable decisions and develop innovative and dynamic pricing strategies for their customers. Specifically, proper time-of-use tariffs can be designed to help customers in changing their consumption habits, especially during peak hours, thus leading to significant energy saving. Hence, smart meters play a non trivial role in the global transition to a low-carbon economy, with benefits also in financial terms [1]. Hence, the main improvements expected from the usage of smart meters are [56]:

- users can adapt their power consumption habits by exploiting real-time available information, thus achieving financial incentives and improving sustainability and energy saving;
- reduction of the operational costs, since service providers can evaluate and control meters remotely, while minimizing also human readings errors and increasing system security;
- time-saving in performing meters readings;
- reduction of the energy waste, since they allow reacting to power shortages, failures and excesses, with the possibility to redirect energy where it is required.

Finally, Figure 2.8 highlights a comparison between conventional electricity meters and novel smart meters architectures.

2.6 European Guidelines

The green transition has been formalized by EU Commission in December 2019 via the the so-called *European Green Deal*, which relies on disruptive innovations, new technologies, and sustainable solutions to achieve the EU decarbonisation objectives by 2050 [16]. Moved by climate change and environmental degradation, which are dangerous threats for Europe and, in general, for the world, the European Green Deal aims at transforming the EU into a modern, resource-efficient and competitive economy via the achievement of the following objectives:

- no net emissions of greenhouse gases by 2050;
- economic growth decoupled from resource use;
- no person and no place left behind.

Different specifications have been fixed by the European Commission in order to make EU climate, energy, transport and taxation policies oriented towards the reduction of net greenhouse gas emissions by at least 55% by 2030, compared to 1990 levels [57]. Therefore, the final goal for all the 27 EU member states is to turn the EU into the first climate-neutral continent by 2050 by acting, among different sectors, also on the energy one. It is worth noting that, climate neutrality by 2050 means achieving net zero greenhouse gas emissions for EU countries as a whole, mainly by cutting emissions, investing in green technologies and protecting the natural environment [17]. Specifically, it is expected that the greater use of renewable energy will be crucial to achieve the aforementioned objectives, with a energy efficiency increasing. In this context, the first step towards the above objectives has been the European Climate Law, presented in March 2020 [17], which also includes measures to keep track of progress and adjust actions accordingly. Then, in July 2021 the EU Commission presented a new package of proposals, called the Fit For 55 package, i.e., a set of policy instruments tackling the green transition with a cross-sectoral approach (see Figure 2.9), with the aim of ensuring that EU policies are

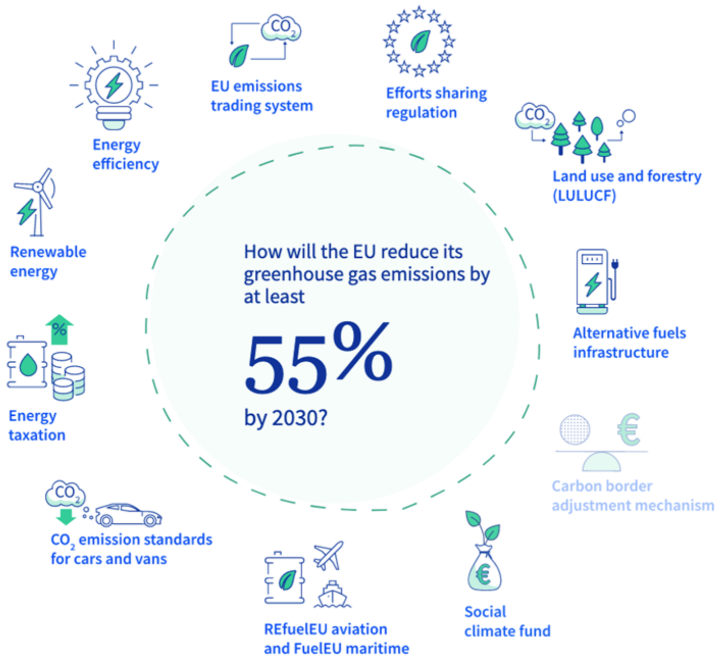

Figure 2.9. What is included into the Fit for 55 Package [5].

in line with the climate goals agreed by the Council and the European Parliament [16, 5].

Based on these considerations, it follows that the development of novel ICT, the widespread of smart meters and advanced distributed control strategies, along with the diffusion of distributed renewable energy sources and ESSs, which lead to SG and MG paradigms, are fundamental part of the energy transition according to the European Green Deal vision. The huge amount of available data coming from high level of connectivity among distributed devices involved into the power network, which is now conceived as CPES, leads to more flexible and reliable power system characterized by a sectoral integration. Besides, DGs and ESSs, together with digitalization, allow designing proper demand-side management strategies aiming at matching energy production and request, thus enhancing the possibility to integrate RESs into the energy system.

However, it should be noted that the actual regulatory framework does not sufficiently encourage innovative investments (mainly based on ICT) in distribution grids. This could lead to some problems in the future, especially with a congestion in the distribution networks, higher risks of blackout, problems for RESs integration with a deterioration of the Quality of Service (QoS) [58]. To face this issue, the Council of European Energy Regulators (CEER) has recognised the National Regulatory Authorities (NRAs) to keep up with changes in the energy sector and to ensure that policy and regulation do not create unjustified barriers against innovation, while continuing to empower and protect consumers during the transition [59]. Furthermore, the technical literature is moving towards a common formulation for regulatory experimentation in energy sector, starting from two pioneer NRAs, i.e., Ofgem in Great Britain and Arera in Italy. From a global point-of-view, the International Smart Grid Action Network (ISGAN) also highlights the need to improve conventional approaches with regulatory experiments, which stand for a deviation from the actual regulatory frameworks in order to test different rules in a real-world application, while at the same time it is possible to evaluate technological advances and new business model. Instead, at the European level, in 2018 the association of CEER introduced a 3D strategy based on digitalization, decarbonization and dynamic regulation, which aims at: *i*) enabling energy transition, *ii*) achieving regulatory goals; *iii*) ensuring a comprehensive approach and more opportunities for new solution to be tested and deployed ona large-scale. For more details on the topic, the interested reader can refer to [16].

Starting from 2005, EU formed the European Technology Platform (ETP) in order to promote SG technology and support the vision of 2020 European electricity networks development, and a large number of pilot projects have been implemented, especially in Portugal, Italy and Czech Republic [60]. Specifically, the Italian framework will be discussed in the next section.

2.6.1 The Italian Framework

Italy is considered as one of the EU states that has been most affected by the increase of intermittent generation, with a wide use of RESs [61]. The Italian Energy Regulator (Autorità per l'Energia Elettrica e il Gas (AEEG)) has promoted the selection process RO ARG/elt 39/10 for

SG demonstration projects, especially focused on Medium Voltage (MV) networks.
Along this line, one of the remarkable project is related to the practical implementation of SG concept to real-life MV network in the urban area of Milan, developed by A2A Reti Elettriche (which owns and operates the distribution network in the cities of Milan and Brescia) [58]. Compered to other pilot projects, A2A Lambrate (Milan) one has two main features: the first one is related to the availability of superfast broadband services (i.e., those with an advertised speed of 30 $[Mbit/s]$ or above); the second one is the presence of customers and industrial applications with very stringent QoS demand. In doing so, this project results to be a demonstration of a SG aiming at reconstructing a specific distribution network through the use of innovative technologies allowing the active RESs management, while ensuring the necessary level of security, availability and QoS. A2A has obtained a grant from the AEEG both for Lambrate and Brescia networks since it overcame current limitations related to several aspects, e.g., interface protection of generators connected to the MV grid and introduction of innovative voltage regulation functionalities, thus encouraging the development of DGs and the use of RESs for electricity generation [62].

Another important initiative approved by AEEG is the one carried out by Azienda San SEverino Marche SpA (A.S.SE.M SpA), a small Distributed System Operators (DSO) located in Central Italy with a submission of an experiment proposal aimed at introducing novel automation and control features within its distribution networks [63]. This pilot project is implemented on the 20 $[kV]$ electricity distribution network of San Sverino, Marche (Macerata province), which is equipped with real-time monitoring systems able to collect data required for the project evaluation. The project provides important features, such as: *i*) increasing of the grid reliability by preventing the unintentional island operations of DGs or their unwanted disconnections; *ii*) novel fault management based on the selective interlocking and the remote control of switches along lines, with the purpose of improving users service continuity; *iii*) centralized voltage regulation aimed at increasing the network hosting capacity for RESs; *iv*) monitoring and control of DGs injections.

Important efforts have been done also by the University of Genoa, which is working on mathematical modeling of optimal operation for poly-

generation MG, an important stepping stone towards advance large scale metering [64]. The Smart Polygeneration Microgrid (SPM) of the University of Genoa is located in the Savona University Campus and its objective is the investigation of different issues related to modeling and simulation, energy efficiency, new protocols and paradigms. It includes heterogeneous DGs, such as gas microturbines, PV and concentrating solar power, integrated with ESSs, such as sodiumenickel batteries, on a low voltage distribution system. The aim is to produce clean energy for the University loads and to operate as a test-bed facility for research, testing and development of management strategies and power components [64], by performing the following main activities: *i*) implementation and validation of algorithm to predict generation from RESs; *ii*) implementation and validation of methods for the optimal operations of ESSs and dispatchable sources; *iii*) power flow control at the interface with the external grid in order to control the exchange of active/reactive power; *iv*) gathering of energy measurements in a centralized database in order to find pattern that can be useful for further researches; *v*) testing of new smart power converters for improving the integration of RESs.
Therefore, these initiatives, along with other important projects devoted to the implementation and the development of a set of environmental and sustainable policies, confirm that Italy with the AEEG is working a lot towards novel regulation for SG diffusion in order to promote a clean energy framework according to European Green Deal perspective [65].

Chapter 3

Microgrid Modeling and Control Architecture

The MG infrastructure consists of heterogeneous DGs, which could be RESs and ESSs and local loads. All these entities have to be collectively managed in order to enhance energy security and reliability, while offering flexible services to the grid. In this perspective, it is mandatory to integrate MG with a proper control infrastructure. A hierarchical structure is usually employed for MG control architecture since it meets fundamental infrastructure and dynamic interface requirements, while providing integrity through both centralized and distributed control systems. Therefore, this chapter presents the typical multi-layer hierarchical control architecture used in MG applications, which consists of three main layers to be endowed with intelligence and flexibility, namely: PC, aiming at both maintaining voltage/frequency stability and providing power-sharing capability among DGs; SC, which restores frequency and voltage deviations naturally induced by PC; TC, which guarantees power flow management between the MG and the main grid, by taking into account also economic aspects. A complete description of each layer, as well as the respective control objectives, will be given.

As stated in previous chapters, the main objective of this thesis is the design of fully-distributed cooperative control strategies for voltage/frequency regulation in invert-based islanded MG in MASs perspective. Along this line, the MG can be studied as NCS, i.e., *a set of spatially distributed* *systems in which the communication between sensors, actuators and controllers occurs through a shared band limited digital communication network*. In this perspective, all the DGs can be assumed as fully controllable players and the allowed information flow among them can be studied via algebraic graph theory. Therefore, this chapter aims also at introducing preliminary concepts related to cooperative control of MASs linked by a communication graph where, in particular, the most important properties of algebraic graph theory are recalled. Basic controllers guaranteeing the achievement of *consensus* and *synchronization* are briefly presented in order to highlight that in cooperative systems, any control protocol of each agent must be distributed, meaning that it respects the prescribed graph topology and depends only on local information about itself and its neighbors in the graph. Finally, the derivation of the AC inverter based isladend MG model will be presented along with the classical framework adopted in the technical literature to study voltage and frequency MG stability.

3.1 Microgrid Hierachical Control Architecture

In order to guarantee stable and economically efficient MG operations, a proper control architecture is a prerequisite in MG, whose main objectives are [66]:

- voltage and frequency regulation both in grid-connected and in islanded modes;
- proper load sharing and DGs coordination;
- MG synchronization with the utility grid;
- power flow control;
- MG operating costs optimization.

These requirements have different impact and time scales, thus requiring a multilayer hierarchical control architecture, which has become a standard paradigm for DGs systems. By exploting the hierarchical control architecture, it is possible to control MG variables, i.e., frequeny and voltage values, while guaranteeing power sharing capability, meaning that each

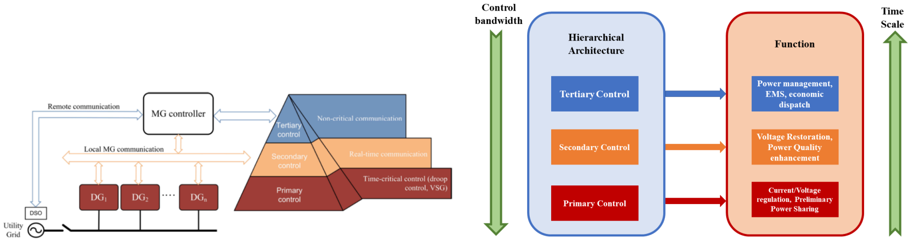

(a) (b)

Figure 3.1. Hierarchical Control Architecture in Microgrid [6].

DG is able to generate a desired steady-state power [1].
MG hiearchical control architecture consists of three different layers:

1. PC layer: it is the droop control used to share load between converters;

2. SC layer: it is responsible for removing steady-state voltage and frequency error induced by PC;

3. TC layer: it deals with global responsabilities in terms of import/-export of energy for the MG.

Each layer has different control objectives and a specific speed of response in term of control bandwidth. This latter consideration enables the decoupling of the dynamics of each layer and facilitates their individual design [1]. Moreover, whereas the performance of PC and SC affects the MG stability and its power quality as they involve fast control mechanisms, the TC provides support for optimizing the MG power flow or the power transfer to/from the utility grid [67]. Figure 3.1 shows the typical MG hierarchical control architecture involving PC, SC and TC layers. From Figure 3.1 (a), it is possible to observe that PC layer, commonly based on the droop method to mimic the behavior of the synchronous generators, is usually implemented without communication among the DGs. Conversely, SC, aiming at compensating frequency and voltage deviations induced by droop control, is based on real-time communication and different approaches can be applied on the basis of communication scheme implemented (centralized, decentralized or distributed). Finally, TC, which works with a longer timescale, usually is based on centralized communication system depending on a central controller from the main grid. Therefore, this three-layer control architecture is implemented by leveraging both local converter and digital communication links along with coordinated control approaches, which are separated by at least an order of magnitude in control bandwidth. Indeed, from PC to TC layers, control bandwidth decreases while time scale increases (see Figure 3.1 (b)).

A more detailed explanation of each layer functionalities, along with their respective control objectives, will be provided below.

3.1.1 Primary Control

The PC layer (*level one of IEC/ISO 62264 std)*) is designed to satisfy the following control objectives [68]:

- stabilize voltage and frequency, especially after an islanding event which could bring to MG instability phenomena due to mismatch between power generated and consumed;
- provide DGs with plug-and-play capability, while sharing active and reactive power among them without any communication links;
- mitigate circulating currents, which may cause over-current phenomena in the power electronic devices and damage them.

The PC is the first level in the hierarchy and it is locally implemented at DGs terminals. Typically, it consists of inner current and voltage control loops, a virtual impedence loop and droop mechanism controller [7]. Current and voltage inner control loops deal with frequency and voltage stabilization, while droop control mechanism addresses the power sharing task. Moreover, virtual impedance is an optional loop acting via a mismatched inductive/resistive feeder impedance in order to enhance the power quality and power sharing accuracy into the MG. To increase the power system stability, the PC should have the fastes response to any sources or demand variation, i.e., of the order of milliseconds. Moreover, the PC can be used also to balance energy among DGs and ESSs [68].

Hence, the PC is essentially designed by mimicking the behaviour of synchronous generator in conventional power systems, where it drops the operating frequency and voltage magnitudes when an increasing of active and reactive power demand occur. This is the main objective of conventional droop control scheme, where the active power-frequency $(P-\omega)$ and reactive power-voltage $(Q-v)$ droop-based controllers are used to reach power sharing according to the following relations:

$$\omega_i = \omega^\star - k_{P_i} P_i, \qquad\qquad v_i = v^\star - k_{Q_i} Q_i, \tag{3.1}$$

where v_i and ω_i are the i-th DG output voltage magnitude and operating frequency; Q_i and P_i are the output reactive and active power, respectively; k_{Q_i} and k_{P_i} are the droop gains selected on the basis of DGs rating; $v^\star$ and $\omega^\star$ are the PC set-points to be sent to inner voltage and current control loops [69]. From (3.1), it follows that no communication links are required for droop control implementation, thus resulting in a higher reliability with respect to different control approaches along with a simple implementation [68, 69]. However, some limitations exist in PC based on droop control, which can be listed as follows [69]:

- droop control can be applied only for dominantly inductive transmission lines and DGs interconnecting lines, while it fails for low-voltage MG with dominantly resistive interconnecting impedance;
- it is prone to frequency and voltage deviations induced by load variations;
- it is not suitable for non-linear loads since it neglects the resulting harmonic current circulation, which leads to poor power quality and slow dynamic response;
- poor voltage regulation under critical loads since voltage is not a global variable in MG.

Despite these drawbacks, droop-based controllers are largely employed in PC layer. However, different methods based on communication links have been suggested in the technical literature, such as concentrated control, master/slave, instantaneous current sharing and circular chain control methods (see [68] and references therein).

3.1.2 Secondary Control

The SC layer (*second level of IEC/ISO 62264 std*) works to fulfill the following control objectives [54]:

- frequency and voltage restoration to nominal values whenever load change occurs;
- frequency and voltage steady-state errors compensation induced by droop-based PC;
- synchronization with the utility grid during transition from islanded to grid-connected mode.

Taking into account (3.1), these objectives can be mathematically formulated as follows:

$$\lim_{t\to\infty} \omega_i(t) = \omega^\star, \qquad \lim_{t\to\infty} v_i(t) = v^\star, \tag{3.2}$$

$$\lim_{t\to\infty} (k_{P_i} P_i(t) - k_{P_j} P_j(t)) = 0, \quad \lim_{t\to\infty} (k_{Q_i} Q_i(t) - k_{Q_j} Q_j(t)) = 0, \tag{3.3}$$

for all $i, j = 1, \ldots, N$, where (3.2) and (3.3) stand for frequency and voltage regulation and power sharing control objectives in the steady-state. Compared to PC, the SC uses a low bandwidth communication (see Figure 3.1(b)) and has more global responsibilities.
As disclosed in Figure 3.2, SC architectures are classifies into three main classes, namely: centralized SC, decentralized SC and distributed SC.

Centralized control structure has been the traditional control architecture for SC layer, where there exists a central controller whose task is to coordinate voltage and frequency values of all the DGs involved into the grid to the desired set-point (i.e., $v^\star$ and $\omega^\star$, respectively) (see Figure 3.2(a)). However, by exploiting this kind of SC architecture, the entire stability and the performance of the MG are strongly compromised by possible failures of the centralized infrastructure. Therefore, since all the required data are transmitted via a high-data rate centralized infrastructure, any deficiency or failure of this latter degrades the MG efficiency [7]. In the technical literature, although this kind of SC architecture is applied to deal with harmonic cancellation, unbalanced current reduction and other quality and management issues, the flexibility and the reliability of the MG result to be strongly weakened and the whole system may

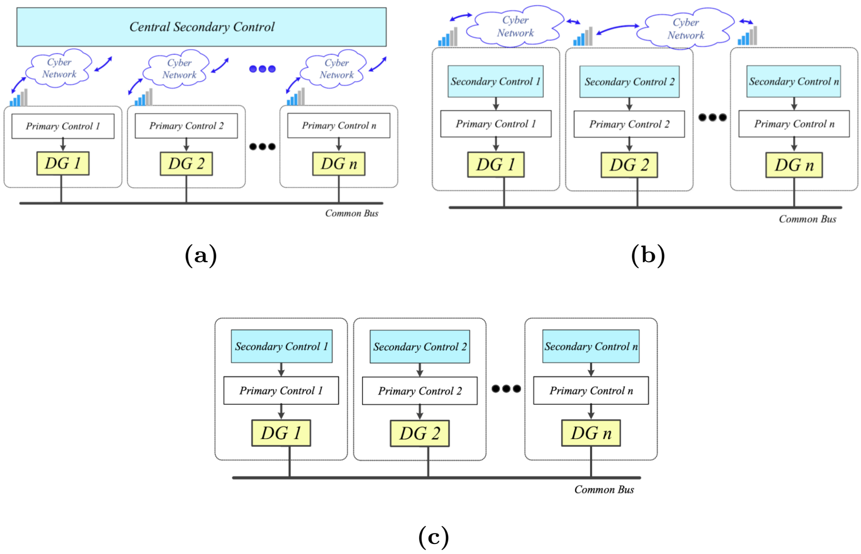

Figure 3.2. Secondary Control layer Architectures: *a*) Centralized SC; *b*) Distributed SC; *c*) Decentralized SC [7].

collapse [7, 67].

In decentralized SC approach (Figure 3.2(c)), frequency and voltage regulation is carried out by multiple secondary controllers locally embedded into each DG, without data sharing with other DGs [67]. Although this communication-less control structure may provide important advantages due to the absence of a central infrastructure for SC purposes, fully-decentralized approaches have different issues related to, e.g., clock-drift phenomena. Based on the above considerations, communication-free decentralized control strategies do not represent a suitable solution and, hence, the majority of the works in the technical literature focus on communication-based structures, i.e. centralized and distributed ones (Figure 3.2(a) and 3.2(b)). However, besides the above mentioned drawbacks related to centralized SC architecture, it is worth noting that this latter becomes even more tricky when system scale is larger since the central controller suffers from extensive computation and communication burden.

To overcome this issue, distributed SC architecture, disclosed in Figure 3.2(b), has become the most suitable solution [8], where MASs paradigm can be exploited to model the MG. According to this mathematical framework, each MG component is represented by a dynamic system which, sharing information with the neighboring agents, aims at achieving a common coordinated behavior at the global level via distributed control protocols [42]. In this case, the behavior of the MG depends on the agents dynamics, i.e., on the DGs, as well as on the communication topology employed to model the information sharing process among them. The distributed structure of the communication network is able to improve MG reliability since the requirement for a central controller is obviated and, by exploiting control protocols distributed on all the DGs, the control system does not fail down subsequent to outage of a single unit [8]. In this perspective, the MG can be viewed as a CPS or, even better, as a CPES, where NCS framework, along with distributed consensus algorithms, can be helpful to achieve secondary control purposes. Specifically, the SC of MG via distributed control architecture can be recast as a tracking synchronization problem of MASs, where DGs voltage and frequency are required to track the nominal values $v^\star$ and $\omega^\star$, respectively. More details on synchronization process in MASs will be given in Section 3.2.

3.1.3 Tertiary Control

The TC layer (*level three of IEC/ISO 62264 std.*) is the last and the slowest control level in MG control architecture. It considers the economical aspects in the optimal operation of the MG and manages the power flow between the MG and the utility grid [66]. Therefore, this level involves the EMS and, hence, it deals with non-critical tasks required for power flow optimization. Specifically, the optimal scheduling of the MG resources is provided by a centralized system at a low sampling rate (several seconds or minutes), where low priority data packets are transferred via the MG communication network [67]. Summarizing, the key tasks of TC layer can be listed as follows:

- control and optimization of the power flow between the MG and the utility grid;
- transmission of the frequency and voltage reference values to the SC

layer;

- performing islanding events detection and voltage harmonic reduction;
- improvement of the power quality at the PCC.

Therefore, in grid-connected mode, the TC layer exploits the power references provided by the DSO to control the power flow between the MG and the main grid, thus requiring a communication link between the EMS (embedded into the TC) and the DSO. Conversely, in the presence of a multi MG scenario, the TC is used also to provide information exchange between the neighboring MGs.

Since the focus of the thesis falls into the design of fully-distributed control strategies for MG at the SC layer of the hierarchical control architecture in a NCS perspective by exploiting MASs theory, some preliminary concepts related to cooperative control of MASs will be presented in the next section.

3.2 Cooperative Control of Multi-Agent Systems

The communication network interconnecting a set of N dynamical systems, called also as *agents*, can be modeled by leveraging MASs theory over a graph. A graph is a pair $\mathscr{G} = (\mathscr{V}, \mathscr{E})$, with $\mathscr{V} = \{V_1, V_2, \ldots, V_N\}$ the set of N nodes (or vertices) and $\mathscr{E}$ the set of edges or arcs. Elements of $\mathscr{E}$ are (V_i, V_j), standing for an arc from V_i to V_j. These arcs represent the information flow in the graph. It is assumed that the graph is *simple*, i.e., $(V_i, V_i) \neq \mathscr{E}$, $\forall i$, i.e. no self-loops are allowed. Edge (V_i, V_j) means to be outgoing with respect to node V_i and incoming with respect to V_j. The neighbors set of the i-th node V_i is denoted as $\mathscr{N}_i = \{V_j : (V_j, V_i) \in \mathscr{E}\}$, i.e., the set of nodes with edges incoming to V_i. The graph is said to be *balanced* if the in-degree are equal to the out-degree for nodes $V_i \in \mathscr{V}$. Moreover, if $(V_i, V_j) \in \mathscr{E} \rightarrow (V_j, V_i) \in \mathscr{E}$, $\forall i, j$, the graph is said *bidirectional*; otherwise it is denoted as a *directed graph* or *digraph* (see Figure 3.3(a)).
According to the algebraic graph theory [8], graph structure and properties can be investigated by studying the properties of some associated matrices. In particular, it is possible to introduce the adjacency or connectivity

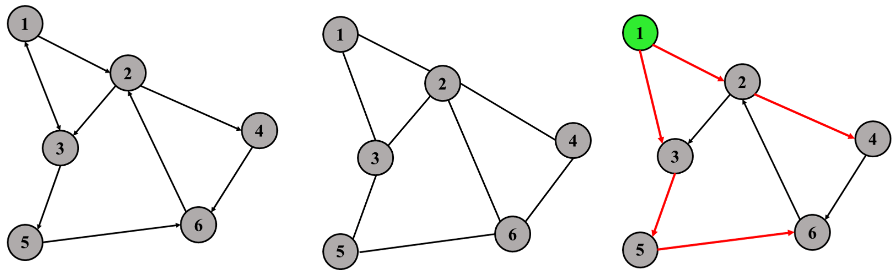

(a) (b) (c)

Figure 3.3. Graph examples: *a*) Direct Graph; *b*) Undirected Graph; *c*) A spanning tree for the graph in *a*) with root node 1 [8].

matrix $\mathscr{A} = [a_{ij}] \in \mathbb{R}^{N\times N}$, whose generic element $a_{ij} = 1$ if there exists a link between agent j and agent i, $a_{ij} = 0$ otherwise. Note that, $a_{ii} = 0$. If $a_{ij} = a_{ji}$, $\forall i, j$, i.e., if the graph is bidirectional and the weights of edges (V_i, V_j) and (V_j, V_i) are the same, the graph is said to be *undirected* (see Figure 3.3(b)).

A directed path is a sequence of nodes $V_1,\ V_2, \dots, V_r$ such that $V_i, V_{i+1} \in \mathscr{E},\ i \in \{0, 1, \dots, r-1\}$. Node V_i is said to be connected to node V_j if there exists a directed path from V_i to V_j and the distance between them is the length of the shortest path from V_i to V_j. The graph $\mathscr{G}$ is said to be *strongly connected* if $V_i,\ V_j$ are connected for all distinct nodes $V_i,\ V_j \in \mathscr{V}$.

A (directed) tree is a connected digraph where every node except one, called the root, has in-degree equal to one. A *spanning tree* of a digraph is a directed tree formed by graph edges that connects all the nodes of the graph. A graph is said to have a spanning tree if a subset of the edges forms a directed tree, meaning that all nodes in the graph are reachable from a single root node by following the edge arrows (Figure 3.3(c)).

If a graph is strongly connected, then all nodes are root nodes.

Furthermore, the diagonal in-degree matrix $\mathscr{D} = diag\{d_1, d_2, \dots, d_N\} \in \mathbb{R}^{N\times N}$ is defined as $d_i = \sum_{j=1}^{N} a_{ij}$, which indicates the number of nodes communicating with i-th agent. Hence, the Laplacian matrix is computed as $\mathscr{L} = \mathscr{D} - \mathscr{A}$ and it has all row sums equal to zero. Note that, the properties of the graph may be studied in terms of Laplacian matrix and, in particular, of its eigenvalues.

Cooperative control of MASs has received a lot of attention during the last decades due to its potential application in different areas, e.g., sensor networks, intelligent transportation systems, electric power system and so on. In this networked system, each agent is endowed with its own state variable and dynamics. The fundamental problem is to design distributed protocols guaranteeing *consensus* or *synchronization*, meaning that, by leveraging local information of each agent along with the ones of its neighbours $j \in \mathscr{N}_i$, it is possible to achieve a common group behaviour, i.e., the states of all the agents reach the same value.
In the sequel, for the sake of completeness, the definition of consensus and syncrhonization problems will be formalized according to the technical literature.

3.2.1 Consensus and Cooperative Regulator Problem

Let consider a MASs consisting of N agents with a simple first-order single-integrator dynamics as

$$\dot{x}_i(t) = u_i(t), \tag{3.4}$$

with $x_i(t),\ u_i(t) \in \mathbb{R}$ the state and the control input of the i-th agent. The following definition is given for the sake of completeness.

Definition 1 (*Consensus - Cooperative Regulator Problem*[8])**.** *Find a distributed control protocol for each agent i that drives all the states to the same constant steady-state values, i.e., $x_i(t) \to x_j(t) \to c = const,\ \forall i, j$. This value is known as a consensus value.*

To solve problem in Definition 1, the simpler distributed control protocol for the i-th agent is:

$$u_i(t) = \sum_{j \in \mathscr{N}_i} a_{ij}(x_j(t) - x_i(t)), \tag{3.5}$$

where a_{ij} is the element of the adjacency matrix modeling the presence/absence of a communication link between the i-th and j-th agents. Controller in (3.5) is known as *cooperative regulator* since no external reference input is involved. By introducing enlarged vector $x(t) = [x_1(t),\ \dots, x_N(t)]^\top \in$

$\mathbb{R}^N$, the closed-loop dynamics of the entire MASs can be presented as

$$\dot{x}(t) = -\mathscr{L}x(t), \tag{3.6}$$

with $\mathscr{L} = \mathscr{D} - \mathscr{A}$ the Laplacian matrix. Note that, the global control input vector $u = [u_1, \ldots, u_N]^\top \in \mathbb{R}^N$ is given as $u = -\mathscr{L}x(t)$, meaning that the eigenvalues λ_i of $\mathscr{L}$ are instrumental through the analysis of the MASs stability. By ordering these eigenvalues in increasing magnitude as $\{\lambda_1, \ldots, \lambda_N\}$ and assuming the existence of a spanning tree in the graph, it follows that $\lambda_1 = 0$, whereas the remainder of the eigenvalues has positive real parts. According to (3.6), at steady state, it results $0 = -\mathscr{L}x_{ss}$. The consensus problem for the MASs (3.4)-(3.5) can be solved according to the following theorem [8].

Theorem 1. *(Cooperative Regulation for First-order Systems [8]) The cooperative regulator* (3.5) *guarantees the consensus of the single-integrator dynamics* (3.4) *if and only if the graph has a spanning tree. Then, all node states come to the same steady-state values $x_i = x_j = c$, $\forall i, j$ given as*

$$c = \sum_{i=1}^{N} p_i x_i(0),$$

where $w_1 = [p_1 \ldots p_N]^\top$ is the normalized left eigenvector of the Laplacian $\mathscr{L}$ for $\lambda_1 = 0$ such that $w_1^\top \mathscr{L} = 0$ and $\|w_1\| = 1$. Moreover, the consensus is achieved with a time constant given by

$$\tau = \frac{1}{Re\{\lambda_2\}},$$

with λ_2 being the second eigenvalue of $\mathscr{L}$, that is, the Fiedler eigenvalue.

Proof. Proof of Theorem 1 can be found in [8]. □

Note that, from Theorem 1, it is clear that agents states go to a constant value c depending on the initial conditions of all the agents involved in the MASs due to interrelation among them captured by Laplacian matrix $\mathscr{L}$.

3.2.2 Syncrhonization or Cooperative Tracker Problem

Let consider a MASs consisting of N agents with a simple first-order single-integrator dynamics as in (3.4), plus an additional node, labeled with index 0, i.e., $x_0(t)$, acting as a leader in providing the reference behaviour to be imposed to the whole network. For the sake of simplicity, assume $\dot{x}_0(t) = 0$.

Definition 2. *(Synchronization - Cooperative Tracker Problem [8]). Find a distributed control protocol for each agent i that drives all states to the state of the leader node, i.e., $x_i(t) \to x_0(t)$, $\forall i$.*

The above problem in Definition 2 is also known as *leader-tracking problem*. To solve this latter, it is usually considered a distributed cooperative tracker protocol as

$$u_i(t) = \sum_{j \in \mathscr{N}_i} a_{ij}(x_j(t) - x_i(t)) + p_i(x_0(t) - x_i(t)), \tag{3.7}$$

where a_{ij} is the element of the adjacency matrix modeling the presence/absence of a communication link between agent i and agent j, respectively; p_i is the i-th element of the Pinning matrix $\mathscr{P} = diag\{p_1, \dots, p_N\}$ such that $p_i = 1$ when the leader information is directly available for the i-th agent, 0 otherwise. It means that if the agent i can obtain the leader information directly, the node i is pinned to the leader.
To analyze the closed-loop MASs network, define the synchronization errors as $e_i(t) = x_0(t) - x_i(t)$, $\forall i$ and, hence, the global tracking error vector $e(t) = [e_1(t), \dots, e_N(t)]^\top \in \mathbb{R}^N$. Taking into account (3.7), the global synchronization error dynamics results to be:

$$\dot{e}(t) = -(\mathscr{L} + \mathscr{P})e(t),$$

meaning that, the global synchronization error $e(t)$ goes to zero if $(\mathscr{L} + \mathscr{P})$ is stable. This result is given according to the following theorem.

Theorem 2. *(Cooparative Tracking for First-order Systems [8]) The cooperative tracking protocol (3.7) guarantees tracking of the single-integrator dynamics (3.4) if and only if the augmented graph $\mathscr{G}_{N+1}$ resulting from the presence of the leader node has a spanning tree. Then, $x_i(t) \to x_0(t)$, $\forall i$.*

Proof. Proof of Theorem 2 can be found in [8]. □

Note that, results of Theorem 1 and Theorem 2 can be easily extended to more general agent dynamics, including vector states and general state variable dynamics. Specifically, in the case of vector states, i.e., $x_i(t),\ u_i(t) \in \mathbb{R}^N,\ \forall i$, previous results can be extended by using Kronecker product properties [70] and Theorem 1 and Theorem 2 remain still valid. For more details, the interested reader can refer to [8, 71]. It is worth noting that, although in Definition 2 the leader is assumed as a constant reference profile, controller (3.7) (and, thus, Theorem 2) can be easily adapted to the case of non-constant reference behavior. According to the technical literature, the leader dynamics is usually modeled as an autonomous system, i.e., $\dot{x}_0(t) = Ax_0(t)$, useful to generate a large class of command trajectories (unit step, ramp, sinusoidal waveforms, and more). Also in this case, distributed controller has to be designed by tacking into account the local neighborhood tracking errors as in (3.7). On the other hand, very few results deal with a non-autonomous (but bounded) reference behavior [72].

3.3 Microgrid Modeling

Consider an islanded operating AC MG consisting of N DGs and M local loads, physically interconnected via power transmission lines. Each DG i, $\forall i = 1, \dots, N$ is equipped with smart devices allowing information sharing among them so to achieve SC objectives. Hence, a double layer modeling approach is used to model the entire network, which involves a *physical layer*, involving power transmission lines to connect DGs with local loads, and a *cyber-layer*, for the connections among DGs in the cyber-space, which are able to guarantee fulfillment of SC objectives via their on-board devices.
In what follows, to create a detailed framework, the problem formulation will be discussed starting from an accurate mathematical model for DGs and for the overall stand-alone MG network. Note that, according to the technical literature [73], MG modeling can be categorized into two main classes: inverter-interfaced DGs [74] and the so-called small signal model [75]. Although in the former the model derivation is restricted to single

DG, while the current and power flows between different units are non explicitly considered, in the sequel the inverter-based modelling will be considered since the future electrical networks will be composed of inverter-based electrical devices [73].

3.3.1 DG Model

A PC layer is locally implemented in each inverter-based DG unit, consisting of three-phase dc/ac inverter, a dc source, RL output connector and an LCL filter [30]. Moreover, an inner voltage control loop and current control loop along with the power control are included in order to regulate the inverter voltage and current and to help power sharing task [76], thus reacting the instability phenomenon both in frequency and voltage magnitudes after PCC disconnection process [77]. Since power control loop dynamics is slower than the voltage and current control loops, usually the technical literature focuses on the stability of the reactive/active power control loop. The study of voltage and current control loops usually follows the traditional PI controllers (see [28] and references therein).
Although the PC of each DG is generally formulated under its own $d-q$ (direct-quadrature) reference frame rotating at the frequency ω_i, all the DGs choose a common reference frame to operate with the rotating frequency ω_{com}. Denote the angle of the i-th DG reference frame with respect to the common reference frame as

$$\delta_i = \int (\omega_i - \omega_{com})\, dt. \tag{3.8}$$

Therefore, according to the CERTS and taking into account (3.1), the dynamics of the i-the DG unit is expressed by the following approximated droop equations ($\forall i = 1, \ldots, N$) [78]:

$$\begin{cases} \begin{cases} k_{v_i} \dot{v}_i^{od} = v_i^n - v_i^{od} - k_{Q_i} Q_i^m \\ v_i^{oq} = 0 \end{cases} \\ \omega_i = \omega_i^n - k_{P_i} P_i^m \end{cases} \tag{3.9}$$

where v_i^n and ω_i^n, provided by the SC layer, represent the PC voltage and frequency set-points; P_i^m and Q_i^m are the measured active and re-

active power at the i-th DG terminal; $k_{v_i} \in \mathbb{R}^+$ is the voltage control gain; $k_{Q_i} \in \mathbb{R}^+$ and $k_{P_i} \in \mathbb{R}^+$ are its voltage and frequency droop coefficients, properly selected by considering its corresponding active and reactive power ratings. Note that $\omega_i^n = u_i^\omega$, $v_i^n = u_i^V$. Hence, $u_i^\omega = u_i^V = 0$ means that SC is inactive.
Moreover, the measured real and reactive power, i.e. P_i^m and Q_i^m respectively, are given via the following first-order low-pass filter [30]:

$$\tau_{P_i}\dot{P}_i^m = -P_i^m + P_i, \tag{3.10a}$$

$$\tau_{Q_i}\dot{Q}_i^m = -Q_i^m + Q_i, \tag{3.10b}$$

where τ_{P_i} and τ_{Q_i} are the filter time constants, P_i and Q_i are the active and reactive power outputs of the i-th DG.

For SC purposes, each DG i within the network, $\forall i = 1, \dots, N$, exchanges its information with the corresponding neighbors via onboard smart devices enabling the communication. Hence, the MG resembles a MASs, where each DG is an agent and distributed cooperative SC strategies can be applied to solve voltage/frequency regulation problem. These latter can be recast as a leader-tracking problems, where the objective is to design $v_i^n = u_i^V$ and $\omega_i^n = u_i^\omega$ in (3.9) such that the terminal voltage and frequency amplitude of each DG, i.e., v_i^{out} and ω_i, converges to the desired reference value $v^\star$ and $\omega^\star$, respectively, i.e., $v_i^{out} \to v^\star$, $\omega_i \to \omega^\star$, $\forall i$, where

$$v_i^{out} = \sqrt{(v_i^{od})^2 + (v_i^{oq})^2}. \tag{3.11}$$

This latter implies that SC voltage input u_i^V has to guarantee that $v_i^{od} \to v^\star$ due to $v_i^{oq} = 0$.

3.3.2 Double-Layer Microgrid Network Model

The *cyber layer*, i.e., the communication layer describing the information exchange among the smart controllers associated with each DG i, $\forall i = 1, \dots, N$ within the MG in the cyber-physical space, can be modeled according to graph theory (see previous Section 3.2). Specifically, this *cyber layer* can be described via the graph $\mathscr{G}_N^c = \{\mathscr{V}_N^c, \mathscr{E}_N^c, \mathscr{A}_N^c\}$, where $\mathscr{V}_N^c$ is the nodes set, i.e. the DGs, while $\mathscr{E}_N^c \subseteq \mathscr{V}_N^c \times \mathscr{V}_N^c$ is the edges set representing the communication links among the inverters. $\mathscr{A}_N^c = [a_{ij}]^c \in \mathbb{R}^{N\times N}$ is the

adjacency matrix defined as $a_{ij} = 1$ if there is a link from DG j to DG i, $a_{ij} = 0$ otherwise. The Laplacian matrix $\mathscr{L}^c = [l_{ij}] \in \mathbb{R}^{N \times N}$ is such that $l_{ii} = \sum_{j \neq i}^{N} a_{ij}$ and $l_{ij} = -a_{ij}$, with $i \neq j$.
The reference voltage and frequency values (i.e. v_0 and $\omega_0 \in \mathbb{R}$, respectively) of secondary distributed consensus control are shared by a virtual leader DG, labeled with 0 index. Hence, the resulting augmented graph is defined as $\mathscr{G}^c_{N+1} = \{\mathscr{V}^c_{N+1}, \mathscr{E}^c_{N+1}\}$, to which it is possible associating a Pinning matrix $\mathscr{P} = diag\{a_{10}, a_{20}, \cdots, a_{N0}\} \in \mathbb{R}^{N \times N}$, whose generic element $a_{i0} = 1$ if the leader information is directly available for the ith DG, $a_{i0} = 0$ otherwise.
By defining the leader node 0 globally reachable in $\mathscr{G}^c_{N+1}$ if there exists a path from every DGs node i, $\forall i = 1, \ldots, N$ to leader node 0, throughout the thesis, unless otherwise specified, it will be assumed the global reachability property for the leader agent. Finally, $\mathscr{N}_i^c = \{j : (i,j) \in \mathscr{E}^c_{N+1}\}$ denotes the neighboring set of the DG unit i, $\forall i = 1, \ldots, N$.

Besides the communication network topology, the *physical layer*, i.e. the electrical network topology, also needs to be presented, which describes the physical interconnections among the N DG units and M local loads enabled via power transmission lines. To this aim, by leveraging again graph theory, a directed graph $\mathscr{G}^e_{N+M} = \{\mathscr{V}^e_{N+M}, \mathscr{E}^e_{N+M}, \mathscr{A}^e\}$ can be introduced, being $\mathscr{V}^e_{N+M}$ the electrical entities set and $\mathscr{E}^e_{N+M}$ the set of the electric edges, i.e. the impedences of the power lines. Indeed, $\mathscr{A}^e$ represents the adjacency matrix associated to the electrical topology, whose complex weights are the admittance between different buses. For example, the generic $a_{\rho k} = Y_{\rho k} = G_{\rho k} + jB_{\rho k}$, being $Y_{\rho k} \in \mathbb{C}, G_{\rho k} \in \mathbb{R}$ and $B_{\rho k} \in \mathbb{R}$ the admittance, the conductance and susceptance, respectively. $Y_{\rho k} = 0$ means that does not exists a power line between the ρ-th and the k-th bus. Similarly, $\mathscr{N}_\rho^e = \{k : k \in \mathscr{V}^e_{N+M}, k \neq \rho, Y_{\rho k} \neq 0\}$ denotes the set of neighbors of the ρ-th electrical unit. In addition, it results $G_{\rho\rho} = \sum_{k \in \mathscr{N}_\rho^e} G_{\rho k}$ and $B_{\rho\rho} = \sum_{k \in \mathscr{N}_\rho^e} B_{\rho k}$.
Note that, this kind of representation for the communication and the electrical layers is possible according to the appraised inverter-based MG modelling [73].

Cyber-layer and *electrical layer* topologies are such that the following assumptions hold [13].

Assumption 1. *The power transmission lines within the MG, describing* *the electrical network topology* $\mathscr{G}^e_{N+M}$, *are lossless. This implies that the conductance is always zero, i.e.* $G_{\rho k} = 0$, *and* $Y_{\rho k} = jB_{\rho k}, \forall \rho \in \mathscr{V}_{M+M}, k \in \mathscr{N}^e_\rho$.

Note that, the above assumption is common and reasonable in power system analysis (see e.g. [79, 80] and references therein). Indeed, the lossless line admittance may be justified as follows: in MV and LV networks the line impedance is usually not purely inductive, but has a non-negligible resistive part. On the other hand, the inverter output impedance is typically inductive (due to the output inductance and/or the possible presence of an output transformer). Under these circumstances, the inductive parts dominate the resistive parts [79]. Moreover, Assumption 1 is also crucial for control design phase. Indeed, by considering dominant inductive networks, the influence of the dynamics of the phase angles on the reactive power flows can be neglected [81].

Taking into account the above Assumption 1 together with the power balance equations [82], the following relations hold:

$$\hat{P}_\rho = \sum_{k \in \mathscr{N}^e_\rho} v_\rho v_k B_{\rho k} \sin(\delta_\rho - \delta_k), \tag{3.12a}$$

$$\hat{Q}_\rho = v_\rho^2 B_{\rho\rho} - \sum_{k \in \mathscr{N}^e_\rho} v_\rho v_k B_{\rho k} \cos(\delta_\rho - \delta_k), \tag{3.12b}$$

where $\hat{P}_\rho$, $\hat{Q}_\rho$, v_ρ and δ_ρ are the active injected power, the reactive injected power, the measured voltage and phase angle of the bus ρ, $\forall \rho \in \mathscr{V}^e_{N+M}$, respectively.
Moreover, to integrate the presence of a local load within a specific bus ρ, the so-called ZIP load model can be exploited, whose expression is given as [83]

$$P_{L_\rho} = P_{1_\rho} v_\rho^2 + P_{2_\rho} v_\rho + P_{3_\rho}, \tag{3.13a}$$

$$Q_{L_\rho} = Q_{1_\rho} v_\rho^2 + Q_{2_\rho} v_\rho + Q_{3_\rho}, \tag{3.13b}$$

where the pair (P_{1_ρ}, Q_{1_ρ}) represents the nominal constant impedence loads, (P_{2_ρ}, Q_{2_ρ}) indicates the pair for the nominal constant current loads, while (P_{3_ρ}, Q_{3_ρ}) the ones related to nominal constant power loads.

Putting together (3.12)-(3.13), we can have:

$$P_i = \sum_{\rho \in \mathcal{N}_i^e} P_{L_\rho} + \sum_{\rho \in \mathcal{N}_i^e} \hat{P}_\rho, \tag{3.14a}$$

$$Q_i = \sum_{\rho \in \mathcal{N}_i^e} Q_{L_\varepsilon} + \sum_{\rho \in \mathcal{N}_i^e} \hat{Q}_\rho, \tag{3.14b}$$

where P_i and Q_i are the total active and reactive power output of the DG $i, \forall i = 1, \dots, N$.

Assumption 2. *There exist prescribed known constants* $\Pi^Q, \Pi^P \in \mathbb{R}^+$ *such that*

$$|Q_i| \leq \Pi^Q, \ |P_i| \leq \Pi^P \ \ \forall i.$$

This ensures that reactive and active power (3.14b) and (3.14a), as well as (3.10b) and (3.10a), are bounded.

Remark 1. *Assumption 2 is reasonable in power system analysis since, by considering a fixed operating point of the inverter, the magnitudes of these powers do not exceed their tresholds, thus preventing any instability conditions [30].*

Remark 2. *According to* (3.9)-(3.14)*, DGs voltage and frequency dynamics are coupled each other. However, decoupling voltage and frequency control design phases is a common practise in power system analysis and stabilization (see [84] and references therein). Accordingly, through the next chapters, frequency and voltage controllers will be discussed separately.*

3.4 Concluding Remarks and Setting for the Next Chapters

This chapter has presented the typical hierarchical control architecture employed in MG, which consists of three different layers, namely, PC, SC and TC. Their main features and control objectives have been deeply presented.

In order to guarantee voltage/frequency stability in the MG, which falls into SC objectives and will be the main interest of the thesis, preliminary concepts on distributed control for MASs have been presented, along with the fundamental properties of algebraic graph theory, useful to investigate the allowed information flow among DGs involved into the MG. Thus, the derivation of a proper MG control-oriented model in CPES perspective has been carried-out.

In the remainder chapters, these preliminaries will be used to design fully distributed cooperative control strategies both for general MASs and for MG. However, before presenting the main theoretical results of the thesis, in the next chapter a discussion about the more crucial problems arising in cooperative control of NCS and, in particular, in MG, will be provided so to motivate and highlight the contributions of the book.

Chapter 4

Open Challenges in Distributed Secondary Control of Microgrids

This chapter aims to briefly present the most important issues arising in distributed control of MASs and, in particular, in the specific MG application, in order to highlight the motivations and contributions of the next chapters. The MG performance depends on the distributed control strategies employed to coordinate different DGs involved into the network, which are enabled in the cyber space via the interaction among these different electrical entities properly equipped with smart devices. The combination of electrical and physical layers leads to the vision of MG as a CPES as disclosed in Figure 4.1, where advanced ICT are exploited for information transmission and distributed decision making process, thus allowing a control performance improvement, with more effective, resilient and reliable operations. However, the large amount of connected devices along with the widespread of ICT causes several communication constraints that require to be analysed in control design phase in order to ensure acceptable performance for the entire network. Examples of communication impairments arising in distributed control are, e.g., communication time delays, data-loss and network bandwidth limitation, which could lead to time synchronization loss of state variables, thus degrading dynamic performance, even bringing to instability phenomena. Besides communication impair-

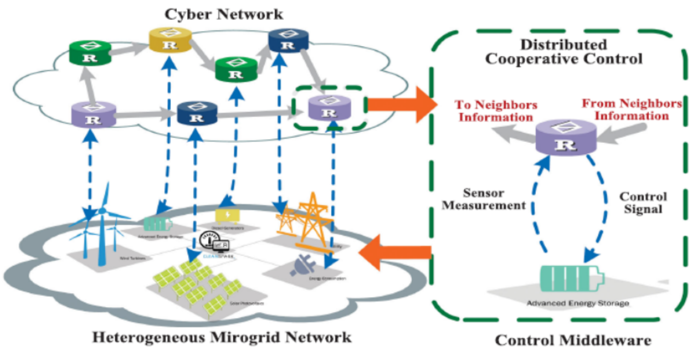

Figure 4.1. Cyber-enabled distributed cooperative control scheme for Microgrids [9].

ments, other control requirements crucial in MG application emerge from a careful analysis of the technical overview, which are highlighted since they need to be further investigated. Firstly, since from a practical view point loads require nominal operating conditions in terms of state variables, the problem of speeding-up the convergence rate of frequency/voltage magnitudes to the desired set-point results to be fundamental in MG. Hence, finite-time stability methods are a promising solution in order to ensure the synchronization in finite-time interval. Moreover, it is also proven that these strategies are able to provide robust performance and stability, as well as higher accuracy and disturbance rejections. Furthermore, unknown model mismatches, external disturbances and uncertainties always affect DGs dynamics due to the inner control loops (usually neglected in the technical literature to derive a control-oriented DG model) and all the complex phenomena, such as topological changes, unbalanced and nonlinear loads, high-frequency pulse-width voltage modulation and transition between modes of operation. Therefore, in the sequel, an explanation of the emerging open challenges in distributed SC of MG addressed through the book will be provided.

4.1 Fundamental Issues of Distributed Secondary Control in Microgrids

As discussed in previous chapters, the MG can be considered as a smart cyber-physical network consisting of heterogeneous intelligent nodes, i.e., the electronically interfaced DERs (which include DGs, loads, ESSs), endowed with the sensing/actuation, control and communication capabilities, which interact among them to efficiently deliver power and electricity to the consumers [9].
However, different challenging issues arise due to the widespread of intermittent DERs, especially in islanded mode operations, such as voltage and frequency fluctuations, as well as the entire MG stability. As the hierarchical control architecture is the most suitable solution to manage with multiple control requirements and different time-scales, the cyber-enabled distributed control theory embedded into the SC layer is expected to constitute a key analytical tool in the design of cyber-physical MG systems [9]. In order to guarantee effective, resilient and reliable MG operations, it is required to proper manage and coordinate all the involved and geographically dispersed DERs via the design of appropriate distributed control strategies. These latter rely on advanced ICT, which play a crucial role in cooperative control of DERs. However, communication constraints result from the usage of large number of communication devices in MG, such as communication delay, data-loss, and cyber attack, while at the same time a limited communication bandwidth should be considered. Moreover, besides the fulfillment of SC objectives, the technical literature on the topic introduces some important control requirements for MG applications aiming at improving the effectiveness and robustness of the entire electrical network.

In the sequel, communication constraints and control requirements for distributed SC strategies, as well as for general MASs, will be highlighted in order to better motivate the next chapters.

4.2 Communication Constraints

The cyber network, enabled via the exploitation of advanced ICT, allows the interaction among the different spatially distributed electrical units in the cyber-space in order to reach global objectives by exploiting the two-way communication network. On the one hand, the exploitation of distributed communication medium improves MG flexibility, scalability and stability [9]. On the other hand, the information sharing process among different smart devices leads to different communication constraints, such as switching topology, delay, noise disturbances, bandwidth limitation and cyber attacks, which could deteriorate the cooperation performance even bringing to instability phenomena of the whole network [9]. Thus, it is crucial to consider communication constraints during the control design phase in order to prevent undesirable events, while capturing their impact on control performance.

In the following, two communication constraints, addressed in this book, will be highlighted.

4.2.1 Communication Time Delay Effects

Time-delay is one of the universal phenomena arising in MASs and in practical MG systems since it is an integral part of communication network [85, 9]. The hypothesis of an ideal communication network in MASs applications results to be unrealistic since, in practise, agents share their state information through a wireless network and, hence, communication time-delays in data-acquisition and transmission naturally arise [25]. Hence, communication delays both in nominal and troublesome scenarios must be considered in the designing of distributed secondary control strategies, regardless of high or low bandwidth communication links. Limited communication speed, extra time for the measurement message reception, computation time for the control input generation and execution time for the input acted are some of the main reasons for time delays appearing in MG. If load changes and disturbances occur, the electronically interfaced DERs are able to fast respond to the control commands on the basis of data exchanged with their neighbors due to their low inertia. This implies that, compared to conventional bulk power systems, time delays in MG have a more significant impact on system performance and stability due to the low system inertia and high response speed.

The presence of communication time-delays is usually addressed in MASs literature under the assumption of constant and unique time-delay affecting the communication structure [25, 26]. However, this assumption results to

be unrealistic in practical applications as in MG control since, when dealing with wireless/wired communication networks, each communication links connecting a pair of agents is affected by variable time-delays depending on actual conditions and impairments of the communication channel. If follows that communication time-delays, affecting the outdated information used to compute the control input, have to be considered as time-varying functions.
It is worth noting that one of the most important distinction in delays arising in distributed control theory is related to *symmetric and asymmetric communication delay* [9]. Denote with $\tau(t)$ the time when the information is transmitted to DER_j to DER_i; then, a generic distributed control protocols embedding asymmetric communication delays has the following form:

$$u_i(t) = \sum_{j \in \mathscr{N}_i} a_{ij}[y_j(t - \tau(t)) - y_i(t)] + a_{i0}[y^{ref} - y_i(t)], \tag{4.1}$$

where $y_i(t)$ and $y_j(t - \tau(t))$ are the measured information variable of i-th DER from itself without delays and its neighbors with time-varying delays, respectively. It means that, the i-th DER receives message from the j-th DER, $\forall j \in \mathscr{N}_i$, at time t and utilizes messages $y_j(t-\tau(t))$ instead of $y_j(t)$. Note that, the delay in (4.1) is asymmetric since the i-th agent can receive it own information $y_i(t)$ instantaneously, meaning the sum of computation and execution times for each single agent is neglected.
Conversely, if these computation and execution times for each agents are considered, then delays become *symmetric*, i.e.:

$$u_i(t) = \sum_{j \in \mathscr{N}_i} a_{ij}[y_j(t - \tau(t)) - y_i(t - \tau(t))] + a_{i0}[y^{ref} - y_i(t - \tau(t))]. \tag{4.2}$$

Note that, if $\tau(t) = \tau = constant$, the delay is unique and fixed.

Remark 3. *It should be clarified that, in (4.2), self and communication delays are homogeneous for all the agents, i.e. $\tau(t)$ affects both $y_i(t)$ and $y_j(t)$. Although this assumption could represent a limitation from a practical point-of-view, it does not impact on the so-called delay consensus margin. Moreover, in the case of homogeneous agents dynamics, it would be also reasonable to assume that their delays, likewise, are homogeneous [86].*

Based on the above considerations, it results that delays have to be considered in control design and it is desirable to find stability conditions depending on a maximum tolerable delay in order to highlight the stability margin with respect to these communication latencies [42].

4.2.2 Limited Communication Bandwidth

In practical MASs applications as MG control, agents are spatially distributed over a monitoring area and controlled through some communication networks by a digital control platform or controller, which usually runs with limited energy resources and computing capability [12, 9]. Moreover, distributed control protocols are usually designed under the assumption of point-to-point data transmission, meaning that the information sharing process relies on continuous states or continuous output measurements. This leads to a continuous inter-agent interaction, which results to be unrealistic since the advances communication networks only ensure digital information dissemination. It follows that traditional continuous time control strategies have to be reformulated by taking into account the following two main requirements:

1. although agents to be controlled live in the continuous physical world and their states/outputs are analog signals, the novel cooperative distributed control strategies are implemented in software on digital computers, which require analog-to-digital and digital-to-analog converters during data acquisition, communication, computation and actuation; this implies that it would be more practical to design and implement distributed controllers in *sampled-data* fashion [36, 12];

2. the communication network bandwidth sometimes may also be restricted and, in practical applications as in MG control, it would be unrealistic to assume always available the limited communication bandwidths and channels; furthermore, the overuse of limited communication resources might lead to possible communication congestion, long delays and packet losses [9].

According to requirement 1), the crucial issue is to study how the sampling process impacts on control performances of the whole network, whose stability can be ensured via a proper selection of the sampling period [36]. Thus, it has been proven that distributed sampled-data controllers allow

achieving a preliminary reduction of the amount of control signals used for stabilization purposes, while their implementation in digital control platform results to be easier with respect continuous-time controllers [14].
On the other hand, an even more efficient use of the communication infrastructure is desirable according to requirement 2), which can be achieved by exploiting Event-Triggered (ET) control theory [9]. According to this latter control paradigm, the violation of some state - and/or time-dependent conditions will trigger a sampling event and, then, the controller will update the feedback signal with the newly sampled information [87]. In this perspective, ET approaches are able to reduce the communication and computation burden since the controllers are only updated when a local measurement error exceeds a tolerable bound. Hence, it results a significant reduction of the communication network workload and a mitigation of the communication resources waste, while maintaining satisfactory control performance. Note that, traditional distributed state-dependent ET strategies have two main drawbacks: *i*) they are sensitive to external interference; *ii*) it is difficult to prove Zeno freeness property and ensure the existence of a minimum inter-execution time [9].

4.3 Control Requirements

Besides the above mentioned communication constraints, in the sequel some control requirements will be discussed, which seem to be crucial in the design of distributed control strategies for MASs and, in particular, in MG applications.

4.3.1 The Convergence Time

As the settling time of distributed control protocols characterizes the convergence rate of the closed-loop system, it represents one of the fundamental requirements for control system design [88]. Fast convergence is usually desirable in order to achieve better performance and robustness. This is particularly crucial in MG applications since a short convergence time allows adapting to frequent and fast disturbances induced by the high variability of RESs and continuously changing loads [89].
As shown in previous Section 3.2, the convergence rate depends on the

algebraic connectivity, i.e., the second smallest eigenvalue of the Laplacian matrix of the communication graph [71]. Although the convergence time of the conventional asymptotic distributed control laws can be improved by designing *ad-hoc* communication topologies and control parameters, in practical MASs, it is of particular interest to realize cooperative control in a finite time to meet the specific system requirements, while avoiding an asymptotic convergence over an unbounded time [89, 88].

Thus, the finite-time control theory is gaining momentum, especially in low-inertia MG with a high penetration of renewable energy generation in order to accommodate its fast changing operating conditions [42]. By combining distributed control theory with finite-time stability tools in MG application field, the frequency and voltage restoration can be achieved in a finite-time horizon, featuring an improved convergence performance than the conventional asymptotic control strategies [89].

4.3.2 Unknown Model Mismatches, External Disturbances and Uncertainties

Unknown model mismatches, external disturbances and uncertainties widely exist in practical system and, hence, research on cooperative anti-disturbance control schemes for MASs is significant [90].

In the context of distributed control of MG, it should be considered that DGs have a nonidentical dynamics, as well as their nature is usually nonlinear. Different linearization approaches have been suggested in order to handle with a control-oriented model, but many simplifications result, which need to be proper managed in order to ensure the stability of the whole network.

Therefore, the following key points should be considered in the control design phase [84]:

- the DGs models used in the technical literature suffer from incomplete plant dynamics since they usually ignore the impact of the inner controllers on the secondary one; therefore, they are simpler for control purposes but, at the same time, they lack of global stability;
- in practise, the MG parameters are unknown, meaning that it is required to consider unmodeled dynamics, which could include unknown disturbances and uncertainties;

- high uncertainties have to be also considered in order to embed the no-predictable nature of renewable sources generations.

Note that, model mismatches, external disturbances and uncertainties acting on the generic i-th DG also arise due to all the related complex phenomena, such as topological changes, unbalanced and nonlinear loads, high-frequency pulse-width voltage modulation and transition between modes of operations [8, 32].

Adaptive control theory seems to be a good solution to handle with all the above mentioned issues and it needs to be further investigated. Specifically, it could be suitable both for the compensation of nonlinear and uncertain DGs dynamics and for counteracting fluctuations arising in system operating conditions, without any manual intervention and by adjusting control parameters in real-time via self-tuning mechanisms. Moreover, if properly designed, adaptive control strategies could be independent of DGs parameters, thus allowing their implementation on DGs regardless their specific parameters and connector specifications [8].

4.4 Concluding Remarks

The objective of this chapter was to highlight the fundamental issues arising in distributed secondary control of inverter-based islanded MG. From the literature overview, both the main communication impairments and the control requirements have been deeply discussed in order to motivate and point-out the contributions and the strength points of the next chapters.

In the remaining chapters, different distributed cooperative control strategies will be suggested in order to address and solve the above mentioned concerns.

Chapter 5

Resilience with respect to communication time-delays

This chapter deals with the problem of resilience with respect to communication time-delays arising during information sharing process in MASs. Firstly, the exponential leader-tracking consensus control problem of a general high-order MASs in the presence of a non-ideal communication network is addressed. To emulate a more realistic cyber communication environment, a specific time-varying delay is associated with each communication link within the network, whose value, at each time instant, depends on the real conditions of the communication channel. To solve this problem, a fully-distributed delayed PI control protocol able to guarantee the exponential stability of the entire delayed closed-loop MASs is proposed. The stability of this latter is analytically proved by exploiting Lyapunov-Krasovskii theory combined with Halanay Inequality, thus obtaining exponential stability conditions expressed as a feasible LMIs. Exemplary numerical simulations corroborate the effectiveness of the theoretical derivation. Based on the above theoretical results, the second part of the chapter recasts the secondary voltage regulation problem in standalone MG as a leader-tracking one, where communication latency during information exchange among the electrical busses is considered. Besides robustness with respect to communication delays, since in MG applications a faster convergence rate is usually desired due to the presence of variable loads, the requirement of speeding-up voltage synchronization process is also taken into account. Therefore, to guarantee that all DGs reach in a finite-time and maintain the voltage set-point, imposed by a virtual DG acting as a leader, a novel robust networked-based control protocol is suggested, able to counteract both the time-varying communication delays and natural fluctuations caused by the PC. The finite-time stability of the whole MG is analytically proven by exploiting again Lyapunov-Krasovskii theory along with finite-time stability mathematical tools. In doing so, delay-dependent stability conditions are derived as a set of LMIs, whose solution allows the proper tuning of the control gains such that the control objective is achieved with required transient and steady-state performances. A thorough numerical analysis is carried out on the IEEE 14-bus test system. Simulation results confirm the analytical derivation and reveal both the effectiveness and the robustness of the suggested controller in ensuring the voltage restoration in finite-time in spite of the effects of time-varying communication delays.

5.1 Input Time-varying delays in Cyber-Physical Systems

Cooperative control of MASs has gained momentum in the last decades due to its variety of application fields, e.g. sensor networks, robotics, electric power systems, autonomous vehicles, and so on [25, 91]. Since the main objective within a MASs is to achieve a common group behavior, while agents interact among them and with the environment via communication networks, the design of distributed controller for each agent becomes a crucial task to guarantee the achievement of state consensus [92] or output consensus [93]. Up to now, important results have been achieved in the technical literature on the leader-follower consensus problem. Among the various control approaches, PI and PID control strategies have been widely used in control systems, due to their closed-loop performances, robustness with respect to model mismatches, and ease of implementation. Indeed, attenuation of unknown disturbances, as well as model uncertainties can be achieved via the introduction of integral action [94], while improving also steady-state performances and tracking capabilities of the closed-loop system [95]. However, despite these advantages, distributed PI or PID protocols are still slightly covered in the current literature [96] and, generally, they are implemented under some simple assumptions for communication constraints, which make the scenario under investigation less realistic [92, 93]. Indeed, the presence of unavoidable technological constraints during information exchange among agents through wireless/wired network cannot be neglected, thus implying the need to consider communication time delays in information sharing. Moreover, since the communication time-delay can compromise the closed-loop performances of the entire MASs, even bringing to instability phenomena [97], it is important to consider them from the beginning of the control design phase, thus obtaining a controller running via outdated information. Along this line, the presence of both time-varying parameter uncertainties and homogeneous time-varying delays has been tackled in [98, 25] via a distributed robust PID control strategy to solve the leader-tracking problem for a platoon of connected autonomous vehicles, while [99] introduced an observer-based PID controller for a linear discrete-time system subject to cyber-attacks to solve the mean-square ISS problem. Furthermore, in real communication networks, e.g. based on IEEE 802.11 protocol, for each communication channel connecting a pair of agents, different communication impairments and packet losses may occur, thus introducing heterogeneous time-varying delays. Then, according to [98], delays have to be considered as time-varying functions depending on the specific communication link under investigation.

As a CPS, the stability of a MG is threatened by the presence of communication time-delays. Indeed, besides the physical electrical layer, networked and distributed control theory has to be applied in the cyber-space in order to enhance the flexibility and reliability of MG systems, with application of MASs theory and peer-to-peer communications for the designing of the SC layer [100]. Leveraging this paradigm, the voltage/frequency restoration, as well as the power sharing control problems, for stand-alone MG have been solved without considering communication impairments in [101, 102], which propose an event-triggered distributed controller, while [103, 10] present a nonlinear robust consensus-based strategy. Neglecting again communication delays, [104] proposes a distributed economic power dispatch and bus voltage control solution for droop-controlled DC MG, while a coordination among the three control layers is discussed in [105] in order to realize a method for their joint operations. Modelling communication impairments as a white noise, both linear and nonlinear consensus-based approach have been very recently addressed in [106, 24]. However, in practise, when dealing with control of connected DGs leveraging wireless communication, also communication time delay into the shared information and sudden packet losses, originated by communication active links, naturally arise. Therefore the hypothesis of perfect and ideal communication among agents is not realistic, as well as the one of modeling impairments only via additive noises may be restrictive. Nevertheless, few papers address the presence of communication time-delays in the MG control. For example, a linear quadratic regulator have been exploited in [26] under the hypothesis of a unique constant time-delay. Along this direction, a robust neighbor-based distributed cooperative control strategy is proposed in [107] for DC MG by considering slow switching topologies and a constant and homogeneous time delay for the overall communication network. However, in practice information shared via a wireless communication networks is affected by time-varying delays depending on the actual condition of the specific communication channel, thus making the assumption of unique delays too restrictive [108]. Considering communication delays as time-varying functions, [28, 27] have suggested a droop-based distributed cooperative control, but no delay-dependent gain-tuning rule has been provided. This implies that no stability margin with respect to delays, also larger than the typical average value of the end-to-end communication, can be guaranteed by the proposed controllers.

In light of the above, the objective of this chapter is to analyze the presence of input time-varying delays in MASs and, hence, in MG applications so to study their impact on stability performance. In doing so, the present chapter aim is twofold. Specifically, the first part of the chapter focuses on an exemplary high-order MASs with the aim to investigate the effectiveness of a distributed PI control strategy in guaranteeing the exponential leader-tracking performance, while counteracting heterogeneous time-varying delays. It is worth noting that, all the above-mentioned distributed PI/PID control strategies, both with and without communication time-delays, only guarantee the asymptotic stability for the overall MASs, thus neglecting the benefit of finding exponential stability conditions depending on the decay rate of the entire network, which plays an important role for control performances [109],[110]. The exponential convergence of

the entire MASs closed-loop error dynamics is proven by exploiting the Lyapunov-Krasovskii theory combined with Halanay's inequality, which allow finding stability conditions expressed in the form of LMIs. An exemplary numerical analysis, involving a network of linear oscillators, confirms the theoretical derivation.
The second part of the chapter is devoted to the voltage recovery problem in the presence of communication time-varying latencies in inverter-based islanded MG, which falls into the SC layer, and it is investigated by leveraging MASs modeling approach. Besides the presence of communication time-delays, in this second part, the additional requirement related to the finite-time convergence is also considered during the control design phase since, in these practical applications, it is particularly desirable to reach the nominal set-point in a certain time-interval. Specifically, in MG framework, a faster convergence rate would be desiderable due to the presence of variable loads, that require nominal operating conditions in terms of both frequency and voltage magnitudes [84]. On the basis of these considerations and to guarantee that DGs voltage restores to the reference value in a specific finite-time interval, while counteracting communication latency arising from the information sharing process, the goal of this second part is to design a novel distributed robust networked-based finite-time controller able to guarantee voltage recovery despite the presence of model mismatches, load changes, as well as plug-and-play phenomena, occurring in real practical operative scenarios. The main contributions of this latter approach can be summarized as follows:

- Unlike [24, 111, 107], the proposed control approach ensures the finite-time stability of the MG, thus allowing both to speed-up the synchronization process to the reference behaviour despite the presence of sensitive loads and communication latencies and to guarantee prescribed transient performances;

- Differently from [24, 111], by exploiting Lyapunov-Krasovskii theory and Finite-Time stability tools, a delay-dependent control gain tuning procedure is provided in the form of feasible LMIs, whose solution allows finding the voltage controller gains and state trajectories bound as function of the upper bound for the communication time-delay; this guarantees a certain stability margin with respect to sudden packet losses, which can be modeled as hard delays;

- Differently from [28, 111, 30, 24], an extensive simulation analysis is carried out by considering a practical case-of-study of the IEEE 14-bus Test system, where no overlapping between electrical and communication layers is considered. Moreover, the worst case scenarios of hard load variations and plug-and-play of DGs are also discussed in order to confirm the robustness of the proposed control approach with respect to sudden changing into the surrounding electrical environment;

- The validation of the proposed networked-based finite-time delayed control action also in the IEEE 30 bus test system with more distributed energy resources corroborates its applicability on larger networks.

5.2 Exponential leader-tracking control for high-order MASs via distributed PI strategy in the presence of time-varying delays

Consider a high-order MAS consisting of N agents sharing information about their states via a wireless network affected by multiple time-varying communication delays. The single-agent dynamics are assumed to be a Linear Time-Invariant (LTI) system as

$$\dot{x}_i(t) = Ax_i(t) + Bu_i(t, \tau_{ij}(t)), \tag{5.1}$$

where $x_i(t) \in \mathbb{R}^n$ represents the i-th agent state vector, $\forall i = 1, \ldots, N$, while $A \in \mathbb{R}^{n\times n}$ and $B \in \mathbb{R}^{n\times 1}$ are known matrices with the following expressions:

$$A = \begin{bmatrix} 0 & 1 & 0 & \dots & 0 \\ 0 & 0 & 1 & \ddots & 0 \\ \dots & \dots & \dots & \ddots & \vdots \\ 0 & 0 & 0 & \ddots & 1 \\ a_1 & a_2 & \dots & \dots & a_n \end{bmatrix}, \quad B = \begin{bmatrix} 0 \\ 0 \\ \vdots \\ 0 \\ b \end{bmatrix}, \tag{5.2}$$

with $b > 0$ and $a_1, a_2, \dots, a_n$ are constants depending on system dynamics; $u_i(t, \tau_{ij}(t)) \in \mathbb{R}$ is the delayed control input evaluated by each agent by exploiting local measurements and network information. Indeed, the information exchanging among agents induces time-varying delays depending on the specific conditions of the communication channel, i.e. $\tau_{ij}(t)$, for $j = 0, 1, \dots, N$ with $j \neq i$.

The aim is to solve a cooperative leader-tracking problem, i.e. to guarantee that all agents synchronize to a reference behavior imposed by a leader agent, indexed with 0. The reference leader dynamics are described as

$$\dot{x}_0(t) = Ax_0(t), \tag{5.3}$$

with $x_0(t) \in \mathbb{R}^n$ and $A \in \mathbb{R}^{n\times n}$. Note that, a large class of useful command trajectories (e.g. ramp, step, sinusoidal waveform and so on) can be generated by the leader dynamic in (5.3) [71]. To address leader-tracking problem of general MASs in the presence of multiple time-varying delays, the distributed control input $u_i(t, \tau_{ij}(t))$ has to be designed such that $\|x_i(t) - x_0(t)\| \to 0$, $\forall i$ as $t \to \infty$. To solve this problem, the following cooperative networked-based delayed PI control strategy is suggested:

$$\begin{aligned} u_i(t, \tau_{ij}(t)) = -\tilde{K}_p \textstyle\sum_{j=0}^{N} a_{ij} \Big(x_i(t - \tau_{ij}(t)) - x_j(t - \tau_{ij}(t)) \Big) \\ -\tilde{K}_i \textstyle\sum_{j=0}^{N} a_{ij} \int_0^{t-\tau_{ij}(t)} (x_i(s) - x_j(s))\, ds \end{aligned} \tag{5.4}$$

where $\tilde{K}_p = K_p[1_{1\times n}]$ and $\tilde{K}_i = K_i[1_{1\times n}]$, being $1_{1\times n}$ the n-th unit vector and $K_p \in \mathbb{R}_+$, $K_i \in \mathbb{R}_+$ the proportional and integral control gains, respectively; a_{ij} models the network topology according to presence/absence of a communication link between agent i and agent j, according to graph theory (see Section 3.2).

Note that, it is crucial to not neglect any possible communication delays that might arise during information sharing among agents and, hence, consider them from the beginning of the control design phase, thus designing a proper control action robust with respect to communication delays based on outdated information.

Remark 4. *In (5.4), no distinction between self- and inter-agent delays is done, i.e., τ_{ij} affects both $x_i(t)$ and $x_j(t)$ in $u_i(t)$, meaning that τ_{ij} can be interpreted as the signal processing delay at the i-th agent communication* *channel level. This is reasonable under homogeneous agents dynamics and does not compromise the delay consensus margin [86].*

The following assumptions hold.

Assumption 3. *[98] To give a more compact notation, the delays affecting the communication among agents are such that $\tau_{ij} \in \{\sigma_p(t) : p = 1, 2, \ldots, m \leq N^2\}$, where $m = N^2$ means that the communication network topology is described by a directed complete graph and all time-delays are different.*

Assumption 4. *[112] The unknown heterogeneous time-varying communication delays are such that $\tau_{ij} \in \{\sigma_p(t) : p = 1, 2, \ldots, m \leq N^2\}$ are bounded and slowly varying signals, i.e. $\sigma_p(t) \in [0, \sigma_p^\star]$ and $\dot{\sigma}_p(t) \leq \mu_p < 1 \;\; \forall p = 1, \ldots, m$.*

5.2.1 Exponential Stability Analysis

In order to tackle with the leader-tracking consensus problem and analytically formalize the resulting exponential stability conditions, the multi-agent closed loop network under the action of control protocol (5.4) is firstly derived.

Closed-Loop Network

Let (5.1) and (5.3) to be the i-th single agent and leader dynamics. By defining the error with respect to the leader, $\forall i = 1, \ldots, N$, as

$$e_i(t) = x_i(t) - x_0(t) \in \mathbb{R}^{n \times 1}, \tag{5.5}$$

the i-th closed-loop error system can be derived as:

$$\begin{aligned} \dot{e}_i(t) &= Ae_i(t) + Bu_i(t, \tau_{ij}(t)) \\ &= Ae_i(t) - B\tilde{K}_p \sum_{j=0}^{N} a_{ij} \Big(e_i(t - \tau_{ij}(t)) - e_j(t - \tau_{ij}(t)) \Big) \\ &\quad - B\tilde{K}_i \sum_{j=0}^{N} \int_0^{t-\tau_{ij}(t)} \Big(e_i(s) - e_j(s) \Big)\, ds. \end{aligned} \tag{5.6}$$

In order to tackle with the overall delayed closed-loop MASs dynamics, introduce the augmented vector $e(t) = [e_1^\top(t),\ e_2^\top(t),\ \dots,\ e_N^\top(t)]^\top \in \mathbb{R}^\nu$, with $\nu = Nn$, and let Assumption 3 holds. In doing so, the overall closed-loop network dynamics can be written as

$$\begin{aligned}\dot{e}(t) =&(I_N \otimes A)e(t) - \sum_{p=1}^{m}(\mathscr{H}_p \otimes B\tilde{K}_p)e(t-\sigma_p(t))\\ &- \sum_{p=1}^{m}(\mathscr{H}_p \otimes B\tilde{K}_i)\int_0^{t-\sigma_p(t)} e(s)\,ds,\end{aligned} \tag{5.7}$$

being $\mathscr{H}_p$ the matrix $\mathscr{H} = \mathscr{L} + \mathscr{P}$, defined in Section 3.2, partitioned according to the m-th decomposition of the complete graph, whose elements are:

$$h_{ij}^{(p)} = \begin{cases} -a_{ij}, & j \neq i, \sigma_p(\cdot) = \tau_{ij}(\cdot),\\ 0, & j \neq i, \sigma_p(\cdot) \neq \tau_{ij}(\cdot),\\ \sum_{j=1}^{N+1} h_{ij}^{(p)} & j = i,\end{cases}$$

and $\sum_{p=1}^{m} \mathscr{H}_p = \mathscr{H}$. Finally, by letting $z(t) = \int_0^t e(s)\,ds \in \mathbb{R}^\nu$ and $\tilde{x}(t) = [z^\top(t), e^\top(t)]^\top \in \mathbb{R}^{2\nu}$, the closed-loop dynamics in (5.7) can be recast in the following more compact form:

$$\dot{\tilde{x}}(t) = \hat{A}\tilde{x}(t) + \sum_{p=1}^{m} \hat{A}_{(p,\sigma)}\tilde{x}(t-\sigma_p(t)), \tag{5.8}$$

where $\hat{A}$ and $\hat{A}_{(p,\sigma)} \in \mathbb{R}^{2\nu\times 2\nu}$ are the following block matrices:

$$\hat{A} = \begin{bmatrix} 0_\nu & I_\nu \\ 0_\nu & \bar{A}\end{bmatrix}, \quad \hat{A}_{(p,\sigma)} = \begin{bmatrix} 0_\nu & 0_\nu \\ -(\mathscr{H}_p \otimes B\tilde{K}_i) & -(\mathscr{H}_p \otimes B\tilde{K}_p)\end{bmatrix}, \tag{5.9}$$

with $\bar{A} = (I_N \otimes A)$. Note that, $\sum_{p=1}^{m} \hat{A}_{(p,\sigma)} = \hat{A}_\sigma$, where $\hat{A}_\sigma$ is structured as

$$\hat{A}_\sigma = \begin{bmatrix} 0_\nu & 0_\nu \\ -(\mathscr{H} \otimes B\tilde{K}_i) & -(\mathscr{H} \otimes B\tilde{K}_p)\end{bmatrix}. \tag{5.10}$$

Letting matrices $\hat{A}$, $\hat{A}_{(p,\sigma)}$ and $\hat{A}_\sigma$ to be defined as in Eqs. (5.9) and (5.10), it holds:

$$\Phi = \hat{A} + \hat{A}_\sigma = \begin{bmatrix} 0_\nu & I_\nu \\ -(\mathscr{H} \otimes B\tilde{K}_i) & \bar{A} - (\mathscr{H} \otimes B\tilde{K}_p) \end{bmatrix} \in \mathbb{R}^{2\nu \times 2\nu}. \tag{5.11}$$

Proof of Exponential Stability

Here the exponential stability of closed-loop MASs network (5.8) under the action of the networked-based PI control action in (5.4) is proven. Delay-dependent stability conditions guaranteeing the exponential stability can be obtained according to the following theorem.

Theorem 3. *Let the closed-loop system defined in (5.8) under the action of networked-based PI delayed control strategy in (5.4) and let Assumptions 3-4 hold. Given control gains $\tilde{K}_p$ and $\tilde{K}_i$, an upper bound of time-delay function $\sigma^\star = \max_p\{\sigma_p^\star\} > 0$ and tuning parameters $\gamma > 0$ and $\alpha > 0$, with $\alpha > \beta$, being*

$$\beta = \frac{m(m+1)\sigma^{\star 2}\bar{\lambda}_{(\hat{A}^\top \hat{A})} + m(m+1)\sigma^{\star 2} \sum_{q=1}^{m} \bar{\lambda}_{(\hat{A}^\top_{(q,\sigma)} \hat{A}_{(q,\sigma)})}}{\underline{\lambda}_{(P)}}, \tag{5.12}$$

if there exists symmetric positive definite matrix $P \in \mathbb{R}^{2\nu}$ and free matrices M_p, N_p and $T_p \in \mathbb{R}^{2\nu}$ such that

$$\begin{bmatrix} \gamma I & \begin{bmatrix} 2(N_1^\top - M_1) & 2(N_2^\top - M_2) & \dots & 2(N_m^\top - M_m) \end{bmatrix} & \begin{bmatrix} 2(N_1^\top - T_1) & 2(N_2^\top - T_2) & \dots & 2(N_m^\top - T_m) \end{bmatrix} \\ 0 & \begin{bmatrix} (M_1^\top + M_1) & 0 & \dots & 0 \\ 0 & (M_2^\top + M_2) & \dots & 0 \\ 0 & \dots & \ddots & \vdots \\ 0 & \dots & 0 & (M_m^\top + M_m) \end{bmatrix} & \begin{bmatrix} 2(M_1^\top + T_1) & 0 & \dots & 0 \\ 0 & 2(M_2^\top + T_2) & \dots & 0 \\ 0 & \dots & \ddots & \vdots \\ 0 & \dots & 0 & 2(M_m^\top + T_m) \end{bmatrix} \\ 0 & 0 & \begin{bmatrix} (T_1^\top + T_1) & 0 & \dots & 0 \\ 0 & (T_2^\top + T_2) & \dots & 0 \\ 0 & \dots & \ddots & \vdots \\ \vdots & \dots & 0 & (T_m^\top + T_m) \end{bmatrix} \end{bmatrix} > 0, \tag{5.13}$$

$$P\Phi + \Phi^\top P + P \sum_{p=1}^{m} \hat{A}_{(p,\sigma)} \hat{A}^\top_{(p,\sigma)} P + \gamma I + \alpha P + 2mN < 0, \tag{5.14}$$

being Φ defined as in (5.11) and $N_p = N_p^\top$ with $N_p = N$, $\forall p = 1, \dots, m$, *then the delayed closed-loop MAS network* (5.8) *is exponentially stable with a decay rate* $\delta \in (0, \alpha)$.

Proof. Consider the following Lyapunov candidate function:

$$V(\tilde{x}(t)) = \tilde{x}^\top(t) P \tilde{x}(t), \tag{5.15}$$

with $P \in \mathbb{R}^{2\nu}$ constant symmetric and positive definite matrix to be determined. By differentiating $V(\tilde{x}(t))$ along the trajectories of the closed-loop system in (5.8), it yields:

$$\dot{V}(\tilde{x}(t)) = \tilde{x}^\top(t)(P\hat{A} + \hat{A}^\top P)\tilde{x}(t) + 2\tilde{x}^\top(t) P \sum_{p=1}^{m} \hat{A}_{(p,\sigma)} \tilde{x}(t - \sigma_p(t)). \tag{5.16}$$

By applying Newton-Liebnitz formula [97] (see A.13 in Appendix), i.e. $\tilde{x}(t-\sigma_p(t)) = \tilde{x}(t) - \int_{t-\sigma_p(t)}^{t} \dot{\tilde{x}}(s)\, ds$, (5.16) can be rewritten as

$$\dot{V}(\tilde{x}(t)) = \tilde{x}^\top(t)(P\Phi + \Phi^\top P)\tilde{x}(t) - 2\tilde{x}^\top(t) P \sum_{p=1}^{m} \hat{A}_{(p,\sigma)} \int_{t-\sigma_p(t)}^{t} \dot{x}(s)\, ds, \tag{5.17}$$

with Φ as in (5.11). Moreover, for generic vectors a, c of suitable dimensions and given a generic positive definite matrix Υ, it holds [113]:

$$\pm 2a^\top c \leq a^\top \Upsilon a + c^\top \Upsilon^{-1} c. \tag{5.18}$$

Setting $a^\top = \tilde{x}^\top(t) P \hat{A}_{(p,\sigma)}$, $c = \int_{t-\sigma_p(t)}^{t} \dot{\tilde{x}}(s)\, ds$ and $\Upsilon = I$ and applying Jensens inequality [97] (see Lemma 4 in Appendix), it yields:

$$\begin{aligned} &\sum_{p=1}^{m} -2\tilde{x}^\top(t) P \hat{A}_{(p,\sigma)} \int_{t-\sigma_p(t)}^{t} \dot{\tilde{x}}(s)\, ds \leq \\ &\leq \sum_{p=1}^{m} \left(\tilde{x}^\top(t) P \hat{A}_{(p,\sigma)} \hat{A}_{(p,\sigma)}^\top P \tilde{x}(t) + \sigma_p^\star \int_{t-\sigma_p(t)} \dot{\tilde{x}}^\top(s) \dot{\tilde{x}}(s)\, ds \right). \end{aligned} \tag{5.19}$$

Hence, (5.17) can be rewritten as

$$\begin{aligned}\dot{V}(\tilde{x}(t)) \leq& \tilde{x}^\top(t)\Big(P\Phi + \Phi^\top P + P\sum_{p=1}^{m} \hat{A}_{(p,\sigma)}\hat{A}_{(p,\sigma)}^\top P\Big)\tilde{x}(t) \\ &+ \sum_{p=1}^{m} \sigma_p^\star \int_{t-\sigma_p(t)}^{t} \dot{\tilde{x}}^\top(s)\dot{\tilde{x}}(s)\, ds.\end{aligned} \tag{5.20}$$

By leveraging Free-Matrices method [97] (see Appendix A.2.3), it follows:

$$\begin{aligned}&2\sum_{p=1}^{m}\left[\tilde{x}^\top(t)N_p^\top + \tilde{x}^\top(t-\sigma_p(t))M_p^\top + \Big(\int_{t-\sigma_p(t)}^{t} \dot{\tilde{x}}(s)\, ds\Big)^\top T_p^\top\right]\times \\ &\times \left[\tilde{x}(t) - \tilde{x}(t-\sigma_p(t)) - \int_{t-\sigma_p(t)}^{t} \dot{\tilde{x}}(s)\, ds\right] = 0,\end{aligned} \tag{5.21}$$

being N_p, M_p and $T_p \in \mathbb{R}^{2\nu\times 2\nu}$ free matrices. Defining the following enlarged vector $\eta(t) \in \mathbb{R}^{2\nu(2m+1)}$ as

$$\begin{aligned}\eta(t) =&\Big[\tilde{x}^\top(t), \tilde{x}^\top(t-\sigma_1(t)), \tilde{x}(t-\sigma_2(t)), \ldots, \tilde{x}^\top(t-\sigma_m(t)), \\ &\Big(\int_{t-\sigma_1(t)}^{t} \dot{\tilde{x}}(s)\, ds\Big)^\top, \ldots, \Big(\int_{t-\sigma_m(t)}^{t} \dot{\tilde{x}}(s)\, ds\Big)^\top\Big]^\top,\end{aligned}$$

and summing the null terms (5.21) and $\gamma\tilde{x}^\top(t)\tilde{x}(t) - \gamma\tilde{x}^\top(t)\tilde{x}(t)$ to the right-side of inequality (5.20) (with $\gamma > 0$), after some algebraic manipulation it results:

$$\begin{aligned}\dot{V}(\tilde{x}(t)) \leq& \tilde{x}^\top(t)\Big(P\Phi + \Phi^\top P + P\sum_{p=1}^{m} \hat{A}_{(p,\sigma)}\hat{A}_{(p,\sigma)}^\top P \\ &+ \sum_{p=1}^{m}(N_p + N_p^\top) + \gamma I\Big)\tilde{x}(t) - \eta^\top(t)\Theta\eta(t) \\ &+ \sum_{p=1}^{m} \sigma_p^\star \int_{t-\sigma_p(t)}^{t} \dot{\tilde{x}}^\top(s)\dot{\tilde{x}}(s)\, ds,\end{aligned} \tag{5.22}$$

being $\Theta \in \mathbb{R}^{2\nu(2m+1)\times 2\nu(2m+1)}$ the upper triangular block matrix defined in (5.13). Now, substituting the closed-loop system as in (5.8) in the integral term of (5.22) and letting $r = l = p$, it follows:

$$
\begin{aligned}
\dot{\tilde{x}}^\top(s)\dot{\tilde{x}}(s) &= \Big(\hat{A}\dot{\tilde{x}}^\top(s) + \sum_{p=1}^{m}\hat{A}_{(p,\sigma)}\tilde{x}(s-\sigma_p(s))\Big)^\top \\
&\times (\hat{A}\dot{\tilde{x}}^\top(s) + \sum_{p=1}^{m}\hat{A}_{(p,\sigma)}\tilde{x}(s-\sigma_p(s)) \\
&= \tilde{x}^\top(s)\hat{A}^\top\hat{A}\tilde{x}(s) + \tilde{x}^\top(s)\hat{A}^\top\sum_{l=1}^{m}\hat{A}_{(l,\sigma)}\tilde{x}(s-\sigma_l(s)) \\
&+ \sum_{r=1}^{m}\tilde{x}^\top(s-\sigma_r(s))\hat{A}^\top_{(r,\sigma)}\hat{A}\tilde{x}(s) \\
&+ \sum_{r=1}^{m}\sum_{l=1}^{m}\tilde{x}(s-\sigma_r(s))\hat{A}^\top_{(r,\sigma)}\hat{A}_{(l,\sigma)}\tilde{x}(s-\sigma_l(s))
\end{aligned}
\tag{5.23}
$$

Furthermore, exploiting again (5.18) with $\Upsilon = I$, (5.23) can be rewritten as:

$$
\begin{aligned}
\dot{\tilde{x}}^\top(s)\dot{\tilde{x}}(s) &\le \tilde{x}^\top(s)\hat{A}^\top\hat{A}\tilde{x}(s) + m\Big(\tilde{x}^\top(s)\hat{A}^\top\hat{A}\tilde{x}(s)\Big) \\
&+ \sum_{l=1}^{m}\frac{1}{2}\tilde{x}^\top(s-\sigma_l(s))\hat{A}^\top_{(l,\sigma)}\hat{A}_{(l,\sigma)}\tilde{x}(s-\sigma_l(s)) \\
&+ \sum_{r=1}^{m}\frac{1}{2}\tilde{x}^\top(s-\sigma_r(s))\hat{A}^\top_{(r,\sigma)}\hat{A}_{(r,\sigma)}\tilde{x}(s-\sigma_r(s)) \\
&+ \sum_{r=1}^{m}\sum_{l=1}^{m}\Big(\frac{1}{2}\tilde{x}^\top(s-\sigma_r(s))\hat{A}^\top_{(r,\sigma)}\hat{A}_{(r,\sigma)}\tilde{x}(s-\sigma_r(s)) \\
&+ \frac{1}{2}\tilde{x}^\top(s-\sigma_l(s))\hat{A}_{(l,\sigma)}\hat{A}_{(l,\sigma)}\tilde{x}(s-\sigma_l(s))\Big) \\
&\le (m+1)\tilde{x}^\top(s)\hat{A}^\top\hat{A}\tilde{x}(s) \\
&+ (m+1)\sum_{q=1}^{m}\tilde{x}^\top(s-\sigma_q(s))\hat{A}^\top_{(q,\sigma)}\hat{A}_{(q,\sigma)}\tilde{x}(s-\sigma_q(s))
\end{aligned}
\tag{5.24}
$$

being $q = r = l = p$.
Taking into account (5.24) and Rayleigh inequality [114] (see Lemma 9 in Appendix), relation (5.22) can be recast as

$$\begin{aligned}\dot{V}(\tilde{x}(t)) &\leq \tilde{x}^\top(t)\Big(P\Phi + \Phi^\top P + P\sum_{p=1}^{m}\hat{A}_{(p,\sigma)}\hat{A}^\top_{(p,\sigma)}P + \sum_{p=1}^{m}(N_p \\ &\quad + N_p^\top) + \gamma I\Big)\tilde{x}(t) - \eta^\top(t)\Theta\eta(t) + (m+1) \\ &\quad \times \sum_{p=1}^{m}\sigma_p^\star\int_{t-\sigma_p(t)}^{t}\tilde{x}^\top(s)\hat{A}^\top\hat{A}\tilde{x}(s)\,ds + (m+1)\sum_{p=1}^{m} \\ &\quad \sigma_p^\star\sum_{q=1}^{m}\int_{t-\sigma_p(t)}^{t}\tilde{x}^\top(s-\sigma_q(s))\hat{A}^\top_{(q,\sigma)}\hat{A}_{(q,\sigma)}\tilde{x}(s-\sigma_q(s))\,ds \\ &\leq \tilde{x}^\top(t)\Big(P\Phi + \Phi^\top P + P\sum_{p=1}^{m}\hat{A}_{(p,\sigma)}\hat{A}^\top_{(p,\sigma)}P + \sum_{p=1}^{m}(N_p \\ &\quad + N_p^\top) + \gamma I\Big)\tilde{x}(t) - \eta^\top(t)\Theta\eta(t) + m(m+1)\sigma^\star\bar{\lambda}_{(\hat{A}^\top\hat{A})} \\ &\quad \times \int_{t-\sigma^\star}^{t}\tilde{x}^\top(s)\tilde{x}(s)\,ds + m(m+1)\sigma^\star\sum_{q=1}^{m}\bar{\lambda}_{(\hat{A}^\top_{(q,\sigma)}\hat{A}_{(q,\sigma)})} \\ &\quad \times \int_{t-\sigma^\star}^{t}\tilde{x}^\top(s-\sigma_q(s))\tilde{x}(s-\sigma_q(s))\,ds\end{aligned} \tag{5.25}$$

being $\sigma^\star = max_p\{\sigma_p^\star\}$. Now, providing an upper-bound for the integral terms in (5.25) according to [115], exploiting delay upper-bounds and the Rayleigh inequality on the symmetric matrices P in (5.15), it follows $\underline{\lambda}_{(P)}\tilde{x}^\top(t)\tilde{x}(t) \leq V(\tilde{x}(t)) \leq \bar{\lambda}_{(P)}\tilde{x}^\top(t)\tilde{x}(t)$. This implies $\tilde{x}^\top(t-\sigma_q(t))\tilde{x}(t-\sigma_q(t)) \leq \frac{1}{\underline{\lambda}_{(P)}}V(t-\sigma_q(t))$ and, hence, inequality (5.25) can be re-written as

$$\begin{aligned}\dot{V}(\tilde{x}(t)) &\leq \tilde{x}^\top(t)\Big(P\Phi + \Phi^\top P + P\sum_{p=1}^{m}\hat{A}_{(p,\sigma)}\hat{A}^\top_{(p,\sigma)}P + \sum_{p=1}^{m}(N_p \\ &\quad + N_p^\top) + \gamma I\Big)\tilde{x}(t) - \eta^\top(t)\Theta\eta(t) + \frac{m(m+1)\sigma^{\star 2}\bar{\lambda}_{(\hat{A}^\top\hat{A})}}{\underline{\lambda}_{(P)}}\end{aligned}$$

$$
\begin{aligned}
&\times \sup_{t-\sigma^\star \le s \le t} V(\tilde{x}(s)) + \frac{m(m+1)\sigma^{\star 2} \sum_{q=1}^{m} \bar{\lambda}_{(\hat{A}^\top_{(q,\sigma)} \hat{A}_{(q,\sigma)})}}{\underline{\lambda}_{(P)}} \\
&\times \sup_{t-\sigma^\star \le s \le t} V(\tilde{x}(s-\sigma_q(s))) \\
&\le \tilde{x}^\top(t) \Big(P\Phi + \Phi^\top P + P \sum_{p=1}^{m} \hat{A}_{(p,\sigma)} \hat{A}^\top_{(p,\sigma)} P + \sum_{p=1}^{m} (N_p \\
&+ N_p^\top) + \gamma I \Big) \tilde{x}(t) - \eta^\top(t) \Theta \eta(t) + \beta \sup_{t-\sigma^\star \le s \le t} V(\tilde{x}(s)),
\end{aligned} \tag{5.26}
$$

being β as in (5.12). To guarantee $\dot{V}(\tilde{x}(t)) < 0$, it is necessary that condition in (5.13) holds. Since Θ is an upper triangular block matrix, to guarantee $\Theta > 0$ it suffices to select $M_p > 0$ and $T_p > 0$, $\forall p = 1, \ldots, m$. In doing so, for the sake of easiness, it is possible to select $N_p = N_p^\top$ with $N_p = N$, $\forall p = 1, \ldots, m$. Hence, inequality (5.2.1) can be finally recast as follows:

$$
\begin{aligned}
\dot{V}(\tilde{x}(t)) \le & \tilde{x}^\top(t) \Big(P\Phi + \Phi^\top P + P \sum_{p=1}^{m} \hat{A}_{(p,\sigma)} \hat{A}^\top_{(p,\sigma)} P \\
& + 2mN + \gamma I \Big) \tilde{x}(t) + \beta \sup_{t-\sigma^\star \le s \le t} V(\tilde{x}(s)).
\end{aligned} \tag{5.27}
$$

By selecting a positive constant α, with $\alpha > \beta$, if condition (5.14) holds, from (5.27), it yields:

$$
\dot{V}(\tilde{x}(t)) \le -\alpha V(\tilde{x}(t)) + \beta \sup_{t-\sigma^\star \le s \le t} V(\tilde{x}(s)) \tag{5.28}
$$

Since $\alpha > \beta$, Halanay Inequality (see Lemma 6 in Appendix) implies the existence of a positive value $\delta \in (0, \alpha)$ such that

$$
V(\tilde{x}(t)) \le \sup_{t_0-\sigma^\star \le s \le t_0} V(\tilde{x}(s)) e^{-\delta(t-t_0)}, \qquad \forall t \ge t_0. \tag{5.29}
$$

According to (5.29), the exploitation of Rayleigh inequality [116] on (5.15) leads to $\underline{\lambda}_{(P)} \|\tilde{x}(t)\|^2 \le \tilde{x}^\top(t) P \tilde{x}(t) \le \bar{\lambda}_{(P)} \|\tilde{x}(t)\|^2$. According to (5.15), the

Table 5.1. Example 5.2.2: simulation parameters.

Agent	0	1	2	3	4	5
$x_{i,1}(0)$	1	-1	1.85	0.5	2	4
$x_{i,2}(0)$	3	4	-0.6	2.5	-1	-2
m	7					
γ	0.7					

following relation holds:

$$\|\tilde{x}(t)\| \leq \sqrt{\frac{\bar{\lambda}_{(P)}}{\underline{\lambda}_{(P)}}} \sup_{t_0-\sigma^\star \leq s \leq t_0} \|\tilde{x}(s)\| e^{-\frac{\delta}{2}(t-t_0)}, \tag{5.30}$$

thus proving that the error vector $\|\tilde{x}(t)\| \to 0$ exponentially as $t \to \infty$. In doing so, each agent exponentially converges toward the leader-behavior, solving the consensus leader-tracking problem. This completes the proof. □

5.2.2 Numerical Analysis

Here the effectiveness of the suggested networked-based delayed PI control strategy (5.4) in solving the exponential stability leader-following consensus problem is highlighted via an exemplary numerical simulation. Consider a MASs consisting of $N = 5$ linear oscillators plus a leader, labeled as 0, sharing their state information through a delayed communication network. The exemplary i-th agent dynamics are:

$$\dot{x}_i(t) = \begin{bmatrix} 0 & 1 \\ -1 & 0 \end{bmatrix} x_i(t) + \begin{bmatrix} 0 \\ 1 \end{bmatrix} u_i(t, \tau_{ij}(t)).$$

The communication graph topology is described by the following Laplacian and Pinning matrices:

$$\mathscr{L} = \begin{bmatrix} 0 & 0 & 0 & 0 & 0 \\ -1 & 1 & 0 & 0 & 0 \\ 0 & -1 & 1 & 0 & 0 \\ -1 & 0 & -1 & 2 & 0 \\ 0 & 0 & 0 & -1 & 1 \end{bmatrix}, \quad \mathscr{P} = \begin{bmatrix} 1 & 0 & 0 & 0 & 0 \\ 0 & 0 & 0 & 0 & 0 \\ 0 & 0 & 1 & 0 & 0 \\ 0 & 0 & 0 & 0 & 0 \\ 0 & 0 & 0 & 0 & 0 \end{bmatrix}.$$

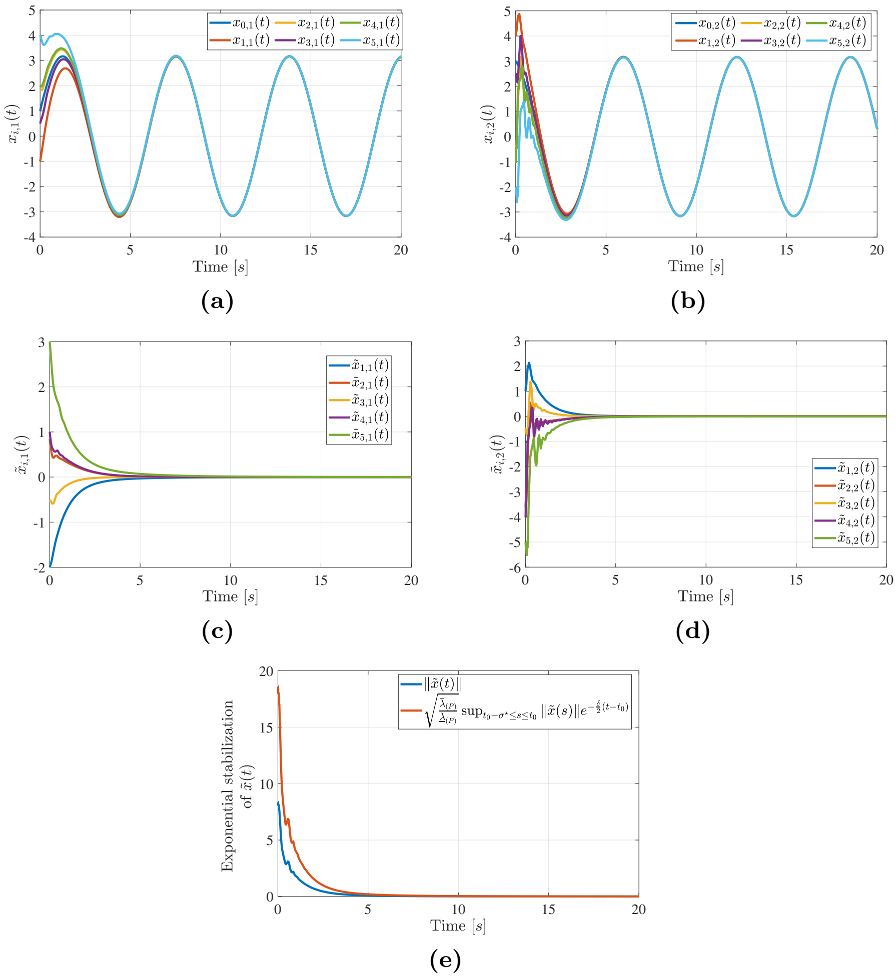

Figure 5.1. Leader-Following consensus problem for 5 linear oscillators. Time history of: a) first state variable $x_{i,1}(t)$, $i = 0, \ldots, 5$; b) second state variable $x_{i,2}(t)$, $i = 0, \ldots, 5$; c) synchronization error $\tilde{x}_{i,1}(t) = x_{i,1}(t) - x_{0,1}(t)$ $i = 1, \ldots, 5$; d) synchronization error $\tilde{x}_{i,2}(t) = x_{i,2}(t) - x_{0,2}(t)$ $i = 1, \ldots, 5$; e) Relation (5.30) with $\delta = 0.78 \in (0, \alpha)$.

The multiple time-varying delays, one for any link, have been emulated as random variables with uniform distribution within the range $[0, 0.1]$ $[s]$, whose maximum value $\sigma^\star = 0.1$ $[s]$, that is greater of the typical average end-to-end communication delay in wireless networks, which is of the order of hundredths of a second (i.e. 10^{-2} $[s]$) [117]. Moreover, the initial conditions, as well as the number of communication links, have been randomly chosen as in Table 5.1. Leader tracking performances have been evaluated leveraging the Matlab/Simulink simulation platform, while Yalmip Toolbox with SeDuMi solver [118] is exploited to solve the LMIs problem defined in Theorem 3. The distributed PI control gains in (5.4) are selected as $K_p = 15$ and $K_i = 5.5$. Since these control gains lead to $\beta = 0.1716$, it is possible to select $\alpha > \beta$ as $\alpha = 0.8$ in order to guarantee exponential stability of the closed-loop oscillator MAS system. These values ensure the fulfillment Theorem 3, thus implying that closed-loop MAS is exponentially stable with a decay rate $\delta \in (0, \alpha)$. Finally, the feasibility of Theorem 3 allows to find matrix P and, hence, it is possible to compute the ratio as $\sqrt{\frac{\bar{\lambda}_{(P)}}{\underline{\lambda}_{(P)}}} = 3.3165$ depending on its minimum and maximum eigenvalues.

Results in Figure 5.1 confirm the theoretical derivation highlighting that, under the proposed networked-based PI delayed control strategy (5.4), good leader-tracking performances are achieved. The time-history of the state variables is disclosed in Figure 5.1(a)-(b), while the one of synchronization errors is reported in Figure 5.1(c)-(d). In doing so, each oscillator exponentially converges towards the leader behavior despite the presence of multiple time-varying delays. Moreover, the exponential stability of the overall MAS is corroborated by Figure 5.1(e), where it is possible to observe the fulfillment of relation in (5.30) for the maximum admissible value of δ according to Lemma 6, i.e. $\delta = 0.78 \in (0, 0.8)$.

5.3 Finite-Time Voltage Control for stand-alone MGs with time-varying communication delays

The aim of this section is to handle the problem of voltage restoration arising at SC level in inverter-based stand-alone MG, i.e., to guarantee that all the DGs within the MG track the reference behaviour as imposed by the leader node, indexed with 0. Specifically, the objective is to design a finite-time control strategy meant to be distributed, i.e. it has to induce a common required behaviour for the overall network of DGs, that is also able to counteract time-varying communication latency arising from the information exchange. To deal with the above problem, the control objective is to design a distributed networked-based delayed strategy $u_i^V(t, \tau(t))$ such that:

- $\|v_i(t) - v_0(t)\| \to 0$ as $t \to T^f$, being v_i, v_0, T^f the voltage of i-th DG within the MG, the voltage set-point and desired settling time respectively;

- there exists constant $c_2 \in \mathbb{R}^+$ acting as a threshold for all voltage error trajectories with respect to the reference voltage set-point within each transient time interval $[t, t + T^f]$.

The voltage leader dynamic is given by the following differential equation:

$$\dot{x}_0(t) = Ax_0(t), \tag{5.31}$$

where $x_0(t) = \begin{bmatrix} v_0(t) & \dot{v}_0(t) \end{bmatrix} \in \mathbb{R}^2$ is the state vector of the leader.
Note that, for sake of brevity, throughout the chapter the dependence on $d - q$ reference frame of v_i^{od} in (3.9) will be omitted, i.e., $v_i^{od} = v_i$. Hence, to put the DG voltage dynamic into state-space form, it is possible to differentiate voltage dynamics in (3.9) as:

$$k_{v_i}\ddot{v}_i(t) + \dot{v}_i(t) - k_{Q_i}\dot{Q}_i^m(t) + u_i^V(t, \tau(t)) = 0, \tag{5.32}$$

being u_i^V the cooperative SC input for voltage regulation computed by leveraging the outdated information shared via communication links, described by $\mathscr{G}_{N+1}^c$, due to communication latency [119]. Indeed, in order to avoid instability phenomenon, it is necessary to consider communication time-delays $\tau(t)$ from the control design phase. Finally, equation (5.32) can be rewritten as

$$\dot{x}_i(t) = Ax_i(t) + B_i u_i^V(t, \tau(t)) + G_i w_i(t). \tag{5.33}$$

Note that, equation (5.33) is a delayed-input system, where $x_i(t) = [v_i(t)\ \dot{v}_i(t)]^\top$ is the state vector; $w_i(t) = [0,\ (-\dot{v}_i(t) - k_{Q_i}\dot{Q}_i^m(t))]^T$ is the time-varying disturbance vector that take into account the voltage deviation induced by droop-PC, while A, B_i, and G_i are

$$A = \begin{bmatrix} 0 & 1 \\ 0 & 0 \end{bmatrix}, \; B_i = G_i = \begin{bmatrix} 0 \\ \frac{1}{k_{v_i}} \end{bmatrix},$$

respectively. In addition, Assumption 2 and Remark 1 guarantee that

$$\exists \quad \Pi \in \mathbb{R}^+ : |w_i(t)| \leq \Pi, \tag{5.34}$$

which means that the disturbances are bounded. The achievement of the aforementioned control objectives is guaranteed under the following distributed delayed finite-time control strategy:

$$u_i^V(t, \tau(t)) = K \sum_{j \in \mathcal{N}_i^c} a_{ij}\big(x_i(t-\tau(t)) - x_j(t-\tau(t))\big), \tag{5.35}$$

where $K \in \mathbb{R}^{1\times 2}$ is the control gains vector to be proper tuned; coefficient a_{ij} models the communication network topology emerging from the presence/absence of a communication link between the DG i and DG j in the SC level (see Section 3.2); $\tau(t)$ is the communication time-varying latency which is detectable by timestamp. Note that, the presence of $\tau(t)$ over the network leads to the need of running the controller on the basis of outdated information as in (5.35). Moreover, for the sake of simplicity, in this section the dependence of $\tau(t)$ from the specific communication channel connecting the each pair of DGs is omitted. In addition, self and interagent delays are the same in (5.35), which does not compromise the *delay consensus margin* (see previous Remark 3 in Chapter 4).
We highlight that the proposed control protocol in (5.35) is homogeneous and continuous, thus allowing to prevent chattering phenomenon arising from discontinuous control law.

5.3.1 Finite-Time Voltage Recovery

In this section, stability conditions guaranteeing the robust finite-time voltage recovery in an islanded MG despite the presence of communication delays are provided. This conditions are expressed as a set of LMIs, whose solution allows finding the suitable control gains vector $K \in \mathbb{R}^{1\times 2}$ in (5.35).

To this aim, firstly the mathematical representation of the MG closed-loop system under the action of the distributed control (5.35) is derived. Hence, given the dynamics of DG i in (5.33) and the ones of the leading agent as in (5.31), the voltage error vector for each DG i with respect to the leader DG 0 can be defined as

$$e_i(t) = x_i(t) - x_0(t) \qquad \forall i \in \mathscr{V}^c_{N+1} - \{0\}.$$

According to the above definition and considering the control input u_i^V as in (5.35), it is possible to derive the closed-loop error dynamics for the i-th DG as

$$\dot{e}_i(t) = Ae_i(t) + B_iK \sum_{j \in \mathscr{N}_i^c} a_{ij}(e_i(t-\tau(t)) - e_j(t-\tau(t))) + G_i w_i(t). \quad (5.36)$$

Now, in order to describe the closed-loop network for the overall MG in a more compact form, by taking into account the communication topology, the following enlarged state and disturbances vectors are introduced as $\tilde{x}(t) = [e_1^\top(t), e_2^\top(t), \cdots, e_N^\top(t)]^\top \in \mathbb{R}^{2N\times 1}$ and $\bar{w}(t) = [w_1^\top(t), w_2^\top(t), \cdots, w_N^\top(t)] \in \mathbb{R}^{2N\times 1}$, respectively. Therefore, the delayed closed-loop system results as follows:

$$\dot{\tilde{x}}(t) = \bar{A}\tilde{x}(t) + A_\tau \tilde{x}(t-\tau(t)) + G\bar{w}(t), \quad (5.37)$$

where $\bar{A} = (I_N \otimes A)$; $A_\tau = \sum_i (\mathscr{H} \otimes B_iK)$; $G = \sum_i (I_N \otimes G_i)$, with the symbol $\otimes$ standing for the Kronecker product and $\mathscr{H} = \mathscr{L} + \mathscr{P}$, being $\mathscr{L}$ and $\mathscr{P}$ the Laplacian and Pinning matrices of the graph $\mathscr{G}^c_{N+1}$.
The following common assumption holds.

Assumption 5. *[97] The unknown homogeneous time-varying communication delay $\tau(t)$ is bounded, i.e. $\tau(t) \in [0, \tau^\star]$ and $\dot{\tau}(t) \in [0, \mu[$ with $\tau^\star$ and $\mu < 1 \in R^+$.*

Sufficient conditions guaranteeing the robust finite-time stability of the closed-loop dynamical system (5.37) are derived according to the following Theorem.

Theorem 4. *Consider the closed-loop MG network as in (5.37) and let Assumption 5 holds. Given positive scalars α, T^f, Π, c_1, $c_2 > c_1$ and* *positive matrix* $\Psi \in \mathbb{R}^{2N}$, *let free matrices* M, $T \in \mathbb{R}^{2N}$ *and free-invertible matrix* $F \in \mathbb{R}^{2N}$, *being* $F^{-1} = X$. *Assume there exist a positive constant* γ *and positive matrices* $P, Q, Z \in \mathbb{R}^{2N}$, $\bar{Q} = \Psi^{\frac{-1}{2}} Q \Psi^{\frac{-1}{2}}$ *and* $\bar{Z} = \Psi^{\frac{-1}{2}} Z \Psi^{\frac{-1}{2}}$ *such that:*

$$\begin{bmatrix} \Sigma_{11} & -M^\top + T & -A_\tau - M^\top & \bar{A}^\top & G \\ \star & -Q(1-\mu)e^{\alpha\tau^\star} - T^\top - T & -T & -A_\tau^\top & 0 \\ \star & \star & -Z & 0 & 0 \\ \star & \star & \star & \tau^{\star 2}P + X^\top + X & -G \\ \star & \star & \star & \star & \gamma I \end{bmatrix} < 0, \tag{5.38}$$

$$e^{\alpha T^f}\Big(1 + \lambda_{max}(\bar{Q})\tau^\star + \lambda_{max}(\bar{Z})\frac{{\tau^\star}^2}{2}\Big)c_1 + \gamma \Pi e^{\alpha T^f} < c_2, \tag{5.39}$$

being $\Sigma_{11} = (\bar{A}+A_\tau)+(\bar{A}+A_\tau)^\top + Q + M + M^\top - \alpha I$, $\lambda_{max}(\bar{Q})$ *and* $\lambda_{max}(\bar{Z})$ *the maximum eigenvalues of matrices* $\bar{Q}$ *and* $\bar{Z}$, *respectively. Then system* (5.37) *is robust finite-time stable with respect to* $(c_1, c_2, \tau^\star, T^f, \Psi, \Pi)$ *for all the disturbances satisfying* (5.34).

Proof. Consider the following Lyapunov-Krasovskii functional:

$$V(\tilde{x}(t)) = V_1(\tilde{x}(t)) + V_2(\tilde{x}(t)) + V_3(\tilde{x}(t)), \tag{5.40}$$

where

$$V_1(\tilde{x}(t)) = \tilde{x}^\top(t)\tilde{x}(t), \tag{5.41}$$

$$V_2(\tilde{x}(t)) = \int_{t-\tau(t)}^{t} \tilde{x}^\top(s) e^{\alpha(t-s)} Q \tilde{x}(s)\, ds, \tag{5.42}$$

$$V_3(\tilde{x}(t)) = \tau^\star \int_{-\tau^\star}^{0} \int_{t+\theta}^{t} \dot{\tilde{x}}^\top(s) e^{\alpha(t-s)} Z \dot{\tilde{x}}(s)\, ds\, d\theta, \tag{5.43}$$

being Q and Z symmetric and positive definite matrices.
Differentiating $V_1(\tilde{x}(t))$ in (5.41) along the trajectories of the closed-loop system (5.37), it yields:

$$\begin{aligned} \dot{V}_1(\tilde{x}(t)) &= \dot{\tilde{x}}^\top(t)\tilde{x}(t) + \tilde{x}(t)^\top \dot{\tilde{x}}(t) = 2\tilde{x}^\top(t)\dot{\tilde{x}}(t) \\ &= 2\tilde{x}^\top(t)\bar{A}\tilde{x}(t) + 2\tilde{x}^\top(t)A_\tau \tilde{x}(t-\tau(t)) + 2\tilde{x}^\top(t)G\bar{w}(t). \end{aligned} \tag{5.44}$$

By leveraging the Newton-Leibnitz formula (see Appendix A.13), i.e., $\tilde{x}(t-$

$\tau(t)) = \tilde{x}(t) - \int_{t-\tau(t)}^{t} \dot{\tilde{x}}(s)\, ds$ [97], the equality (5.44) can be rewritten as:

$$\dot{V}_1(\tilde{x}(t)) = \tilde{x}^\top(t)(\Phi + \Phi^\top)\tilde{x}(t) - 2\tilde{x}^\top A_\tau \int_{t-\tau(t)}^{t} \dot{\tilde{x}}(t)\, ds + 2\tilde{x}^\top(t)G\bar{w}(t), \tag{5.45}$$

being $\Phi = \bar{A} + A_\tau$.
Moreover, given Assumption 5, by differentiating $V_2(\tilde{x}(t))$ in (5.42) and $V_3(\tilde{x}(t))$ in (5.43) along the trajectories of (5.37), it yields:

$$\begin{aligned} \dot{V}_2(\tilde{x}(t)) \leq{}& \tilde{x}^\top(t)Q\tilde{x}(t) - \tilde{x}^\top(t-\tau(t))e^{\alpha\tau^\star}Q(1-\mu)\tilde{x}(t-\tau(t)) \\ &+ \alpha V_2(\tilde{x}(t)), \end{aligned} \tag{5.46}$$

$$\begin{aligned} \dot{V}_3(\tilde{x}(t)) &\leq \tau^{\star 2}\dot{\tilde{x}}^\top(t)Z\dot{\tilde{x}}(t) - \int_{t-\tau(t)}^{t} \dot{\tilde{x}}^\top(s)e^{\alpha(t-s)}Z\dot{\tilde{x}}(s)\, ds + \alpha V_3(\tilde{x}(t)) \\ &\leq \tau^{\star 2}\dot{\tilde{x}}^\top(t)Z\dot{\tilde{x}}(t) - \int_{t-\tau(t)}^{t} \dot{\tilde{x}}^\top(s)Z\dot{\tilde{x}}(s)\, ds + \alpha V_3(\tilde{x}(t)). \end{aligned} \tag{5.47}$$

By applying Jensen inequality [97] (refer to Lemma 4 in Appendix) on the integral term of inequality (5.47), it follows:

$$\begin{aligned} \dot{V}_3(\tilde{x}(t)) \leq{}& \alpha V_3(\tilde{x}(t)) + \tau^{2\star}\dot{\tilde{x}}(t)Z\dot{\tilde{x}}(t) \\ &- \left(\int_{t-\tau(t)}^{t} \dot{\tilde{x}}(s)\, ds\right)^\top Z\left(\int_{t-\tau(t)}^{t} \dot{\tilde{x}}(s)\, ds\right). \end{aligned} \tag{5.48}$$

Finally, summing up (5.45), (5.46) and (5.48), the following inequality is obtained:

$$\begin{aligned} \dot{V}(\tilde{x}(t)) \leq{}& \tilde{x}^\top(t)(\Phi + \Phi^\top)\tilde{x}(t) - 2\tilde{x}^\top A_\tau \int_{t-\tau(t)}^{t} \dot{\tilde{x}}(t)\, ds + 2\tilde{x}^\top(t)G\bar{w}(t) \\ &+ \tilde{x}^\top(t)Q\tilde{x}(t) - \tilde{x}^\top(t-\tau(t))e^{\alpha\tau^\star}Q(1-\mu)\tilde{x}(t-\tau(t)) + \alpha V_2(\tilde{x}(t)) \\ &+ \alpha V_3(\tilde{x}(t)) + \tau^{2\star}\dot{\tilde{x}}^\top(t)Z\dot{\tilde{x}}(t) \\ &- \left(\int_{t-\tau(t)}^{t} \dot{\tilde{x}}^\top(s)\, ds\right)^\top Z\left(\int_{t-\tau(t)}^{t} \dot{\tilde{x}}(s)\, ds\right). \end{aligned} \tag{5.49}$$

Now, Free Matrices method (see Section A.2.3) leads to

$$2\left(\tilde{x}^\top(t)M^\top + \tilde{x}^\top(t-\tau(t))T^\top\right)\times$$
$$\times\left[\tilde{x}(t) - \tilde{x}(t-\tau(t)) - \int_{t-\tau(t)}^{t} \dot{\tilde{x}}(s)\,ds\right] = 0 \tag{5.50}$$

and

$$2\dot{\tilde{x}}^\top(t)F^\top\left(\dot{\tilde{x}}(t) - \bar{A}\tilde{x}(t) - A_\tau\tilde{x}(t-\tau(t)) - G\bar{w}(t)\right) = 0, \tag{5.51}$$

being M, T and $F \in \mathbb{R}^{2N\times 2N}$ free matrices.
Summing the null terms (5.50) and (5.51) to the right-side of inequality (5.49), it follows:

$$\begin{aligned}
\dot{V}(\tilde{x}(t)) \leq{}& +\alpha V_2(\tilde{x}(t)) + \alpha V_3(\tilde{x}(t)) + \tilde{x}^\top(t)\left(\Phi + \Phi^\top + Q + M + M^\top\right)\tilde{x}(t)\\
&+ 2\tilde{x}^\top(t)\left(M^\top + T\right)\tilde{x}(t-\tau(t)) + 2\tilde{x}^\top(t)G\bar{w}(t)\\
&- 2\tilde{x}^\top(t)\left(A_\tau + M^\top\right)\int_{t-\tau(t)}^{t}\dot{\tilde{x}}(s)\,ds\\
&+ \tilde{x}^\top(t-\tau(t))\left(-Q(1-\mu)e^{\alpha\tau^\star} + T^\top + T\right)\tilde{x}(t-\tau(t))\\
&- 2\tilde{x}^\top(t-\tau(t))T^\top\int_{t-\tau(t)}^{t}\dot{\tilde{x}}(s)\,ds + \dot{\tilde{x}}^\top(t)\left(\tau^{2\star}Z + F^\top + F\right)\dot{\tilde{x}}(t)\\
&- 2\dot{\tilde{x}}^\top(t)F^\top\bar{A}\tilde{x}(t) - 2\dot{\tilde{x}}^\top(t)F^\top A_\tau\tilde{x}(t-\tau(t)) - 2\dot{\tilde{x}}^\top(t)F^\top G\bar{w}(t)\\
&- \left(\int_{t-\tau(t)}^{t}\dot{\tilde{x}}^\top(s)\,ds\right)^\top Z\left(\int_{t-\tau(t)}^{t}\dot{\tilde{x}}(s)\,ds\right)
\end{aligned} \tag{5.52}$$

Now, by defining the following enlarged state vector:

$$\eta(t) = \begin{bmatrix}\tilde{x}^\top(t) & \tilde{x}^\top(t-\tau(t)) & \int_{t-\tau(t)}^{t}\dot{\tilde{x}}(s)\,ds & \dot{\tilde{x}}^\top(t) & \bar{w}(t)\end{bmatrix}^\top \in \mathbb{R}^{\nu\times\nu}, \tag{5.53}$$

with $\nu = 5\cdot 2N$, the inequality (5.52) can be recast into a more compact form as

$$\dot{V}(\tilde{x}(t)) \leq \eta^\top(t)\Xi\eta(t) + \alpha V_2(\tilde{x}(t)) + \alpha V_3(\tilde{x}(t)), \tag{5.54}$$

where

$$\Xi = \begin{bmatrix} \Xi_{11} & \Xi_{12} & \Xi_{13} & \Xi_{14} & \Xi_{15} \\ \star & \Xi_{22} & \Xi_{23} & \Xi_{24} & \Xi_{25} \\ \star & \star & \Xi_{33} & \Xi_{34} & \Xi_{35} \\ \star & \star & \star & \Xi_{44} & \Xi_{45} \\ \star & \star & \star & \star & \Xi_{55} \end{bmatrix} \in \mathbb{R}^{\nu\times\nu}, \tag{5.55}$$

whose elements are defined as

$$\begin{aligned} &\Xi_{11} = \Phi + \Phi^\top + Q + M^\top + M, \quad \Xi_{12} = -M^\top + T, \\ &\Xi_{13} = -A_\tau - M^\top, \quad \Xi_{14} = \bar{A}^\top F, \quad \Xi_{15} = G, \\ &\Xi_{22} = -Q(1-\mu)e^{\alpha\tau^\star} - T^\top - T, \quad \Xi_{23} = -T^\top, \\ &\Xi_{24} = -A_\tau^\top F, \quad \Xi_{33} = -Z, \quad \Xi_{44} = \tau^{2\star}Z + F^\top + F, \\ &\Xi_{45} = -F^\top G, \quad \Xi_{25} = \Xi_{34} = \Xi_{35} = \Xi_{55} = 0_{2N\times 2N}. \end{aligned}$$

Summing and subtracting the terms $\alpha V(\tilde{x}(t))$ and $\gamma\bar{w}^\top(t)\bar{w}(t)$ to (5.54), after some algebraic manipulations, it results:

$$\dot{V}(\tilde{x}(t)) - \alpha V(\tilde{x}(t)) \leq \eta^\top(t)\Xi'\eta(t) + \gamma\bar{w}^\top(t)\bar{w}(t), \tag{5.56}$$

being Ξ' defined as

$$\begin{bmatrix} \Phi+\Phi^\top+Q+M^\top+M-\alpha I_{2N} & -M^\top+T & -A_\tau-M^\top & \bar{A}^\top F & G \\ \star & -Q(1-\mu)e^{\alpha\tau^\star}-T^\top-T & -T^\top & -A_\tau^\top F & 0_{2N\times 2N} \\ \star & \star & -Z & 0_{2N\times 2N} & 0_{2N\times 2N} \\ \star & \star & \star & \tau^{2\star}Z+F^\top+F & -F^\top G \\ \star & \star & \star & \star & -\gamma I_{2N} \end{bmatrix} \tag{5.57}$$

Choosing positive definitive matrices Q and $Z \in R^{2N}$, free matrices M, T, $F \in R^{2N\times 2N}$ and $\mathscr{L}_2$ gain γ such that $\Xi' < 0$ is fulfilled (with Ξ' defined in (5.57)), from (5.56) it follows:

$$\dot{V}(\tilde{x}(t)) - \alpha V(\tilde{x}(t)) \leq \gamma\bar{w}^\top(t)\bar{w}(t). \tag{5.58}$$

Then, for all $t \in [t_0, t_0 + T^f]$, being T^f the pre-fixed settling time, it holds:

$$
\begin{aligned}
V(\tilde{x}(t)) &\leq e^{\alpha t} V(\tilde{x}(0)) + \gamma \int_0^t \bar{w}^\top(s)\bar{w}(s)\, ds \\
&\leq e^{\alpha T^f} V(\tilde{x}(0)) + \gamma \int_0^{T^f} \bar{w}^\top(s)\bar{w}(s)\, ds. \qquad (5.59)
\end{aligned}
$$

Now, in order to evaluate $V(\tilde{x}(0))$, introduce the following relations:

$$
\bar{Q} = \Psi^{\frac{-1}{2}} Q \Psi^{\frac{-1}{2}}\ , \quad \bar{Z} = \Psi^{\frac{-1}{2}} Z \Psi^{\frac{-1}{2}},
$$

being $\Psi \in R^{2N}$ any positive matrix, i.e. $\Psi > 0$.
Given the above definitions, according to the choice of the Lyapunov-Krasovskii functional (5.40), $V(\tilde{x}(0))$ can be computed as

$$
\begin{aligned}
V(\tilde{x}(0)) &= \tilde{x}^\top(0)\tilde{x}(0) + \int_{-\tau(0)}^{0} \tilde{x}^\top(s) e^{-\alpha s} Q \tilde{x}(s)\, ds \\
&+ \tau^\star \int_{-\tau^\star}^{0} \int_{\theta}^{0} \dot{\tilde{x}}^\top(s) e^{-\alpha s} Z \dot{\tilde{x}}(s)\, ds\, d\theta \\
&\leq \{1 + \lambda_{max}(\bar{Q})\tau^\star + \frac{\tau^{\star 3}}{2}\lambda_{max}(\bar{Z})\} \times \\
&\sup_{-\tau^\star \leq t_0 \leq 0} \{\tilde{x}^\top(t_0)\Psi\tilde{x}(t_0);\ \dot{\tilde{x}}^\top(t_0)\Psi\dot{\tilde{x}}(t_0)\}. \qquad (5.60)
\end{aligned}
$$

Given (5.60) and the boundedness of the disturbance vector as in (5.34), inequality (5.59) finally becomes:

$$
V(\tilde{x}(t)) \leq e^{\alpha T^f}\Big(1 + \lambda_{max}(\bar{Q})\tau^\star + \lambda_{max}(\bar{Z})\frac{\tau^{\star 3}}{2}\Big)c_1 + \gamma \Pi e^{\alpha T^f}, \qquad (5.61)
$$

being Π the maximum value of $\bar{w}(t)$ for all the domains that include the MG operation point.
Furthermore, from (5.40)

$$
V(\tilde{x}(t)) \geq \tilde{x}^\top(t)\tilde{x}(t) \geq \lambda_{min}(I)\tilde{x}^\top(t)\Psi\tilde{x}(t) \qquad (5.62)
$$

holds. Finally, from (5.61) and (5.62) it follows:

$$\tilde{x}^\top(t)\Psi\tilde{x}(t) \leq e^{\alpha T^f}\Big(1+\lambda_{max}(\bar{Q})\tau^\star+\lambda_{max}(\bar{Z})\frac{\tau^{\star 3}}{2}\Big)c_1+\gamma\Pi e^{\alpha T^f} \leq c_2. \tag{5.63}$$

Therefore, if the inequality (5.57) and the LMIs (5.39) hold, the delayed closed-loop system (5.37) is robust finite-time stable according to Definition 7 (see Definition 7 in Appendix).
However, inequality (5.57) is not easy to solve since it is non-linear due to the presence of products between the matrix variable A_τ, depending on the control gains as in (5.35), and the other matrices variables. Hence, for effectively dealing with it, the congruence transformation LMIs property is employed to transform (5.57) into an equivalent LMIs by pre- and post-multiply it with the matrix $\Upsilon = diag\{I, I, I, X, I\}$ and its transpose [120]. In doing so, by defining $X = F^{-1}$ and $P = X^\top Z X$, after some algebraic manipulation, (5.57) is transformed into the LMIs (5.38) depending on the linear combination of the controller gains. This completes the proof. □

Remark 5. *The feasibility of the LMIs problem in* (5.38)-(5.39) *can be numerically verified by using, for example, the interior-point method [120] implemented in the Yalmip Toolbox with SeDuMi solver [118].*

Remark 6. *Since Finite-time control strategies can guarantee both a faster convergence than asymptotically ones and a best features in the presence of disturbances and uncertainties [121], it is particularly suitable adopt them in practical application like MGs control. Indeed, by reaching the voltage synchronization of all the DGs to the reference values in finite-time, the variable loads, which require nominal operating conditions, can be properly managed, thus allowing a proper disturbances rejection [84].*

Remark 7. *Feasible delay-dependent Matrix Inequalities in* (5.38) *and* (5.39) *are obtained through Theorem 4, which guarantee the robust finite-time voltage synchronization of the overall MG in (5.37). By fixing the maximum value $\tau^\star$ for the time delays, the value of c_1, Π (usually prescribed in technical literature [122]) and the couple (T^f, α), which force the overall performances of the entire MG in terms of settling time, thus conditioning state trajectories evolution and their threshold c_2, equalities* (5.38)

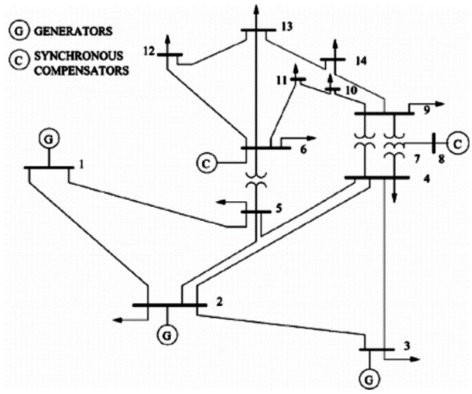

Figure 5.2. The IEEE 14-bus Test System

and (5.39) *can be seen as LMIs. In so doing, the feasibility of the LMIs allows tuning the robust controller gains so to guarantee the achievement of control objectives despite the presence of communication latency.*

Remark 8. *When solving the LMIs in* (5.38) *and* (5.39)*, the upper bound for communication delay* $\tau^\star$ *is set to be greater than the conventional threshold of the wireless communication network in normal operating conditions, e.g. based on the IEEE 802.11 protocol. Note that, hard delays, larger than the typical upper bound allowed by the wireless network, correspond to sudden packet losses. In doing so, the proposed procedure provides a meaningful robust stability margin with respect to the unavoidable latencies that can affect the networked cyber-physical system during some operative conditions [108].*

5.3.2 Performance Analysis

In this section the effectiveness of the control approach (5.35) is verified for the voltage regulation problem in the IEEE 14-bus test system depicted in Figure 5.2. The aim is to show how the proposed distributed finite-time control (5.35), despite the presence of communication time-varying delays, can ensure a desired voltage restoration by eliminating unavoidable deviations due to primary droop-control. The system operates in islanded mode and consists of $N = 5$ droop control DGs setting on buses $1, 2, 3, 6$

Table 5.2. DGs Locations, static droop coefficient and time constants of the LCL filters.

		DG1	DG2	DG3	DG4	DG5
DGs	Location	1	2	3	6	8
	τ_{P_i}	0.016	0.016	0.016	0.016	0.016
	τ_{Q_i}	0.016	0.016	0.016	0.016	0.016
	k_{P_i}	$3.01e^{-5}$	$7.14e^{-5}$	$1e^{-5}$	$1e^{-5}$	$1e^{-5}$
	k_{Q_i}	0.01	0.02	$2.5e^{-3}$	$4.17e^{-3}$	$4.17e^{-3}$
	k_{v_i}	$1e^{-2}$	$1e^{-2}$	$1e^{-2}$	$1e^{-2}$	$1e^{-2}$

Table 5.3. ZIP load model parameters.

Load Bus	$P_{1\rho}$	$P_{2\rho}$	$P_{3\rho}$	$Q_{1\rho}$	$Q_{2\rho}$	$Q_{3\rho}$
4	0.01	1	e^4	0.01	1	e^4
5	0.01	2	e^4	0.01	2	e^4
7	0.01	3	e^4	0.01	3	e^4
9	0.01	4	e^4	0.01	4	e^4
10	0.01	1	e^4	0.01	1	e^4
11	0.01	2	e^4	0.01	2	e^4
12	0.01	3	e^4	0.01	3	e^4
13	0.01	4	e^4	0.01	4	e^4
14	0.01	1	e^4	0.01	1	e^4

and 8, $M = 9$ ZIP-modeled local loads and twenty transmission lines (see the electrical power line topology in 5.2). Information about lines impedance and active and reactive power limits are provided according to [123], while the parameters of both droop-controlled DGs and ZIP local loads are chosen as in Table 5.2 and 5.3, respectively.

The DGs share information via the communication network topology $\mathscr{G}^c_{N+1}$ with $\mathscr{E}^c_{N+1} = \{(0,1),(1,2),(2,3),(3,2),(3,4),(4,5)\}$, where only DG1 has a direct access to virtual leader information. It is worth noting that this connected communication topology is just one among all the possible configuration that can be dealt with the proposed approach (similar results have been omitted here for the sake of brevity).
In the simulation scenario, the communication delay $\tau(t)$ has been simulated as a time-varying function with a maximum value of $\tau^\star = 0.1[s]$. Note that, by considering $\tau^\star = 0.1[s]$, it results an upper bound for the communication delays that is greater than the typical maximum value allowed for wireless channel in normal operating conditions (which is about $10^{-2}[s]$ [124]). In doing so, a meaningful margin of robust stability with

respect to hard delays, which correspond to sudden information packet losses, can be provided.
Moreover, to mimic a more realistic scenario, the secondary frequency controller u_i^ω

$$\begin{aligned} u_i^\omega &= \alpha_i(\hat{\omega}_i - \omega_i) \\ \dot{\hat{\omega}}_i &= \beta_i \sum_{j \in \mathcal{N}_i^c} (\omega_i - \omega_j) + g_i(\omega_i - \omega_0) + \varphi_i \sum_{j \in \mathcal{N}_i^c} (u_j^\omega - u_i^\omega) \end{aligned} \tag{5.64}$$

proposed in [13] is also included in the simulation platform, whose control gains are selected as $\alpha_i = 10.5, \beta_i = -0.3$, and $\gamma = 0.001$, while ω_0 is the frequency reference value to be reached.
Voltage regulation performances are evaluated leveraging the Matlab Simulink simulation platform, while the LMIs defined in Theorem 4 are numerically verified by using the interior-point method implemented in Yalmip Toolbox through the SeDuMi solver. The resulting control gains in (5.35), obtained by verifying the feasibility problem of LMIs (5.38)-(5.39), are $K = [-0.930 \;\; -0.726]$; instead, the weighted $\mathscr{L}_2$ gain and the threshold for state trajectories are $\gamma = 0.94237$ and $c_2 = 0.0459$, respectively.
Note that, as already stated, for solving the LMIs, a fixed value for $\tau^\star$, properly chosen according to technological constraints, is considered. However, this parameter plays an important role for the stability of the whole MG, as well as for solving the LMI problem (5.38)-(5.39). Therefore, before describing the simulation results, a sensitivity analysis of this parameter with respect to L_2 gain γ and state trajectories threshold c_2 is carried out in order to disclose the maximum upper bound of communication delays which guarantees that Theorem 4 still holds as well as the feasibility of LMI problem is confirmed. Specifically, this latter is verified for different value of $\tau^\star$, ranging from $0.1[s]$ to $0.9[s]$ with an iterative step of $0.1\ [s]$. By solving the LMIs problem for each of the selected value for $\tau^\star$, different values for the $\mathscr{L}_2$ gain γ and state trajectories bound c_2 are obtained as shown in Figure 5.3. This sensitivity analysis allows finding a stability margin with respect to the upper bound of the communication delay that can be useful if hard delays occur.
In order to disclose the strength and the robustness of the suggested finite-time control law in ensuring the achievement of voltage restoration to the

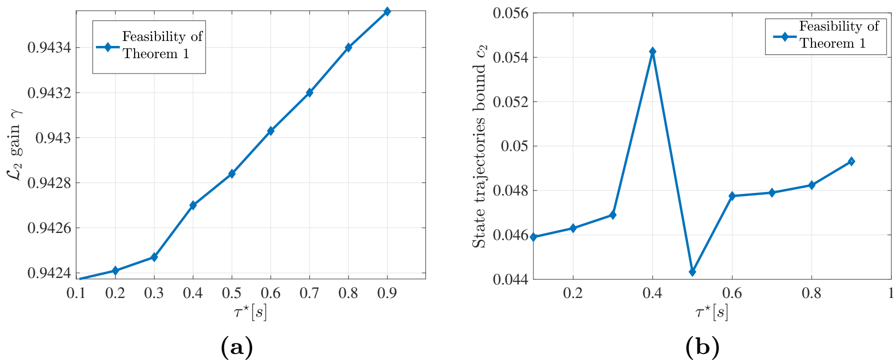

Figure 5.3. Feasibility of LMI (5.38) and (5.39) for different value of $\tau^\star \in [0.1; 0.9][s]$: a) Relation among $\tau^\star$ and L_2 gain γ; b) Relation among $\tau^\star$ and c_2.

set point despite the presence of both communication delays and frequency/voltage deviations, a time-interval of $60[s]$ is considered for simulation purpose. Specifically, three representative simulation scenarios are investigated, namely: *i*) *nominal scenario*, where only voltages reference variations occur; *ii*) *loads changing scenario*, where both voltages reference and loads variations occur; *iii*) *plug-and-play scenario*, where a more troublesome simulation scenario is emulated, where plug-and-play phenomena and load variations occur. Furthermore, the validation on the IEEE 30 bus test system is carried out to disclose the applicability of the proposed approach to larger power network, while a comparison analysis is also provided to show the benefit of the approach with respect to the very recent technical literature.

Nominal Scenario

In this nominal scenario, no loads variations are considered. Particularly, the use-case under test performs only voltage reference changes, i.e.: *i*) at $t = 0$ $[s]$ the frequency and voltage control are enabled with $\omega_0(t) = 1$ $[p.u.]$ and $v_0(t) = 1.02$ $[p.u.]$; *ii*) at $t = 10$ $[s]$ the set-point for the voltage secondary controller is set to $v_0(t) = 1.03$ $[p.u.]$; *iii*) at $t = 40$ $[s]$ the set-point restores to $v_0(t) = 1.02$ $[p.u.]$.

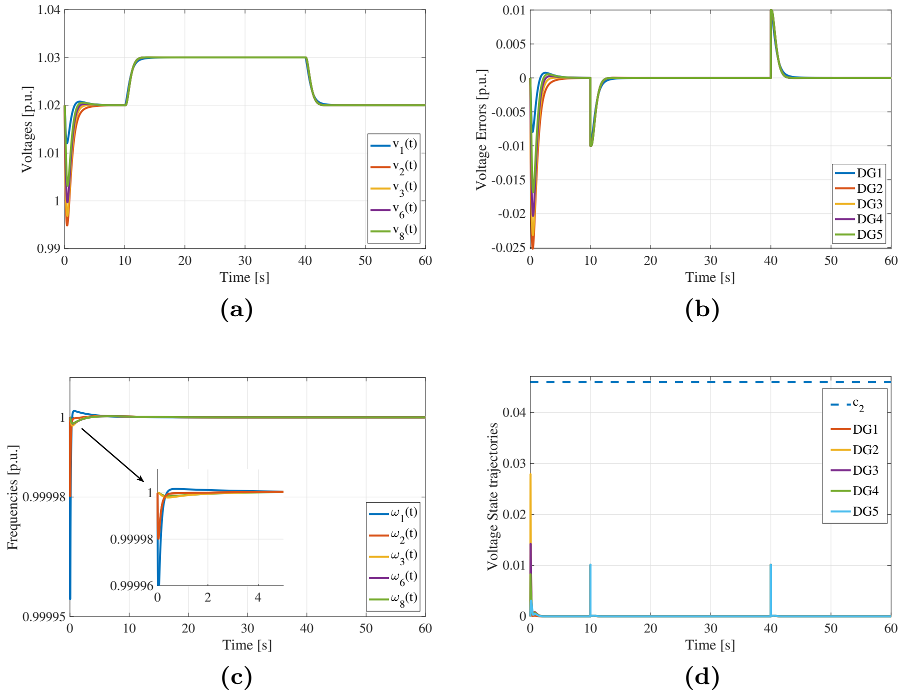

Figure 5.4. Distributed Finite-Time Voltage Restoration Control in the *nominal scenario*. Time history of: a) voltage $v_i(t), i = 1, \dots, 5$; b) voltage error $v_i(t) - v_0(t), i = 1, \dots, 5$; c) frequency $\omega_i(t), i = 1, \dots, 5$; d) Voltage state trajectories $\tilde{x}^\top(t)\Psi\tilde{x}(t)$.

The effectiveness of the proposed finite-time control strategy is confirmed by the results in Figure 5.4, where it is possible to appreciate the voltage synchronization process in spite of the effects of time-varying latency, the unavoidable fluctuation due to PC and the reference changes. Specifically, by activating controller (5.35) at $t = 0$ $[s]$, all the DGs voltages achieve the set-point in $T^f = 6$ $[s]$ as shown in Figure 5.4(a), thus allowing the voltage errors fast approaching to zero value (see Figure 5.4(b)). For completeness, Figure 5.4(c) reports the frequency evolution of all the DGs under the action of (5.64). Finally, state trajectories evolution are disclosed in Figure 5.4(d), thus confirming the boundedness of the whole MG with re-

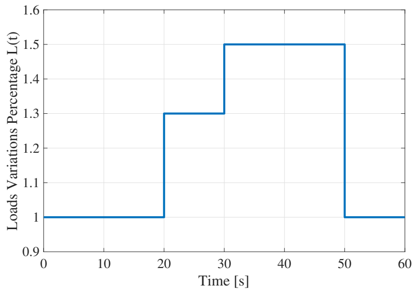

Figure 5.5. Distributed Finite-Time Voltage Restoration Control in the *load changing scenario*. Time history of the loads percentage variation with respect to the nominal values.

spect to the threshold c_2, properly computed by solving LMIs (5.39), i.e. $\tilde{x}^\top(t)\Psi\tilde{x}(t) < c_2 \quad \forall t \in [t_0, t_0 + T^f]$, being t_0 the time instant when the set-points change.

Load Changing Scenario

Since load demand is subjected to frequent changes according to specific and practical requirements, the evaluation of the robustness with respect to load variations is a crucial aspect to be investigated for assessing the performance of the controlled grid, besides the previous one. In particular, a variable load profile $L(t)$ as depicted in Figure 5.5 is considered, where a maximum load variation of $\pm$ 50% can be observed. Specifically, the following scenario is taken into account:

- At $t = 0$ $[s]$, the frequency and voltage controller are switched on, with $\omega_0 = 1$ $[p.u.]$ and $v_0 = 1.02$ $[p.u.]$;
- At $t = 10$ $[s]$, the set-point for voltage control varies to $v_0(t) = 1.03$ $[p.u.]$;
- At $t = 20$ $[s]$, there is a 30% of increasing for the nominal values of the loads;
- At $t = 30$ $[s]$, loads increase of an additional 20%;

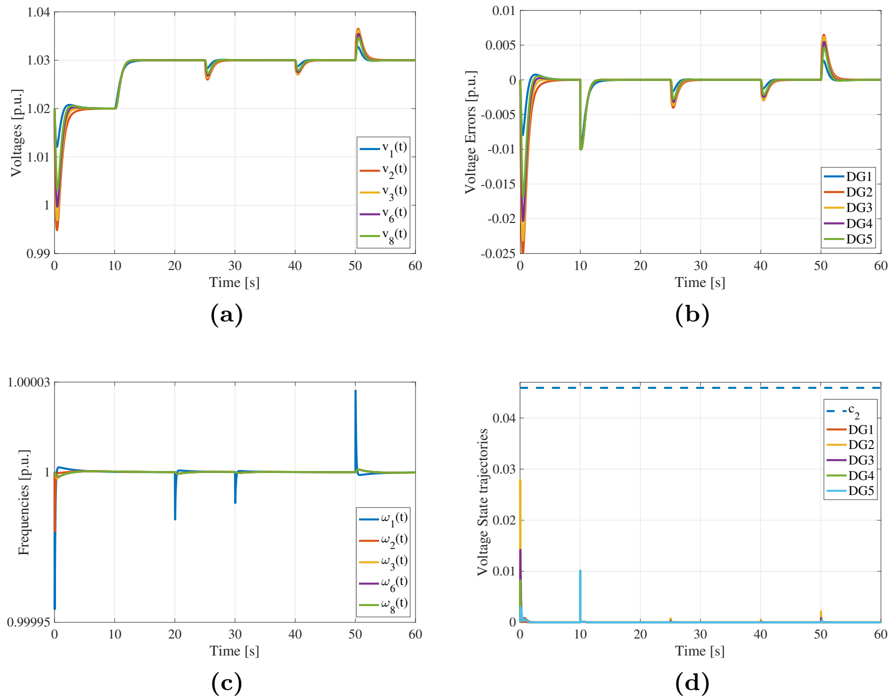

Figure 5.6. Distributed Finite-Time Voltage Restoration Control in the *load changing scenario*. Time history of: a) voltage $v_i(t), i = 1, \dots, 5$; b) voltage error $v_i(t) - v_0(t), i = 1, \dots, 5$; c) frequency $\omega_i(t), i = 1, \dots, 5$; d) Voltage state trajectories $\tilde{x}^\top(t)\Psi\tilde{x}(t)$.

- At $t = 40$ $[s]$ the voltages reference value is restored to $v_0(t) = 1.02$ $[p.u.]$;
- At $t = 50$ $[s]$, loads are restored to their nominal value.

Results in Figure 5.6 show that the proposed approach is able to counteract the sudden variation in the load request, recovering the desired voltage intensity. Moreover, the robustness and the effectiveness of the suggested finite-time distributed controller are confirmed in Figure 5.6 even in this troubled scenario characterized of sudden load changes. Specifically, as the SC is switched on at $t = 0$ $[s]$, the voltages of all DGs restore to the set-point in $T^f = 6$ $[s]$ as shown Figure 5.6(a) and the voltage errors with respect to the references go to zero (see Figure 5.6(b)). Load variation and voltage references changes are performed at the next step of the simulation and the same good performance are achieved in this scenario as well. Indeed, also in this case, the proposed controller allows adjusting the voltages of all the DGs to the desired reference value with the same settling time $T^f = 6$ $[s]$. Tolerable errors can be seen in the voltage time evolution in Figure 5.6(a)-(b) in concurrence of load fluctuations. Figure 5.6(c) points out the time evolution of the DGs frequency with controller in (5.64) switched on. Furthermore, according to Definition 7, Figure 5.6(d) proves the boundedness of the overall state trajectories, i.e. $\tilde{x}^\top(t)\Psi\tilde{x}(t) < c_2 \quad \forall t \in [t_0, t_0 + T^f]$, where t_0 is the time instant when sudden changes in loads and references appear.

Plug-and-Play Scenario

Here the robustness of the proposed control approach is discussed in the more troublesome simulation scenario, where plug-and-play phenomena along with load variations, as in in Figure 5.5, occur. Specifically, DG2 at bus 2 and DG4 at bus 6 are unplugged at $t = 25$ $[s]$ and $t = 50$ $[s]$ respectively, and then plugged-in at $t = 32$ $[s]$ and $t = 52$ $[s]$, respectively. Note that these sources failure also implies communication losses for the links connected to the unplugged DGs [125]. Simulation results, depicted in Figure 5.7, confirm the effectiveness of the proposed control approach in ensuring finite-time voltage control also in this troublesome electrical scenario. Specifically, Figure 5.7(a) shows that voltage controllers successfully face to DGs losses by sharing the excess power among the remaining DG units (see Figure 5.7(b)). Finally as highlighted in Figure 5.7(c), the boundedness of the overall state-trajectories is still guaranteed.

Validation on a larger system: the case of IEEE 30 bus test system

Here the applicability of the proposed control approach also in larger system, with more interconnected DGs sharing information via a communication network affected by time-varying communication delays, is highlighted. Specifically, the IEEE 30-bus system operating in stand-alone

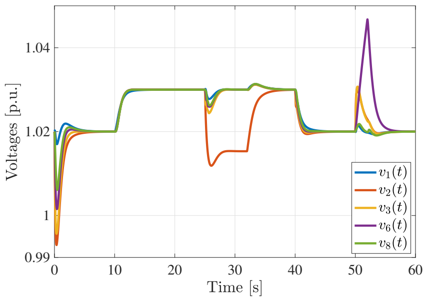

(a)

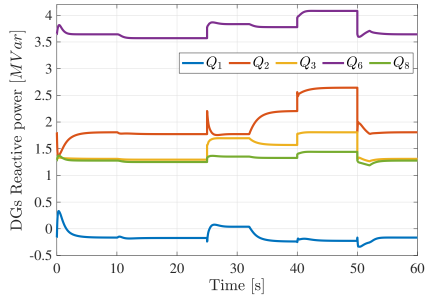

(b)

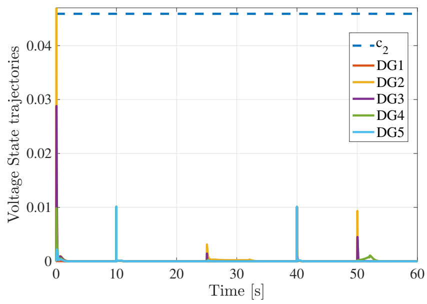

(c)

Figure 5.7. Plug-and-Play scenario for DG2 and DG4 in *load changing scenario*. Time history of: a) voltage $v_i(t), i = 1, \dots, 5$; b) supplied reactive power $Q_i(t), i = 1, \dots, 5$; c) Voltage state trajectories $\tilde{x}^\top(t)\Psi\tilde{x}(t)$.

mode is considered, which consists of $N = 7$ droop control DGs, set on buses $1, 2, 3, 6, 8, 10$ and 13, $M = 23$ ZIP local loads and 41 transmission lines. Parameters of the electrical grid are given in [123]. As exemplar simulation scenario we consider the *nominal scenario* as described above. Results in Figure 5.8 disclose that, also for larger power networks, the proposed control protocol (5.35) is able to ensure the robust finite-time voltage regulation problem despite the presence of communication time-varying delays. Indeed, all the DGs track the reference behaviour (see Figure 5.8(a)-(b)), while counteracting the effects of communication latency as well as the natural deviation due to underlying control layer. Finally,

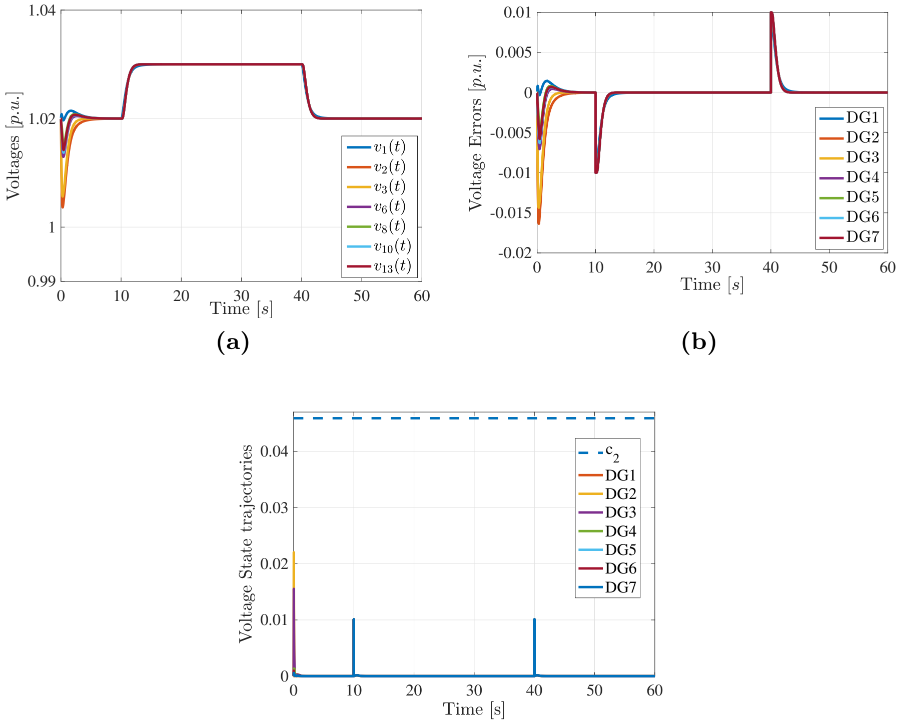

(c)

Figure 5.8. Distributed Finite-Time Voltage Restoration Control in the *nominal scenario* for IEEE 30 bus Test System. Time history of: a) voltage $v_i(t), i = 1, \dots, 7$; b) voltage errors $v_i(t) - v_0(t), i = 1, \dots, 7$; c) Voltage state trajectories $\tilde{x}^\top(t)\Psi\tilde{x}(t)$.

the boundedness of the state trajectories evolution is still guaranteed as shown in Figure 5.8(c), thus confirming that $\tilde{x}^\top \Psi \tilde{x} < c_2 \forall t \in [t_0, t_0 + T^f]$, being t_0 the time instant when reference variations occur. The obtained results confirm how the proposed approach successes in guaranteeing the control objectives also for larger test-bus power network.

Comparison Analysis

To further disclose the benefit of the proposed finite-time networked-based delayed control input in guaranteeing voltage regulation in MG, herein the resulting performances are compared with the ones achievable via the nonlinear distributed voltage controller, very recently proposed in [10], which neglects the unavoidable presence of communication impairments. For the comparison analysis, the *nominal scenario* as detailed above is considered. The performances achievable with the nonlinear controller [10] are disclosed in Figure 5.9, which highlights how time-varying delays dramatically affect the MG stability. By observing both Figure 5.4 and Figure 5.9, it is possible to appreciate how the proposed control approach allows achieving improved performances in terms voltage regulation, while counteracting time-varying communication delays as well as voltage deviations due to PC layer and references variations. This benefit straightly comes from the fact that the communication delays are taken into account from the beginning of the control design phase.

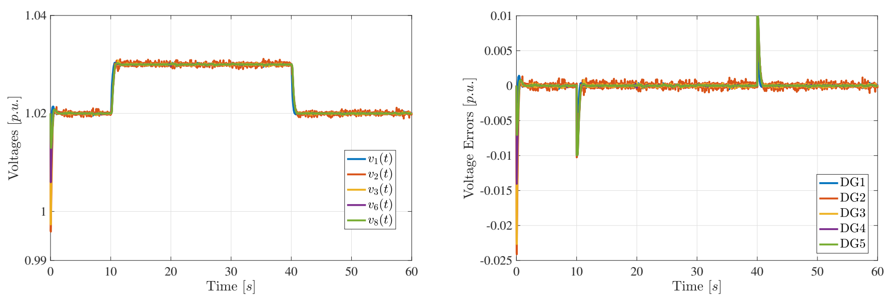

(a) **(b)**

Figure 5.9. Comparison with nonlinear controller proposed in [10] for the *nominal scenario*. Time history of: a) voltage $v_i(t), i = 1, \dots, 5$; b) voltage errors $v_i(t) - v_0(t), i = 1, \dots, 5$.

5.4 Concluding Remarks

This chapter has investigated the effect of time-varying communication delays in MASs and, in particular, in MG application. Firstly, a novel networked-based PI control strategy is introduced to solve the leader tracking problem for high-order LTI MASs with heterogeneous time-varying delays depending on the specific communication channel connecting a pair

of agents. Exponential stability conditions are derived by exploiting both Lyapunov-Krasovskii theory and Halanay Lemma, thus guaranteeing that each agent exponentially tracks the leader behavior while coping with heterogeneous time-varying delays. The effectiveness of the approach is validated for the application of linear oscillator networks. Exemplary numerical simulations corroborate the theoretical derivation.
Then, MASs modeling paradigm is exploited to address the secondary voltage control in stand-alone inverter-based MG in the presence of communication latencies. The problem is solved via a fully distributed finite-time voltage control strategy able to guarantee that all DGs voltages track the reference value in a finite-time interval despite model mismatches, load fluctuation and natural deviation induced by droop-based PC. Exploiting Lyapunov-Krasosovskii theory combined with Finite-Time Stability tools, the effectiveness and the robustness of the proposed control law are analytically proven, thus resulting in delay-dependent stability criteria expressed as a set of LMIs allowing the tuning of the control gains. An extensive numerical simulation, carried out on a realistic case study using the popular benchmark of the IEEE 14 bus test system, is performed. Numerical results have revealed the robustness and the effectiveness of the proposed control architecture in guaranteeing that all the DGs involved in the MG track the reference leader behaviour with specified transient and steady-state performances, in spite of communication time-varying latencies, as well as natural voltage fluctuations induced by the PC layer.

Chapter 6

Resilience with respect to unknown and unbounded uncertainties

As modern DGs always involve heterogeneous and unknown disturbances/model mismatches, a lack of accurate knowledge about the entire MG dynamics arises. Hence, an appropriate SC strategy is helpful to improve the voltage regulation process in an uncertain and unknown environment. To this aim, this chapter focuses on designing a novel distributed adaptive PID-like controller able to counteract unknown uncertainties arising from external disturbances and parameter mismatches, as well as unavoidable deviations induced by primary droop control, while recovering desired voltage reference value. By leveraging Lyapunov theory, an adaptive mechanism is provided to adjust control parameters for dealing with different operating conditions. The stability of the entire MG, analytically derived by also exploiting the Barbalat lemma, proves that all DGs within the electrical grid track the reference signal despite the presence of unknown uncertainties, with bounded adaptive control gains in steady-state phases. A detailed simulation analysis confirms the theoretical derivation and the effectiveness of the proposed controller in ensuring the voltage restoration in different troublesome scenarios, where both reference/loads variations and plug-and-play phenomena occur.

6.1 Need for Robust Secondary Voltage Control

Modern power systems are increasingly moved towards MG-based distribution network framework in order to improve system resilience with respect to troublesome operating situations, e.g. downstream of natural disasters, physical and cyber attacks [126]. Moreover, MG solution allows also facing with both environmental issues and huge costs of development of traditional power systems via the extensive integration of RESs, such as solar and wind, thus generating more and green electricity [127]. The main benefits of the usage of RESs rely in: *i*) reducing carbon dioxide (CO_2) generation from power generation units, *ii*) reducing power losses and voltage drop, *iii*) delivering power to the new load centers that are geographically located far from power grids. However, the investment and maintenance costs of such energy sources are high [128]. Besides, the uncertainty of RESs and the nonlinear nature of generation facilities impose unprecedented changes on improving the control performance [127]. Indeed, a MG with its control mechanism is a nonlinear system and it is always prone to disturbances and matched/unmatched uncertainties. Matched uncertainties are logged through the input channels, while unmatched uncertainties are those that act through channels other than control inputs [11]. Load changes, DGs tripping, unmodeled dynamics, noises, communication delays, and network and PC parameters variations are some examples of uncertainties, which may affect the MG control system performance, even bringing to instability phenomena [11, 129]. Therefore, distributed SC of dispersed DGs into the MG is a tricky problem and it could be desirable to design and implement efficient and proper control techniques able to compensate for the adverse effects of disturbances/uncertainties. Robust control theory is the best solutions to overcome uncertainty, disturbance, and the nonlinear nature of RESs [127]. Different attempts are made towards the design of secondary robust controllers and implementation of various robust control algorithms.
For instance, a Distributed Sliding Mode Controller (DSMC) is introduced in [10] in order to achieve voltage regulation and satisfy power sharing requirements, while robustness with respect to randomness and uncertainty of DGs and loads has been proved via phase trajectory method. Again, [130] combines an extended state Kalman-Bucy filter to estimate the DGs state information in the presence of parameters perturbations and mea-

surement noises, with a Sliding Mode Controller (SMC) able to maintain the system stability and improve SC performances. To overcome chattering phenomena that may arise when SMC solutions are adopted, [131] introduces a RBF Neural Network (NN) to adjust switching gain of the sliding mode control in real time, while restoring MG voltage values. Moreover, an active disturbance rejection control technique has been suggested in [132] in order to enhance robustness against unmodeled dynamics, model uncertainties and external disturbance, while the problem of finite-time stabilization of MG voltages has been addressed and solved in [42, 133]. By leveraging backstepping technique and NonZero-Sum (NZS) differential game strategy, [134] has tackled the problem of voltage recovery of islanded MG, where the model identifier has been established to reconstruct the unknown NZS games systems based on a three-layer NN.

From the control point of view, steady-state and transient performances can be highly improved by using PID controller, which allows considering at the same time both past and future information together with the present ones [135]. Versatility and ease of implementation are the main features of PID-like control and its variations, which enable the usage of this kind of controllers in different application fields (see [93, 136] and references therein). For the specific MG application, PI/PID approaches have been widely used in the SC [35], since they can not only remove voltage deviations induced by the PC layer, but also provide fast response to the transient change [14, 137]. For instance, a fully distributed robust delayed sampled-data PID controller has been used in [14] to solve voltage regulation control problem by exploiting artificial delays approach and finite difference approximation. Again, the problem of designing a robust centralized PID protocol for grid voltage control of an islanded MG has been addressed and solved in [138] by comparing four different methods, hence providing an optimal selection of central PID controller parameters.

As the conventional SC is based on PI/PID controllers with fixed parameters, this kind of control strategies result in poor performance against uncertianties, model inaccuracies and sudden load variations. To improve MG performance with respect to its frequently changing behavior, while taking into account different kind of DGs, adaptive and intelligent PI/PID controllers with dynamically updated coefficients are needed [139]. Along this line, an adaptive PI control approach has been proposed in [139] where

an adaptive neuro-fuzzy interface system is designed to adapt the PI coefficients at MG operating conditions. Conversely, the nonlinear constrained minimization method has been exploited in [140] in order to design decentralized voltage PI controllers aiming at regulating the voltage amplitude of the grid nodes to which DGs are connected. Herein, the nonlinear problem has been formulated in the frequency domain, with the purpose of finding proportional and integral control gains; however, the accurate choice of a proper cost function on the basis of the electrical grid operating conditions is required. A robust model reference adaptive PID controller is suggested in [141] to obtain desired voltage performance in the presence of unknown parameters. However, herein, the reference model has to be chosen such that it matches with the nominal plant model, which could be a hard task due to unavailability of accurate MG information. Hence, the technical literature overview highlights that most of adaptive mechanisms are based on ANN [33], backstepping [34, 142] and Fuzzy technique [35]. However, these latter methods result in high computational complexity, which make difficult their implementation in real-time applications [143].
Given the above considerations, by taking advantages of the PID-like control strategies, this chapter is devoted to the design of a novel distributed PID controller endowed with self-tuning adaptive mechanisms able to restore the voltage synchronization for all the current MG operating conditions. Most notably, unlike existing distributed adaptive protocols for the voltage recovery problem, the design is performed in a fully distributed fashion, i.e. without requiring any knowledge about global information, such as the communication graph topology, system dynamics and/or bound of external disturbances. Specifically, by exploiting the solely information flow in the communication network from NCS perspective, the updating control laws are derived via Lyapunov theory along with the Barbalat lemma, thus coping with variable loads, completely-unknown external disturbances and unmodeled dynamics. In doing so, the asymptotic MG voltage synchronization is achieved in different highly varying operating conditions, as well as the boundedness of the adaptive signals is guaranteed with a reduction of computational burden and communication channel bandwidth. Motivations and contributions of the chapter can be highlighted as follows:

- to solve the voltage recovery problem in inverter-based islanded MG, a fully-distributed adaptive PID-like controller is designed, which, leveraging self-adaptive mechanisms, does not require any information/assumption about DGs model uncertainties and external disturbances, arising from the different operating conditions in which DGs are involved. Indeed, in order to provide to the electrical grid anti-disturbance capability, uncertainties and external disturbance are not assumed to be known and bounded as in [130, 133, 33, 11];

- the proposed distributed controller embeds additional distributed adaptive integral and derivative actions which allow ensuring better performances both in steady-state and transient phases in terms of maximum voltage deviation percentage, differently from e.g. [11];

- the distributed adaptive mechanisms, required to handle all MG unavoidable uncertainties, are able to overcome the control gains tuning issue, crucial in PI/PID/Proportional-Derivative (PD)-based strategies; moreover, differently from alternative adaptive methods based on ANN [33], backstepping [34], fuzzy technique [35], the ones proposed through this chapter involve a reduced computational burden and network communication resources savings, according to the metric in [37], thus being more performing from an implementation perspective;

- differently from [33, 34, 35], which ensure the solely UUB stability for the voltage error trajectories, the proposed control strategy is able to ensure the asymptotic stability of these tracking errors, while guaranteeing the boundedness property for all the involved signals to be adapted.

6.2 Cooperative Robust Voltage Control Problem

In this section, the problem of voltage restoration arising at the SC level in inverter-based islanded MG is addressed. The control objective is to achieve the voltage synchronization of all the DGs to the reference behavior imposed by the leader node (labeled with 0), despite the lack of accurate knowledge of MG information, such as network topology, sudden load variations, external and unknown disturbances and uncertain dynamics. To pursue this scope, a novel distributed cooperative PID control is presented, which, exploiting the networked shared information, is able to counteract all the external disturbances and parameter mismatches thanks to a suitable adaptive mechanism for the proportional, integral and derivative control gains. The advantages of the proposed approach rely on: *i*) the improvement of the closed-loop performances, due to the additional integral and derivative actions for the steady-state and the transient phases, respectively; *ii*) the capability in dealing with all unavoidable unknown uncertainties affecting the DGs network.

Hence, from the control point of view, given voltage dynamics

$$k_{vi}\dot{v}_i = v^{nom} - v_i - k_{Qi}Q_i^m + u_i^v, \qquad i = 1, 2, \cdots N, \tag{6.1}$$

the aim is to design a networked-based control strategy $u_i^v(t)$ in (6.1) such that:

$$\|v_i(t) - v_0(t)\| \to 0, \qquad i = 1, \ldots, N, \tag{6.2}$$

where $v_i(t)$ is the voltage of the i-th DG within the MG, while $v_0(t)$ is the desired voltage set-point imposed by the leader DG0.

To deal with this problem, let us introducing the state vector for the leader node $x_0(t) = [x_{0,1}(t),\ x_{0,2}(t)]^\top = [v_0(t),\ \dot{v}_0(t)]^\top \in \mathbb{R}^{2\times 1}$. Hence, the voltage leader dynamics can be expressed by the following differential equations:

$$\dot{x}_{0,1}(t) = x_{0,2}(t), \quad \dot{x}_{0,2}(t) = 0. \tag{6.3}$$

Then, the i-th DG voltage dynamics can be obtained by differentiating (6.1), $\forall i = 1, \cdots, N$, i.e.:

$$\ddot{v}_i(t) = -\frac{1}{k_{vi}}\dot{v}_i(t) - \frac{k_{Qi}}{k_{vi}}\dot{Q}_i^m(t) + \frac{1}{k_{vi}}u_i^v(t), \tag{6.4}$$

where $u_i^v(t)$ is the distributed SC input for voltage regulation to be computed by leveraging the networked information, exchanged through the communication links according to the topology described by $\mathscr{G}_{N+1}^c$.

Now, by defining the i-th DG state vector and its disturbance as

$$x_i(t) = [x_{i,1}(t),\ x_{i,2}(t)]^\top = [v_i(t),\ \dot{v}_i(t)]^\top \in \mathbb{R}^{2\times 1},$$

$$d_i(t) = (-\dot{v}_i(t) - k_{Qi}\dot{Q}_i^m(t)),$$

it is possible deriving the following state-space form for (6.4):

$$\begin{aligned} \dot{x}_{i,1}(t) &= x_{i,2}(t), \\ \dot{x}_{i,2}(t) &= \frac{1}{k_{vi}}u_i^v(t) + \frac{1}{k_{vi}}d_i(t). \end{aligned} \tag{6.5}$$

To recast the voltage restoration control problem (6.2) as a consensus leader-tracking one, for each DG i within the MG, it is possible to define the following state error with respect to the leading DG0:

$$e_i(t) = \begin{bmatrix} e_{i,1}(t) \\ e_{i,2}(t) \end{bmatrix} = \begin{bmatrix} x_{i,1}(t) - x_{0,1}(t) \\ x_{i,2}(t) - x_{0,2}(t) \end{bmatrix} = x_i(t) - x_0(t). \tag{6.6}$$

Given (6.3)-(6.5), the dynamics of $e_i(t)$, $\forall i$, can be derived as:

$$\begin{aligned} \dot{e}_{i,1}(t) &= e_{i,2}(t), \\ \dot{e}_{i,2}(t) &= \frac{1}{k_{vi}}u_i^v(t) + \frac{1}{k_{vi}}d_i(t). \end{aligned} \tag{6.7}$$

Moreover, to handle voltage leader tracking consensus problem, introduce the following synchronization signal for the i-th DG ($i = 1, \cdots, N$):

$$\eta_i(t) = \sum_{j=1}^{N} a_{ij}(x_i(t) - x_j(t)) + a_{i0}(x_i(t) - x_0(t)) \in \mathbb{R}^{2\times 1}, \tag{6.8}$$

where a_{ij} is the element of the adjacency matrix $\mathscr{A}_N^c$ associated to communication network topology in the cyber-space; a_{i0} stands for the i-th element of the pinning matrix $\mathscr{P}$ and models the interactions among follower DGs and the virtual DG0 (see Section 3.2). According to (6.6), it is possible to rewrite the synchronization signal for the i-th DG in (6.8) as

$$\eta_i(t) = \sum_{j=1}^{N} a_{ij}(e_i(t) - e_j(t)) + a_{i0}e_i(t) = c_i e_i(t) - \sum_{j=1}^{N} a_{ij}e_j(t), \tag{6.9}$$

where $c_i = \sum_{j=1}^{N} a_{ij} + a_{i0}$.
The following common assumption holds.

Assumption 6. *The communication graph $\mathscr{G}^c_{N+1}$ contains a directed spanning tree rooted at the leader node. Therefore, each node receives the leader information, directly or indirectly.*

Remark 9. *Assumption 6 ensures the positiveness of parameter c_i for all the time interval, i.e. $c_i \in \mathbb{R}_+$, $\forall i$, $\forall t$. This implies that there is no time instant such that the DG i can be isolated.*

Synchronization signal in (6.9) can be written in explicit vector form as

$$\eta_i(t) = \begin{bmatrix} \eta_{i,1}(t) \\ \eta_{i,2}(t) \end{bmatrix} = c_i \begin{bmatrix} e_{i,1}(t) \\ e_{i,2}(t) \end{bmatrix} - \begin{bmatrix} \sum_{j=1}^{N} a_{ij} e_{j,1}(t) \\ \sum_{j=1}^{N} a_{ij} e_{j,2}(t) \end{bmatrix}. \tag{6.10}$$

Given error dynamics in (6.7), by differentiating (6.10), the following dynamics for the synchronization signal can be derived:

$$\begin{aligned} \dot{\eta}_{i,1}(t) &= \eta_{i,2}(t), \\ \dot{\eta}_{i,2}(t) &= \frac{c_i}{k_{vi}}(u_i^v(t) + d_i(t) - \frac{k_{vi}}{c_i} \sum_{j=1}^{N} a_{ij} \dot{e}_{j,2}(t)) = \frac{c_i}{k_{vi}}(u_i^v(t) + w_i(t)), \end{aligned} \tag{6.11}$$

where $w_i(t) = d_i(t) - \frac{k_{vi}}{c_i} \sum_{j=1}^{N} a_{ij} \dot{e}_{j,2}(t)$.

Remark 10. *The variable $w_i(t)$ in (6.11) embeds any kind of unknown model mismatches and external disturbances acting on the i-th DG. Specifically, it accounts for the uncertain and nonlinear terms due to all the related complex phenomena, such as topological changes, unbalanced and nonlinear loads, high-frequency pulse-width voltage modulation and transition between modes of operation (more details about this topic can be found in [32, 8]).*

Finally, the dynamics of the synchronization signal in (6.11) can be written in the state-space form as follows:

$$\dot{\eta}_i(t) = A\eta_i(t) + B_i(u_i^v(t) + w_i(t)), \tag{6.12}$$

with $A = [0 \;\; 1; 0 \;\; 0]$, $\quad B_i = [0 \;\; \frac{c_i}{k_{vi}}]^\top$.

Remark 11. *For each DG i, since $c_i \in \mathbb{R}_+$ and $k_{vi} \in \mathbb{R}_+$, the couple (A, B_i) is controllable.*

6.3 Distributed Robust Adaptive PID-like Control

To solve voltage regulation problem in (6.2) despite the presence of unknown uncertainties and external disturbances acting on each DG i within the network, the idea is to design a cooperative and adaptive PID-like controller, whose action is able to emulate an ideal controller acting in the case of fully known agents conditions.
Specifically, from (6.12), when all the disturbances and mismatches involved in $w_i(t)$ term are completely known ($\forall i = 1, \ldots, N$), the ideal controller

$$u_i^{v\star}(t) = -w_i(t) - K_i^\star \eta_i(t) \tag{6.13}$$

guarantees the achievement of voltage synchronization within the MG according to control objective (6.2), where $K_i^\star \in \mathbb{R}^{1\times 2}$ is the ideal gain vector. This latter can be tuned by considering the closed-loop dynamics for each DG i under the action of the controller (6.13), i.e.:

$$\dot{\eta}_i(t) = (A - B_i K_i^\star)\eta_i(t) = \Phi_i \eta_i(t). \tag{6.14}$$

The asymptotic stability of each DG i within the network is ensured according to Remark 11 by choosing control gain $K_i^\star \in \mathbb{R}^{1\times 2}$ such that Φ_i $\forall i$ is Hurwitz stable [135]. Different control methods can be exploited to deal with tuning procedure of $K_i^\star$, e.g., pole-placement, LQR and so on.

Now, for dealing with the unknown nature of w_i-term and solving the voltage regulation control problem (6.2) $\forall i$, the following distributed adaptive PID-like control law is designed:

$$\begin{aligned} u_i^v(t) =& u_{i,PID}^v(t) + \chi_i(t) = K_{Pi}(t)\eta_i(t) + K_{Ii}(t)\int_0^t \eta_i(s)ds \\ &+ K_{Di}(t)\dot{\eta}_i(t) + \chi_i(t), \end{aligned} \tag{6.15}$$

where $K_{Pi}(t), K_{Ii}(t)$ and $K_{Di}(t) \in \mathbb{R}^{1\times 2}$ are the control gains shaping the proportional, integral and derivative actions, respectively, to be adapted in order to emulate the ideal control action (6.13); $\chi_i(t) \in \mathbb{R}$ is an auxiliary control signal that has to be properly chosen so to counteract the presence of uncertainties and model mismatches.

By denoting

$$\theta_i^\top(t) = [K_{Pi}(t)\ K_{Ii}(t)\ K_{Di}(t)] \in \mathbb{R}^{1\times 6},$$

$$\varphi_i(t) = \left[\eta_i(t)\ \int_0^t \eta_i(s)ds\ \dot{\eta}_i(t)\right]^\top \in \mathbb{R}^{6\times 1},$$

the control action $u_{i,PID}^v(t)$ in (6.15) can be re-written in a more compact form as

$$u_i^v(t) = u_{i,PID}^v(t) + \chi_i(t) = \theta_i^\top(t)\varphi_i(t) + \chi_i(t). \tag{6.16}$$

Now, let $u_{i,PID}^{v\star}(t) = \theta_i^{\star\top}\varphi_i(t)$ to be the optimal distributed PID controller with fixed optimal proportional, integral and derivative control gains $\theta_i^\star = [K_{Pi}^\star\ K_{Ii}^\star\ K_{Di}^\star]$, which is able to uniformly approximate the ideal controller $u_i^{v\star}(t)$ in (6.13). Accordingly, the following bounded error approximation can be introduced:

$$u_{i,PID}^{v\star}(t) - u_i^{v\star} = \xi_i(t), \tag{6.17}$$

with $|\xi_i(t)| \leq \bar{\xi}_i < \infty,\ i = 1, \cdots, N$, the maximum unknown approximation error between the two ideal control laws $u_i^{v\star}(t)$ and $u_{i,PID}^{v\star}(t)$.
Finally, the ith closed-loop system of DG i under the action of the proposed augmented distributed adaptive PID controller $u_i^v(t)$ in (6.16) can be derived by substituting this latter in (6.12) and adding the zero sum terms (6.17), thus obtaining:

$$\begin{aligned}\dot{\eta}_i(t) &= A\eta_i(t) + B_i(\theta_i^\top(t)\varphi_i(t) + \chi_i(t) + w_i(t)) + B_i(\xi_i(t)\\ &+ u_i^{v\star}(t) - \theta_i^{\star\top}\varphi_i(t)) = \Phi_i\eta_i(t) + B_i\tilde{\theta}_i^\top(t)\varphi_i(t) + B_i\chi_i(t) + B_i\xi_i(t),\end{aligned} \tag{6.18}$$

with $\tilde{\theta}_i(t) = \theta^\top{}_i(t) - \theta^\star{}_i{}^\top$ and $\Phi_i = (A - B_iK_i^\star)$ the Hurwitx stable matrix as in (6.14).

6.3.1 Control Design and Stability Analysis

Here, firstly the adaptive mechanisms for the control gains $\theta_i^\top(t) = [K_{Pi}(t)\ K_{Ii}(t)\ K_{Di}(t)]$, as well as for the control action $\chi_i(t)\ \forall i = 1, \ldots, N$, are designed. Then, the asymptotic stability of the overall MG network under the action of the proposed cooperative adaptive PID-like controller (6.16) is analytically proven, thus resulting in stability conditions summarized in the following Theorem.

Theorem 5. *Consider the closed-loop system of the i-th DG within the MG as in (6.18), $\forall i = 1, \ldots, N$. Let Assumption 6 holds. Given scalars $\alpha_i \in \mathbb{R}_+$ ($\forall i = 1, \ldots, N$), symmetric and positive definite matrices $P_i \in \mathbb{R}^{2\times 2}$ satisfying the Lyapunov equation $P_i\Phi_i + \Phi_i^\top P_i = -Q_i$ ($\forall i = 1, \ldots, N$), a positive diagonal matrix $\Gamma_i \in \mathbb{R}^{6\times 6}$($\forall i = 1, \ldots, N$), positive free function $\phi_i(t)$ such that $\int_0^t \phi_i(s)\,ds \leq \bar{\phi}_i < +\infty$ (with $\bar{\phi}_i$ a positive constant) ($\forall i = 1, \ldots, N$), and the auxiliary control signal in (6.15) as*

$$\chi_i(t) = -\frac{B_i^\top P_i \eta_i(t)}{\sqrt{\|B_i^\top P_i \eta_i(t)\|^2 + \phi_i^2(t)}}\hat{\xi}_i(t), \tag{6.19}$$

with $\hat{\xi}_i(t)$ the estimation of the unknown upper-bound $\bar{\xi}_i$ in (6.17), updating according to following mechanism

$$\dot{\hat{\xi}}_i(t) = \alpha_i \frac{\|B_i^\top P_i \eta_i(t)\|^2}{\sqrt{\|B_i^\top P_i \eta_i(t)\|^2 + \phi_i^2(t)}}, \tag{6.20}$$

then, the augmented distributed adaptive PID controller (6.15) with adaptive gains $\theta_i(t)$ as

$$\dot{\theta}_i(t) = -\Gamma_i \varphi_i(t) \eta_i^\top(t) P_i B_i \tag{6.21}$$

can asymptotically solve voltage regulation problem according to control objective (6.2). Moreover, as the i-th DG voltage v_i goes to v_0 as $t \to \infty$, signals $\theta_i(t)$ and $\hat{\xi}_i(t)$ remain bounded over the time.

Proof. Consider the following Lyapunov candidate function:

$$\begin{aligned} V(t) &= V_1(t) + V_2(t) + V_3(t) \\ &= \sum_{i=1}^{N} \eta_i^\top(t) P_i \eta_i(t) + \sum_{i=1}^{N} \frac{1}{\alpha_i}\tilde{\xi}_i^2(t) + \sum_{i=1}^{N} \tilde{\theta}_i^\top(t)\Gamma_i^{-1}\tilde{\theta}_i(t) \quad \forall i, \end{aligned} \tag{6.22}$$

with $P_i = P_i^\top > 0 \in \mathbb{R}^{2\times 2}$ a symmetric positive definite matrix, $\alpha_i \in \mathbb{R}_+$ a positive scalar and $\Gamma_i^{-1} \in \mathbb{R}^{6\times 6}$ a positive diagonal matrix. Moreover, the variable $\tilde{\xi}_i(t)$ represents the estimation error of the unknown upper bound $\bar{\xi}_i$ in (6.17), computed on the basis of its actual estimation $\hat{\xi}_i(t)$ as $\tilde{\xi}_i(t) = \bar{\xi}_i - \hat{\xi}_i(t)$.

Differentiating $V_1(t)$ in (6.22) along the trajectories of (6.18), it results:

$$\begin{aligned}\dot{V}_1(t) = &\sum_{i=1}^{N} \eta_i^\top(t)(P_i\Phi_i + \Phi_i^\top P_i)\eta_i(t) + 2\sum_{i=1}^{N} \eta_i^\top(t)P_iB_i\tilde{\theta}_i^\top(t)\varphi_i(t) \\ &+ 2\sum_{i=1}^{N} \eta_i^\top(t)P_iB_i\chi_i(t) + 2\sum_{i=1}^{N} \eta_i^\top(t)P_iB_i\xi_i(t).\end{aligned} \tag{6.23}$$

The last cross term in (6.23) can be bounded by exploiting the upper bound of $\xi_i(t)$ in (6.17) as follows:

$$2\sum_{i=1}^{N} \eta_i^\top(t)P_iB_i\xi_i(t) \leq 2\sum_{i=1}^{N} \|\eta_i^\top(t)P_iB_i\|\bar{\xi}_i. \tag{6.24}$$

Moreover, since Assumption 6 ensures that matrix Φ_i in (6.23) is Hurwitz stable, there always exists a symmetric and positive definite matrix $Q_i = Q_i^\top > 0$ solving the Lyapunov equation $P_i\Phi_i + \Phi_i^\top P_i = -Q_i$, $\forall i$ [144]. Thus, (6.23) can be rewritten as:

$$\begin{aligned}\dot{V}_1(t) \leq &-\sum_{i=1}^{N} \eta_i^\top(t)Q_i\eta_i(t) + 2\sum_{i=1}^{N} \eta_i^\top(t)P_iB_i\tilde{\theta}_i^\top(t)\varphi_i(t) \\ &+ 2\sum_{i=1}^{N} \eta_i^\top(t)P_iB_i\chi_i(t) + 2\sum_{i=1}^{N} \|\eta_i^\top(t)P_iB_i\|\bar{\xi}_i.\end{aligned} \tag{6.25}$$

Given the estimation $\hat{\xi}_i(t)$ of the unknown upper bound $\bar{\xi}_i(t)$ as $\hat{\xi}_i(t) = \bar{\xi}_i - \tilde{\xi}_i(t)$ and $\chi_i(t)$ in (6.19), inequality (6.25) can be recast as:

$$\begin{aligned}\dot{V}_1(t) \leq &-\sum_{i=1}^{N} \eta_i^\top(t)Q_i\eta_i(t) + 2\sum_{i=1}^{N} \eta_i^\top(t)P_iB_i\tilde{\theta}_i^\top(t)\varphi_i(t) \\ &+ 2\sum_{i=1}^{N} \left(\|\eta_i^\top(t)P_iB_i\| - \frac{\|B_i^\top P_i\eta_i(t)\|^2}{\sqrt{\|B_i^\top P_i\eta_i(t)\|^2 + \phi_i^2(t)}}\right)\bar{\xi}_i \\ &+ 2\sum_{i=1}^{N} \frac{\|B_i^\top P_i\eta_i(t)\|^2}{\sqrt{\|B_i^\top P_i\eta_i(t)\|^2 + \phi_i^2(t)}}\tilde{\xi}_i(t),\end{aligned} \tag{6.26}$$

where $\phi_i(t)$, $\forall i = 1, \dots, N$ is a positive free function satisfying $\int_0^t \phi_i(s)\,ds \leq \bar{\phi} : i < +\infty$, with $\bar{\phi}_i > 0$ a positive scalar. Note that, the definition of P_i ensures that $\|\eta_i^\top(t) P_i B_i\| = \|B_i^\top P_i \eta_i(t)\|$, $\forall i$. By recalling the property $z^\top z = \|z\|^2$ with $z = B_i^\top P_i \eta_i(t)$, since for any variable $z \in \mathbb{R}^n$, $\|z\| \geq 0$ (with $\|z\| = 0$ iff $z = 0$) implies $\|\|z\|\| = \|z\| > 0$, it is possible to leverage Lemma 8. In doing so, (6.26) can be rewritten as follows:

$$\begin{aligned}\dot{V}_1(t) \leq & -\sum_{i=1}^{N} \eta_i^\top(t) Q_i \eta_i(t) + 2\sum_{i=1}^{N} \eta_i^\top(t) P_i B_i \tilde{\theta}_i^\top(t) \varphi_i(t) \\ & + 2\sum_{i=1}^{N} \bar{\xi}_i \phi_i(t) + 2\sum_{i=1}^{N} \frac{\|B_i^\top P_i \eta_i(t)\|^2}{\sqrt{\|B_i^\top P_i \eta_i(t)\|^2 + \phi_i^2(t)}} \tilde{\xi}_i(t).\end{aligned} \tag{6.27}$$

Now, differentiating $V_2(t)$ and $V_3(t)$ in (6.22) along (6.18), it holds:

$$\dot{V}_2(t) = -2\sum_{i=1}^{N} \frac{1}{\alpha_i} \tilde{\xi}_i(t) \dot{\hat{\xi}}_i(t), \quad \dot{V}_3(t) = 2\sum_{i=1}^{N} \tilde{\theta}_i^\top(t) \Gamma_i^{-1} \dot{\theta}_i(t). \tag{6.28}$$

After summing up (6.27)-(6.28), by selecting the adaptive law for the estimation of $\hat{\xi}_i(t)$ as in (6.20) and considering the equality

$$2\sum_{i=1}^{N} \eta_i^\top(t) P_i B_i \tilde{\theta}_i^\top(t) \varphi_i(t) = 2\sum_{i=1}^{N} \tilde{\theta}_i^\top(t) \varphi_i(t) \eta_i^\top(t) P_i B_i,$$

the following inequality can be derived:

$$\begin{aligned}\dot{V}(t) \leq & -\sum_{i=1}^{N} \eta_i^\top(t) Q_i \eta_i(t) + 2\sum_{i=1}^{N} \tilde{\theta}_i^\top(t) \varphi_i(t) \eta_i^\top(t) P_i B_i \\ & + 2\sum_{i=1}^{N} \bar{\xi}_i \phi_i(t) + 2\sum_{i=1}^{N} \tilde{\theta}_i^\top(t) \Gamma_i^{-1} \dot{\theta}_i(t).\end{aligned} \tag{6.29}$$

Furthermore, by considering the adaptive mechanism for control gains θ_i

as in (6.21), (6.29) becomes:

$$\dot{V}(t) \leq -\sum_{i=1}^{N} \eta_i^\top(t) Q_i \eta_i(t) + 2\sum_{i=1}^{N} \bar{\xi}_i \phi_i(t). \tag{6.30}$$

Integrating (6.30) on the time interval $[0, t]$, the application of Rayleigh inequality in Lemma 9 and the boundedness property of $\phi_i(t)$ ensure that:

$$V(t) + \sum_{i=1}^{N} \underline{\lambda}_{Q_i} \int_0^t \|\eta_i(s)\|^2 ds \leq V(0) + 2\sum_{i=1}^{N} \bar{\xi}_i \bar{\phi}_i < \infty, \tag{6.31}$$

where $\underline{\lambda}_{Q_i}$ is the smallest eigenvalue of the symmetric matrix Q_i. Inequality (6.31) guarantees the existence of an upper bound for the Lyapunov function in (6.22) and this implies that signals $\eta_i(t)$, $\theta_i(t)$ and $\hat{\xi}_i(t)$ are also bounded $\forall i = 1, \ldots, N$. Furthermore, (6.31) also suggests that [145]:

$$\lim_{t \to +\infty} \sum_{i=1}^{N} \underline{\lambda}_{Q_i} \int_0^t \|\eta_i(s)\|^2 ds \leq V(0) + 2\sum_{i=1}^{N} \bar{\xi}_i \bar{\phi}_i < \infty. \tag{6.32}$$

Therefore, from Lemma 7, it is possible to conclude that

$$\lim_{t \to +\infty} \|\eta_i(s)\| = 0, \quad \forall i = 1, \ldots, N. \tag{6.33}$$

Now, to prove the stability of the entire MG network under the action of augmented distributed adaptive PID controller in (6.15), let

$$\eta(t) = [\eta_1^\top(t), \eta_2^\top(t), \cdots, \eta_N^\top(t)]^\top \in \mathbb{R}^{2N \times 1},$$

$$e(t) = [e_1^\top(t), e_2^\top(t), \cdots, e_N^\top(t)]^\top \in \mathbb{R}^{2N \times 1},$$

to be global vectors of the whole power network. From the definition of $\eta_i(t)$ in (6.9), it yields:

$$\eta(t) = (\mathscr{L} + \mathscr{P} \otimes I_2) e(t), \tag{6.34}$$

where the positiveness of $\mathscr{L} + \mathscr{P}$ is ensured by Assumption 6.
Therefore, the convergence of $\eta(t)$ towards zero (i.e. condition (6.33)) also

implies that $e(t) \to 0$ [146]. This confirms the achievement of the voltage regulation control as in (6.2).

$\square$

Remark 12. *It is worth noting how the proposed approach involves a limited amount of time-varying information for computing the adaptive control, guaranteeing at the same time the asymptotic stability of the synchronization errors. According to the metric proposed in [37], this results in a reduction of the computational burden and optimal usage of the communication channel bandwidth than the current adaptive control methodologies (see e.g. [147, 148] and the references therein). Moreover, the real-time updating of the control gains parameters can be ensured by exploiting the novel computation technologies proposed in the field of MG control [149].*

Remark 13. *The proposed control* (6.15) *along with the adaptive mechanisms* (6.20)-(6.21) *is fully-distributed since their computation do not leverage the knowledge about neither the eigenvalues of the Laplacian matrix, modelling the communication structure, or the leader dynamics, whose behavior could be completely unknown [146].*

6.4 Numerical simulations

In this section, the proposed distributed adaptive PID-like in (6.15) is validated on a $220V_{RMS}$, $50[Hz]$ islanded MG composed of $N = 4$ DGs and their respective local loads, connected via three power transmission lines. Parameters of the test system are chosen as in [14]. The communication network topology $\mathscr{G}^c_{N+1}$ is chosen such that Assumption 6 holds, i.e. $\mathscr{E}^c_{N+1} = \{(0,1),(1,2),(1,3),(2,3),(1,4),(3,4)\}$. In so doing $\mathscr{L} + \mathscr{P}$ is a positive definite M-matrix. It is important to point out that this communication topology is just one among the possible configurations that can be dealt with the proposed approach.
The positive free functions are selected $\forall i$ as $\phi_i(t) = e^{-0.1t}$, while the ideal control gains vectors $K^\star_i$ in (6.13), tuned via pole-placement technique, are: $K^\star_1 = K^\star_2 = [1.0827, 0.8120]$, $K^\star_3 = K^\star_4 = [0.5413, 0.4060]$. Other parameters involved in Theorem 5 are selected $\forall i = 1,2,3,4$ as follows: $\Gamma_i = 50 I_{6\times 6}$, $\alpha_i = 1$ and $Q_i = 10 I_{2\times 2}$.

Moreover, to mimic a more realistic scenario, the secondary frequency controller u_i^{ω}

$$\begin{aligned} u_i^{\omega} &= \alpha_i(\hat{\omega}_i - \omega_i) \\ \dot{\hat{\omega}}_i &= \beta_i \sum_{j \in \mathcal{N}_i^c} (\omega_i - \omega_j) + g_i(\omega_i - \omega_0) + \varphi_i \sum_{j \in \mathcal{N}_i^c} (u_j^{\omega} - u_i^{\omega}) \end{aligned} \tag{6.35}$$

proposed in [13] has been involved in the simulation platform in order to test the proposed voltage controller (6.15) in a more reasonable and practical case-of-study. Specifically, frequency control gains in (6.35) are selected as $\alpha_i^{\omega} = 500,\ \beta_i^{\omega} = 20,\ \phi_i^{\omega} = 250,\ i = 1, 2, 3, 4$, while the desired set-point ω_0 is such that $\omega_0 = 50$ $[Hz]$ for $t \in [0, 20)$ $[s]$ and $\omega_0 = 50.2$ $[Hz]$ for $t \in [20, 40)$ $[s]$.
Here, the objective is to highlight the effectiveness of the proposed fully-distributed adaptive PID-like controller in solving voltage restoration problem by removing unavoidable deviations induced by PC, despite the lack of knowledge of process dynamics and the presence of external heterogeneous disturbances. To this aim, the numerical analysis is carried out by leveraging Matlab/Simulink simulation platform, with time-interval of 40 $[s]$ for simulation purpose. Three representative simulation scenarios are considered, namely: *i*) *nominal scenario*, which involves voltage reference variations to highlight the leader-tracking capability of the proposed controller; *ii*) *loads changing scenario*, where voltage reference and loads changes occur; *iii*) *plug-and-play scenario*, which shows the ability of the proposed controller in dealing with the plug-and-play phenomena and reference variations. Moreover, a comparison analysis is also provided to further highlight the advantages of the proposed approach with respect to an alternative adaptive control law, recently suggested in the technical literature. Finally, it is worth mentioning that frequency responses are maintained within the operating range $[50, 50.2]$ $[Hz]$ and can be restored via (6.35) in all the appraised simulation scenarios. However, for the sake of brevity, frequency time histories are omitted.

6.4.1 Nominal Scenario

The use-case under test in this nominal scenario is characterized by changes in voltage set points, according to the following list of events:

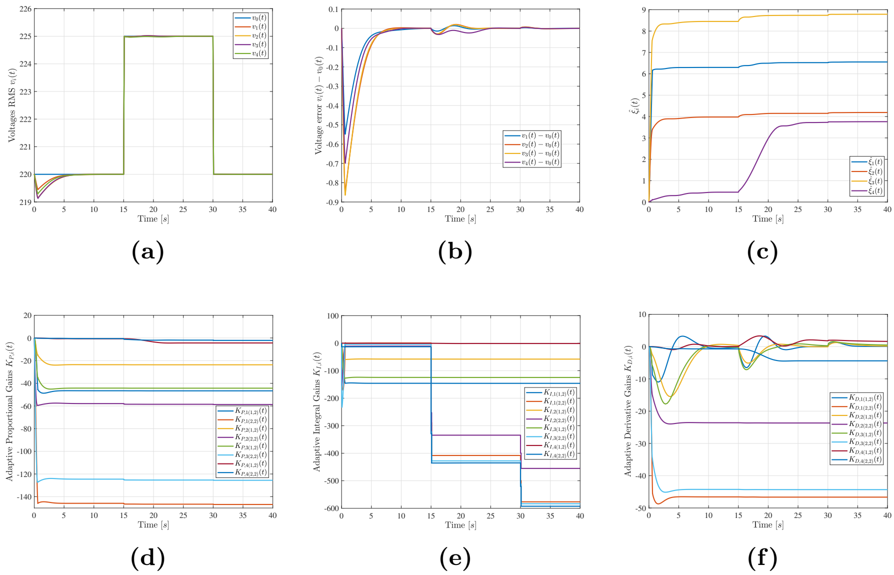

Figure 6.1. Cooperative adaptive PID-like voltage regulation in *nominal scenario*. Time history of: *a*) voltage $v_i(t)$, $i = 1, \dots, 4$; *b*) voltage error $v_i(t) - v_0(t)$, $i = 1, \dots, 4$; *c*) estimated signal $\hat{\xi}_i(t)$ $i = 1, \dots, 4$; *d*) adaptive proportional gain vector $K_{Pi} \in \mathbb{R}^{2\times 1}$, $i = 1, \dots, 4$; *e*) adaptive integral gain vector $K_{Ii} \in \mathbb{R}^{2\times 1}$, $i = 1, \dots, 4$; *f*) adaptive derivative gain vector $K_{Di} \in \mathbb{R}^{2\times 1}$, $i = 1, \dots, 4$.

- at $t = 0$ $[s]$ the voltage SC in (6.15) is activated with $v_0(t) = 220$ $[V_{RMS}]$;
- at $t = 15$ $[s]$ the voltage set-point is changed to $v_0(t) = 225$ $[V_{RMS}]$;
- at $t = 30$ $[s]$ the desired voltage is restored to $v_0(t) = 220$ $[V_{RMS}]$.

Results in Figure 6.1 confirm the effectiveness of the proposed adaptive control strategy in ensuring the voltage synchronization process despite the presence of fluctuation due to droop control, different external disturbances and lack of knowledge about the global dynamics of each DG involved in the electrical network. Specifically, by activating the SC (6.15) at $t = 0$ $[s]$, all the DGs track the voltage reference behaviour imposed by the virtual DG 0 in spite of the effects of unavoidable fluctuation induced by PC and the reference changes as shown in Figure 6.1(a), while voltage errors approach to zero after each transient phase involved in the investigated simulation scenario (see Figure 6.1(b)). Specifically, as it is possible to observe in Figure 6.1(b), small bounded voltage errors occur at $t = 15$ $[s]$ and $t = 30$ $[s]$, which correspond to leader voltage variations. Meanwhile, these latter voltage reference variations at $t = 15$ $[s]$ and $t = 30$ $[s]$ imply also changes in the adaptive control gains behavior as disclosed in Figure 6.1(d)-(e)-(f). However, according to Theorem 5, once the voltage synchronization process is completed, the adaptive proportional, integral and derivative control gains $K_{Pi}(t)$, $K_{Ii}(t)$ and $K_{Di}(t) \in \mathbb{R}^{2\times 1}$, $\forall i = 1, \ldots, 4$ converge to constant steady-state values as shown in Figure 6.1(d)-(e)-(f), along with the estimated signal $\hat{\xi}_i(t)$, $\forall i = 1, \ldots, 4$ (see Figure 6.1(c)).

6.4.2 Load changing scenario

Since robustness with respect to load variations is a crucial requirement in real applications due to strongly variable load demand, here a more troublesome scenario with variable loads has been analyzed. Specifically, the following scenario is considered:

- at $t = 0$ $[s]$ voltage SC in (6.15) is activated with $v_0(t) = 220$ $[V_{RMS}]$;
- at $t = 5$ $[s]$ Load 1 is removed while re-added at $t = 8$ $[s]$;
- at $t = 15$ $[s]$ the voltage set-point is changed to $v_0(t) = 225$ $[V_{RMS}]$, until it restores to initial value at $t = 30$ $[s]$;
- at $t = 16$ $[s]$ Load 4 is removed while re-added at $t = 20$ $[s]$;
- at $t = 23$ $[s]$ there is a 20% of increasing for Load 2, until it restore its nominal values at $t = 30$ $[s]$;
- at $t = 30$ $[s]$ Load 3 is removed while re-added at $t = 34$ $[s]$.

Robustness performances with respect to sudden variation in the load requests are highlighted in Figure 6.2. Herein it is possible observing that the proposed approach allows counteracting load changes, while restoring the desired voltage set-point. Specifically, once the adaptive controller (6.15) is switched on at $t = 0$ $[s]$, DGs voltages promptly react

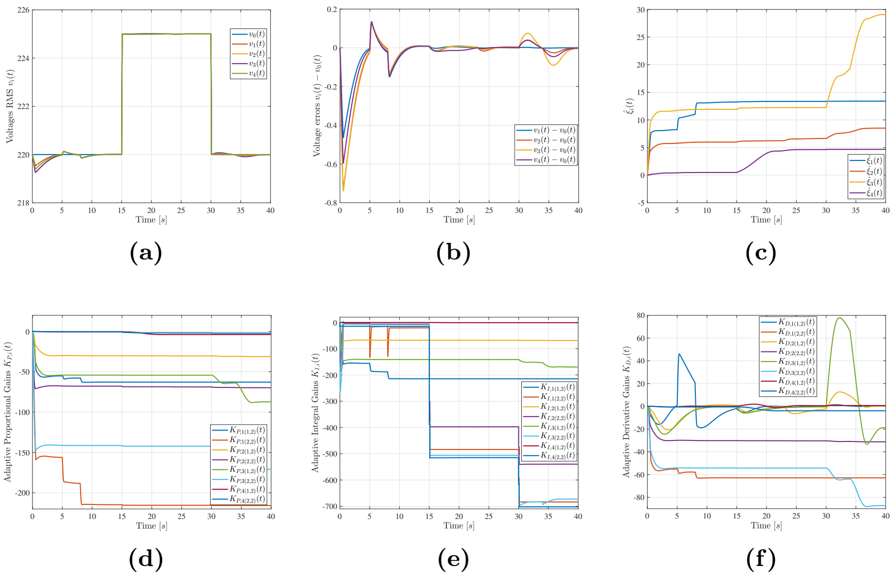

Figure 6.2. Cooperative adaptive PID-like voltage regulation in *load changing scenario*. Time history of: *a*) voltage $v_i(t)$, $i = 1, \ldots, 4$; *b*) voltage error $v_i(t) - v_0(t)$, $i = 1, \ldots, 4$; *c*) estimated signal $\hat{\xi}_i(t)$ $i = 1, \ldots, 4$; *d*) adaptive proportional gain vector $K_{Pi} \in \mathbb{R}^{2\times 1}$, $i = 1, \ldots, 4$; *e*) adaptive integral gain vector $K_{Ii} \in \mathbb{R}^{2\times 1}$, $i = 1, \ldots, 4$; *f*) adaptive derivative gain vector $K_{Di} \in \mathbb{R}^{2\times 1}$, $i = 1, \ldots, 4$.

to loads variations and synchronize to the reference value, as shown in Figure 6.2(a), while voltage errors with respect to virtual DG 0 converge to zero (Figure 6.2(b)). Also in this case, acceptable errors can be appreciated in transient phases when load/reference changes occur as shown in Figure 6.2(b), which confirms the same good performances also in this case. Again, each transient phase due to loads and/or voltage reference variations leads to changes into control gains, which have to adapt their behaviour in order to guarantee successfully desired voltage recovery (see Figure 6.2(d)-(e)-(f)). Similarly to the *nominal scenario*, whenever steady-state conditions are reached, adaptive control gain vectors $K_{Pi}(t)$, $K_{Ii}(t)$ and $K_{Di}(t) \in \mathbb{R}^{2\times 1}$, $i = 1, \ldots, 4$, converge to finite values as highlighted in Figure 6.2(d)-(e)-(f), along with the estimated signal $\hat{\xi}_i(t)$, $i = 1, \ldots, 4$

(see Figure 6.2(c)-(f)).

6.4.3 Plug-and-play scenario

In this simulation scenario the robustness of the proposed distributed adaptive PID-like controller (6.15) is proved in a more troublesome environment, where plug-and-play phenomena affect some DGs within the test system. Specifically, the following events are performed:

- at $t = 0$ $[s]$, the voltage SC (6.15) is activated with $v_0(t) = 220$ $[V_{RMS}]$;
- DG 2 and DG 3 are unplugged at $t = 10$ $[s]$ and $t = 18$ $[s]$, respectively;
- DG 2 and DG 3 are plugged-in at $t = 15$ $[s]$ and $t = 27$ $[s]$, respectively;
- at $t = 15$ $[s]$ voltage set-point is changed to $v_0(t) = 225$ $[V_{RMS}]$, while its nominal value $v_0(t) = 220$ $[V_{RMS}]$ is restored at $t = 30$ $[s]$.

Figure 6.3 illustrates the results of the above-described cumbersome scenario, thus proving the effectiveness of the approach in successfully dealing with voltage regulation problem despite DGs losses and changes in voltage set-points (see Figure 6.3(a)-(b)). Note that, these sources failure also implies communication losses for the links connected to the unplugged DGs [125]. Specifically, when DG 2 and DG 3 fail at $t = 10$ $[s]$ and $t = 18$ $[s]$, respectively, they automatically render the links $2-3$ (between DGs 2 and 3) and 3–4 (between DGs 3 and 4) inoperable. However, this does not compromise the steady-state performance of the proposed control methodology, as long as Assumption 6 is still guaranteed, thus proving the resilience of the approach also with respect to packet losses. For the sake of completeness and according to theoretical derivation, time-histories of adaptive proportional, integral and derivative control gain vectors $K_{Pi}(t)$, $K_{Ii}(t)$ and $K_{Di}(t) \in \mathbb{R}^{2\times 1}$, $i = 1, \ldots, 4$, are reported in Figure 6.3(d)-(f), respectively, which show the achievement of constant values once synchronization process is done after each transient phase, along with signal $\hat{\xi}_i(t)$, $i = 1, \ldots, 4$ (see Figure 6.3(c)).

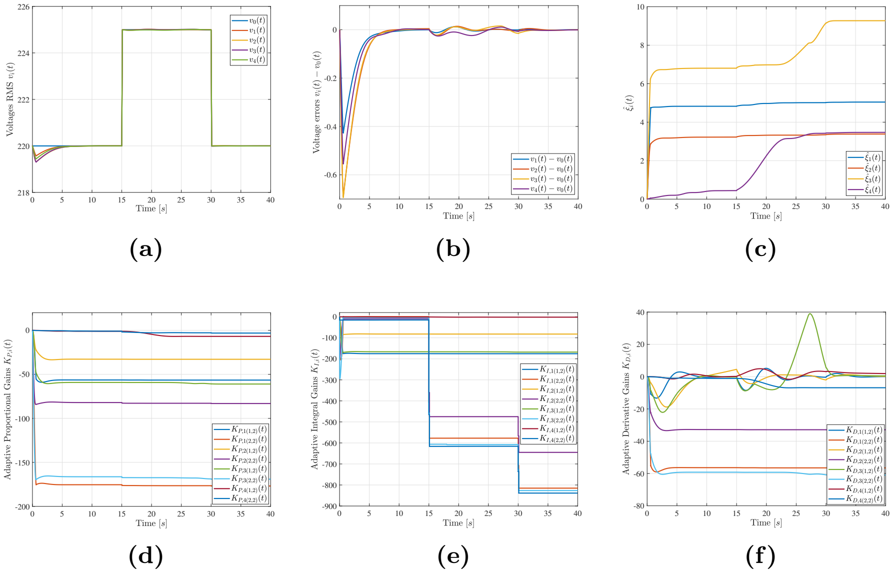

Figure 6.3. Cooperative adaptive PID-like voltage regulation in *plug-and-play scenario*. Time history of: $a)$ voltage $v_i(t)$, $i = 1, \ldots, 4$; $b)$ voltage error $v_i(t) - v_0(t)$, $i = 1, \ldots, 4$; $c)$ estimated signal $\hat{\xi}_i(t)$ $i = 1, \ldots, 4$; $d)$ adaptive proportional gain vector $K_{Pi} \in \mathbb{R}^{2\times 1}$, $i = 1, \ldots, 4$; $e)$ adaptive integral gain vector $K_{Ii} \in \mathbb{R}^{2\times 1}$, $i = 1, \ldots, 4$; $f)$ adaptive derivative gain vector $K_{Di} \in \mathbb{R}^{2\times 1}$, $i = 1, \ldots, 4$.

6.4.4 Comparison Analysis

In order to further highlight the advantages of the proposed distributed adaptive PID-like controller in guaranteeing voltage recovery in islanded MG, here the performance of the proposed controller are compered with the one achievable through the alternative adaptive control approach recently suggested in [11]. For the comparison analysis, the *load changing scenario* as detailed in Section 6.4.2 is considered with a constant voltage reference value $v_0 = 225$ $[V_{RMS}]$ so to compute the maximum percentage of voltage deviation. The performance of both adaptive controllers can be appreciated in Figure 6.4, which discloses the voltage synchronization errors $v_i(t) - v_0$, $\forall i$. Figure 6.4 corroborates the effectiveness of the

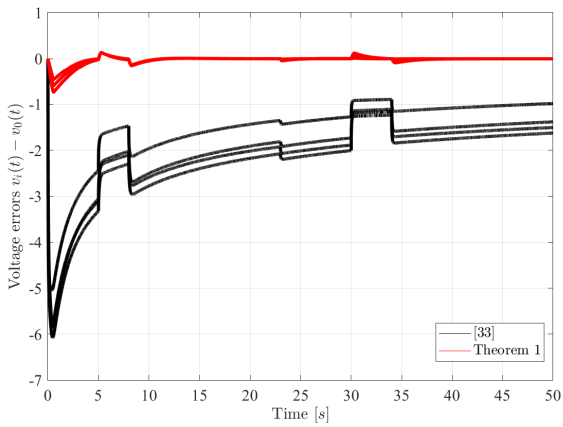

Figure 6.4. Comparison with adaptive controller in [11] for the *load changing scenario: time history of voltage errors $v_i(t) - v_0(t)$, $\forall i$.*

proposed control strategy in achieving improved performances in terms of voltage recovery since smaller synchronization errors (red lines in Figure 6.4) with respect to the ones obtained via [11] (black lines in Figure 6.4) occur. Specifically, for the investigated scenario, it results that the maximum voltage deviation is 0.34% for the proposed controller (6.15), whereas for the adaptive strategy in [11] it is 2.76%. Finally, it is worth mentioning that this benefit straightly comes from the PID-like structure of (6.15), where the derivative and integral actions ensure improved transient and steady-state performance with respect to [11] which, instead, adaptively weights the local voltage neighborhood consensus error with a proportional-based action.

6.5 Concluding Remarks

This chapter has addressed the secondary voltage regulation problem in inverter-based islanded MG under unknown and unbounded uncertainties, which is a crucial issue in these practical application due to the related complex phenomena arising in modern power systems. A cooperative adaptive PID-like control protocol is introduced to solve the problem which, thanks to its PID-based structure, is able to guarantee strongly improved steady-state and transient performance. Novel adaptive mechanisms are derived by exploiting Lyapunov theory, which allowed improving performances by adjusting control parameters on the basis of different operating conditions and guaranteeing the anti-disturbances capability of the electrical network. Lyapunov theory along with Barbalat lemma are also exploited to analytically demonstrate the stability of the entire MG network, thus ensuring the effectiveness and the robustness of the control strategy in reaching voltage synchronization despite the presence of unknown and unbounded external disturbances and parameter mismatches affecting distributed generators dynamics. Extensive numerical simulations have highlighted the effectiveness of the approach in different troublesome scenarios, where both reference/load variations and plug-and-play phenomena are considered.

Chapter 7

From continuous to periodic inter-agent interactions

In distributed cooperative control frame, agents are spatially distributed over a monitoring/operational area and controlled through some communication networks by a digital control platform. Each agent works autonomously with the aim of achieving a common group behaviour at the global level by exploiting only local information from itself and its neighborhood. Hence, the inter-agent interactions play a crucial role in control design phase of distributed control laws. Conventional consensus control protocols for NCS are designed on the basis of continuous data transmissions. However, advanced communication networks only permit digital or periodical information dissemination. In this cases, continuous interactions among agents are not suitable and may incur heavy burden on the communication networks. Therefore, classical distributed control strategies derived from point-to-point information exchanges should be re-evaluated in a sampled-data/periodic fashion. In light of the above, this chapter focuses on designing sampled data and periodic distributed control strategies both for a general high-order MASs and, in particular, for CPES as MG. Specifically, this chapter consists of two main results. The first part is devoted to the design of a fully-distributed delayed sampled-data PID controller to solve secondary voltage recovery problem in inverter-based islanded MG, whose derivative action is approximated using finite difference. By choosing a small enough sampling period and leveraging artificial delays approach, the proposed strategy ensures the secondary voltage regulation, with closed-loop performances similar to ones achievable via a continuous-time PID controller, but with a significant reduction of the communication burden, thus improving the efficiency of the entire MG. Exponential stability of the closed-loop MG network is analytically proved via Lyapunov-Krasovskii theory and the derived sampling-dependent stability conditions are expressed as a set of LMIs, whose solution allows finding the weighted L_2 gain. A detailed simulation analysis confirms the effectiveness and the robustness of the proposed approach. On the other hand, the second part of the chapter considers the leader-tracking problem of a general MASs under a periodic time-varying communication topology, without requiring the connectivity of the network for all $t \geq 0$. Both state and input delays are considered. A fully distributed control protocol, along with the constructive time-delay approach to periodic averaging, are combined in order to solve the problem, thus ensuring that a time-dependent switching control rule preserves the ISS of the entire network, despite the presence of disconnected topologies, state and communication delays. The original closed-loop error systems is transformed into a neutral-type system with discrete and distributed delays. ISS analysis of the neutral system employs appropriate Lyapunov-Krasovskii functionals leading to simple ISS conditions in terms of LMIs, whose solution allows finding upper bounds on small parameter, state and communication delays that preserve ISS. Numerical simulations illustrate the effectiveness of the theoretical results.

7.1 Communication Resources Saving-Oriented Control Strategies

Conventional distributed consensus control strategies rely on some ideal and unrealistic hypothesis regarding the information exchange processes happening into the cyber space. One of the most simplifying assumptions concerns the capability of each agent within the network to continuously obtain state information about itself and its neighbors so to continuously update its controller [150]. This hypothesis may result absurd in practical applications since the communication network bandwidth and computing resources are limited for the existing agents. Moreover, although agents involved in the network requiring proper control algorithm to reach a coordinated behavior live into continuous physical world, it should be noted that these cooperative control laws are implemented in terms of software on digital computers [12]. Therefore, there is a need to use analog-to-digital and digital-to-analog converters during data acquisition, communication, computation, and control actuation, as disclosed in Figure 7.1.

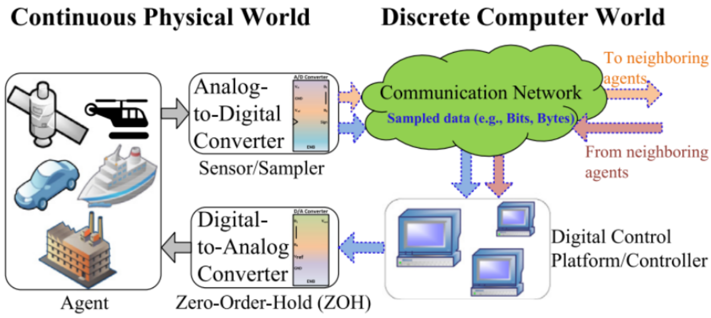

Figure 7.1. Schematic diagram of distributed sampled-data cooperative control for MASs [12].

In this control perspective, the objective is to decrease the number of control update among agents as much as possible in order to save limited resources in message delivery [151]. Therefore, a good consensus algorithm for distributed MASs must be capable of saving the limited resources of communication capacity and energy supply, while guaranteeing the control performance [152]. A widely used method is sampled-data control since it allows periodic execution of control and measurement tasks, which is beneficial for resource saving [150].

Although the above mentioned benefits related to sampled-data control, in the context of voltage SC in inverter-based islanded MG the majority of distributed control strategies are still designed under the assumption of continuous communication among DGs [153, 23], which may result in a communication network congestion, especially when the number of DGs involved into the MG increases [154]. Few recent attempts in considering the MG communication network bandwidth and energy constraints problems from the beginning of control design phase can be found in [24, 154], which are moving towards diffusive event-triggered control strategies.

Besides the advantages of digital control scheme, another crucial aspect is related to the wide use of PI [155] and PID compensators [156] in SC for voltage restoring as well as for removing steady-state deviations. Specifically, PID control strategy cannot only remove voltage/frequency deviations caused by PC, but also provide fast response to the transient changes. However, poor robustness, low bandwidth, as well as the gains tuning problem limit the practical application of PID controllers in MG framework [141].
Based on the above considerations, the first main objective of this chapter is related to the design of a fully-distributed sampled-data PID-based controller for voltage restoration problem in inverter-based islanded MG able to counteract unavoidable deviations due to PC, as well as loads fluctuations. According to [157, 158, 159], the proposed controller exploits finite-difference approximation for derivative actions, thus leading to a time-delayed controller whose delayed term is tackled with its Taylor's expansion with the remainder in the integral form. Indeed, it has been shown that this approximation preserve the stability if the delay is small enough [160], thus confirming that the presence of delays is not always detrimental [161]. The proposed sampled-data distributed PID control strategy, where the data sampling is studied using time-delay approach [97], allows to reduce the amount of control signals used for stabilization, thus saving limited network communication resources. To analytically prove the exponential stability of the closed-loop MG network under the proposed sampled-data PID, Lyapunov-Krasovskii theory is employed. The obtained robust sampling-dependent stability conditions are expressed as a LMIs depending on the proportional, integral and derivative controller gains tuned in the original continuous PID according to Routh-Hurwitz criterion, whose solution allows finding the weighted L_2 gain. A non trivial numerical analysis, involving set-point references/load variations, as well as DG plug-and-play functionality, confirm the effectiveness of the approach.

An alternative way to impose a resources-saving oriented control action is to consider switching communication networks, which exclude that agents can communicate with their neighbors all the time [162]. This leads to the need to consider time-varying communication network, which bring to more challenging scenarios with respect to the ones where more simple

situations with fixed and connected topologies have been analyzed [163]. Furthermore, when dealing with switching communication networks, the hypothesis of at least one connected topology in the finite set of switching is often required, which allows to easily formulate the problem as the stabilization of a switched system with at least one stable mode.
To overcome the above-mentioned restrictive assumption, periodic switching communication topology may be an effective policy to model both teams of autonomous agents that coordinate via periodic communication and networks of chaotic oscillators that synchronize through periodic coupling (see [164] and references therein). Along this line, [163] addresses the ISS of nonlinear switched MASs under jointly connected communication topology, while [165] studies the output-consensus of linear MASs under fast switching topology by exploiting classical averaging tools. Note that, classical averaging theory has been widely employed to study stability properties of systems with fast-switching behavior, including synchronization of chaotic oscillators and control of multiple agents [166]. Although authors in [165] do not require the connectivity of the network for all $t \geq 0$, it applies classical averaging for stability [144]. This leads to qualitative results that do not allow to find an upper bound on the small parameter $\epsilon > 0$ (standing for the variation speed of the time-varying topology) that guarantees the stability of MASs. The quantitative upper bound is found via simulation analysis.
Therefore, the second part of the chapter deals with the leader-tracking problem for a general high-order MASs with both state and communication delays under periodic time-varying communication network, which does not require the connectivity for all t. To solve the problem, the recent constructive time-delay approach to periodic averaging is exploited [40], which allows formulating ISS condition in the form of LMIs, whose solutions provide upper bounds on the small parameter ϵ, as well as on the state and communication delays. Moreover, this work represents the first practical application on MASs of novel theoretical results [47], where the main novelty is the presence of non-small state delays of order of $\mathscr{O}(1)$ that may arise in many practical systems [167].

7.2 Distributed Sampled-data PID Control for Voltage Regulation in Islanded MGs using Artificial Delays

Here, the aim is to design a novel robust distributed sampled-data PID controller for voltage regulation in a stand-alone MG, where the derivative terms are approximated using finite difference as in [158], thus obtaining a delayed sampled-data PID controller which guarantees that all DG units within the MG track the leader reference behaviour.
To represent i-th DG voltage dynamics, by taking into account (3.10b), the derivative of voltage equation in (3.9) leads to [23]:

$$k_{v_i}\ddot{v}_i(t) + w_i(t) + u_i^V(t) = 0, \tag{7.1}$$

being $w_i(t) = -\dot{v}_i(t) - k_{Q_i}\dot{Q}_i^m(t)$ the bounded disturbances due to the droop-PC model, such that $|w_i(t)| \leq \Pi$ [23] . Now, leveraging state-space formalism, system (7.1) can be rewritten as

$$\dot{x}_i(t) = Ax_i(t) + B(u_i^V(t) + w_i(t)), \tag{7.2}$$

where $x_i(t) = [v_i(t)\ \dot{v}_i(t)]^\top \in \mathbb{R}^2$, while $A \in \mathbb{R}^{2\times2}$ and $B \in \mathbb{R}^{2\times1}$ assume the following expressions:

$$A = \begin{bmatrix} 0 & 1 \\ 0 & 0 \end{bmatrix}, \quad B = \begin{bmatrix} 0 \\ -\frac{1}{k_{v_i}} \end{bmatrix}. \tag{7.3}$$

Conversely, the leader reference behaviour is described as the following autonomous system:

$$\dot{x}_0(t) = Ax_0(t), \tag{7.4}$$

where $x_0(t) = [v_0(t)\ \dot{v}_0(t)]^\top \in \mathbb{R}^2$ is the leader state vector embedding the voltage reference. To deal with the problem of voltage regulation in islanded MG, it is useful to look for a distributed PID controller as

$$\begin{aligned} u_i^V(t) =& \bar{k}_p \sum_{j\in\mathcal{N}_i^c} a_{ij}(v_i(t) - v_j(t)) + \bar{k}_i \sum_{j\in\mathcal{N}_i^c} a_{ij} \int_0^t (v_i(s) - v_j(s))\, ds \\ &+ \bar{k}_d \sum_{j\in\mathcal{N}_i^c} a_{ij}(\dot{v}_i(t) - \dot{v}_j(t)), \end{aligned} \tag{7.5}$$

where $\bar{k}_p, \bar{k}_i$ and $\bar{k}_d$ are the proportional, integral and derivative control gains, respectively, while a_{ij} models the communication network topology emerging from the presence/absence of the communication link between i-th and j-th DG. By defining voltages errors of the i-th and j-th DG with respect to the leader as $e_i = v_i - v_0$ and $e_j = v_j - v_0$, the PID control input in (7.5) can be recast as

$$\begin{aligned} u_i^V(t) =& \bar{k}_p \sum_{j\in\mathcal{N}_i^c} a_{ij}(e_i(t) - e_j(t)) + \bar{k}_i \sum_{j\in\mathcal{N}_i^c} a_{ij} \int_0^t (e_i(s) - e_j(s))\, ds \\ &+ \bar{k}_d \sum_{j\in\mathcal{N}_i^c} a_{ij}(\dot{e}_i(t) - \dot{e}_j(t)). \end{aligned} \tag{7.6}$$

As in [157], the finite-difference approximation for the derivative term leads to

$$\dot{e}_i(t) = \bar{e}_i = \frac{e_i(t) - e_i(t-h)}{h}, \qquad \dot{e}_j(t) = \bar{e}_j = \frac{e_j(t) - e_j(t-h)}{h}, \tag{7.7}$$

with $h > 0$. Hence, by leveraging (7.7), (7.6) becomes a delay-dependent controller as

$$\begin{aligned} u_i^V(t) =& k_p \sum_{j\in\mathcal{N}_i^c} a_{ij}(e_i(t) - e_j(t)) + k_i \sum_{j\in\mathcal{N}_i^c} a_{ij} \int_0^t (e_i(s) - e_j(s))\, ds \\ &+ k_d \sum_{j\in\mathcal{N}_i^c} a_{ij}(e_i(t-h) - e_j(t-h)), \end{aligned} \tag{7.8}$$

being

$$k_p = \bar{k}_p + \frac{\bar{k}_d}{h}, \quad k_i = \bar{k}_i, \quad k_d = -\frac{\bar{k}_d}{h}. \tag{7.9}$$

The above delay-dependent controller (7.8) can be implemented in sampled-data fashion by using the following relations [158]:

$$\begin{aligned} &\int_0^t e_i(s)\, ds \approx \int_0^{t_k} e_i(s)\, ds \approx h \sum_{s=0}^{k-1} e_i(t_s), \\ &\dot{e}_i(t) \approx \dot{e}_i(t_k) \approx \bar{e}_i(t_k) = \frac{e_i(t_k) - e_i(t_{k-1})}{h}, \qquad t \in [t_k, t_{k+1}), \end{aligned} \tag{7.10}$$

being $h > 0$ and $t_k = kh,\ k \in \mathbb{N}_0$ the sampling period and the sampling instants, respectively. Exploiting (7.10), the PID controller in (7.6) can be, hence, approximated by the following sampled-data PID controller:

$$\begin{aligned}u_i^V(t) =&\bar{k}_p \sum_{j\in\mathcal{N}_i^c} a_{ij}(e_i(t_k) - e_j(t_k)) + \bar{k}_i h \sum_{j\in\mathcal{N}_i^c}\sum_{s=0}^{k-1}(e_i(t_s) - e_j(t_s))\\ &+ \bar{k}_d \sum_{j\in\mathcal{N}_i^c} a_{ij}(\bar{e}_i(t_k) - \bar{e}_j(t_k))\\ =&k_p \sum_{j\in\mathcal{N}_i^c} a_{ij}(e_i(t_k) - e_j(t_k)) + k_i h \sum_{j\in\mathcal{N}_i^c}\sum_{s=0}^{k-1}(e_i(t_s) - e_j(t_s))\\ &+ k_d \sum_{j\in\mathcal{N}_i^c} a_{ij}(\bar{e}_i(t_{k-1}) - \bar{e}_j(t_{k-1})), \qquad t \in [t_k, t_{k+1}),\ k \in \mathbb{N}_0\end{aligned} \tag{7.11}$$

where k_p, k_i and k_d are defined in (7.9).

Remark 14. *Although studies on asynchronous nonuniform sampling are recently arising, the rapid advances in wireless sensing and communication technologies may help to develop advanced time synchronization protocols for wireless sensor. In this case, it would be reasonable to keep all the samplers synchronized through software time synchronization algorithms, thus justifying uniform synchronous sampling mechanism [12]. Asynchronous nonuniform and random sampling mechanisms may be considered as a future work.*

7.2.1 Exponential Stability Analysis

To prove the stability of the islanded MG under the action of sampled-data PID controller in (7.11), the following vectors associated with the i-th DG are introduced:

$$\tilde{x}_i(t) = \begin{bmatrix}\tilde{x}_{i,1}(t)\\ \tilde{x}_{i,2}(t)\\ \tilde{x}_{i,3}(t)\end{bmatrix} = \begin{bmatrix} e_i(t)\\ \dot{e}_i(t)\\ (t-t_k)e_i(t_k)+h\sum_{s=0}^{k-1} e_i(t_s)\end{bmatrix} \in \mathbb{R}^3, \tag{7.12}$$

$$\rho_i(t) = \tilde{x}_i(t_k) - \tilde{x}_i(t) \in \mathbb{R}^3, \quad \delta_i(t) = \bar{e}_i(t_k) - \bar{e}_i(t) \in \mathbb{R}, \tag{7.13}$$

for $t \in [t_k, t_{k+1})$, $k \in \mathbb{N}_0$, being $\rho_i(t)$ and $\delta_i(t)$ in (7.13) the errors due to sampling. Following [158], Taylor's expansion leads to

$$e_i(t-h) = e_i(t) - \dot{e}_i(t)h - \kappa_i(t), \tag{7.14}$$

being $\kappa_i(t) = \int_{t-h}^{t}(t-h-s)\ddot{e}_i(s)\,ds$. Therefore, the control input (7.11) can be, finally, re-written as:

$$\begin{aligned} u_i^V(t) =& K_1 \sum_{j\in\mathscr{N}_i^c} a_{ij}(\tilde{x}_i - \tilde{x}_j) + K_2 \sum_{j\in\mathscr{N}_i^c} a_{ij}(\rho_i - \rho_j) \\ &+ \bar{k}_d \sum_{j\in\mathscr{N}_i^c} (\kappa_i + \delta_i - \kappa_j - \delta_j), \end{aligned} \tag{7.15}$$

with $K_1 = [\bar{k}_p \;\; \bar{k}_d \;\; \bar{k}_i] \in \mathbb{R}^{1\times 3}$ and $K_2 = [\bar{k}_p \;\; 0 \;\; \bar{k}_i] \in \mathbb{R}^{1\times 3}$.
Given (7.1), (7.4) and (7.15), the closed-loop single DG dynamics can be derived as:

$$\begin{aligned} \dot{\tilde{x}}_i(t) =& \mathscr{A} \sum_{j\in\mathscr{N}_i^c} a_{ij}(\tilde{x}_i - \tilde{x}_j) + BK_2 \sum_{j\in\mathscr{N}_i^c} a_{ij}(\rho_i - \rho_j) \\ &+ B\bar{k}_d \sum_{j\in\mathscr{N}_i^c} a_{ij}(\kappa_i + \delta_i - \kappa_j - \delta_j) + B(w_i - w_j), \end{aligned} \tag{7.16}$$

where $\mathscr{A} = A + BK_1$, being matrices A and B defined in (7.3). To describe the overall MG network, define the following enlarged vector as

$$\begin{aligned} &\eta(t) = [\tilde{x}_1^\top(t), \tilde{x}_2^\top(t), \ldots, \tilde{x}_N^\top(t)] \in \mathbb{R}^{3N}, \quad \theta(t) = [\kappa_1(t), \kappa_2(t), \ldots, \kappa_N(t)] \in \mathbb{R}^N, \\ &\bar{\rho}(t) = [\rho_1^\top(t), \rho_2^\top(t), \ldots, \rho_N^\top(t)] \in \mathbb{R}^{3N}, \quad \bar{\delta}(t) = [\delta_1(t), \delta_2(t), \ldots, \delta_N(t)] \in \mathbb{R}^N, \\ &\dot{\zeta}(t) = [\dot{e}_1(t), \dot{e}_2(t), \ldots, \dot{e}_N(t)] \in \mathbb{R}^N, \quad \bar{\zeta}(t) = [\bar{e}_1(t), \bar{e}_2(t), \ldots, \bar{e}_N(t)] \in \mathbb{R}^N, \\ &\bar{w}(t) = [w_1(t), w_2(t), \ldots, w_N(t)] \in \mathbb{R}^N. \end{aligned} \tag{7.17}$$

Hence, the closed-loop dynamics of the entire MG network under the action of sampled-data PID controller (7.15) can be obtained:

$$\dot{\eta}(t) = \Phi\eta(t) + A_1\bar{\rho}(t) + A_2(\theta(t) + \bar{\delta}(t)) + D\bar{w}(t) \tag{7.18}$$

being $\Phi = (I_N \otimes A) + (\mathscr{H} \otimes BK_1) \in \mathbb{R}^{3N\times 3N}$, $A_1 = (\mathscr{H} \otimes BK_1) \in \mathbb{R}^{3N\times 3N}$, $A_2 = (\mathscr{H} \otimes B\bar{k}_d) \in \mathbb{R}^{3N\times 3N}$ and $D = (I_N \otimes B) \in \mathbb{R}^{3N\times 3N}$, with $\mathscr{H} = \mathscr{L} + \mathscr{P}$, where $\mathscr{L}$ and $\mathscr{P}$ are the Laplacian and Pinning matrices, respectively. Furthermore, Φ is a block matrix defined as

$$\Phi = (I_N \otimes A) + (H \otimes BK_1) = \begin{bmatrix} \Phi_{11} & \Phi_{12} & \dots & \Phi_{1N} \\ \Phi_{21} & \Phi_{22} & \dots & \Phi_{2N} \\ \vdots & \dots & \ddots & \vdots \\ \Phi_{N1} & \Phi_{N2} & \dots & \Phi_{NN} \end{bmatrix}, \tag{7.19}$$

being

$$\Phi_{ii} = \begin{bmatrix} 0 & 1 & 0 \\ -\frac{\Delta_i}{k_{v_i}}\bar{k}_p & -\frac{\Delta_i}{k_{v_i}}\bar{k}_d & -\frac{\Delta_i}{k_{v_i}}\bar{k}_i \\ 1 & 0 & 0 \end{bmatrix}, \quad \Phi_{ij} = \begin{bmatrix} 0 & 0 & 0 \\ -\frac{a_{ij}}{k_{v_i}}\bar{k}_p & -\frac{a_{ij}}{k_{v_i}}\bar{k}_d & -\frac{a_{ij}}{k_{v_i}}\bar{k}_i \\ 0 & 0 & 0 \end{bmatrix} \tag{7.20}$$

with Δ_i the i-th element of the degree matrix (see Section 3.2). Note that, the closed-loop system of the whole MG network under the action of PID controller (7.6) takes the form

$$\dot{\eta}(t) = \Phi\eta(t) + D\bar{w}(t). \tag{7.21}$$

A useful lemma that will be instrumental for the proof of Theorem 6 is presented.

Lemma 1. *Consider the closed-loop system in (7.21) and assume the leader agent to be globally reachable in $\mathscr{G}^c_{N+1}$. Given a decay rate $\bar{\alpha} > 0$, by selecting the control gains such that the matrix Φ is Hurwitz, i.e.*

$$\bar{k}_d > 0, \qquad \bar{k}_i > 0, \qquad \bar{k}_p > \max_i \left\{ \frac{\bar{k}_i k_{v_i}}{\bar{k}_d \Delta_i} \right\}, \tag{7.22}$$

if there exist a positive definite matrix $P \in \mathbb{R}^{3N\times 3N}$ and a positive constant γ such that

$$\begin{bmatrix} P\Phi + \Phi^\top P + \bar{\alpha}P + I & PD \\ \star & -\gamma^2 I \end{bmatrix} < 0, \tag{7.23}$$

the PID controller (7.5) exponentially stabilizes the closed-loop system (7.21).

Proof. Consider the Lyapunov function $V = \eta^\top(t)P\eta(t)$ and the disturbance attenuation index

$$J = \int_0^\infty [\eta^\top(s)\eta(s) - \gamma^2\bar{w}^\top(s)\bar{w}(s)]ds.$$

Following the analytical steps in [168], LMI in (7.23) is obtained. Note that this LMI is feasible when the matrix Φ is Hurwitz. To this aim, control gains in (7.5) have to be selected such that $\Phi < 0$. Specifically, since the leader is globally reachable, by construction, Φ is negative definite if each main diagonal block Φ_{ii} in (7.20) is a negative definite matrix, $\forall i = 1, \dots, N$ [169]. Therefore, by computing the characteristic equation of the matrix Φ_{ii} as $det(\lambda I_{3\times 3} - \Phi_{ii}) = \lambda^3 + \lambda^2 \frac{\Delta_i}{k_{v_i}} \bar{k}_d + \lambda \frac{\Delta_i}{k_{v_i}} \bar{k}_p + \frac{\Delta_i}{k_{v_i}} \bar{k}_i$, by applying Routh-Hurwitz criterion [170] and by setting the control gains as in (7.22), the exponential stability of the closed-loop system (7.21) is ensured. □

In the sequel, it will be proven that, if system (7.21) is exponentially stable with a decay rate $\bar{\alpha} > 0$, then the closed-loop MG (7.18) is exponentially stable with a decay rate $\alpha \in (0, \bar{\alpha})$ and a small enough $h > 0$.

Theorem 6. *Let control gains $\bar{k}_p, \bar{k}_i$ and $\bar{k}_d$ to be chosen according to Lemma 1 and consider the closed-loop MG network as in (7.18) under the action of sampled-data PID controller in (7.11). Given tuning parameters $h > 0$ and $\alpha \in (0, \bar{\alpha})$, if there exist positive definite symmetric matrices $P \in \mathbb{R}^{3N\times 3N}$, $S \in \mathbb{R}^{3N\times 3N}$, $W \in \mathbb{R}^{N\times N}$, $Q \in \mathbb{R}^{N\times N}$, $R \in \mathbb{R}^{N\times N}$, free matrices $M \in \mathbb{R}^{3N\times 3N}$, $T \in \mathbb{R}^{3N\times 3N}$ and a weighted L_2 gain $\gamma > 0$ satisfying*

$$\begin{bmatrix} P\Phi+\Phi^\top P+2\alpha P & -(T^\top-P)A_1 & -(T^\top-P)A_2 & -(T^\top-P)A_2 & -(T^\top-P)D & T^\top-\Phi^\top M \\ \star & -\frac{\pi^2}{4}S & 0 & 0 & 0 & -A_1^\top M \\ \star & \star & -\frac{\pi^2 h^2}{4}Q & 0 & 0 & -A_2^\top M \\ \star & \star & \star & -e^{-2\alpha h}R & 0 & -A_2^\top M \\ \star & \star & \star & \star & -\gamma I & -D^\top M \\ \star & \star & \star & \star & \star & \Psi+M^\top \end{bmatrix} < 0, \tag{7.24}$$

where

$$\Psi = h^2 e^{2\alpha h} S + \begin{bmatrix} 0 & 0 & 0 \\ 0 & h^2(e^{2\alpha h}Q+\frac{1}{4}R) & 0 \\ 0 & 0 & 0 \end{bmatrix}, \tag{7.25}$$

then, voltage consensus is exponentially achieved under distributed sampled-data PID controller (7.11).

Proof. Consider the following Lyapunov-Krasovskii functional:

$$V = V_1 + V_2 + V_3 + V_4 + V_5, \tag{7.26}$$

where

$$
\begin{aligned}
V_1 &= \eta^\top P \eta, \\
V_2 &= h^2 e^{2\alpha h} \int_{t_k}^{t} e^{-2\alpha(t-s)} \dot{\eta}(s)^\top S \dot{\eta}(s)\, ds - \frac{\pi^2}{4} \int_{t_k}^{t} e^{-2\alpha(t-s)} \bar{\rho}^\top(s) S \bar{\rho}(s)\, ds, \\
V_3 &= \int_{t_k}^{t} e^{-2\alpha(t-s)} \dot{\bar{\zeta}}^\top(s) W \dot{\bar{\zeta}}(s)\, ds - \frac{\pi^2}{4} \int_{t_k}^{t} e^{-2\alpha(t-s)} \bar{\delta}^\top(s) W \bar{\delta}(s)\, ds, \\
V_4 &= h^2 e^{2\alpha h} \int_{t-h}^{t} e^{-2\alpha(t-s)} \frac{s-t+h}{h} \ddot{\zeta}^\top(s) Q \ddot{\zeta}(s)\, ds, \\
V_5 &= \int_{t-h}^{t} e^{-2\alpha(t-s)} \frac{(s-t+h)^2}{4} \ddot{\zeta}^\top(s) R \ddot{\zeta}(s)\, ds.
\end{aligned}
\tag{7.27}
$$

Note that, Lemma 5 ensures that V_2 and V_3 defined in (7.26)-(7.27) are such that $V_2 \geq 0$ and $V_3 \geq 0$. By differentiating V along the trajectories of the closed-loop system in (7.18), it follows:

$$
\begin{aligned}
\dot{V}_1 &= \eta^\top (P\Phi + \Phi^\top P)\eta + 2\eta^\top P D \bar{w} + 2\eta^\top P A_1 \bar{\rho} + 2\eta^\top P A_2 (\theta + \bar{\delta}), \\
\dot{V}_2 &= -2\alpha V_2 + h^2 e^{2\alpha h} \dot{\eta}^\top S \dot{\eta} - \frac{\pi^2}{4} \bar{\rho}^\top S \bar{\rho}, \\
\dot{V}_3 &= -2\alpha V_3 + \dot{\bar{\zeta}}^\top W \dot{\bar{\zeta}} - \frac{\pi^2}{4} \bar{\delta}^\top W \bar{\delta}, \\
\dot{V}_4 &= -2\alpha V_4 + h^2 e^{2\alpha h} \ddot{\zeta}^\top Q \ddot{\zeta} - e^{2\alpha h} h \int_{t-h}^{t} e^{-2\alpha(t-s)} \ddot{\zeta}^\top(s) Q \ddot{\zeta}(s)\, ds, \\
\dot{V}_5 &= -2\alpha V_5 + \frac{h^2}{4} \ddot{\zeta}^\top R \ddot{\zeta} - \frac{1}{2} \int_{t-h}^{t} e^{-2\alpha(t-s)} (s-t+h) \ddot{\zeta}^\top(s) R \ddot{\zeta}(s)\, ds.
\end{aligned}
\tag{7.28}
$$

By applying Jensen inequality as in Lemma 4 with $\rho \equiv 1$ and $\rho \equiv s-t+h$ on the integral terms in $\dot{V}_4$ and $\dot{V}_5$ respectively, it results:

$$
\dot{V}_4 \leq -2\alpha V_4 + h^2 e^{2\alpha h} \ddot{\zeta}^\top Q \ddot{\zeta} - \Big(\int_{t-h}^{t} \ddot{\zeta}(s)\, ds \Big)^\top Q \Big(\int_{t-h}^{t} \ddot{\zeta}(s)\, ds \Big),
$$

$$\begin{aligned}\dot{V}_5 \leq -2\alpha V_5 + \frac{h^2}{4}\ddot{\zeta}^\top R\ddot{\zeta} - e^{-2\alpha h}\Big(\int_{t-h}^{t}(s-t+h)\ddot{\zeta}(s)\,ds\Big)^\top R \\ \times\Big(\int_{t-h}^{t}(s-t+h)\ddot{\zeta}(s)\,ds\Big) = -2\alpha V_5 + \frac{h^2}{4}\ddot{\zeta}^\top R\ddot{\zeta} - e^{-2\alpha h}\theta^\top R\theta.\end{aligned} \tag{7.29}$$

Since equation (7.14) can be written in vector form by using the enlarged vector in (7.17) as $\bar{\zeta} = \dot{\zeta} + \theta$, by differentiating this latter, it yields $\int_{t-h}^{t}\ddot{\zeta}(s)\,ds = h\dot{\bar{\zeta}}$. The exploitation of this latter relation for the integral term of $\dot{V}_4$ in (7.2.1) leads to

$$\dot{V}_4 \leq -2\alpha V_4 + h^2 e^{2\alpha h}\ddot{\zeta}^\top Q\ddot{\zeta} - h^2\dot{\bar{\zeta}}^\top Q\dot{\bar{\zeta}}. \tag{7.30}$$

Summing-up $\dot{V}_1$, $\dot{V}_2$ and $\dot{V}_3$ in (7.28), $\dot{V}_4$ in (7.30) and $\dot{V}_5$ in (7.2.1), it follows:

$$\begin{aligned}\dot{V} \leq & \eta^\top(P\Phi + \Phi^\top P + 2\alpha P)\eta + 2\eta^\top PD\bar{w} + 2\eta^\top PA_1\bar{\rho} + 2\eta^\top PA_2(\theta+\bar{\delta}) \\ & + h^2 e^{2\alpha h}\dot{\eta}^\top S\dot{\eta} - \frac{\pi^2}{4}\bar{\rho}^\top S\bar{\rho} - \frac{\pi^2 h^2}{4}\bar{\delta}^\top Q\bar{\delta} + h^2 e^{2\alpha h}\ddot{\zeta}^\top Q\ddot{\zeta} + \frac{h^2}{4}\ddot{\zeta}^\top R\ddot{\zeta} \\ & - e^{-2\alpha h}\theta^\top R\theta - 2\alpha V.\end{aligned} \tag{7.31}$$

By adding the null term $\gamma\bar{w}^\top\bar{w} - \gamma\bar{w}^\top\bar{w}$ and introducing the augmented vector $\chi^\top = [\eta^\top \quad \bar{\rho}^\top \quad \bar{\delta}^\top \quad \theta^\top \quad \bar{w}^\top] \in \mathbb{R}^{9N\times 9N}$, inequality (7.31) can be presented in a more compact form as

$$\dot{V} \leq -2\alpha V + \chi^\top\Omega\chi + \dot{\eta}^\top\Psi\dot{\eta} + \gamma\bar{w}^\top\bar{w}, \tag{7.32}$$

being $\Psi \in \mathbb{R}^{3N\times 3N}$ as defined in (7.25) and

$$\Omega = \begin{bmatrix} P\Phi+\Phi^\top P+2\alpha P & PA_1 & PA_2 & PA_2 & PD \\ \star & -\frac{\pi^2}{4}S & 0 & 0 & 0 \\ \star & \star & -\frac{pi^2 h^2}{4}Q & 0 & 0 \\ \star & \star & \star & -e^{-2\alpha h}R & 0 \\ \star & \star & \star & \star & -\gamma I \end{bmatrix} \in \mathbb{R}^{9N\times 9N}, \tag{7.33}$$

Now, the descriptor method leads to [97]:

$$\Big(\dot{\eta}^\top M^\top + \eta^\top T^\top\Big)\Big(\dot{\eta} - \Phi\eta - D\bar{w} - A_1\bar{\rho} - A_2(\theta+\bar{\delta})\Big) = 0 \tag{7.34}$$

being $M, T \in \mathbb{R}^{3N \times 3N}$ free matrices. Summing the null term (7.34) to the right-side of inequality (7.32) and denoting $\bar{\chi}^\top = [\chi^\top \quad \dot{\eta}^\top]^\top \in \mathbb{R}^{12N}$, it follows:

$$\dot{V} \leq -2\alpha V + \bar{\chi}^\top \Omega' \bar{\chi} + \gamma \bar{w}^\top \bar{w}, \tag{7.35}$$

with $\Omega' \in \mathbb{R}^{12N \times 12N}$ the matrix defined in (7.24). Therefore, if LMIs in (7.24) holds, then closed-loop system in (7.18) is exponential stable with a decay rate α and a L_2 gain γ. □

7.2.2 Numerical Analysis

In this section, the proposed distributed-sampled data PID controller (7.11) is validated in a $220V_{RMS}$, $50[Hz]$ islanded MG consisting of four DGs and four respective loads, whose parameters are as in [23]. The communication topology is chosen such that globally reachability property of DG_0 is satisfied, i.e. $\mathscr{E}^c_{N+1} = \{(0,1),(1,2),(1,3),(2,3),(1,4),(3,4)\}$. To consider a more realistic scenario, the frequency SC is the one proposed in [13]. The numerical simulations are carried out by exploiting Matlab/Simulink platform and the Runge-Kutta fixed step solver with sampling time $T_s = 0.5 \times 10^{-3}$, while Yalmip Toolbox with SeDuMi solver is exploited to solve LMIs problem defined in Lemma 1 and in Theorem 6. The computed continuous-time PID control gains as in (7.5) are $\bar{k}_p = 350$, $\bar{k}_i = 110$ and $\bar{k}_d = 80$. The LMIs in Theorem 6 are feasible for $\alpha = 0.4 \in (0, \bar{\alpha})$, with $\bar{\alpha} = 0.6$ and $h = 0.002$, thus providing a weighted L_2 gain $\gamma = 0.79941$. This leads to the control gains in (7.9) $k_p = 40350$, $k_i = 110$ and $k_d = -4000$. To show the effectiveness of the proposed distributed sampled-data PID controller in guaranteeing successfully resolution of voltage regulation problem, while counteracting references changes and load variation, a time interval of 40 $[s]$ is considered, where a troublesome scenario is performed. Specifically, at the startup SC references value are $v_0 = 220[V_{RMS}]$ and $\omega_0 = 2\pi 50$ $[rad/s]$, until they change at $t = 15[s]$ with $v_0 = 225$ $[V_{RMS}]$ and at $t = 20[s]$ with $\omega_0 = 2\pi 50.2$ $[rad/s]$, respectively. In the meantime, DG_3 is unplugged at $t = 8[s]$ and plugged-in at $t = 17[s]$. Moreover, at $t = 25[s]$, the load 4 is removed, while at $t = 30[s]$ the SC voltage set-point changes at $v_0 = 220[V_{RMS}]$. Finally, load 4 is re-added at $t = 35[s]$.
Results in Figure 7.2 disclose the robustness of the distributed sampled-

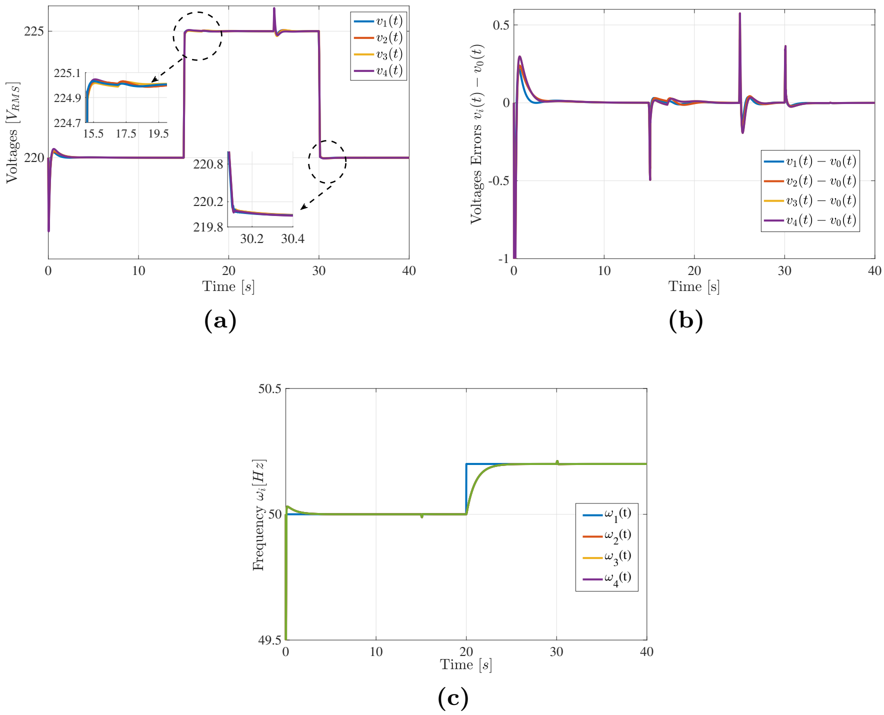

Figure 7.2. Robust Voltage Regulation via distributed sampled-data PID controller with $h = 0.002$. Time history of: a) voltage $v_i(t)[V_{RMS}]$, $i = 1, \ldots, 4$; b) voltage errors $v_i(t) - v_0(t)$, $i = 1, \ldots, 4$; c) frequencies with control input as in [13] $\omega_i(t)[Hz]$ $i = 1, \ldots, 4$.

data PID control strategy in guaranteeing the voltages restoration with small transient time despite the presence of unavoidable deviations due to primary control, references variations, as well as under the plug-and-play functionality of DGs within the MG. More specifically, Figure 7.2(a) highlights the robustness of the proposed strategy in ensuring that all DGs voltage track the reference behavior as imposed by the virtual DG_0, while small-acceptable errors can be seen when load/references variations, as well as plug-and-play events of $DG3$, occur (see Figure 7.2). Note that, although, due to plug-and-play operation, all the connection attached to DG_3, i.e. DG_1, DG_2, DG_4 are lost, the proposed control strategy is able

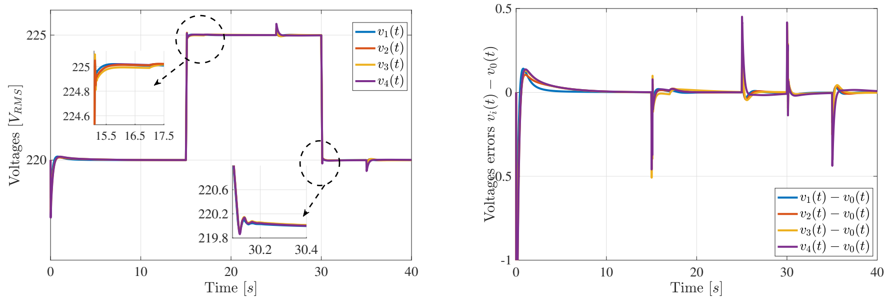

(a) **(b)**

Figure 7.3. Robust Voltage Regulation via distributed PID controller (7.5). Time history of: a) voltage $v_i(t)[V_{RMS}]$, $i = 1, \dots, 4$; b) voltage errors $v_i(t) - v_0(t)$, $i = 1, \dots, 4$.

to regulate DGs voltages with zero steady state errors and small transient time (see Figure 7.2(a)-(b)). For the sake of completeness, Figure 7.2(c) discloses the time history of DGs frequency with distributed control action in [13]. The similar performances of the distributed continuous-time PID controller in (7.5) are also shown in Figure 7.3. However, sampled-data PID controller (7.11) requires to transmit $\lfloor 40/h \rfloor + 1 = 20001$ control signals during $40[s]$ of simulation, thus reducing the total amount of transmitted signal by almost 75%.

7.3 Synchronization of Multi-Agent Systems under Time-Varying Network via Time-Delay Approach to Averaging

Consider a MASs consisting of N dynamical agents plus a leader, interconnected via a communication network. The dynamics of the leader and followers are given as the following delayed differential equations:

$$\dot{x}_0(t) = Ax_0(t) + A_d x_0(t - h_1(t)), \tag{7.36}$$

$$\dot{x}_i(t) = Ax_i(t) + A_d x_i(t - h_1(t)) + Bu_i(t - h_2(t)) + w_i(t), \tag{7.37}$$

where $x_0 \in \mathbb{R}^{n\times 1}$ and $x_i(t) \in \mathbb{R}^{n\times 1}$ are the leader and ith follower state, respectively, while $w_i(t) \in \mathbb{R}^{n\times 1}$ represents the external disturbance acting on the ith agent dynamics and assumed to be locally essentially bounded, i.e. $\sup_{[0,t]} |w(t)| < +\infty$, $\forall t \geq 0$. Moreover, A, $A_d \in \mathbb{R}^{n\times n}$ and $B \in \mathbb{R}^{n\times 1}$ are known matrices, while $u_i(t - h_2(t))$ stands for the delayed control input of agent i. Time-varying piecewise continuous functions $h_1(t)$ and $h_2(t)$ denote the unknown state and input delays, respectively, which are assumed to be bounded, i.e., $0 < h_1(t) \leq d_1$, $0 < h_2(t) \leq d_2$, with $d_1 > d_2$.
In the sequel, a periodic switching communication network is considered for the MAS (7.36)-(7.37), which is properly orchestrated via a time-dependent switching control signal $\sigma(\frac{t}{\epsilon})$ able to guarantee a periodic communication among agents. Hence, the resulting time-varying graph can be modeled as $\mathscr{G}_{N+1}(\frac{t}{\epsilon})\{\mathscr{V}_{N+1}(\frac{t}{\epsilon}), \mathscr{E}_{N+1}(\frac{t}{\epsilon})\}$, with time-varying Laplacian and Pinning matrices, i.e. $\mathscr{L}(\frac{t}{\epsilon})$, $\mathscr{P}(\frac{t}{\epsilon})$ such that $\mathscr{H}(\frac{t}{\epsilon}) = \mathscr{L}(\frac{t}{\epsilon}) + \mathscr{P}(\frac{t}{\epsilon})$. Moreover, different from [171], it is only required the uniform connectivity on average according to Definition 8, which does not imply the connectivity of the network $\forall t \geq 0$.
Based on the above considerations, the aim of this section is twofold: i) achieve the practical leader-tracking consensus by guaranteeing that the error trajectories $e_i(t) = x_i(t) - x_0(t)$ of each agent i with respect to the leader converge to a certain small enough ball $\mathscr{X}_\rho$, with ρ its radius, i.e., $\inf_{y\in\mathscr{X}_\rho} \|e_i(t) - y\| \to 0$, $\forall i$ as $t \to \infty$, being $y \in \mathscr{X}_\rho$, in the presence of both non-small state and input delays $h_1(t)$ and $h_2(t)$, respectively, as well as the time-varying graph $\mathscr{G}(\frac{t}{\epsilon})$ [172]; ii) find upper bound $\epsilon^\star > 0$ on ϵ, which shows how rapidly the network should be switched among different M communication topologies (even disconnected), each of them identified via an indicator function $\chi_s = \chi[(k + \sum_{r=1}^{s-1} \beta_r)\epsilon, (k + \sum_{r=1}^{s} \beta_r)\epsilon)$, $\forall s = 1, \ldots, M$, with $\sum_{s=1}^{M} \chi_s(\tau) = 1$, $k = 0, 1, \ldots$ and $\tau = \frac{1}{\epsilon}$, preserving control objective i). Control objectives i) and ii) are achieved via the following fully distributed control input:

$$u_i(t - h_2(t)) = K \sum_{j=0}^{N} a_{ij_{\sigma(\frac{t}{\epsilon})}} (x_i(t - h_2(t)) - x_j(t - h_2(t))), \tag{7.38}$$

where K is the control gain vector, $\sigma(\frac{t}{\epsilon})$ is the time-dependent switching role such that $\sigma : \mathbb{R}_{\geq 0} \to \mathscr{I} = \{1, 2, \ldots, M\}$ and $a_{ij_{\sigma(\frac{t}{\epsilon})}} = a_{ij}(\frac{t}{\epsilon})$ is the element of the adjacency matrix that accounts for the presence of a communication link between agent i and j and referring to the time varying graph $\mathscr{G}(\frac{t}{\epsilon})$, which switches faster than $\mathscr{G}(t)$.
Note that, compared with [165], time-delay approach to averaging as in [40] leads to LMI-based ISS conditions for the MASs (7.36)-(7.37) under control input (7.38), whose solution allows finding bounds $\epsilon^\star > 0$, d_1 and d_2 on ϵ, $h_1(t)$ and $h_2(t)$, respectively, preserving ISS for all $\epsilon \in (0, \epsilon^\star]$, $h_1(t) \in [0, d_1]$, $h_2(t) \in [0, d_2]$ and a small enough decay rate $\alpha > 0$, which seems to be not possible via classical averaging theory from [144].
By considering (7.36)-(7.37), $\forall i = 1, \ldots, N$, define the error of each agent i with respect to leader dynamics as $e_i(t) = x_i(t) - x_0(t) \in \mathbb{R}^{n\times 1}$. By differentiating $e_i(t)$ and taking into account (7.38), the following ith closed-loop error system is obtained:

$$\begin{aligned} \dot{e}_i(t) &= Ae_i(t) + A_d e_i(t - h_1(t)) + w_i(t) \\ &\quad + BK \sum_{j=0}^{N} a_{ij}(\tfrac{t}{\epsilon})(e_i(t - h_2(t)) - e_j(t - h_2(t))). \end{aligned} \tag{7.39}$$

By introducing augmented vectors $\tilde{x}(t) = [e_1^\top(t), e_2^\top(t), \ldots, e_N^\top(t)] \in \mathbb{R}^{Nn}$ and $\tilde{w}(t) = [w_1^\top(t), w_2^\top(t), \ldots, w_N^\top(t)] \in \mathbb{R}^{Nn}$, the following closed-loop MASs system results to be:

$$\dot{\tilde{x}}(t) = \tilde{A}\tilde{x}(t) + \tilde{A}_d\tilde{x}(t - h_1(t)) + \tilde{w}(t) + D(\tfrac{t}{\epsilon})\tilde{x}(t - h_2(t)), \tag{7.40}$$

with $\tilde{A} = (I_N \otimes A)$, $\tilde{A}_d = (I_N \otimes A_d)$ and the $T = 1$-periodic $D(\frac{t}{\epsilon}) = (\mathscr{H}(\frac{t}{\epsilon}) \otimes BK)$. The following assumptions hold.

Assumption 7. *According to Definition 8, the graph $\mathscr{G}_{N+1}(\frac{t}{\epsilon})$ is connected on average.*

Remark 15. *Uniformly connected on average networks include periodic ones. In this case, $\mathscr{L}_{av} = \frac{1}{T}\int_0^T \mathscr{L}(\tau)\, d\tau$, with T the period of the network. Let $T_s = \epsilon\beta_s$ be the length of time during one period for which $\sigma(\frac{t}{\epsilon}) = s$. Then, $\mathscr{L}_{av} = \frac{1}{T}\sum_s \mathscr{L}_s T_s = \sum_s \beta_s \mathscr{L}_s$ where, by definition, $\beta_s = \frac{T_s}{T}$ and $\sum_s \beta_s = 1$ [166].*

Assumption 8. *Let Assumption 7 holds. Furthermore, it holds*

$$\frac{1}{\epsilon}\int_{t-\epsilon}^{t} D(\tfrac{s}{\epsilon}) = D_{av} + \Delta D(\tfrac{t}{\epsilon}), \qquad \|\Delta D(\tfrac{t}{\epsilon})\| \leq \sigma_D, \quad \forall \tfrac{t}{\epsilon} \geq 1,$$

with constant matrix $D_{av} = (\mathscr{H}_{av} \otimes BK)$ and small enough $\sigma_D > 0$. Matrix $\Delta D(\frac{t}{\epsilon}) = (\Delta\mathscr{H}(\frac{t}{\epsilon}) \otimes BK)$ stands for communication topology uncertainties due to possible communication link failures, whose norm is upper bounded by constant σ_D.

Given $\mathscr{H}_s = \mathscr{L}_s + \mathscr{P}_s$, $\forall s = 1, \dots, M$, describing all the communication topologies activating on the periodic time-interval $[k\epsilon, (k+1)\epsilon]$, $k \in \mathbb{Z}^+$, each of them with a duration period of β_s, $s \in \mathscr{I}$, system (7.40) can be presented as

$$\dot{\tilde{x}}(t) =$$
$$\begin{cases} \tilde{A}\tilde{x}(t) + \tilde{A}_d\tilde{x}(t-h_1(t)) + \tilde{w}(t) + D_1\tilde{x}(t-h_2(t)), \quad t \in [k\epsilon, (k+\beta_1)\epsilon) \\ \tilde{A}\tilde{x}(t) + \tilde{A}_d\tilde{x}(t-h_1(t)) + \tilde{w}(t) + D_2\tilde{x}(t-h_2(t)), t \in [(k+\beta_1)\epsilon, (k+\sum_{s=1}^{2}\beta_s)\epsilon) \\ \qquad\qquad\vdots \\ \tilde{A}\tilde{x}(t) + \tilde{A}_d\tilde{x}(t-h_1(t)) + \tilde{w}(t) + D_M\tilde{x}(t-h_2(t)), t \in [(k+\sum_{s=1}^{M-1}\beta_s)\epsilon, (k+1)\epsilon). \end{cases} \tag{7.41}$$

From (7.41), $D(\tau)$ in (7.40) can be expressed as a convex combination of constant matrices $D_s = \mathscr{H}_s \otimes BK$, i.e.,

$$D(\tau) = \sum_{s=1}^{M} \chi_s(\tau) D_s, \quad \tau \in [k\epsilon, (k+1)\epsilon), \; k = 0, 1, \dots, \tag{7.42}$$

where $\chi_s(\tau)$ is the indicator function of the time interval $[(k+\sum_{r=1}^{s-1}\beta_r)\epsilon, (k+\sum_{r=1}^{s}\beta_r)\epsilon)$, $\forall s = 1, \dots, M$, such that $\sum_{s=1}^{M}\chi_s(\tau) = 1$. Following time-delay procedure [46], let consider the following notation:

$$f(\tfrac{t}{\epsilon}) = D(\tfrac{t}{\epsilon})x(t-h_2(t)), \qquad G(\tfrac{t}{\epsilon}) = \frac{1}{\epsilon}\int_{t-\epsilon}^{t} (s-t+\epsilon) f(\tfrac{t}{\epsilon})\, ds. \tag{7.43}$$

Moreover, the following holds:

$$\begin{aligned}
&\tfrac{1}{\epsilon}\int_{t-\epsilon}^{t} \dot{\tilde{x}}(s)\,ds = \tfrac{1}{\epsilon}[x(t)-x(t-\epsilon)] = \tfrac{d}{dt}[x(t)-G(t) \\
&-\tfrac{1}{\epsilon}\tilde{A}\int_{t-\epsilon}^{t}(s-t+\epsilon)\tilde{x}(s)\,ds - \tfrac{1}{\epsilon}\tilde{A}_d\int_{t-\epsilon}^{t}(s-t+\epsilon)\tilde{x}(s-h_1(s))\,ds \\
&-\tfrac{1}{\epsilon}\int_{t-\epsilon}^{t}(s-t+\epsilon)\tilde{w}(s)\,ds] \qquad (7.44) \\
&= \tfrac{d}{dt}[x(t)-G(t)] + \tfrac{1}{\epsilon}\tilde{A}\int_{t-\epsilon}^{t}\tilde{x}(s)\,ds - \tilde{A}\tilde{x}(t) - \tilde{A}_d\tilde{x}(t-h_1(t)) \\
&+\tfrac{1}{\epsilon}\tilde{A}_d\int_{t-\epsilon}^{t}\tilde{x}(s-h_1(s))\,ds + \tfrac{1}{\epsilon}\int_{t-\epsilon}^{t}\tilde{w}(s)\,ds - \tilde{w}(t).
\end{aligned}$$

Integrating (7.40) on $[t-\epsilon, t]$, for $t \geq \epsilon + d_1$ and denoting $z(t) = \tilde{x}(t) - G(t)$, it yields:

$$\dot{z}(t) = \tilde{A}\tilde{x}(t) + \tilde{A}_d\tilde{x}(t-h_1(t)) + \tfrac{1}{\epsilon}\int_{t-\epsilon}^{t} D(\tfrac{s}{\epsilon})\tilde{x}(s-h_2(s))\,ds + \tilde{w}(t). \quad (7.45)$$

Under Assumption 8, integral term in (7.45) can be presented as

$$\begin{aligned}
&\tfrac{1}{\epsilon}\int_{t-\epsilon}^{t} D(\tfrac{s}{\epsilon})[\tilde{x}(s-h_2(s)) + \tilde{x}(t) - \tilde{x}(t)]\,ds = \tfrac{1}{\epsilon}\int_{t-\epsilon}^{t} D(\tfrac{s}{\epsilon})\,ds\tilde{x}(t) \\
&\quad -\tfrac{1}{\epsilon}\int_{t-\epsilon}^{t} D(\tfrac{s}{\epsilon})[\tilde{x}(t) - \tilde{x}(s-h_2(s))]\,ds = (D_{av} + \Delta D(\tfrac{t}{\epsilon}))\tilde{x}(t) - Y(t),
\end{aligned} \quad (7.46)$$

being

$$Y(t) = \tfrac{1}{\epsilon}\int_{t-\epsilon}^{t} D(\tfrac{s}{\epsilon})\int_{s-h_2(s)}^{t}\dot{\tilde{x}}(\theta)\,d\theta\,ds. \quad (7.47)$$

In doing so, (7.45) can be rewritten as follows:

$$\dot{z}(t) = (\Phi + \Delta D(\tfrac{t}{\epsilon}))\tilde{x}(t) + \tilde{A}_d\tilde{x}(t-h_1(t)) - Y(t) + \tilde{w}(t), \quad t \geq \epsilon \quad (7.48)$$

with $\Phi = \tilde{A} + D_{av}$.

Assumption 9. *Matrices* $\Phi + \tilde{A}_d$ *are Hurwitz.*

Note that, system in (7.48) with $\dot{\tilde{x}}$ defined by the righ-hand side of (7.40) is a kind of neutral type system (i.e., Hale's form of neutral differential equations [97, 173]). If $\tilde{w} = 0$ and $\Delta D = 0$, (7.48) can be considered as a $\mathscr{O}(\epsilon)$ perturbation of the averaged system

$$\dot{\tilde{x}}_{av} = \Phi\tilde{x}_{av}(t) + \tilde{A}_d\tilde{x}_{av}(t - h_1(t)), \tag{7.49}$$

due to the presence of additional terms $G(t)$ and $Y(t)$.
Since if the function $\tilde{x}(t)$ is a solution of (7.40), then it satisfies also time-delay system (7.48) [40], it follows that ISS of time-delay system (7.48) ensures the ISS of the original closed-loop MAS network (7.40). Hence, in the sequel the Lyapunov-Krasovskii theory for time-delay systems is exploited in order to find conditions expressed as LMIs whose feasibility leads to upper bounds $\epsilon^\star$ on ϵ and d_1, d_2 on $h_1(t)$ and $h_2(t)$, respectively, preserving ISS of (7.48) for all $\epsilon \in (0, \epsilon^\star]$ and for a small enough decay rate $\alpha > 0$, as well as the fulfillment of control objectives i) and ii).

7.3.1 Input-to-State Stability

Here the ISS of neutral system (7.48) is analytically proven, thus implying the ISS of (7.40) under the action of the networked-based control law in (7.38).

Theorem 7. *Consider the closed-loop system in (7.40) obtained from (7.36)-(7.37) under the action of control law (7.38). Let Assumptions 7-9 hold and assume delays to be bounded, i.e.,* $0 < h_1(t) \le d_1$ *and* $0 < h_2(t) \le d_2$. *Given control gain vector* $K \in \mathbb{R}^{1\times n}$, *matrices* $\mathscr{H}_{av}$, $\mathscr{H}_s$, D_{av}, D_s, $s \in \mathscr{I}$ *and constants* $\sigma_D > 0$, $\alpha > 0$, $\epsilon^\star > 0$, $d_1 > 0$ *and* $d_2 > 0$, *let there exist* $Nn \times Nn$ *positive definite matrices* P, R, H, S_p, W_p, $p = 1, 2$ *and* $\bar{H}$, *matrices* $U_p \in \mathbb{R}^{Nn\times Nn}$ *and scalars* $\gamma > 0$, $\lambda > 0$ *that satisfy the following LMIs:*

$$\begin{bmatrix} P & -P \\ \star & P + e^{-2\alpha\epsilon^\star} R \end{bmatrix} \ge 0, \tag{7.50}$$

$$\begin{bmatrix} W_p & U_p \\ \star & W_p \end{bmatrix} \ge 0, \quad p = 1, 2 \tag{7.51}$$

$$\int_{\tau-1}^{\tau} (\zeta - \tau + 1 + \tfrac{d_2}{\epsilon}) D^\top(\zeta) H D(\zeta)\, d\zeta \leq \bar{H}, \tag{7.52}$$

$$\begin{bmatrix} \Omega & \begin{bmatrix} \begin{bmatrix} 0_{6Nn} \\ \sqrt{\epsilon^\star} D_s^\top R \\ 0_{6Nn} \end{bmatrix} & \begin{bmatrix} \sqrt{d_1}\tilde{A}^\top W_1 \\ 0_{3Nn} \\ \sqrt{d_1} D_s^\top W_1 \\ 0_{Nn} \\ \sqrt{d_1} D_s^\top W_1 \\ 0_{Nn} \\ \sqrt{d_1} W_1 \end{bmatrix} & \begin{bmatrix} \sqrt{d_2}\tilde{A}^\top W_2 \\ 0_{3Nn} \\ \sqrt{d_2} D_s^\top W_2 \\ 0_{Nn} \\ \sqrt{d_2} D_s^\top W_2 \\ 0_{Nn} \\ \sqrt{d_2} W_2 \end{bmatrix} & \begin{bmatrix} \sqrt{\epsilon^\star}\tilde{A}^\top W_2 \\ 0_{3Nn} \\ \sqrt{\epsilon^\star} D_s^\top W_2 \\ 0_{Nn} \\ \sqrt{\epsilon^\star} D_s^\top W_2 \\ 0_{Nn} \\ \sqrt{\epsilon^\star} W_2 \end{bmatrix} \end{bmatrix} \\ \star & \begin{bmatrix} -R & 0_{Nn\times Nn} & 0_{Nn\times Nn} & 0_{Nn\times Nn} \\ \star & -W_1 & 0_{Nn\times Nn} & 0_{Nn\times Nn} \\ \star & \star & -W_2 & 0_{Nn\times Nn} \\ \star & \star & \star & -\bar{H} \end{bmatrix} \end{bmatrix} < 0, \; \forall s \in \mathscr{I} \tag{7.53}$$

where Ω is the symmetric block matrix whose elements are given as

$$\begin{aligned}
&\Omega_{11} = P\Phi + \Phi^\top P + 2\alpha P + S_1 + S_2 + \lambda\sigma_D^2 I_n - \frac{1}{d_1}\rho_{d_1} W_1 - \frac{1}{d_2}\rho_{d_2} W_2, \\
&\Omega_{12} = -\Phi^\top P - 2\alpha P, \quad \Omega_{13} = \Omega_{24} = P, \quad \Omega_{14} = \Omega_{23} = -P, \\
&\Omega_{15} = P\tilde{A}_d + \frac{1}{d_1}\rho_{d_1}(W_1 - U_1), \quad \Omega_{16} = \frac{1}{d_1}\rho_{d_1} U_1, \quad \Omega_{17} = \frac{1}{d_2}\rho_{d_2}(W_2 - U_2), \\
&\Omega_{18} = \frac{1}{d_2}\rho_{d_2} U_2, \quad \Omega_{19} = -\Omega_{29} = P, \quad \Omega_{22} = -\frac{4}{\epsilon^\star}\rho_\epsilon R + 2\alpha P, \quad \Omega_{25} = -P\tilde{A}_d, \\
&\Omega_{33} = -\lambda I_n, \quad \Omega_{44} = -\frac{2}{\epsilon^\star}\rho_\epsilon \rho_{d_2} H, \quad \Omega_{55} = -\frac{1}{d_1}\rho_{d_1}(2W_1 - U_1 - U_1^\top), \\
&\Omega_{56} = -\frac{1}{d_1}\rho_{d_1}(W_1 - U_1), \quad \Omega_{66} = -\rho_{d_1}\left(S_1 + \frac{1}{d_1} W_1\right), \\
&\Omega_{77} = -\frac{1}{d_2}\rho_{d_2}(2W_2 - U_2 - U_2^\top), \quad \Omega_{78} = -\frac{1}{d_2}\rho_{d_2}(W_2 - U_2), \\
&\Omega_{88} = -\rho_{d_2}\left(S_2 + \frac{1}{d_2} W_2\right), \quad \Omega_{99} = -\gamma^2 I_N \quad \rho_{d_1} = e^{-2\alpha d_1}, \\
&\rho_{d_2} = e^{-2\alpha d_2}, \quad \rho_\epsilon = e^{-2\alpha\epsilon^\star}
\end{aligned} \tag{7.54}$$

and other blocks are assumed to be null matrices. Then, system (7.40) *is ISS for all $\epsilon \in (0, \epsilon^\star]$, $h_1(t) \in (0, d_1]$, $h_2(t) \in (0, d_2]$, a small enough decay rate $\alpha > 0$ and locally essentially bounded $\tilde{w}(t)$, meaning that practical leader tracking consensus is achieved and the solutions of* (7.40) *initialized* *by* $\phi \in W[-d_1, 0]$ *satisfy*

$$|\tilde{x}(t)|^2 \leq \bar{\kappa} e^{-2\alpha(t-\epsilon^\star-d_1)}\|\phi\|_W^2 + \left[\bar{\kappa} e^{-2\alpha(t-\epsilon^\star-d_1)} + \frac{\gamma^2}{2\alpha}\right]\|\tilde{w}[0,t]\|_\infty^2, \quad (7.55)$$

$\forall t \geq 0$*, i.e., given* $\Delta > 0$*, the ellipsoid*

$$\mathscr{X} = \left\{\tilde{x} \in \mathbb{R}^n : |\tilde{x}|^2 \leq \frac{\gamma^2}{2\alpha}\Delta^2\right\} \quad (7.56)$$

is exponentially attractive with a decay rate $\alpha > 0$*.*

Proof. Consider the following Lyapunov-Krasovskii functional:

$$V(t) = V_P(t) + V_R(t) + V_H(t) + V_{S_p}(t) + V_{W_p}(t), \quad p = 1, 2, \quad (7.57)$$

with

$$V_P(t) = z^\top(t) P z(t), \quad (7.58)$$

$$V_R(t) = \tfrac{1}{\epsilon}\int_{t-\epsilon}^{t} e^{-2\alpha(t-s)}(s-t+\epsilon)^2 f(\tfrac{s}{\epsilon})^\top R f(\tfrac{s}{\epsilon})\, ds, \quad (7.59)$$

$$V_H(t) = \tfrac{1}{\epsilon}\int_{t-\epsilon}^{t}\int_{s-d_2}^{t} e^{-2\alpha(t-\theta)}(s-t+\epsilon+d_2)\dot{\tilde{x}}^\top(\theta) D^\top(\tfrac{s}{\epsilon}) H D(\tfrac{s}{\epsilon})\dot{\tilde{x}}(\theta)\, d\theta\, ds, \quad (7.60)$$

$$V_{S_p}(t) = \int_{t-d_p}^{t} e^{-2\alpha(t-s)}\tilde{x}^\top(s) S_p \tilde{x}(s)\, ds, \quad (7.61)$$

$$V_{W_p}(t) = \int_{t-d_p}^{t} (s-t+d_p) e^{-2\alpha(t-s)}\dot{\tilde{x}}^\top(s) W_p \dot{\tilde{x}}(s)\, ds. \quad (7.62)$$

Note that $V_R(t)$ is required to compensate $G(t)$ in (7.48), while $V_{S_p}(t)$ and $V_{W_p}(t)$, $p = 1, 2$ in (7.61)-(7.62) are standard terms for delay-dependent stability to compensate delays $h_1(t)$ and $h_2(t)$, respectively. Moreover, to compensate Y-term in (7.48), $V_H(t)$ in (7.60) is introduced [97].

Differentiating $V_P(t)$ and $V_R(t)$ along the trajectories of (7.48), it follows:

$$\begin{aligned}\dot{V}_P(t) + 2\alpha V_P(t) =& 2\left[\tilde{x}(t) - G(t)\right]^\top P[(\tilde{A} + D_{av} + \Delta D(\tfrac{t}{\epsilon}))\tilde{x}(t)\\ &+ \tilde{A}_d\tilde{x}(t - h_1(t)) - Y(t) + \tilde{w}(t)]\\ &+ 2\alpha\left[\tilde{x}(t) - G(t)\right]^\top P\left[\tilde{x}(t) - G(t)\right], \qquad (7.63)\\ \dot{V}_R(t) + 2\alpha V_R(t) =& \epsilon f^\top(\tfrac{t}{\epsilon})Rf(\tfrac{t}{\epsilon})\\ &- \frac{2}{\epsilon}\int_{t-\epsilon}^{t} e^{-2\alpha(t-s)}(s - t + \epsilon)f^\top(\tfrac{s}{\epsilon})Rf(\tfrac{s}{\epsilon})\,ds\\ &\le \epsilon f^\top(\tfrac{t}{\epsilon})Rf(\tfrac{t}{\epsilon}) - \frac{4}{\epsilon}e^{-2\alpha\epsilon}G^\top(t)RG(t), \qquad (7.64)\end{aligned}$$

where Jensen inequality in Lemma 4 has been applied in (7.64). Moreover, for $V_{S_p}(t)$ in (7.61) and $V_{W_p}(t)$ in (7.62), with $p = 1, 2$, it yields:

$$\begin{aligned}\dot{V}_{S_p}(t) + 2\alpha V_{S_p}(t) =& \tilde{x}^\top(t)S_p\tilde{x}(t) - e^{-2\alpha d_p}\tilde{x}^\top(t - d_p)S_p\tilde{x}(t - d_p),\\ \dot{V}_{W_p}(t) + 2\alpha V_{W_p}(t) =& d_p\dot{\tilde{x}}^\top(t)W_p\dot{\tilde{x}}(t) - \int_{t-d_p}^{t} e^{-2\alpha(t-s)}\dot{\tilde{x}}^\top(s)W_p\dot{\tilde{x}}(s)\,ds\\ &= d_p\dot{\tilde{x}}^\top(t)W_p\dot{\tilde{x}}(t) - \frac{e^{-2\alpha d_p}}{d_p}\begin{bmatrix} \tilde{x}(t)-\tilde{x}(t-h_p(t)) \\ \tilde{x}(t-h_p(t))-\tilde{x}(t-d_p) \end{bmatrix}^\top\\ &\times \begin{bmatrix} W_p & U_p \\ \star & W_p \end{bmatrix}\begin{bmatrix} \tilde{x}(t)-\tilde{x}(t-h_p(t)) \\ \tilde{x}(t-h_p(t))-\tilde{x}(t-d_p) \end{bmatrix},\end{aligned} \qquad (7.65)$$

where matrices $U_p \in \mathbb{R}^{Nn\times Nn}$, $p = 1, 2$ are subject to inequalities (7.51) arising from Park inequality [174] on the integral term in (7.65). Again, by differentiating $V_H(t)$ in (7.60) along (7.48), it holds:

$$\begin{aligned}\dot{V}_H(t) + 2\alpha V_H(t) \le& \dot{\tilde{x}}^\top(t)\Big(\frac{1}{\epsilon}\int_{t-\epsilon}^{t}(s - t + \epsilon + d_2)D^\top(\tfrac{s}{\epsilon})HD(\tfrac{s}{\epsilon})\,ds\Big)\dot{\tilde{x}}(t)\\ &- \frac{1}{\epsilon}e^{-2\alpha(\epsilon+d_2)}\int_{t-\epsilon}^{t}\int_{s-d_2}^{t}\dot{\tilde{x}}^\top(\theta)D^\top(\tfrac{s}{\epsilon})HD(\tfrac{s}{\epsilon})\dot{\tilde{x}}(\theta)\,d\theta\,ds.\end{aligned} \qquad (7.66)$$

Similar to [46], by changing variable $s = \epsilon\zeta$ and exploiting (7.52), for the first integral term in (7.66) it follows:

$$\begin{aligned}&\frac{1}{\epsilon^2}\int_{t-\epsilon}^{t}(s-t+\epsilon+d_2)D^\top(\tfrac{s}{\epsilon})HD(\tfrac{s}{\epsilon})\,ds\\&=\int_{\frac{t}{\epsilon}-1}^{\frac{t}{\epsilon}}(\zeta-\tfrac{t}{\epsilon}+1+\tfrac{d_2}{\epsilon})D^\top(\zeta)HD(\zeta)\,d\zeta\le\bar{H},\end{aligned}\tag{7.67}$$

while for the second integral term in (7.66) it is possible to leverage extended Jensen's inequality in Lemma 4, thus recasting (7.66) as

$$\dot{V}_H(t)+2\alpha V_H(t)\le\epsilon\dot{\tilde{x}}^\top(t)\bar{H}\dot{\tilde{x}}(t)-\frac{2}{\epsilon}e^{-2\alpha(\epsilon+d_2)}Y^\top(t)HY(t).\tag{7.68}$$

In order to compensate $\Delta D(\frac{t}{\epsilon})\tilde{x}(t)$ in (7.63), the S-procedure in Lemma 13 (see Appendix) can be applied, i.e.,

$$\begin{aligned}\dot{V}(t)+2\alpha V(t)-\gamma^2|\tilde{w}(t)|^2&\le\dot{V}(t)+2\alpha V(t)+\lambda(\sigma_D^2|\tilde{x}(t)|^2\\&\quad-|\Delta D(\tfrac{t}{\epsilon})\tilde{x}(t)|^2)-\gamma^2|\tilde{w}(t)|^2\\&\le\xi^\top(t)\Omega\xi(t)+\epsilon^\star f^\top(\tfrac{t}{\epsilon})Rf(\tfrac{t}{\epsilon})\\&\quad+\dot{\tilde{x}}^\top(t)(d_1W_1+d_2W_2+\epsilon^\star\bar{H})\dot{\tilde{x}}(t),\end{aligned}\tag{7.69}$$

for $t\ge\epsilon$, with some positive scalars $\lambda>0$ and $\gamma>0$, augmented vector $\xi^\top(t)=[\tilde{x}^\top(t),\ G^\top(t),\Delta D^\top(\frac{t}{\epsilon})\tilde{x}^\top(t),\ Y^\top(t),\tilde{x}^\top(t-h_1(t)),\ \tilde{x}^\top(t-d_1),\ \tilde{x}^\top(t-h_2(t)),\ \tilde{x}^\top(t-d_2),\ \tilde{w}^\top(t)]\in\mathbb{R}^{9Nn\times 9Nn}$ and symmetric block matrix Ω defined in (7.54). Moreover, by leveraging (7.42), $f(\frac{t}{\epsilon})$ and $\dot{\tilde{x}}(t)$ in (7.69) can be presented as

$$\begin{aligned}f(\tfrac{t}{\epsilon})&=\sum_{s=1}^{M}\chi_s(\tfrac{t}{\epsilon})D_s\tilde{x}(t-h_2(t)),\\\dot{\tilde{x}}(t)&=\tilde{A}\tilde{x}(t)+\tilde{A}_d\tilde{x}(t-h_1(t))+\tilde{w}(t)+\sum_{s=1}^{M}\chi_s(\tfrac{t}{\epsilon})D_s\tilde{x}(t-h_2(t)).\end{aligned}\tag{7.70}$$

By Schur complements, if inequality

$$\begin{bmatrix} \Omega & \Omega_{12} \\ \star & \begin{bmatrix} -R & 0_{Nn} & 0_{Nn} & 0_{Nn} \\ \star & -W_1 & 0_{Nn} & 0_{Nn} \\ \star & \star & -W_2 & 0_{Nn} \\ \star & \star & \star & -\bar{H} \end{bmatrix} \end{bmatrix} < 0 \tag{7.71}$$

holds, with Ω_{12} defined as

$$\begin{bmatrix} \begin{bmatrix} 0_{6Nn} \\ \sqrt{\epsilon^\star}\chi(\frac{t}{\epsilon})D_s^\top R \\ 0_{6Nn} \end{bmatrix} & \begin{bmatrix} \sqrt{d_1}\tilde{A}^\top W_1 \\ 0_{3Nn} \\ \sqrt{d_1}\chi(\frac{t}{\epsilon})D_s^\top W_1 \\ 0_{Nn} \\ \sqrt{d_1}\chi(\frac{t}{\epsilon})D_s^\top W_1 \\ 0_{Nn} \\ \sqrt{d_1}W_1 \end{bmatrix} & \begin{bmatrix} \sqrt{d_2}\tilde{A}^\top W_2 \\ 0_{3Nn} \\ \sqrt{d_2}\chi(\frac{t}{\epsilon})D_s^\top W_2 \\ 0_{Nn} \\ \sqrt{d_2}\chi(\frac{t}{\epsilon})D_s^\top W_2 \\ 0_{Nn} \\ \sqrt{d_2}W_2 \end{bmatrix} & \begin{bmatrix} \sqrt{\epsilon^\star}\tilde{A}^\top W_2 \\ 0_{3Nn} \\ \sqrt{\epsilon^\star}\chi(\frac{t}{\epsilon})D_s^\top W_2 \\ 0_{Nn} \\ \sqrt{\epsilon^\star}\chi(\frac{t}{\epsilon})D_s^\top W_2 \\ 0_{Nn} \\ \sqrt{\epsilon^\star}W_2 \end{bmatrix} \end{bmatrix}, \tag{7.72}$$

with $\chi(\frac{t}{\epsilon}) = \sum_{s=1}^{M} \chi_s(\frac{t}{\epsilon})$, then

$$\dot{V}(t) + 2\alpha V(t) - \gamma^2 |\tilde{w}(t)|^2 < 0. \tag{7.73}$$

Note that, (7.53) implies both (7.71) and (7.73) since it is affine in $\sum_{s=1}^{M} \chi_s(\frac{t}{\epsilon})D_s^\top$. Furthermore, for all $\epsilon \in (0, \epsilon^\star]$, the positiveness of the functional is guaranteed by the following bound:

$$V(t) \geq V_P(t) + V_R(t) \geq \begin{bmatrix} \tilde{x}(t) \\ G(t) \end{bmatrix}^\top \begin{bmatrix} P & -P \\ \star & P + e^{-2\alpha\epsilon^\star} R \end{bmatrix} \begin{bmatrix} \tilde{x}(t) \\ G(t) \end{bmatrix} \geq |\tilde{x}(t)|^2. \tag{7.74}$$

Hence, if (7.50) is satisfied, then comparison principle ensures

$$|\tilde{x}(t)|^2 \leq V(t) \leq e^{-2\alpha(t-\epsilon-d_1)} V(\epsilon) + \frac{\gamma^2}{2\alpha} \|\tilde{w}[0,t]\|_\infty^2 \qquad t \geq \epsilon. \tag{7.75}$$

From (7.57), for some positive ϵ-independent κ_1 it holds:

$$V(\epsilon) \leq \kappa_1 \left[\|\tilde{x}_\epsilon\|_W^2 + \int_{-d_1}^{\epsilon} |\dot{\tilde{x}}(s)|^2 \, ds \right]. \tag{7.76}$$

By denoting $\tilde{x}_t(\theta) = \tilde{x}(t+\theta)$ with $\theta \in [-d_1, 0]$, from (7.40), it follows:

$$\tilde{x}_t(\theta) = \begin{cases} \phi(t+\theta), & t+\theta < 0 \\ \phi(0) + \int_0^{t+\theta} [Ax(s) + A_d x(s - h_1(s)) + B(\frac{s}{\epsilon})w(s)]\, ds, & t+\theta \geq 0. \end{cases} \tag{7.77}$$

From (7.77), the following holds:

$$\|x_t\|_W \leq \|\phi\|_W + \int_{-\theta}^{0} \kappa_2 \|\phi(s)\|_W\, ds + b(\epsilon T + d_1)\|w[0,t]\|_\infty, \quad t \geq 0, \tag{7.78}$$

for some ϵ-independent $\kappa_2 > 0$. From (9.50) and Gronwall inequality, it results:

$$\|\tilde{x}_t\|_W \leq e^{\kappa_2 d_1}\|\phi\|_W + (\epsilon + d_1)\|\tilde{w}[0,t]\|_\infty \quad t \in [0, \epsilon + d_1], \tag{7.79}$$

and, hence,

$$\|\tilde{x}_t\|_W^2 \leq e^{2\kappa_2 d_1}\|\phi\|_W + (\epsilon + d_1)^2\|\tilde{w}[0,t]\|_\infty^2\, ds \quad t \in [0, \epsilon T + d_1]. \tag{7.80}$$

Similarly, from (7.40):

$$|\dot{\tilde{x}}(t)|^2 \leq \kappa_3 \|\phi\|_W^2 + \|\tilde{w}[0,t]\|_\infty^2 \qquad t \in [0, \epsilon + d_1], \tag{7.81}$$

for some positive ϵ-independent κ_3. Tacking into account (7.80)-(7.81), the following inequality can be derived:

$$V(\epsilon) \leq \kappa_1 \left[e^{2\kappa_2 d_1}\|\phi\|_W^2 + \|\tilde{w}[0,t]\|_\infty^2 \right] \tag{7.82}$$

Substitution of this latter into (7.75) leads to the fulfillment of (7.55) (and, thus, (7.56)) for some ϵ-independent $\bar{\kappa} > 0$, thus completing the proof. □

Remark 16. *It is worth noting that decision variable γ, as a component of ISS gain, strongly impacts on ellipsoid radius according to (7.56). To reduce the attractive ball dimension, one can minimize the value of γ. However, from (7.54), this contraction leads to poor convergence rate which,* *conversely, needs for larger values of γ. It follows that a good trade-off between attractive ball dimension and convergence rate has to be reached. Moreover, several optimization software tools are available to deal with minimization problems subject to LMIs constraints, such as MOSEK [175], which has a MATLAB API accessible via the YALMIP parser and exploits, e.g., bisection algorithm.*

Remark 17. *It is worth noting that, linear systems and nonlinear Lipshitz systems with constant delay which are Globally Exponentially Stable in absence of an input (0-GES) are ISS as well [176]. In Theorem 7 ISS analysis is also required due to the presence of non-small delays, whose length can strongly compromise the practical stability of the system. According to the recent literature, if the delay exceeds a prescribed size the ISS may be no-longer preserved [177].*

7.3.2 Numerical Analysis

In this section some numerical simulations are provided in order to confirm the effectiveness of the theoretical derivation. Let us considering a MASs consisting of $N = 10$ dynamical followers plus a leader sharing information via delayed switching communication network and whose delayed dynamics (7.36)-(7.37) are characterized by the following matrices:

$$A = \begin{bmatrix} 0 & 1 \\ -1 & 0 \end{bmatrix}, \; A_d = \begin{bmatrix} -1 & 1 \\ -2.5 & 0 \end{bmatrix}, \; B = \begin{bmatrix} 0 \\ 1 \end{bmatrix}.$$

The initial conditions of the agents are randomly selected, while their external disturbances are chosen such that $w_1(t) = w_7(t) = \sin(t)$, $w_2(t) = \sin(1.5t)$, $w_3(t) = w_6(t) = \sin(0.5t)$, $w_4(t) = w_8(t) = 0.1\sin(t)$, $w_5(t) = w_9(t) = w_10(t) = 0$, for $t \in [0, 5)$ $[s]$, and $w_5(t) = \sin(0.5t)$, $w_9(t) = 0.1\sin(0.5t)$, $w_{10}(t) = 2\sin(0.5t)$, $w_1(t) = w_2(t) = w_3(t) = w_4(t) = w_6(t) = w_7(t) = w_8(t) = 0$ for $t \in [5, 10]$ $[s]$. Let us assume the periodic switching network $\mathscr{G}_{N+1}(\frac{t}{\epsilon})$ among ten agents as depicted in Figure 7.4, which allows to present matrix $D(\tau)$ in (7.42) as the following convex combination of $M = 2$ constant matrices, i.e.:

$$D(\tau) = \sum_{s=1}^{2} \chi_s(\tau) D_s, \quad \tau \in [k, k+1), \quad k = 0, 1, \ldots, \tag{7.83}$$

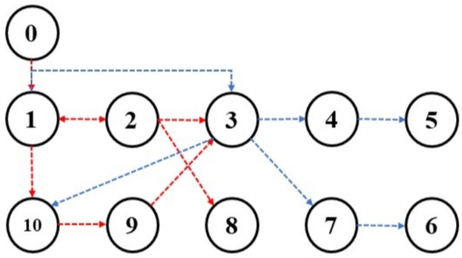

Figure 7.4. Switching communication network graph $\mathscr{G}_{N+1}(\frac{t}{\epsilon}) = \{\mathscr{V}, \mathscr{E}^s_{N+1}(\frac{t}{\epsilon})\}, s = 1, 2$, with $\mathscr{E}^1_{N+1}(\frac{t}{\epsilon})$ and $\mathscr{E}^2_{N+1}(\frac{t}{\epsilon})$ in red and blue dashed lines, respectively.

with $D_1 = \mathscr{H}_1 \otimes BK$ referred to the edge set $\mathscr{E}^1_{N+1}(\frac{t}{\epsilon})$ (red dashed lines in Figure 7.4) and $D_2 = \mathscr{H}_2 \otimes BK$ referred to $\mathscr{E}^2_{N+1}(\frac{t}{\epsilon})$ (blue dashed lines in Figure 7.4), respectively. Moreover, $\chi_1(\tau) = \chi_{[k\epsilon,(k+\beta_1)\epsilon]}(\tau)$ is the indicator function of the time interval $[k\epsilon, (k+\beta_1)\epsilon]$, while $\chi_2(\tau) = 1 - \chi_1(\tau)$. Therefore, $D(\tau)$ is 1-periodic with $\Delta D = 0$ and, hence, $\sigma_D = 0$. By choosing $\beta_1 = 0.6$ and $K = [-15 \ \ -15]$, it results the Hurwitz matrix $\Phi = \tilde{A} + \beta_1 D_1 + (1-\beta_1)D_2 + \tilde{A}_d$. For all $\tau \geq 1$, inequality (7.52) can be presented as

$$\begin{aligned}
&\int_{\tau-1}^{\tau}\Big(\zeta - \tau + 1 - \frac{d_2}{\epsilon}\Big)D^\top(\zeta)HD(\zeta)\,d\zeta \leq \\
&\int_{\tau-\beta_1}^{\tau}\Big(\zeta - \tau + 1 - \frac{d_2}{\epsilon}\Big)\,d\zeta D_1^\top HD_1 + \int_{\tau-(1-\beta_1)}^{\tau}\Big(\zeta - \tau + 1 - \frac{d_2}{\epsilon}\Big)\,d\zeta D_2^\top HD_2 \qquad (7.84)\\
&= \Big(\frac{1-(1-\beta_1)^2}{2} + \beta_1\frac{d_2}{\epsilon}\Big)D_1^\top HD_1 + \Big(\frac{1-\beta_1^2}{2} + \frac{d_2}{\epsilon}(1-\beta_1)\Big)D_2^\top HD_2 = \bar{H}
\end{aligned}$$

The numerical simulations are carried out by exploiting MATLAB platform, while Yalmip Toolbox with MOSEK solver have been exploited to solve the LMIs in (7.50)-(7.53). By verifying the feasibility of LMIs in Theorem 7 for a small enough decay rate $\alpha = 0.005$, it is possible to find upper bounds $\epsilon^\star$, d_1 and d_2 preserving the ISS of the overall MASs network. This means that bounded leader-tracking consensus can be achieved with error trajectories $\tilde{x}(t)$ approaching the attractive ball whose radius is $\sqrt{\frac{\gamma^2}{2\alpha}\Delta^2}$ according to (7.55)-(7.56). Specifically, the analysis is carried-out in a threefold way. Given desired decay rate $\alpha = 0.005$, the values of two parameters among ϵ, d_1 and d_2 is fixed at a time, while iteratevely increas-

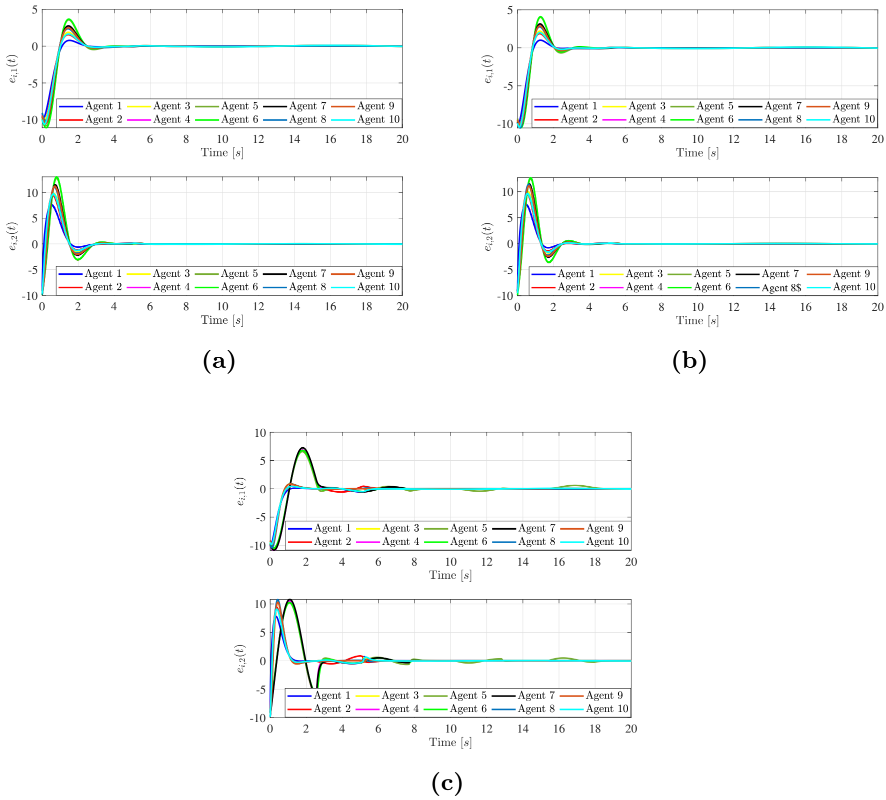

Figure 7.5. Leader-tracking consensus problem. Time history of synchronization errors $e_i(t)$, $i = 1, \ldots, 10$ for: a) $\epsilon^\star = 0.0177$, $d_1 = 0.912$, $d_2 = 0.013$; b) $\epsilon^\star = 0.0177$, $d_1 = 0.5$, $d_2 = 0.0268$; c) $\epsilon^\star = 5.13$, $d_1 = 0.5$, $d_2 = 0.01$.

ing the value of the third one in order to find its upper bound preserving the ISS of the entire network. In doing so, the upper bounds $\epsilon^\star$, d_1 and d_2 on ϵ, $h_1(t)$ and $h_2(t)$, respectively, can be evaluated for a desired decay rate. Table 7.1 shows the results of these analysis. In particular, it is possible to appreciate that for $\alpha = 0.005$, $\epsilon^\star = 0.0177$ and $d_2 = 0.013$, the non-small state delay upper bound and γ are $d_1 = 0.912$ and $\gamma = 26.2879$, while for $\alpha = 0.005$, $\epsilon^\star = 0.0177$ and $d_1 = 0.5$ it results $d_2 \sim \mathscr{O}(\epsilon)$, i.e. $d_2 = 0.0268$, and $\gamma = 17.574$. By numerical simulations of solutions,

Table 7.1. Feasibility of Theorem 7.

	$\epsilon^\star$	d_1	d_2	γ
$\alpha = 0.005,\ \epsilon^\star = 0.0177,\ d_2 = 0.013$	–	0.912	–	26.2879
$\alpha = 0.005,\ \epsilon^\star = 0.0177,\ d_1 = 0.5$	–	–	0.0268	17.574
$\alpha = 0.005,\ d_1 = 0.5,\ d_2 = 0.01$	5.13	–	–	41.9173

$\alpha = 0.005,\ d_1 = 0.5$ and $d_2 = 0.01$ allow finding that the ISS of the overall MASs network is preserved till larger values of ϵ, i.e. $\forall\epsilon \in (0, \epsilon^\star]$ with $\epsilon^\star = 5.13$. Furthermore, numerical simulations have been performed for the above described three cases and the results are shown in Figure 7.5(a)-(c), thus confirming theoretical derivation. In particular, Figure 7.5(a)-(c) report the time-history of the error trajectories of the overall MASs network, thus confirming that, under the proposed networked-based delayed control law and switching communication network, bounded leader-tracking consensus can be achieved for all $\epsilon \in (0, \epsilon^\star],\ h_1(t) \in (0, d_1],\ h_2(t) \in (0, d_2]$, with $\epsilon^\star,\ d_1$ and d_2 properly selected according to Table 7.1, and for a small enough decay rate, even if the network is not connected for all $t \geq 0$. Hence, it is possible to concluded that, compared with [165], our approach allows quantifying the upper bound $\epsilon^\star$, as well as maximum admissible delays d_1 and d_2, which is not possible by exploiting classical averaging theory.

7.4 Concluding Remarks

In this chapter the problem of reducing communication network workload in CPES and, in general, in MASs has been addressed via distributed periodic control strategies, which allow avoiding communication resources waste without compromising stability performance. Firstly, the digital implementation of distributed PID control strategy by using artificial delays approach has been investigated to solve the voltage SC in inverter-based islanded MG. The proposed mechanism has allowed to reduce the number of the control updates, thus saving the limited network communication resource and releasing communication bandwidth. Theoretical analysis has been carried out by exploiting Lyapunov-Krasovskii theory and the derived exponential stability conditions have been expressed as a set of LMIs, whose solution allows finding the weighted L_2 gain. Numerical results have confirmed the effectiveness of the control strategy in guaranteeing the voltage regulation control problem, while coping with references/load variations, natural deviations, as well as plug-and-play situations. On the other hand, for the general class of high-order MASs with both input and state delays, the benefits of using periodic fast-switching communication network has been studied by leveraging the constructive time-delay approach to periodic averaging without requiring the connectivity of the network for all the time. This latter approach has allowed finding a proper time-dependent switching control rule preserving the ISS of the entire MASs, where the Lyapunov-Krasovskii theory has been exploited again to analyticall prove the effectiveness of the method in ensuring bounded-leader tracking performance. Stability conditions expressed as LMIs are derived, whose solution led to upper bounds on small parameter, state and communications delays.

Chapter 8

Towards distributed aperiodic control

This chapter tackles the secondary voltage recovery problem in islanded MG with the aim of further reducing communication frequency among DGs, while maintaining desired performance and saving communication network workload. To pursue this objective, a distributed PID controller is firstly introduced, whose sampled-data implementation is enabled by leveraging the finite-difference approximation for the derivative action, which leads to a distributed Proportional-Integral-Retarded (PIR) controller with a small enough sampling period $h > 0$. Then, the resulting fully-distributed PIR control law is combined with a DETM, which embeds Zeno-freeness property and avoids the requirement of continuous transmission in triggering process. Thus, the communication burden is significantly mitigated and the waste of communication resources is avoided. By exploiting Lyapunov-Krasovkii method, exponential stability conditions expressed as LMIs are derived, whose solution allows evaluating the maximum sampling period and DETM parameters preserving the stability of the MG voltage. A thorough numerical analysis, carried out on the standard IEEE 14-bus test system, confirms the effectiveness of the theoretical derivation.

8.1 A Novel Communication Resources Saving-Oriented control approach

The focus of this chapter is the voltage regulation problem, which falls into SC layer, i.e., the more critical level to guarantee nominal working conditions. At this level, distributed control schemes are gaining momentum since they represent a superior alternative with respect to conventional centralized or decentralized approaches. By exploiting information exchanges among DGs at the local level, distributed control techniques are able to achieve SC objectives, while guaranteeing higher flexibility, reliability and scalability [22].

Along this line, cooperative control of MASs represents one of the main approaches for SC design [178], where each component within the MG is modeled as a dynamical system able to reach a desired coordinated behavior at the global level via its own neighboring information and distributed control protocols [23, 24]. Several distributed control strategies are recently introduced in the technical literature to solve voltage regulation problem in islanded MG, each of them facing with a specific challenge, such as finite-time convergence [42, 31], bounded uncertainties/disturbances [11], cyber attacks [153].

All the above mentioned distributed SC schemes assume continuous communication among DGs and require fast communication ability to ensure the stability of the system, which may lead heavy burden on the communication network, thus representing a no-computationally efficient solution [101, 14]. Moreover, the communication bandwidth will be inevitably limited as the number of DGs involved in the MG increases [179]. Therefore, the design of effective and reliable control schemes able to reduce the data exchange frequency, while maintain MG performance, will be meaningful in order to: *i*) efficiently manage with the limited bandwidth; *ii*) reduce network congestion; *iii*) avoid waste of communication and computation resources [22, 179]. Event-Triggered Control (ETC) has been recognized as a suitable solution to achieve the aforementioned objectives and it avoids costly communication. It guarantees controllers to switch-on only when trigger conditions are fulfilled, meaning that the communication become aperiodic rather than periodic.

Along this direction, [22] has introduced a distributed ETC to achieve

SC objectives, where the design of trigger function/condition has handled through Lyapunov method. To solve voltage recovery problem in a distributed fashion, an ET time generator has considered in [180], whose task is to judge whether a certain measurement error has reached the ET condition which, however, depends on the communication network topology via the Laplacian matrix. Moreover, an ETC has been embedded into a Distributed Model Predictive Control (DMPC) scheme in [181] to regulate the voltage magnitude of each DG, where it is shown that communication/-computation burden is reduced with slightly compromised control performance. Herein, to improve these latter, authors also embed an adaptive observer to mitigate the negative effects of mismatches due to sampling process. The presence of communication time-delays during information sharing process has been considered in [154], where the voltage synchronization is achieved via a distributed ETC, designed by using the low gain feedback technique. Note that, all the above-mentioned ETC methods are designed without considering disturbances acting on DGs dynamics and, hence, they may not guarantee Zeno-freeness in practical applications [179]. From this literature overview, it is clear that most efforts have been done towards the development of static ET rules based on synchronization/sampling voltage errors [182]. However, DETM based on an auxiliary internal variable is gaining attention in the last years since it has been proven that it requires fewer control updated with respect to static ET control and has the capability of eliminating Zeno behavior [183, 184]. It is worth noting that the main difference between static ET and the dynamic one relies in the threshold. Static ET has a fixed and constant threshold into the triggering rule, whereas Dynamic Event-Triggered (DET) endows a dynamically adjustable mechanism provided by the additional internal variable [185].

In light of the above, the aim of the chapter is to introduce a novel robust distributed DET PID-like controller able to solve voltage recovery problem in inverter-based islanded MG, where bounded disturbances arising from MG modeling phase are taken into account without compromise Zeno-freeness property. The PID-like structure of the proposed fully-distributed controller allows to reach highly improved steady-state and transient performance since, both past and future information, together with the present ones, are considered [14]. Moreover, the DET mecha-

nism, based on a comparison between the actual computed control signal and the last imposed one, is able to further reduce the number of the control signals sent compared with the classical static ET via the additional internal variable, which adjusts the triggering threshold and lengthens the inter-event time intervals, thus leading to communication resources saving. Moreover, it is worth noting that the proposed DET mechanism is based on control signals, instead of voltage errors measurements, in order to avoid accumulating errors in the integral terms approximation. By exploiting theoretical results in [157], the fully-distributed PID-like control protocol exploits finite-difference approximation to deal with the derivative terms, which results in a PIR controller. Note that, if the delay length is small enough, the stability is maintained despite this approximation [160]. The data sampling is tackled via time-delay approach and Lyapunov-Krasovskii method [97], where the key point is to express the delayed term via its Taylor's expansion with remainder in the integral form, properly compensated via the Lyapunov Krasovskii functional. Thus, simple robust sampling-dependent stability conditions in the form of LMIs are derived, whose feasibility is ensured for small enough sampling period if the original distributed derivative-dependent controller stabilizes the MG voltage.
Note that, differently from [185], where the DET mechanism (dependent on the voltage error measurements) is applied along with a simple fully-diffusive control protocol without considering disturbances acting on the MG, the proposed stability analysis leads to feasible LMIs whose solution allows finding parameters involved into the DET condition ensuring stability. Furthermore, with respect to the results presented in [14] (see previous Chapter 7), where the sample-data implementation of the distributed PID controller has been carried out without involving an ET mechanism, through the chapter it will be highlighted how the proposed method further reduces the usage of the limited communication resources with a less number of triggering events, which is helpful for saving communication bandwidth.

8.2 Dynamic Event-Triggered PID-like Control Using Artificial Delays

Here the aim is to design the secondary voltage control v_i^n in (3.9) able to synchronize all DGs voltage v_i^{out}, $\forall i = 1, 2, \dots, N$, to the reference voltage v_0, provided by a virtual DG, labeled with index 0. This implies the synchronization of the direct term v_i^{od} in (3.9) $\forall i = 1, 2, \dots, N$.
This control problem, which can be recast as a leader-tracking one, is here tackled by designing a novel distributed dynamic event-triggered control strategy able to reduce the communication burden and saving limited network resources. Note that, for sake of brevity, throughout the chapter the dependence on $d - q$ reference frame of v_i^{od} in (3.9) will be omitted, i.e., $v_i^{od} = v_i$.
By differentiating voltage equation in (3.9) and taking into account equation (3.10b), the following simplified second-order model is derived:

$$k_{v_i}\ddot{v}_i(t) + \dot{v}_i(t) + k_{Q_i}\dot{Q}_i^m + \hat{u}_i(t) = 0, \tag{8.1}$$

where $\hat{u}_i(t) = \dot{v}_i^n$ is the i-th DG control input generating PC voltage reference to be designed later. By leveraging state-space formalism, (8.1) leads to

$$\dot{x}_i(t) = \begin{bmatrix} 0 & 1 \\ 0 & 0 \end{bmatrix} x_i(t) + \begin{bmatrix} 0 \\ -\frac{1}{k_{v_i}} \end{bmatrix} (\hat{u}_i(t) + w_i(t)), \tag{8.2}$$

where $x_i(t) = [v_i(t)\ \dot{v}_i(t)]^\top \in \mathbb{R}^2$ is the voltage state vector, while $w_i(t) = h(t, v_i, Q_i, Q_i^m) \in \mathbb{R}$ is the disturbance taking into account the voltage deviation induced by PC, with $h(t, v_i, Q_i, Q_i^m) = -\dot{v}_i(t) - k_{Q_i}\dot{Q}_i^m$.

Remark 18. *Note that, Assumption 2 ensures the boundedness property for the term $w_i(t)$ in (8.2) [42]. It means that*

$$\exists \quad \Pi \in \mathbb{R}^+ \quad : |w_i(t)| \leq \Pi, \ \forall i = 1, 2, \dots, N.$$

On the other hand, the leading dynamics of the reference generator DG 0 can be modeled as the following autonomous system:

$$\dot{x}_0(t) = \begin{bmatrix} 0 & 1 \\ 0 & 0 \end{bmatrix} x_0(t), \tag{8.3}$$

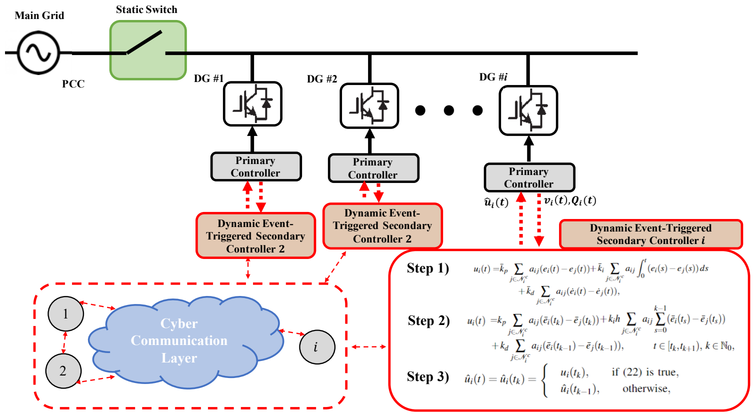

Figure 8.1. Distributed Dynamic Event-trigger PID Control Architecture for SC voltage regulation.

where $x_0(t) = [v_0(t)\ \dot{v}_0(t)]^\top \in \mathbb{R}^2$ is the leader DG 0 reference state vector. Then, for the generic i-th DG, the synchronization error can be presented as:

$$e_i(t) = v_i(t) - v_0(t), \qquad i = 1, 2, \ldots, N. \tag{8.4}$$

Now, the SC control input $\hat{u}_i(t)$ in (8.2) is designed such that:

$$\lim_{t\to\infty} \|e_i(t)\| = 0, \quad \forall i, \tag{8.5}$$

while ensuring the communication resources saving. To this aim, the following three-steps procedure is proposed: 1) introduction of a distributed PID voltage controller $u_i(t)$ which, although leveraging a continuous information sharing over the communication network, is practical to implement thanks to the finite-time difference of the derivative action; 2) sampled-data implementation of the previous designed controller $u_i(t)$ in order to obtain a digital control scheme ensuring a preliminary reduction of transmitted control signal; 3) design of the dynamic event-triggering rule to further decrease the communication network workload from the controller to actuator, while saving its limited resources [186].
In the sequel, all the design steps of the proposed control procedure are described, while a schematization of the resulting control architecture is provided in Figure 8.1 so to clearly highlight how unnecessary sampled-

data transmission is mitigated.

Step 1: From (8.4), the control $u_i(t)$ is designed as a distributed continuous-time PID controller weighting the networked shared information as

$$\begin{aligned} u_i(t) =& \bar{k}_P \sum_{j\in\mathcal{N}_i^c} a_{ij}(e_i(t)-e_j(t)) + \bar{k}_I \sum_{j\in\mathcal{N}_i^c} a_{ij} \int_0^t (e_i(s)-e_j(s))\,ds \\ &+ \bar{k}_D \sum_{j\in\mathcal{N}_i^c} a_{ij}(\dot{e}_i(t)-\dot{e}_j(t)), \end{aligned} \tag{8.6}$$

where $\bar{k}_P$ is the proportional control gain, $\bar{k}_I$ is the integral control gain and $\bar{k}_D$ is the derivative control gain; a_{ij} is the generic element of the adjacency matrix accounting for the presence/absence of a communication link between the i-th and j-th DG.

Note that, in general control engineering practice there is a widely exploitation of PID controller due to their ability in providing fast response to the transient phase while reducing steady-state deviations [156, 14]. However, this class of controllers depends on derivative of the output that can be hardly measured in practice [157, 161]. To deal with this problem, according to [14], the control input in (8.6) can be transformed in a distributed PIR controller by using the following finite-difference approximations for the derivative terms, i.e.:

$$\begin{aligned} \dot{e}_i(t) \approx& \bar{e}_i(t) = \frac{e_i(t)-e_i(t-h)}{h}, \\ \dot{e}_j(t) \approx& \bar{e}_j(t) = \frac{e_j(t)-e_j(t-h)}{h}, \end{aligned} \tag{8.7}$$

with $i,\ j = 1,2,\ldots,N$ and $h > 0$. Hence, by exploiting (8.7), the distributed PIR controller for the i-th DG has the following form:

$$\begin{aligned} u_i(t) =& k_P \sum_{j\in\mathcal{N}_i^c} a_{ij}(e_i(t)-e_j(t)) + k_I \sum_{j\in\mathcal{N}_i^c} a_{ij} \int_0^t (e_i(s)-e_j(s))\,ds \\ &+ k_D \sum_{j\in\mathcal{N}_i^c} a_{ij}(e_i(t-h)-e_j(t-h)), \end{aligned} \tag{8.8}$$

where the control gains, based on the finite-difference method, can be expressed as

$$k_P = \bar{k}_P + \frac{\bar{k}_D}{h}, \quad k_I = \bar{k}_I, \quad k_D = -\frac{\bar{k}_D}{h}. \tag{8.9}$$

Step 2: Now, to ensure a preliminary reduction of communication resources, here the sampled-data implementation of distributed PIR controller in (8.8) is addressed. To this end, it is assumed that the tracking error $e(t)$ is available only at the discrete-time instants $t_k = kh$, where $k \in \mathbb{N}_0$ and $h > 0$ is the sampling period. Specifically, given (8.7), the following approximations are employed for $t \in [t_k, t_{k+1}),\ k \in \mathbb{N}_0$ [157]:

$$\begin{aligned}
e_i(t) &= \bar{e}_i(t) \approx \bar{e}_i(t_k),\\
\int_0^t e_i(s)\,ds &\approx \int_0^{t_k} \bar{e}_i(s)\,ds \approx \sum_{s=0}^{k-1}\int_{t_s}^{t_{s+1}} \bar{e}_i(s)\,ds \approx \sum_{s=0}^{k-1}\int_{t_s}^{t_{s+1}} \bar{e}_i(t_s)\,ds\\
&= h\sum_{s=0}^{k-1}\bar{e}_i(t_s),\\
\dot{e}_i(t) &\approx \dot{\bar{e}}_i(t) \approx \dot{\bar{e}}_i(t_k) = \frac{\bar{e}_i(t_k) - \bar{e}_i(t_{k-1})}{h}.
\end{aligned} \tag{8.10}$$

By leveraging (8.10), (8.8) can be recast in sampled-data fashion as

$$\begin{aligned}
u_i(t) =& \bar{k}_P \sum_{j\in\mathscr{N}_i^c} a_{ij}(\bar{e}_i(t_k) - \bar{e}_j(t_k)) + \bar{k}_I h \sum_{j\in\mathscr{N}_i^c} a_{ij} \sum_{s=0}^{k-1}(\bar{e}_i(t_s) - \bar{e}_j(t_s))\\
&+ \bar{k}_D \sum_{j\in\mathscr{N}_i^c} a_{ij}(\dot{\bar{e}}_i(t_k) - \dot{\bar{e}}_j(t_k))\\
=& k_P \sum_{j\in\mathscr{N}_i^c} a_{ij}(\bar{e}_i(t_k) - \bar{e}_j(t_k)) + k_I h \sum_{j\in\mathscr{N}_i^c} a_{ij} \sum_{s=0}^{k-1}(\bar{e}_i(t_s) - \bar{e}_j(t_s))\\
&+ k_D \sum_{j\in\mathscr{N}_i^c} a_{ij}(\bar{e}_i(t_{k-1}) - \bar{e}_j(t_{k-1})), \qquad t \in [t_k, t_{k+1}),\ k \in \mathbb{N}_0,
\end{aligned} \tag{8.11}$$

with k_P, k_I and k_D defined as in (8.9).

Step 3: To further reduce the network workload demanded by the distributed sampled-data distributed PID control, now it will be enriched with a DETM. To this aim, inspired by [183], firstly the following i-th internal dynamic variable associated with DG i within the MG is introduced:

$$\dot{\lambda}_i(t) = -\theta\lambda_i(t) + \sigma\beta|u_i(t_k)|^2 - \beta|\epsilon_i(t_k)|^2, \quad t \in [t_k, t_{k+1}), \tag{8.12}$$

with design parameters $\theta > 0$, $\sigma \in (0,1)$, $\beta > 0$ and $\lambda_i(t_0) = \lambda_{i,0} > 0$; the term ϵ_i is defined as

$$\epsilon_i(t_k) = u_i(t) - \hat{u}_i(t_k), \qquad t \in [t_k, t_{k+1}), \tag{8.13}$$

where $\hat{u}_i(t_k)$ is the last effective control input sent, at t_k, to the i-th DG. With the aim of ensuring the voltage stability of the whole closed-loop network, the idea of the proposed DETM is not to require that $\beta(\sigma(u_i(t_k)|^2 - |\epsilon_i(t_k)|^2)$ is always non-negative, but to ensure that it is non-negative in average [183]. Accordingly, the control action $\hat{u}_i(t)$ in (8.1) is designed according to the following rule:

$$\hat{u}_i(t) = \hat{u}_i(t_k) = \begin{cases} u_i(t_k), & \text{if (8.15) is true,} \\ \hat{u}_i(t_{k-1}), & \text{otherwise,} \end{cases} \tag{8.14}$$

$$\gamma\lambda_i(t_k) + \sigma\beta|u_i(t_k)|^2 - \beta|\epsilon_i(t_k)|^2 < 0, \tag{8.15}$$

where $u_i(t_k)$ is the control action due to sample-data controller in (8.11) at the time t_k, while $\gamma > 0$ is an additional design parameter of the proposed DETM. Given (8.12), this design choice implies voltage stability to be guaranteed when $\lambda_i(t)$ is non-negative $\forall t \geq 0$, according to the following lemma.

Lemma 2. *Let $\sigma \in (0,1), \lambda_{i,0}, \gamma, \beta \in \mathbb{R}_0^+$ and let u_i, λ_i and ϵ_i defined in (8.11), (8.12) and (8.13). Then, for all $t \in [0, t_\infty)$, the DETM in (8.14)-(8.15) ensures $\gamma\lambda_i(t_k) + \sigma\beta|u_i(t_k)|^2 - \beta|\epsilon_i(t_k)|^2 \geq 0$ and $\lambda_i(t) \geq 0$, for all $i = 1, 2, \ldots, N$.*

Proof. By construction, mechanism (8.14) ensures that, $\forall t \in [0, t_\infty)$,

$$\gamma\lambda_i(t_k) + \sigma\beta|u_i(t_k)|^2 - \beta|\epsilon_i(t_k)|^2 \geq 0, \quad i = 1, 2, \ldots, N,$$

where t_∞ is the limit of $t_k = kh$ when $k \to +\infty$. If $\beta = 0$, then $\lambda_i(t_k) \geq 0$. On the other hand, if $\beta \neq 0$ it follows

$$\sigma\beta|u_i(t_k)|^2 - \beta|\epsilon_i(t_k)|^2 \geq -\gamma\lambda_i(t_k).$$

Then, from (8.12), it yields

$$\dot{\lambda}_i(t) \geq -\theta\lambda_i(t) - \gamma\lambda_i(t_k), \quad t \in [t_k, t_{k+1}),$$

for all $t \in [0, t_\infty)$, with $\lambda(0) = \lambda_0 \geq 0$. Comparison lemma [144] guarantees $\lambda(t) \geq 0$, $\forall t \in [0, t_\infty)$. □

Remark 19. *Compared to ET mechanism provided in [24], the proposed DETM* (8.14)-(8.15) *has an additional tuning parameter $\gamma \geq 0$ due to the presence of the novel interval variable λ that may allow to further reduce workload. Note that, the worst case $\gamma = 0$ means that* (8.15) *becomes a static ET. However, according to [183], a positive γ may improve the result and lead to a smaller number of signals.*

8.3 Stability Analysis

To prove how the proposed distributed PID control, embedded with DETM, as in (8.14)-(8.15), can synchronize the DGs output voltage v_i to the references state v_0 (hence solving the control objective (8.5) with limited communication resources), the following proposition is introduced, which will be instrumental for the Lyapunov-Krasovskii stability analysis.

Proposition 1. *For the i-th DG within the MG, the error derivative $\dot{\bar{e}}_i(t)$ defined in* (8.10) *satisfies the following equalities [157, 187]:*

$$\dot{\bar{e}}_i(t) = \dot{e}_i(t) + \kappa_i(t), \quad \kappa_i(t) = \int_{t-h}^{t} \frac{t-h-s}{h} \ddot{e}_i(s)\, ds, \ \forall i. \tag{8.16}$$

Proof. Following arguments in [158], by exploiting Taylor's expansion with the remainder in the integral form, it yields:

$$e_i(t-h) = e_i(t) + \dot{e}_i(t)h - \int_{t-h}^{t} (t-h-s)\ddot{e}_i(s)\, ds. \tag{8.17}$$

Proposition 1 can be obtained by recasting terms in (8.17), i.e.:

$$\dot{\bar{e}}_i(t) = \frac{e_i(t) - e_i(t-h)}{h} = \dot{e}_i(t) + \int_{t-h}^{t} \frac{t-h-s}{h} \ddot{e}_i(t). \tag{8.18}$$

□

8.3.1 Closed-loop MG Network

In order to derive the closed-loop MG network, introduce the following enlarged vectors:

$$\begin{aligned}
&\zeta(t) = [e_1(t), e_2(t), \ldots, e_N(t)] \in \mathbb{R}^N, \quad \bar{\zeta}(t) = [\dot{\bar{e}}_1(t), \dot{\bar{e}}_2(t), \ldots, \dot{\bar{e}}_N(t)] \in \mathbb{R}^N,\\
&\hat{\zeta}(t) = \Bigg[(t-t_k)\bar{e}_1(t_k) + h\sum_{s=0}^{k-1} \bar{e}_1(t_s),\ (t-t_k)\bar{e}_2(t_k) + h\sum_{s=0}^{k-1} \bar{e}_2(t_s),\\
&\qquad \ldots,\ (t-t_k)\bar{e}_N(t_k) + h\sum_{s=0}^{k-1} \bar{e}_N(t_s)\Bigg] \in \mathbb{R}^N,\\
&\chi(t) = [\zeta^\top(t)\ \bar{\zeta}^\top(t)\ \hat{\zeta}^\top(t)] \in \mathbb{R}^{3N\times 3N},
\end{aligned} \tag{8.19}$$

with $t \in [t_k, t_{k+1}),\ k \in \mathbb{N}_0$.
Moreover, denote the errors due to sampling as

$$\begin{aligned}
\varsigma(t) &= \chi(t_k) - \chi(t) \in \mathbb{R}^{3N},\\
\varphi(t) &= \bar{\zeta}(t_k) - \bar{\zeta}(t) \in \mathbb{R}^N, \quad t \in [t_k, t_{k+1}),\ k \in \mathbb{N}_0.
\end{aligned} \tag{8.20}$$

Furthermore, given Proposition 1, the additional augmented vector $\varkappa(t) = [\kappa_1(t), \kappa_2(t), \ldots, \kappa_N(t)] \in \mathbb{R}^N$ is defined.
In light of the above notation, the distributed digital-controller input vector $\bar{u}(t) = [u_1(t),\ u_2(t), \ldots, u_N(t)] \in \mathbb{R}^N$ can be re-written as

$$\begin{aligned}
\bar{u}(t) =& [\bar{k}_P\mathscr{H}\quad \bar{k}_D\mathscr{H}\quad \bar{k}_I\mathscr{H}]\chi(t) + [\bar{k}_P\mathscr{H}\quad 0_{N\times N}\quad \bar{k}_I\mathscr{H}]\varsigma(t)\\
&+ \bar{k}_D\mathscr{H}(\varkappa(t) + \varphi(t)), \qquad t \in [t_k, t_{k+1}],
\end{aligned} \tag{8.21}$$

with $\mathscr{H} = \mathscr{L} + \mathscr{P}$, where $\mathscr{L}$ and $\mathscr{P}$ are the Laplacian and Pinning matrices.

Given (8.1), (8.3), (8.21), the closed-loop system under the action of DETM (8.14) and (8.15) can be derived as:

$$\dot{\chi}(t) = \Phi\chi(t) + \mathscr{A}_1\varsigma(t) + \mathscr{A}_2(\varkappa(t) + \varphi(t)) + \mathscr{B}(\bar{w}(t) + \varepsilon(t)), \tag{8.22}$$

with matrices

$$\Phi = \begin{bmatrix} 0_{N\times N} & I_{N\times N} & 0_{N\times N} \\ \bar{k}_P\bar{B}\mathscr{H} & \bar{k}_D\bar{B}\mathscr{H} & \bar{k}_I\bar{B}\mathscr{H} \\ I_{N\times N} & 0_{N\times N} & 0_{N\times N} \end{bmatrix}, \quad \mathscr{A}_1 = \begin{bmatrix} 0_{N\times N} & 0_{N\times N} & 0_{N\times N} \\ \bar{k}_P\bar{B}\mathscr{H} & 0_{N\times N} & \bar{k}_I\bar{B}\mathscr{H} \\ 0_{N\times N} & 0_{N\times N} & 0_{N\times N} \end{bmatrix},$$
$$\mathscr{A}_2 = \begin{bmatrix} 0_{N\times N} \\ \bar{k}_D\bar{B}\mathscr{H} \\ 0_{N\times N} \end{bmatrix}, \quad \mathscr{B} = \begin{bmatrix} 0_{N\times N} \\ \bar{B} \\ 0_{N\times N} \end{bmatrix}, \quad \bar{B} = -diag\left\{\frac{1}{k_{v1}}, \frac{1}{k_{v2}}, \ldots, \frac{1}{k_{vN}}\right\}, \tag{8.23}$$

and enlarged vectors $\varepsilon(t) = [\epsilon_1(t),\ \epsilon_2(t),\ \ldots,\ \epsilon_N(t)] \in \mathbb{R}^N$ and $\bar{w}(t) = [w_1(t), w_2(t), \ldots, w_N(t)] \in \mathbb{R}^N$, with ϵ_i and $w_i(t)$ defined in (8.13) and (8.2), respectively.
Note that, the MG closed-loop system with continuous controller (8.6) has the following form:

$$\dot{\chi}(t) = \Phi\chi(t) + \mathscr{B}\bar{w}(t), \tag{8.24}$$

and satisfies the following lemma.

Lemma 3. *Let μ_i, $i = 1, \ldots, N$ the i-th eigenvalue of matrix $\bar{B}\mathscr{H}$. Given a decay rate $\bar{\alpha} > 0$, under the assumption of global reachability of the leader DG 0, by choosing control gains in (8.6) as*

$$\bar{k}_D > 0, \qquad \bar{k}_P > 0 \qquad \frac{\bar{k}_I}{\bar{k}_D} > \max_i\{\bar{k}_P\mu_i\}, \tag{8.25}$$

if there exists a positive definite matrix $P \in \mathbb{R}^{3N\times 3N}$ and a positive scalar c satisfying the following LMI

$$\begin{bmatrix} P\Phi+\Phi^\top P+\bar{\alpha}P+I_{3N} & P\mathscr{B} \\ \star & -c^2 I_{3N} \end{bmatrix} < 0, \tag{8.26}$$

then controller (8.6) exponentially stabilizes system (8.24).

Proof. Consider the Lyapunov function $V = \chi^\top(t)P\chi(t)$. By differentiating this latter and considering the attenuation index

$$J = \int_0^\infty [\chi^\top(s)\chi(s) - c^2\bar{w}^\top(s)\bar{w}(s)]\, ds,$$

LMI in (8.26) can be derived. Note that, the feasibility of (8.26) is ensured if and only if Φ is a Hurwitz stable matrix. Therefore, it is required to select $\bar{k}_P, \bar{k}_D$ and $\bar{k}_I$ guaranteeing $\Phi < 0$. According to [188], the characteristic polynomial of Φ can be computed as

$$\begin{aligned} |\lambda I - \Phi| =& |\lambda I_N| \times |\lambda^2 I_N - \lambda\bar{k}_D\bar{B}\mathscr{H} - \bar{k}_P\bar{B}\mathscr{H} + \frac{1}{\lambda}\bar{k}_I\bar{B}\mathscr{H}| \\ &= |\lambda^3 I_N + (-\lambda^2\bar{k}_D - \lambda\bar{k}_P + \bar{k}_I)\bar{B}\mathscr{H}|. \end{aligned} \tag{8.27}$$

Given the expression of $\bar{B}$ in (8.23), if the leader DG 0 is globally reachable in the communication graph, $\bar{B}\mathscr{H}$ has no zero eigenvalues, which are indicated with μ_i $(i = 1, \ldots, N)$. Since $|\xi I_N + \bar{B}\mathscr{H}| = \prod_{i=1}^{N}(\xi + \mu_i)$ [188], (8.27) can be rewritten as

$$|\lambda I - \Phi| = \prod_{i=1}^{N}\big(\lambda^3 + (-\lambda^2\bar{k}_D - \lambda\bar{k}_P + \bar{k}_I)\mu_i\big). \tag{8.28}$$

Therefore, control gains can be designed such that the roots of

$$p_{\mu_i}(\lambda) = \lambda^3 - \bar{k}_D\mu_i\lambda^2 - \bar{k}_P\mu_i\lambda + \bar{k}_I\mu_i \tag{8.29}$$

have a negative real part $\forall p_{\mu_i},\ i = 1, \ldots, N$. Then, by exploiting Routh-Hurwitz criterion, (8.29) is Hurwitz stable $\forall i$ if (8.25) holds. Therefore, the statement is proven. □

8.3.2 Proof of Convergence

The voltage synchronization process of the entire closed-loop MG network (8.22) is ensured according to the following LMIs-based stability criteria.

Theorem 8. *Consider the closed-loop voltage dynamics (8.22) under the action of distributed DET controller (8.14)-(8.15), whose control gains are tuned according to Lemma 3. Assume the leader to be globally reachable in*

$\mathscr{G}^c_{N+1}$ and let Assumptions 1-2 hold. Given sampling period $h > 0$, decay rate $\alpha < \bar{\alpha}$, and positive parameters $\sigma \in (0,1)$, β, θ and γ, if there exist positive definite matrices P, $S \in \mathbb{R}^{3N\times 3N}$, W, Q, $R \in \mathbb{R}^{N\times N}$ and a scalar $b > 0$ such that

$$\left[\begin{array}{c|c} \Theta & \begin{array}{cc} \Phi^\top\Gamma & \sqrt{\sigma\beta e^{-2\alpha h}}[\bar{k}_P\mathscr{H}\ \ \bar{k}_D\mathscr{H}\ \ \bar{k}_I\mathscr{H}]^\top \\ \mathscr{A}_1^\top\Gamma & \sqrt{\sigma\beta e^{-2\alpha h}}[\bar{k}_P\mathscr{H}\ \ 0_{N\times N}\ \ \bar{k}_I\mathscr{H}]^\top \\ \mathscr{A}_2^\top\Gamma & \sqrt{\sigma\beta e^{-2\alpha h}}\bar{k}_D\mathscr{H}^\top \\ \mathscr{A}_2^\top\Gamma & \sqrt{\sigma\beta e^{-2\alpha h}}\bar{k}_D\mathscr{H}^\top \\ \mathscr{B}^\top\Gamma & 0_{N\times N} \\ \mathscr{B}^\top\Gamma & 0_{N\times N} \end{array} \\ \hline \star & \begin{array}{cc} -\Gamma & 0_{3N\times N} \\ \star & -I_{N\times N} \end{array} \end{array}\right] < 0, \tag{8.30}$$

with

$$\Theta = \begin{bmatrix} P\Phi+\Phi^\top P+2\alpha P & P\mathscr{A}_1 & P\mathscr{A}_2 & P\mathscr{A}_2 & P\mathscr{B} & P\mathscr{B} \\ \star & -\frac{\pi^2}{4}S & 0_{3N\times N} & 0_{3N\times N} & 0_{3N\times N} & 0_{3N\times N} \\ \star & \star & -\frac{\pi^2}{4}h^2Q & 0_{N\times N} & 0_{N\times N} & 0_{N\times N} \\ \star & \star & \star & -e^{-2\alpha h}R & 0_{N\times N} & 0_{N\times N} \\ \star & \star & \star & \star & -bI_{N\times N} & 0_{N\times N} \\ \star & \star & \star & \star & \star & -\beta e^{-2\alpha h}I_{N\times N} \end{bmatrix} \tag{8.31}$$

$$\Gamma = h^2e^{2\alpha h}S + \begin{bmatrix} 0_{N\times N} & 0_{N\times N} & 0_{N\times N} \\ 0_{N\times N} & h^2(e^{2\alpha h}Q + \frac{1}{4}R) & 0_{N\times N} \\ 0_{N\times N} & 0_{N\times N} & 0_{N\times N} \end{bmatrix}, \tag{8.32}$$

then, the voltage recovery is exponentially achieved with a decay rate α and a small enough $h > 0$.

Proof. Introduce the following additional vector:

$$\bar{\lambda}(t) = [\lambda_1(t),\ \lambda_2(t), \ldots, \lambda_N(t)] \in \mathbb{R}^N, \tag{8.33}$$

with λ_i, $i = 1, \ldots, N$ defined as in (8.12). Note that, for sake of brevity, throughout the proof we omit the dependence on the time t for all variables. Consider the following Lyapunov Krasovskii functional:

$$V = V_P + V_S + V_W + V_Q + V_R + V_{\bar{\lambda}}\ , \tag{8.34}$$

where

$$
\begin{aligned}
V_P =& \chi^\top P\chi,\\
V_S =& h^2 e^{2\alpha h}\int_{t_k}^{t} e^{-2\alpha(t-s)}\dot{\chi}(s)^\top S\dot{\chi}(s)\,ds - \frac{\pi^2}{4}\int_{t_k}^{t} e^{-2\alpha(t-s)}\varsigma^\top(s)S\varsigma(s)\,ds,\\
V_W =& \int_{t_k}^{t} e^{-2\alpha(t-s)}\dot{\zeta}^\top(s)W\dot{\zeta}(s)\,ds - \frac{\pi^2}{4}\int_{t_k}^{t} e^{-2\alpha(t-s)}\varphi^\top(s)W\varphi(s)\,ds,\\
V_Q =& h^2 e^{2\alpha h}\int_{t-h}^{t} e^{-2\alpha(t-s)}\frac{s-t+h}{h}\ddot{\zeta}^\top(s)Q\ddot{\zeta}(s)\,ds,\\
V_R =& \int_{t-h}^{t} e^{-2\alpha(t-s)}\frac{(s-t+h)^2}{4}\ddot{\zeta}^\top(s)R\ddot{\zeta}(s)\,ds\\
V_{\bar{\lambda}} =& e^{-2\alpha(t-t_k)}\bar{\lambda}.
\end{aligned}
\tag{8.35}
$$

It is worth mentioning that the functional $V(t)$ in (8.34) is positive due to Lemma 5, ensuring $V_S \geq 0$ and $V_W \geq 0$, and Lemma 2, guaranteeing $V_\lambda > 0$.
Differentiating V_P along the trajectories of (8.22), it yields:

$$
\begin{aligned}
\dot{V}_P + 2\alpha V_P =& 2\chi^\top P\dot{\chi} + 2\alpha\chi^\top P\chi = \chi^\top(P\Phi + \Phi^\top P + 2\alpha P)\chi\\
&+ 2\chi^\top P\mathscr{A}_1\varsigma + 2\chi^\top P\mathscr{A}_2(\varkappa + \varphi)\\
&+ 2\chi^\top P\mathscr{B}(\bar{w} + \varepsilon).
\end{aligned}
\tag{8.36}
$$

Moreover, by differentiating V_S and V_W along (8.22), it holds:

$$
\begin{aligned}
\dot{V}_S + 2\alpha V_S &= h^2 e^{2\alpha h}\dot{\chi}^\top S\dot{\chi} - \frac{\pi^2}{4}\varsigma^\top S\varsigma,\\
\dot{V}_W + 2\alpha V_W &= \dot{\zeta}^\top W\dot{\zeta} - \frac{\pi^2}{4}\varphi^\top W\varphi.
\end{aligned}
\tag{8.37}
$$

The derivative of V_Q in (8.35) leads to

$$
\dot{V}_Q + 2\alpha V_Q = h^2 e^{2\alpha h}\ddot{\zeta}^\top Q\ddot{\zeta} - he^{2\alpha h}\int_{t-h}^{t} e^{-2\alpha(t-s)}\ddot{\zeta}^\top(s)Q\ddot{\zeta}(d)\,ds. \tag{8.38}
$$

By employing Lemma 4 to deal with the integral term of (8.38), it results:

$$\dot{V}_Q + 2\alpha V_Q \leq h^2 e^{2\alpha h} \ddot{\zeta}^\top Q \ddot{\zeta} - \Big(\int_{t-h}^{t} \ddot{\zeta}(s)\, ds\Big)^\top Q \Big(\int_{t-h}^{t} \ddot{\zeta}(s)\, ds\Big). \tag{8.39}$$

Then, after differentiating (8.16), i.e. $\dddot{e}_i(t) = \int_{t-h}^{t} \frac{\ddot{e}_i(s)}{h}\, ds$, and considering its vector form:

$$\dot{\ddot{\zeta}} = \int_{t-h}^{t} \frac{\ddot{\zeta}(s)}{h}\, ds, \tag{8.40}$$

inequality (8.39) can be finally recast as

$$\dot{V}_Q + 2\alpha V_Q \leq h^2 e^{2\alpha h} \ddot{\zeta}^\top Q \ddot{\zeta} - h^2 \dot{\ddot{\zeta}}^\top Q \dot{\ddot{\zeta}}. \tag{8.41}$$

Furthermore, by differentiating V_R along the trajectories of (8.22), it follows:

$$\dot{V}_R + 2\alpha V_R = \frac{h^2}{4} \ddot{\zeta}^\top R \ddot{\zeta} - \int_{t-h}^{t} e^{-2\alpha(t-s)} \frac{(s-t+h)}{2} \ddot{\zeta}^\top(s) R \ddot{\zeta}(s)\, ds, \tag{8.42}$$

and by using Jensen inequality in Lemma 4 for the integral term, (8.42) can be re-written as:

$$\dot{V}_R + 2\alpha V_R \leq \frac{h^2}{4} \ddot{\zeta}^\top R \ddot{\zeta} - e^{-2\alpha h} \varkappa^\top R \varkappa. \tag{8.43}$$

Finally, by differentiating $V_{\bar{\lambda}}$ in (8.35), it yields:

$$\dot{V}_{\bar{\lambda}} + 2\alpha V_{\bar{\lambda}} = e^{-2\alpha(t-t_k)} \dot{\bar{\lambda}}. \tag{8.44}$$

Moreover, given Lemma 2, from (8.12), the following inequality holds:

$$\dot{\bar{\lambda}} \leq \sigma\beta |\bar{u}(t_k)|^2 - \beta |\varepsilon(t_k)|^2, \quad t \in [t_k, t_{k+1}], \tag{8.45}$$

with $\bar{u}(t_k)$ defined in (8.21). Exploiting (8.45), (8.44) can be re-written as:

$$\dot{V}_{\bar{\lambda}} + 2\alpha V_{\bar{\lambda}} \leq e^{-2\alpha h} (\sigma\beta |\bar{u}(t_k)|^2 - \beta |\varepsilon(t_k)|^2) \tag{8.46}$$

Summing up (8.36), (8.37), (8.41), (8.43), (8.46) and choosing $W = h^2 Q$, it yields:

$$\begin{aligned}\dot V + 2\alpha V \leq & \chi^\top (P\Phi + \Phi^\top P + \alpha P)\chi + 2\chi^\top P\mathscr{A}_1\varsigma + 2\chi^\top P\mathscr{A}_2(\varkappa + \varphi)\\ & + 2\chi^\top P\mathscr{B}(\bar w + \varepsilon) + h^2 e^{2\alpha h}\dot\chi^\top S\dot\chi - \frac{\pi^2}{4}\varsigma^\top S\varsigma - \frac{\pi^2 h^2}{4}\varphi^\top Q\varphi\\ & + \ddot\zeta^\top [h^2(e^{2\alpha h}Q + \tfrac{1}{4}R)]\ddot\zeta - e^{-2\alpha h}\varkappa^\top R\varkappa\\ & + e^{-2\alpha h}(\sigma\beta|\bar u(t_k)|^2 - \beta|\varepsilon(t_k)|^2) \qquad t\in[t_k, t_{k+1}].\end{aligned} \tag{8.47}$$

Now, introduce the following enlarged vector:

$$\xi^\top = [\chi^\top\ \varsigma^\top\ \varphi^\top\ \varkappa^\top\ \bar w^\top\ \varepsilon^\top] \in \mathbb{R}^{10N}. \tag{8.48}$$

Thus, inequality (8.47) can be re-written as:

$$\dot V + 2\alpha V - b\bar w^\top \bar w \leq \xi^\top \Theta \xi + \dot\chi^\top \Gamma \dot\chi + e^{-2\alpha h}\sigma\beta|\bar u(t_k)|^2, \tag{8.49}$$

for $t \in [t_k, t_{k+1}]$, where $\Theta \in \mathbb{R}^{10N\times 10N}$ and $\Gamma \in \mathbb{R}^{3N\times 3N}$ are defined in (8.31) and (8.32), respectively. Taking into account (8.21) and (8.22), from Schur complement, if (8.30) holds, the following is satisfied:

$$\dot V + 2\alpha V - b\bar w^\top \bar w \leq 0 \quad t\in[t_k, t_{k+1}]. \tag{8.50}$$

Therefore, the fulfillment of (8.30) implies that voltage recovery process is exponentially achieved with a decay rate $\alpha > 0$ and a L_2 gain b. □

8.4 Numerical Analysis

To validate the effectiveness of the proposed strategy (8.11), (8.14), (8.15) in solving voltage recovery problem in MG, as in [23], the IEEE 14-bus test system working in islanded mode is considered. $N = 5$ DGs on buses 1, 2, 3, 6 and 8 are involved into the grid, along with $M = 9$ local loads and twenty power transmission lines, whose parameters are detailed in [23]. The communication topology is described by the set $\mathscr{E}^c_{N+1} = \{(0,1),(1,2),(2,3),(3,2),(2,4),(3,4),(4,5)\}$, where the leader information is directly available only for DG 1. Note that, since this chapter deals with secondary voltage control, frequency responses will be not

shown for the sake of brevity. However, frequency time history is maintained within the operating range of $\omega_0 = 50$ $[Hz]$ and restored via the distributed controller proposed in [13]. This latter is involved in the simulation platform in order to test the proposed voltage control strategy in a realistic MG environment.
Simulations are performed by leveraging Matlab/Simulink, while the feasibility of LMIs in Theorem 8 is verified via Yalmip Toolbox through SeDuMi solver. Lemma 3 has been exploited to select of $\bar{k}_P$, $\bar{k}_I$ and $\bar{k}_D$, which leads to $\bar{k}_P = 30$, $\bar{k}_I = 0.1$ and $\bar{k}_D = 10$. For $\alpha = 0.1$ and $\beta = 1$, the feasibility of LMIs in Theorem 8 is verified in order to find the maximum values of h and σ ensuring the voltage stability. By solving these LMIs, the fulfillment of Theorem 8 is guaranteed for $h = 0.002$, $\sigma = 0.2$ and $b = 1.1578$.

In order to point-out the capability of the proposed strategy in solving voltage recovery problem, while timely eliminating deviations induced by PC and saving limited network communication resources, in the sequel, three different simulation scenarios will be investigated, i.e.: i) *nominal scenario*, where multiple changing in voltage set-point occur so to prove the tracking ability of the proposed controller; ii) *load changing scenario* where, besides changing in voltage set-points, there exist fluctuations in load demand; iii) *plug and play scenario*, where plug-and-play phenomena are involved to discloses the robustness and the resilience of the control law (8.11), (8.14), (8.15) in facing this more troublesome situation. Finally, a comparison analysis with respect to the conventional static ET mechanism (obtained by selecting $\gamma = 0$) and the sampled-data controller in [14] is discussed with the aim of corroborating the effectiveness of the proposed approach in further reduce the communication burden, while avoiding waste of computation resources.

8.4.1 Case A: Nominal Scenario

Herein multiple voltage reference set-points variations are considered, i.e.: i) at $t = 0$ $[s]$, only the PC works; ii) at $t = 2$ $[s]$, the SC is switched ON with $v_0 = 1.02$ $[p.u.]$; iii) at $t = 20$ $[s]$, the voltage reference is changed as $v_0 = 1.03$ $[p.u.]$; iv) at $t = 45$ $[s]$, voltage set-point restores to the initial value $v_0 = 1.02$ $[p.u.]$.
Figure 8.2 confirms the effectiveness of the proposed distributed DET PID-like controller in successful solving the voltage restoration problem despite

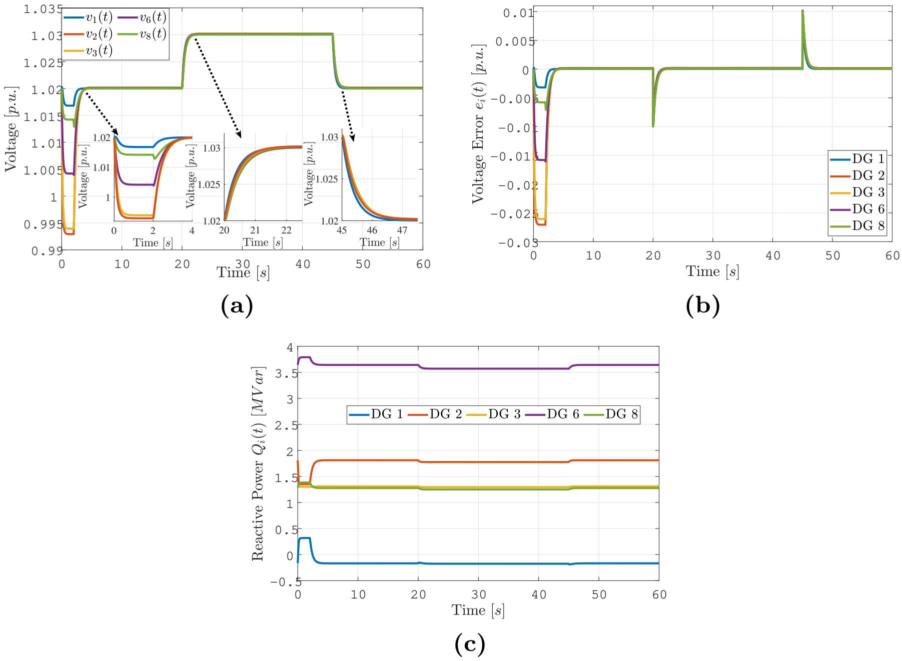

Figure 8.2. Voltage recovery in *nominal scenario* under the Distributed Dynamic Event-Triggered PID-like controller. Time history of: *a*) voltage $v_i(t)$, $i = \{1, 2, 3, 6, 8\}$; *b*) voltage error $v_i(t) - v_0(t)$, $i = \{1, 2, 3, 6, 8\}$, *c*) reactive power Q_i, $i = \{1, 2, 3, 6, 8\}$.

the presence of disturbances acting on DGs dynamics, multiple reference changes and deviations induced by PC. Specifically, from Figure 8.2(a), it is shown that, prior to $t = 2$ $[s]$, where only PC is activated, each DG voltage is deviated from the desired set-point. Then, after activating the proposed DET controller at $t = 2$ $[s]$, voltage deviations are quickly compensated to the reference voltage value $v_0 = 1.02$ $[p.u.]$. Moreover, they are also restored after each reference changing happening at $t = 20$ $[s]$ and $t = 45$ $[s]$, respectively, thus allowing the voltage errors to approach to zero (see Figure 8.2(b)). For completeness, the time history of reactive power Q_i of each DG, $i = 1, \ldots, 5$ has been reported in Figure 8.2(c). Moreover, Figure 8.5(a) shows the detail of the event-trigger time instants of each

DG during the time interval $[2; 4]$ $[s]$ of this simulation scenario where, due to the DET mechanism, each DG is triggered aperiodically rather than continuously. Hence, Figure 8.5(a) highlights that the realise intervals are more frequent in transient phase while, after reaching steady-state, the number of sent control signals is smaller, thus confirming a reduction of the communication network workload.

8.4.2 Case B: Load Changing Scenario

To prove the robustness of the proposed control law with respect to changing in load requests, the following list of events are considered: i) at $t = 0$ $[s]$, only the PC works; ii) at $t = 2$ $[s]$, the voltage SC is switched ON with $v_0 = 1.02$ $[p.u.]$; iii) at $t = 20$ $[s]$, the voltage reference is changed as $v_0 = 1.03$ $[p.u.]$ and the nominal values of the loads increase by 30%; iv) at $t = 30$ $[s]$, there is an additional 20% of increase of the loads, until they restore their initial values at $t = 40$ $[s]$; v) at $t = 45$ $[s]$, voltage set-point restores to the initial value $v_0 = 1.02$ $[p.u.]$.
Results in Figure 8.3 illustrate the performance of the proposed control strategy in solving voltage regulation problem also in this more troublesome scenario where, besides voltage reference variations, there exist sudden changes in load demand. In particular, Figure 8.3(a) shows that, once the proposed SC is activated at $t = 2$ $[s]$, DGs voltages promptly react to both reference and load variations, thus synchronizing their values to the desired set-point imposed by the virtual DG 0. Hence, each DG voltage error with respect to the set-point v_0 converges to zero in the steady-state, with small tolerable errors occurring during each transient phase when reference/load variations occur (Figure 8.3(b)). Moreover, realise intervals of each DG are shown in Figure 8.5(b) for the time interval $[2; 4]$ $[s]$, i.e., after reaching the first steady-state, thus highlighting how the proposed DET mechanism allows reducing the number of control inputs computed at single agent level, while alleviating communication network via an aperiodic control. For completeness, the time-history of the reactive-power Q_i of each DG, has been reported in Figure 8.3(c).

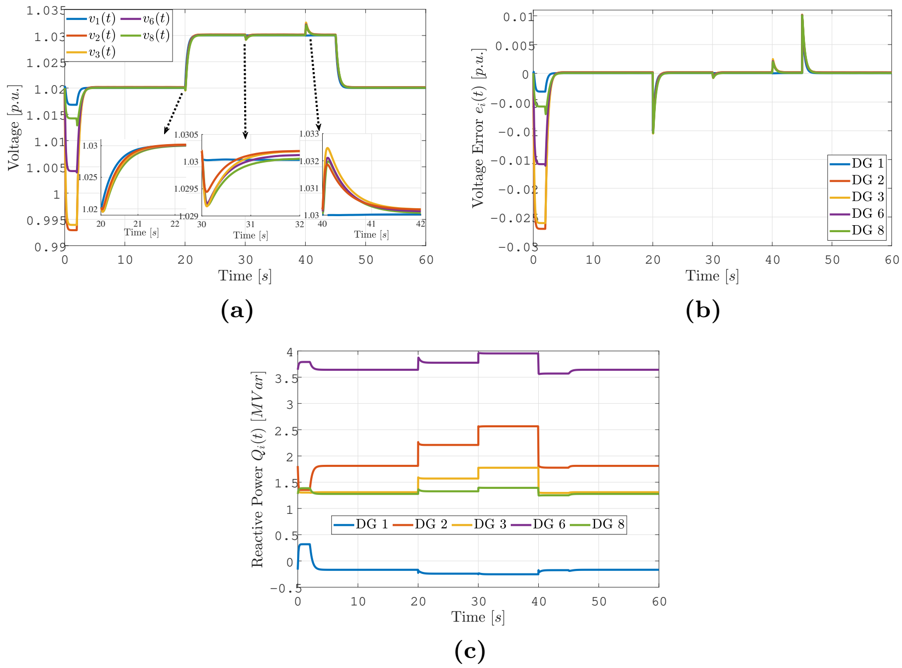

Figure 8.3. Voltage recovery in *load changing scenario* under the Distributed Dynamic Event-Triggered PID-like controller. Time history of: *a*) voltage $v_i(t)$, $i = \{1, 2, 3, 6, 8\}$; *b*) voltage error $v_i(t) - v_0(t)$, $i = \{1, 2, 3, 6, 8\}$, *c*) reactive power Q_i, $i = \{1, 2, 3, 6, 8\}$.

8.4.3 Case C: Plug and Play Scenario

Here, a more challenging scenario, involving multiple complex phenomena to be properly managed in order to maintain MG stability, is considered.

Specifically, the following simulation environment is emulated: *i*) at $t = 0$ [s], only the PC works; *ii*) at $t = 2$ [s], the voltage SC is switched ON with $v_0 = 1.02$ [$p.u.$]; *iii*) at $t = 20$ [s], the voltage reference is changed as $v_0 = 1.03$ [$p.u.$] and a 30% increase of the loads nominal values occur; *iv*) at $t = 24$ [s], DG 4 is unplugged; *v*) at $t = 30$ [s], the loads increase of an additional 20%; *vi*) at $t = 32$ [s], DG 4 is plugged-in; *vii*) at $t = 40$ [s], loads are restored to their nominal values; *viii*) at $t = 45$ [s], voltage set-

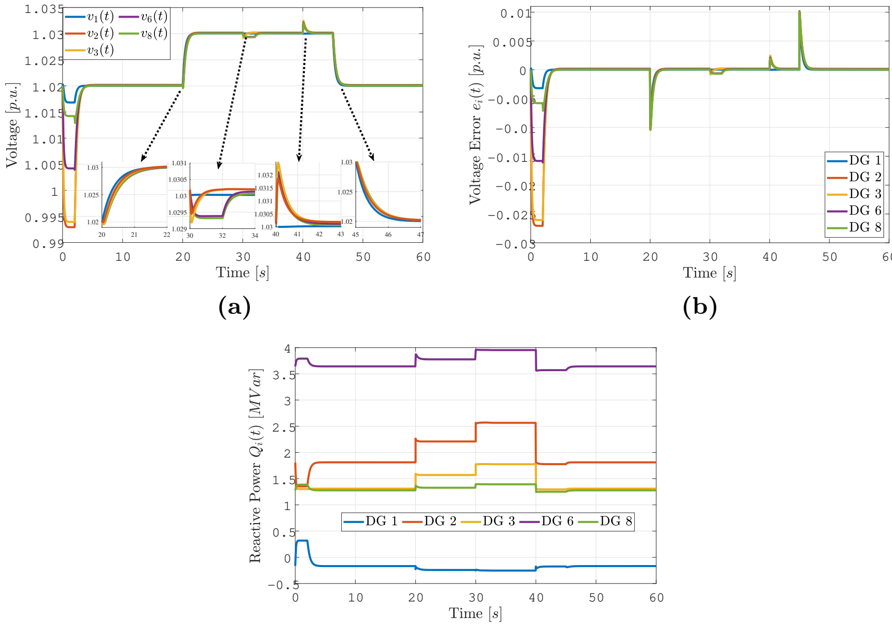

(a) **(b)**

(c)

Figure 8.4. Voltage recovery in *plug-and-play scenario* under the Distributed Dynamic Event-Triggered PID-like controller. Time history of: *a*) voltage $v_i(t)$, $i = \{1, 2, 3, 6, 8\}$; *b*) voltage error $v_i(t) - v_0(t)$, $i = \{1, 2, 3, 6, 8\}$, *c*) reactive power Q_i, $i = \{1, 2, 3, 6, 8\}$.

point restores to the initial value $v_0 = 1.02$ $[p.u.]$.
The effectiveness of the proposed control protocol in successfully achieving voltage synchronization is corroborated also in this worrying environment, as it is possible to observe in Figure 8.4. It is worth noting that the robustness of the proposed control strategy with respect to communication links failures is also guaranteed via this simulation scenario. Indeed, as one DG within the power network fails, it also implies losses for the cyber links connected to the unplugged DGs [125]. It means that when DG 4 is unplugged at $t = 24$ $[s]$, communication links $(2, 4)$, $(3, 4)$ and $(4, 5)$ become useless. Although these plug-and-play phenomena, along with reference/load variations, may compromise MG voltage stability, the

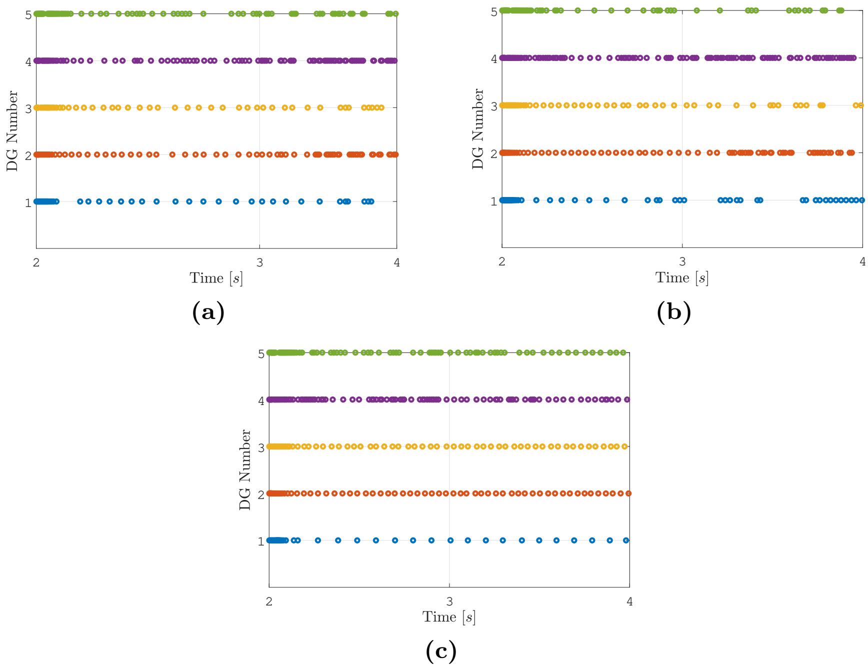

Figure 8.5. Event-triggered time of each DG i, $i = 1, \ldots, 5$ under the Distributed Dynamic Event-Triggered PID-like controller: *a) nominal scenario*; *b) load changing scenario*; *c) plug-and-play scenario*.

performance of the designed SC are confirmed and the voltage recovery problem can be considered as successfully solved also in this case (see Figure 8.4(a)-(c)) with a good trade-off between control performances and number of triggering instants (see Figure 8.5(c)).

8.4.4 Comparison With Conventional Static ET Control and Other State-of-the-Art Digital Controller

To further highlight the advantages of the proposed distributed DET PID-like controller in guaranteeing voltage restoration while reducing communication network workload, by considering the same simulation environment as in Case C, a comparison of its performance with the one achievable

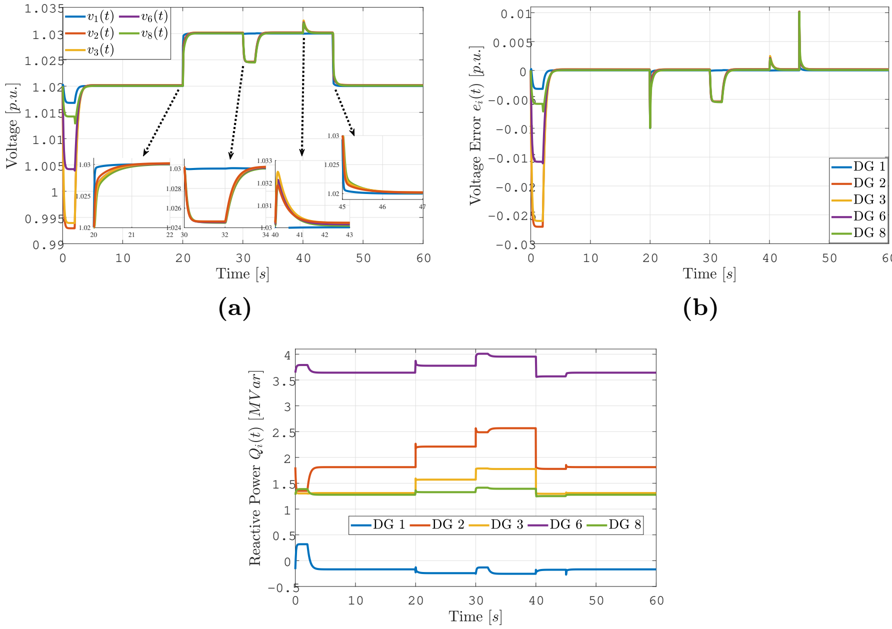

(a) (b) (c)

Figure 8.6. Comparison analysis: voltage recovery in *plug-and-play scenario* under the Distributed Static Event-Triggered PID-like controller. Time history of: a) voltage $v_i(t)$, $i = \{1, 2, 3, 6, 8\}$; b) voltage error $v_i(t) - v_0(t)$, $i = \{1, 2, 3, 6, 8\}$, c) reactive power Q_i, $i = \{1, 2, 3, 6, 8\}$.

via two different kind of controllers is provided. Specifically, for comparison purposes, a conventional Static ET mechanism (resulting from (8.15) with $\gamma = 0$) and the sampled-data controller recently suggested in [14] (see Chapter 7), where no ET conditions are involved, are considered.
The sampling period of the sampled-data controller in [14] is set to be $h = 0.002$, while the static triggered threshold is chosen as $\sigma = 0.2$ so to provide a fair comparison.
Results in Figure 8.6 and Figure 8.7 highlight the performance of the two alternative controllers under comparison in dealing with voltage regulation problem despite the occurrence of the multiple reference/loads changing and plug-and-play phenomena. Performance of static ET (see Figure 8.6)

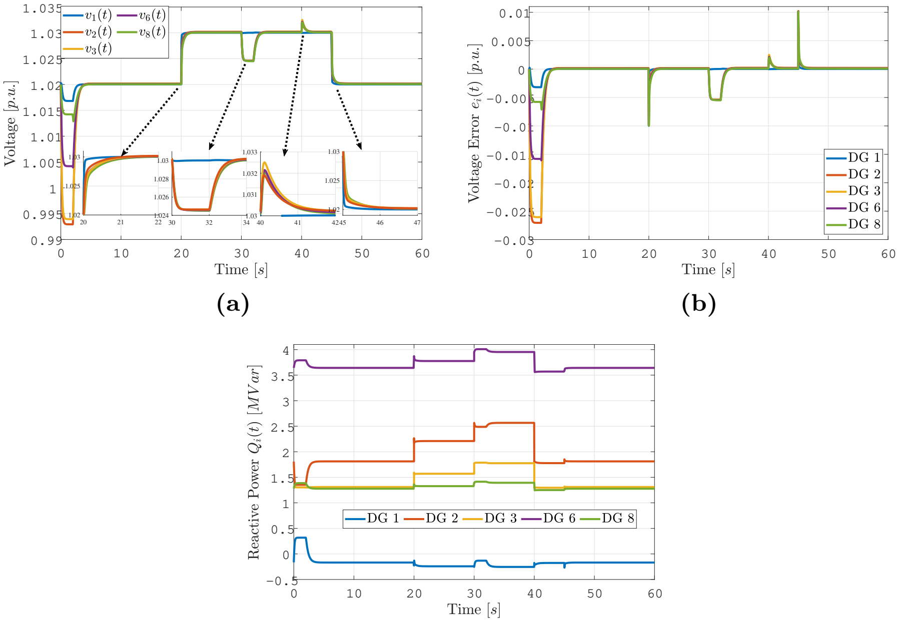

(c)

Figure 8.7. Comparison analysis: voltage recovery in *plug-and-play scenario* under the Distributed Sampled-data PID-like controller in [14]. Time history of: *a*) voltage $v_i(t)$, $i = \{1, 2, 3, 6, 8\}$; *b*) voltage error $v_i(t) - v_0(t)$, $i = \{1, 2, 3, 6, 8\}$, *c*) reactive power Q_i, $i = \{1, 2, 3, 6, 8\}$.

and sampled-data control laws [14] (see Figure 8.7) reveal good voltage recovery performances similar to Figure 8.4. Besides a slight improvement in transient performances ensured by the proposed DET-based distributed controller, it is crucial to note the significant reduction into the number of sent control signals achievable via the proposed controller at single agent level. Comparison among the three controllers in terms of total trigger times are shown in Figure 8.8. More in details, by considering a simulation time interval of 60 $[s]$, each DG under distributed sampled-data controller in [14] computes $60/h + 1 = 30001$ control signals. Conversely, the total number of trigger times for DG i, with $i = 1, \ldots, 5$ under static ET mechanism are 1451, 1997, 1522, 2615 and 2700, respectively. Al-

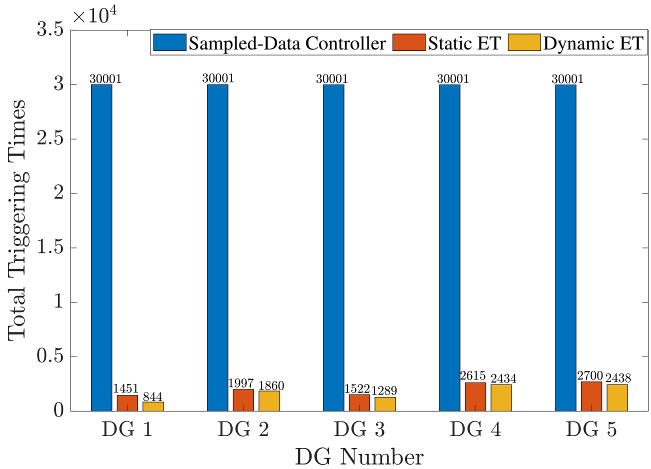

Figure 8.8. Total trigger times of three secondary controllers: sampled-data controller in [14] (blue bar), static ET (red bar), proposed DET (yellow bar).

Table 8.1. Reduction percentage of triggering number w.r.t. Sampled-Data Controller in [14] and Static ET (with $\gamma = 0$ in (8.14)).

Controller	**DG 1**	**DG 2**	**DG 3**	**DG 4**	**DG 5**	**Total**
Sampled Data Controller	−97.18	−93.8	−95.7	−91.89	−91.87	−94.1
Static ET	−41.83	−6.87	−15.31	−6.92	−9.70	−13.81

though the crucial reduction resulting from the static ET, the proposed DET mechanism allows to further decrease the number of the control signals computed by each DG i, whose values are 844, 1860, 1289, 2434 and 2438, respectively. This confirms that static ET triggers more frequently than our DET mechanism. Finally, Table 8.1 summarizes the reduction percentage of triggering number ensured by our approach with respect to the alternative sampled-data controller and static ET mechanism for each DG unit. Herein, it is also possible to appreciate that, at the global level, the reduction of the computational burden is of about 94.1% and 13.81%, respectively.

8.5 Concluding Remarks

This study has introduced a distributed DET PIR control law to solve voltage regulation problem in islanded MG with limited communication network resources. By exploiting artificial delay approach combined with finite-difference approximation, as well as Lyapunov-Krasovskii method, voltage recovery in the whole network is exponentially achieved, meaning that each DG voltage tracks the desired reference, while reducing the number of sent control input and saving network workload. The theoretical derivation provides stability conditions in the form of LMIs, whose solution allows finding upper bounds on sampling period and parameters involved into the DET mechanism preserving voltage stability. Extensive numerical simulation, carried out on the IEEE 14 bus test systems, confirms the effectiveness and the robustness of the approach in successfully solving voltage regulation problem in different challenging situations. Finally, a comparative study shows the advantages of the proposed strategy in reducing network communication burden.

Chapter 9

Control of Switching DC Power Converter via a time-delay approach to averaging

This chapter investigates the stability of systems with fast-varying piecewise-continuous coefficients and non-small delays. Starting from a recent constructive time-delay approach to periodic averaging, that allowed finding upper bound on small parameter $\epsilon > 0$ preserving the stability of the original delay-free systems, here the method is extended to systems with non-small delays, whose ISS is analytically proven. The original time-delay system is transformed into a neutral type one embedding both initial non-small delay, whose upper bound is essentially larger than ϵ and does not vanish for $\epsilon \to 0$, and an additional induced delay due to transformation, whose length is proportional to ϵ. By exploiting Lyapunov-Krasovskii theory, ISS conditions are derived as LMIs, whose solution allows evaluating upper bounds both on small parameter ϵ and non-small delays preserving the ISS of the original time-delay system, as well as the resulting ultimate bound of its solutions. These theoretical results are further applied for stabilization of delayed affine systems by time-dependent switching. Three numerical examples including the stabilization of a flyback power converter illustrate the effectiveness of the approach.

9.1 Averaging of systems with fast-varying coefficients and non-small delays with application to stabilization of affine systems

Averaging is one of the most powerful tools to deal with the stability of time-varying systems with a small parameter $\epsilon > 0$. [144, 189, 190]. The key idea of averaging relies in the approximation of the solution of a time-varying system by the one of the averaged system. It has been proven that, under the assumption of exponential stability of the averaged system, the asymptotic stability of the original one can be also guaranteed if ϵ is small enough [144]. However, as pointed out in [40], the main drawback of this classical approach is the inability to provide an efficient quantitative upper bound on the small parameter ϵ till which stability is still ensured, thus fixing its proper value on the basis of numerical simulations [191]. To overcome this limitation, a time-delay-based approach to periodic averaging has been recently introduced in [40], where the focus is to present original system as a neutral type system whose delay length is equal to ϵ. This kind of representation enables the derivation of ISS conditions in terms of LMIs by leveraging Lyapunov-Krasovskii theory for time-delay systems. These LMIs allow finding the upper bound of the small parameter preserving the stability for a certain decay rate. Moreover, different from classical averaging theory, where system coefficients are assumed continuous in time [144], this new approach allows considering them as piecewise-continuous, thus covering also the class of fast switching systems. An extension of this approach can be found in [46], where ISS and L_2-gain analysis are provided both for deterministic and stochastic systems, while in [192] the time-delay approach has been applied for extremum seeking systems.

The classical averaging for systems with delays was presented in [191], [193] and [194]. For instance, the stabilization of the inverted pendulum in the presence of feedback delays and periodic disturbances has been studied in [191] via classical averaging tools, but fixing both ϵ and delay values on the basis of numerical simulations and without providing stability conditions able to find their upper bounds preserving stability performances.

The significance of [191] is that it shows that the appropriate averaged equations retain the delay term, as opposed to earlier results which suggest that the delay term can be neglected. The time-delay approach to periodic averaging for systems with small delays of the order of ϵ was developed in [40]. However, constructive conditions with efficient quantitative bounds for systems with non-small delays whose upper bound is essentially larger than ϵ and does not vanish for $\epsilon \to 0$ is still an open problem.

As a subclass of hybrid systems, switched systems have received wide attention and there exist many contributions aiming at stabilizability [195], synchronization [196] and fault estimation [197]. Among switched systems family, the switched affine systems have attracted great interests due to its practical applications including DC-DC power conversion [198, 199] and biochemical networks [200]. The control goal is first to find a region of attainable equilibrium points and then designing a proper switching function to drive the state trajectories to the desired one. In general, the switched affine system have several equilibrium points which may not be equilibrium point of any isolated subsystem [201]. Thus, the control is very challenging and requires an appropriate switching rule in order to achieve practical stabilization in the neighborhood of the desirable equilibrium point [199, 202, 203, 204, 205, 206]. For designing the switching function that stabilizes unstable linear systems, the existence of Hurwitz convex combination guarantees existence of both state- and time-dependent stabilizing switching rules [207]. For stabilization of the switched affine systems, most of the works suggest the state-dependent switching [203, 204]. Recently state-dependent switching was extended to affine systems with state delay [208, 38]. Furthermore, to enlarge switching frequency, switching control together with event-triggered mechanism have been employed for general LPV systems [209, 210, 211].

Differently from the state-dependent switching, the time-dependent switching law does not need to perform measurements and calculations. The time-dependent switching law of linear systems with Hurwitz convex combination and uncertainties can be designed by using periodic averaging as was suggested recently in [40], where the switching period can be found from LMIs. However, results of [40] were confined to linear uncertain systems (without the affine terms), whereas the delay was of the order of $\mathscr{O}(\epsilon)$.

The aim of this chapter is to extend the time-delay approach to periodic averaging to the class of linear systems with fast-varying coefficients in the presence of non-small delays. For this class of systems we consider the ISS analysis, which allows providing the explicit expression of the Ultimate Bound (UB) for the solutions of the original systems. The result of the proposed procedure are LMIs-based conditions for finding upper bounds both on small parameter ϵ and non-small delays preserving ISS for desired decay rate. Therefore, the main contributions of the work can be summarized as follows: *i*) different from [40] (see Section 5), where state delays upper bound is of order of $\mathscr{O}(\epsilon)$, through this chapter this assumption on delays size is relaxed by considering non-small delays; *ii*) the ISS analysis for this class of systems via Lyapunov-Krasovskii theory leads to bounds on both delay and ϵ ensuring stability, as well as an explicit form of the UB; *iii*) the results are applied to delayed switched affine systems allowing simple time-dependent switching in the presence of delays and system uncertainties, that is crucial for the stabilization of switch-mode DC power converter. As pointed out in [191], extension of averaging to delays whose upper bound is essentially larger than ϵ is important in many practical applications due to non-small delays that appear in feedback controllers or internal dynamics latencies. To achieve this goal, a novel neutral-type transformation is introduced, which implies also the need of a novel Lyapunov-Krasovskii functional. This latter leads for the first time to stability conditions that allows analytically finding upper bounds on ϵ and non-small delays, whose value is essentially larger than ϵ.

Remark 20. *Note that, a vector function $h(\epsilon)$ is of the order of ϵ, i.e. $h(\epsilon) \sim \mathscr{O}(\delta(\epsilon))$, if there exist positive constants k and c such that $|h(\epsilon)| \leq k|\delta(\epsilon)|$, $\forall |\epsilon| < c$ (see Definition 10.1 on p. 383 of [144]).*

9.2 Periodic averaging of systems with non-small delays

Given piecewise-continuous $A : [0, \infty) \to \mathbb{R}^{n\times n}$ and $B : [0, \infty) \to \mathbb{R}^{n\times n_w}$, a constant matrix $A_d \in \mathbb{R}^{n\times n}$ and a small parameter $\epsilon > 0$, the following class of fast-varying systems is considered (see [193]):

$$\dot{x}(t) = A(\tfrac{t}{\epsilon})x(t) + (A_d + \Delta A_d(t))x(t - h(t)) + B(\tfrac{t}{\epsilon})w(t), \qquad t \geq 0, \quad (9.1)$$

where $x(t) \in \mathbb{R}^n$ is the system state and $w(t) \in \mathbb{R}^{n_w}$ is the disturbance, assumed to be locally essentially bounded, i.e. $w(t) \in L_\infty(0,t), \forall t > 0$. Moreover, $\Delta A_d(t)$ stands for parameter uncertainties affecting the delayed part such that $\|\Delta A_d(t)\| \leq \kappa_d$, with $\kappa_d > 0$ a known constant. The function $h(t)$ is the delay, assumed to be time-varying and bounded, i.e. $0 \leq h(t) \leq h_M$. Initial conditions of system (9.1) are given as $x(\theta) = \phi(\theta), \theta \in [-h_M, 0]$ and ϕ absolutely continuous with $\dot{\phi} \in L_2[-h_M, 0]$.

Remark 21. *System (9.1) contains both fast time $\frac{t}{\epsilon}$ and slow time t. To deal with the interaction of slow and fast variables, classical averaging procedure has been deeply exploited [144, 193]. Note that, compared to classical Linear Parameter-Varying (LPV) system $\dot{x}(t) = A(t)x(t)$, the introduction of small parameter $\epsilon > 0$ re-scales this latter to the fast-time $\frac{t}{\epsilon}$. Thus, for ϵ small enough, $A(\frac{t}{\epsilon})$ varies faster than $A(t)$.*

Let us introduce the following assumptions that are instrumental through the chapter.

Assumption 10. *The following holds:*

$$\frac{1}{\epsilon T}\int_{t-\epsilon T}^{t} A(\tfrac{s}{\epsilon})ds = A_{av} + \Delta A(\tfrac{t}{\epsilon}), \quad \|\Delta A(\tfrac{t}{\epsilon})\| \leq \kappa, \qquad \forall \tfrac{t}{\epsilon} \geq T, \quad (9.2)$$

where $A_{av} + A_d$ is Hurwitz matrix, T is the averaging period and $\kappa > 0$ is a small enough constant.

If $A_{av} + A_d$ is Hurwitz, then the unperturbed averaged system

$$\dot{x}_{av}(t) = [A_{av} + \Delta A(\tfrac{t}{\epsilon})]x_{av}(t) + (A_d + \Delta A_d(t))x_{av}(t - h(t)) \qquad (9.3)$$

is exponentially stable for small enough $\kappa > 0$, $\kappa_d > 0$ and $h_M \sim \mathscr{O}(\epsilon)$ [40, 97]. Here $\Delta A(\frac{t}{\epsilon})$ involves system uncertainty, whose norm is upper bounded by a known constant $\kappa > 0$.

Assumption 11. *Following [40], all the entries $a_{kj}(\frac{t}{\epsilon})$ of $A(\frac{t}{\epsilon})$ in (9.1) belong to some finite intervals, i.e., $a_{kj}(\frac{t}{\epsilon}) \in [\underline{a}_{kj}, \bar{a}_{kj}]$ for $\frac{t}{\epsilon} \geq T$, meaning that all a_{kj} are uniformly bounded, $\forall k, j = 1, \ldots, n$.*

If Assumption 11 is fulfilled, then $A(\tau)$ in (9.1) with $\tau = \frac{t}{\epsilon}$ can be expressed as the following convex combination:

$$A(\tau) = \sum_{i=1}^{N} \rho_i(\tau) A_i \quad \forall \tau \geq T, \quad \rho_i \geq 0, \quad \sum_{i=1}^{N} \rho_i = 1, \quad 1 \leq N \leq 2^{n^2}, \tag{9.4}$$

being A_i constant matrices with entries $\underline{a}_{kj}$ or $\bar{a}_{kj}$.

Assumption 12. *All the entries $b_{kv}(\frac{t}{\epsilon})$, $v = 1, \ldots, n_w$, of $B(\frac{t}{\epsilon})$ in (9.1) belong to some finite intervals, i.e., $b_{kv}(\frac{t}{\epsilon}) \in [\underline{b}_{kv}, \bar{b}_{kv}]$ for $\frac{t}{\epsilon} \geq T$, meaning that all b_{kv} are uniformly bounded.*

If Assumption 12 holds, then $B(\tau)$ can be presented as

$$B(\tau) = \sum_{l=1}^{\bar{N}} f_l(\tau) B_l, \quad \forall \tau \geq T, \quad f_l \geq 0, \quad \sum_{l=1}^{\bar{N}} f_l = 1, \quad 1 \leq \bar{N} \leq 2^{n \times n_w}, \tag{9.5}$$

where B_l are constant matrices whose entries are $\underline{b}_{kv}$ or $\bar{b}_{kv}$.

9.2.1 Transformation to a neutral type system

Following the time-delay approach to averaging [40], (9.1) will be presented in the form of neutral type system with additional distributed delays of the length of ϵT. Let us introduce the following notations:

$$g(t, \epsilon) = A(\tfrac{t}{\epsilon}) x(t) + B(\tfrac{t}{\epsilon}) w(t), \tag{9.6}$$

$$G(t, \epsilon) \triangleq \frac{1}{\epsilon T} \int_{t-\epsilon T}^{t} (s - t + \epsilon T) g(s, \epsilon) \, ds. \tag{9.7}$$

For shortness, the dependence on ϵ of g, G and Y in (9.11) will be omitted below.

Then, by exploiting [46] and [212], it follows:

$$\begin{aligned}\frac{1}{\epsilon T}\int_{t-\epsilon T}^{t}\dot{x}(s)\,ds = \frac{1}{\epsilon T}\left[x(t)-x(t-\epsilon T)\right] = \frac{d}{dt}[x(t)-G(t)\\ -\frac{1}{\epsilon T}\int_{t-\epsilon T}^{t}(A_d+\Delta A_d(s))(s-t+\epsilon T)x(s-h(s))\,ds]\\ = \frac{d}{dt}\left[x(t)-G(t)\right]+\frac{1}{\epsilon T}\int_{t-\epsilon T}^{t}(A_d+\Delta A_d(s))x(s-h(s))\,ds\\ -(A_d+\Delta A_d(t))x(t-h(t)).\end{aligned} \tag{9.8}$$

Integrating (9.1) on $[t-\epsilon T, t]$ for $t \geq \epsilon T + h_M$ and denoting $z(t) = x(t) - G(t)$, it yields:

$$\begin{aligned}\dot{z}(t) =& \frac{1}{\epsilon T}\int_{t-\epsilon T}^{t} A(\tfrac{s}{\epsilon})x(s)\,ds + (A_d+\Delta A_d(t))x(t-h(t))\\ &+ \frac{1}{\epsilon T}\int_{t-\epsilon T}^{t} B(\tfrac{s}{\epsilon})w(s)\,ds.\end{aligned} \tag{9.9}$$

By exploiting Assumption 10, the first integral term of (9.9) can be presented as

$$\begin{aligned}\frac{1}{\epsilon T}\int_{t-\epsilon T}^{t} A(\tfrac{s}{\epsilon})\left[x(s)+x(t)-x(t)\right]\,ds = \frac{1}{\epsilon T}\int_{t-\epsilon T}^{t} A(\tfrac{s}{\epsilon})x(t)\,ds\\ +\frac{1}{\epsilon T}\int_{t-\epsilon T}^{t} A(\tfrac{s}{\epsilon})[x(s)-x(t)]\,ds = \left[A_{av}+\Delta A(\tfrac{t}{\epsilon})\right]x(t)-Y(t),\end{aligned} \tag{9.10}$$

with

$$Y(t) = \frac{1}{\epsilon T}\int_{t-\epsilon T}^{t} A(\tfrac{s}{\epsilon})\int_{s}^{t}\dot{x}(\theta)\,d\theta\,ds, \tag{9.11}$$

while for the second integral term of (9.9) Assumption 12 can be exploited, i.e.,

$$\frac{1}{\epsilon T}\int_{t-\epsilon T}^{t} B(\tfrac{s}{\epsilon})w(s)\,ds = \int_{0}^{1} B(\tfrac{t}{\epsilon}-T\theta)w(t-\epsilon T\theta)\,d\theta = \sum_{l=1}^{\bar{N}} B_l w_l(t), \tag{9.12}$$

with

$$w_l(t) \triangleq \int_0^1 f_l(\tfrac{t}{\epsilon} - T\theta)w(t - \epsilon T\theta)\, d\theta. \tag{9.13}$$

Note that

$$\begin{aligned} |w_l(t)| &= \left|\int_0^1 f_l(\tfrac{t}{\epsilon} - T\theta)w(t - \epsilon T\theta)\, d\theta\right| \\ &\leq \int_0^1 |f_l(\tfrac{t}{\epsilon} - T\theta)||w(t - \epsilon T\theta)|\, d\theta \leq \|w[0,t]\|_\infty, \end{aligned} \tag{9.14}$$

$\forall l = \{1, \ldots, \bar{N}\}$, $t \geq \epsilon T$ due to $0 \leq f_l \leq 1$. Therefore, system (9.9) can be finally rewritten as:

$$\begin{aligned} \dot{z}(t) &= \left[A_{av} + \Delta A(\tfrac{t}{\epsilon})\right] x(t) - Y(t) + (A_d + \Delta A_d(t))x(t - h(t)) \\ &\quad + \sum_{l=1}^{\bar{N}} B_l w_l(t), \qquad t \geq \epsilon T + h_M. \end{aligned} \tag{9.15}$$

System (9.15) is a kind of neutral type system, where $\dot{x}$ is given by (9.1). If $w(t) = 0$, (9.15) can be considered as a perturbation of the averaged system (9.3) due to the presence of additional terms $G(t)$ and $Y(t)$, both of them of the order of $\mathscr{O}(\epsilon)$ provided $x(t)$ and $\dot{x}(t)$ are of the order of $\mathscr{O}(1)$. Therefore, any solution $x(t)$ of (9.1) satisfies (9.15). Thus, ISS of (9.15) guarantees ISS of (9.1).

9.2.2 ISS analysis via direct Lyapunov method

In the sequel, Lyapunov-Krasovskii method for time-delay systems is exploited in order to find ISS conditions expressed as LMIs. Upper bounds $\epsilon^\star$ on ϵ and h_M on the delay $h(t)$ that ensure ISS of (9.15) can be found from these LMIs.

Theorem 9. *Let Assumptions 10-12 hold. Given matrices A_{av}, $A_i(i = 1, \ldots, N)$, A_d, $B_l(l = 1, \ldots, \bar{N})$ and positive constants κ, κ_d, α, $\epsilon^\star$, T and h_M, let there exist positive-definite matrices P, R, H, W, S and $\bar{H} \in \mathbb{R}^{n\times n}$, a matrix $U \in \mathbb{R}^{n\times n}$ and positive scalars b_0, b_1, $\ldots$, $b_{\bar{N}}$, λ, λ_d*

that satisfy the following LMIs:

$$\begin{bmatrix} P & -P \\ \star & P + e^{-2\alpha\epsilon^\star T} R \end{bmatrix} \geq 0, \tag{9.16}$$

$$\begin{bmatrix} W & U \\ \star & W \end{bmatrix} \geq 0, \tag{9.17}$$

$$\frac{1}{T^2} \int_{\tau-T}^{\tau} (\zeta - \tau + T) A^\top(\zeta) H A(\zeta)\, d\zeta \leq \bar{H} \quad \forall \tau \geq T, \tag{9.18}$$

and

$$\left[\begin{array}{c|c} \Omega & \begin{array}{ccc} \sqrt{\epsilon^\star T} A_i^\top R & \sqrt{\epsilon^\star T} A_i^\top \bar{H} & \sqrt{h_M} A_i^\top W \\ 0_{3n\times n} & 0_{3n\times n} & 0_{3n\times n} \\ 0_{n\times n} & \sqrt{\epsilon^\star T} A_d^\top \bar{H} & \sqrt{h_M} A_d^\top W \\ \hline 0_{n\times n} & 0_{n\times n} & 0_{n\times n} \\ 0_{n\times n} & \sqrt{\epsilon^\star T} \bar{H} & \sqrt{h_M} W \\ 0_{\bar{N}\times n} & 0_{\bar{N}\times n} & 0_{\bar{N}\times n} \\ \hline \sqrt{\epsilon^\star T} B_l^\top R & \sqrt{\epsilon^\star T} B_l^\top \bar{H} & \sqrt{h_M} B_l^\top W \end{array} \\ \hline \star & \begin{array}{ccc} -R & 0_{n\times n} & 0_{n\times n} \\ \star & -\bar{H} & 0_{n\times n} \\ \star & \star & -W \end{array} \end{array}\right] < 0, \tag{9.19}$$

$i = 1, \ldots, N$, $l = 1, \ldots, \bar{N}$, where $\Omega \in \mathbb{R}^{\nu\times\nu}$ with $\nu = 7n + (\bar{N}+1)n_w$ is the symmetric block matrix whose elements are

$$\Omega_{11} = PA_{av} + A_{av}^\top P + 2\alpha P + S + \lambda\kappa^2 I_n - \frac{1}{h_M}\rho_H W \in \mathbb{R}^{n\times n},$$

$$\Omega_{12} = -A_{av}^\top P - 2\alpha P \in \mathbb{R}^{n\times n}, \qquad \Omega_{13} = \Omega_{24} = \Omega_{27} = -P \in \mathbb{R}^{n\times n},$$

$$\Omega_{14} = \Omega_{17} = \Omega_{23} = P \in \mathbb{R}^{n\times n}, \quad \Omega_{15} = PA_d + \frac{1}{h_M}\rho_H (W - U) \in \mathbb{R}^{n\times n},$$

$$\Omega_{16} = \frac{1}{h_M}\rho_H U \in \mathbb{R}^{n\times n}, \quad \Omega_{25} = -PA_d \in \mathbb{R}^{n\times n}, \quad \Omega_{44} = -\lambda I_n \in \mathbb{R}^{n\times n},$$

$$\Omega_{18} = P\,[B_1 \;\; B_2 \;\; \ldots \;\; B_{\bar{N}} \;\; 0_{n\times n_w}] \in \mathbb{R}^{n\times(\bar{N}+1)n_w},$$

$$\Omega_{22} = -\frac{4}{\epsilon^\star T}\rho_\epsilon R + 2\alpha P \in \mathbb{R}^{n\times n}, \quad \Omega_{28} = -\Omega_{18},$$

$$
\begin{aligned}
&\Omega_{55} = -\frac{1}{h_M}\rho_H(2W - U - U^\top) + \lambda_d\kappa_d^2 I_n \in \mathbb{R}^{n\times n}, \quad \rho_H = e^{-2\alpha h_M},\\
&\Omega_{56} = -\frac{1}{h_M}\rho_H(W - U) \in \mathbb{R}^{n\times n}, \quad \Omega_{66} = -\rho_H\left(S + \frac{1}{h_M}W\right) \in \mathbb{R}^{n\times n},\\
&\Omega_{33} = -\frac{2}{\epsilon^\star T}\rho_\epsilon H \in \mathbb{R}^{n\times n}, \quad \Omega_{77} = -\lambda_d I_n \in \mathbb{R}^{n\times n}, \quad \rho_\epsilon = e^{-2\alpha\epsilon^\star T},\\
&\Omega_{88} = -diag\{b_1 I_{n_w}, \ \ldots, \ b_{\bar N} I_{n_w}, \ b_0 I_{n_w}\} \in \mathbb{R}^{(\bar N+1)n_w \times (\bar N+1)n_w}.
\end{aligned} \tag{9.20}
$$

Then, for all $\epsilon \in (0, \epsilon^\star]$ *there exists a positive constant* ν *such that the solutions of the delayed system* (9.1) *initialized by* $\phi \in W[-h_M, 0]$ *satisfy*

$$
\begin{aligned}
|x(t)|^2 \leq & \nu e^{-2\alpha(t-\epsilon^\star T - h_M)}\|\phi\|_W^2\\
&+ \left[\nu e^{-2\alpha(t-\epsilon^\star T-h_M)} + \frac{\sum_{l=0}^{\bar N} b_l}{2\alpha}\right]\|w[0,t]\|_\infty^2, \quad \forall t \geq 0
\end{aligned} \tag{9.21}
$$

for all locally essentially bounded $w(t)$ *and* $\phi \in W[-h_M, 0]$*, meaning that* (9.1) *is ISS for all* $\epsilon \in (0, \epsilon^\star]$ *and* $h(t) \in [0, h_M]$*. Moreover, given* $\Delta > 0$*, the ball*

$$
\mathscr{X} = \left\{ x \in \mathbb{R}^n : |x|^2 \leq \frac{b_0 + \cdots + b_{\bar N}}{2\alpha}\Delta^2 \right\} \tag{9.22}
$$

is exponentially attractive with a decay rate α *for* (9.1)*.*

Proof. Consider the following Lyapunov-Krasovskii functional:

$$
V(t) = V_P(t) + V_R(t) + V_H(t) + V_S(t) + V_W(t), \tag{9.23}
$$

with

$$
V_P(t) = z^\top(t)Pz(t), \tag{9.24}
$$

$$
V_R(t) = \frac{1}{\epsilon T}\int_{t-\epsilon T}^{t} e^{-2\alpha(t-s)}(s - t + \epsilon T)^2 g^\top(s)Rg(s)\, ds, \tag{9.25}
$$

$$
V_H(t) = \frac{1}{\epsilon T}\int_{t-\epsilon T}^{t}\int_{s}^{t} e^{-2\alpha(t-\theta)}(s - t + \epsilon T)\dot x^\top(\theta)A^\top(\tfrac{s}{\epsilon})HA(\tfrac{s}{\epsilon})\dot x(\theta)\, d\theta\, ds, \tag{9.26}
$$

$$V_S(t) = \int_{t-h_M}^{t} e^{-2\alpha(t-s)} x^\top(s) S x(s)\, ds, \tag{9.27}$$

$$V_W(t) = \int_{t-h_M}^{t} (s-t+h_M) e^{-2\alpha(t-s)} \dot{x}^\top(s) W \dot{x}(s)\, ds. \tag{9.28}$$

Note that $V_R(t)$ and $V_H(t)$ in (9.25)-(9.26) are to compensate $G(t)$ and $Y(t)$ in (9.15), while $V_S(t)$ and $V_W(t)$ in (9.27)-(9.28) are standard terms for delay-dependent stability to compensate delay $x(t-h(t))$.
Differentiating $V_P(t)$ and $V_R(t)$ along the trajectories of (9.15) it follows:

$$\begin{aligned}\dot{V}_P(t) + 2\alpha V_P(t) =& 2\left[x(t) - G(t)\right]^\top P[(A_{av} + \Delta A(\tfrac{t}{\epsilon}))x(t) - Y(t) \\ &+ (A_d + \Delta A_d(t))x(t-h(t)) + \sum_{l=1}^{\bar{N}} B_l w_l(t)] \\ &+ 2\alpha \left[x(t) - G(t)\right]^\top P \left[x(t) - G(t)\right], \end{aligned} \tag{9.29}$$

$$\begin{aligned}\dot{V}_R(t) + 2\alpha V_R(t) =& (\epsilon T) g^\top(t) R g(t) \\ &- \frac{2}{\epsilon T} \int_{t-\epsilon T}^{t} e^{-2\alpha(t-s)} (s-t+\epsilon T) g^\top(s) R g(s)\, ds. \end{aligned} \tag{9.30}$$

For the integral term in (9.30), Jensen's inequality in Lemma 4 ensures that

$$2G^\top(t) R G(t) \le \int_{t-\epsilon T}^{t} (s-t+\epsilon T) g^\top(s) R g(s)\, ds. \tag{9.31}$$

Then, inequality (9.30) can be re-written as

$$\dot{V}_R(t) + 2\alpha V_R(t) \le (\epsilon T) g^\top(t) R g(t) - \frac{4}{\epsilon T} e^{-2\alpha\epsilon T} G^\top(t) R G(t), \tag{9.32}$$

with $g(t)$ presented as

$$g(t) = \sum_{i=1}^{N} \rho_i(\tfrac{t}{\epsilon}) A_i x(t) + \sum_{l=1}^{\bar{N}} f_l(\tfrac{t}{\epsilon}) B_l w(t), \tag{9.33}$$

where Assumption 11 and Assumption 12 have been exploited. By differentiating $V_H(t)$ in (9.26) along (9.15), it holds:

$$\begin{aligned}\dot{V}_H(t)+2\alpha V_H(t) \leq \dot{x}^\top(t)\Big(\frac{1}{\epsilon T}\int_{t-\epsilon T}^{t}(s-t+\epsilon T)A^\top(\tfrac{s}{\epsilon})HA(\tfrac{s}{\epsilon})\,ds\Big)\dot{x}(t)\\ -\frac{1}{\epsilon T}e^{-2\alpha\epsilon T}\int_{t-\epsilon T}^{t}\int_{s}^{t}\dot{x}^\top(\theta)A^\top(\tfrac{s}{\epsilon})HA(\tfrac{s}{\epsilon})\dot{x}(\theta)\,d\theta\,ds.\end{aligned} \tag{9.34}$$

For the first integral term in (9.34), as in [46], the change of variable $s=\epsilon\zeta$ along with the exploitation of inequality (9.18) lead to

$$\begin{aligned}&\frac{1}{\epsilon^2T^2}\int_{t-\epsilon T}^{t}(s-t+\epsilon T)A^\top(\tfrac{s}{\epsilon})HA(\tfrac{s}{\epsilon})\,ds\\ &\qquad=\frac{1}{T^2}\int_{\frac{t}{\epsilon}-T}^{\frac{t}{\epsilon}}(\zeta-\tfrac{t}{\epsilon}+T)A^\top(\zeta)HA(\zeta)\,d\zeta\leq\bar{H}.\end{aligned} \tag{9.35}$$

For the second integral term of (9.34) it is possible to apply extended Jensen's inequality in of Lemma 4, i.e.,

$$2Y^\top(t)HY(t)\leq\int_{t-\epsilon T}^{t}\int_{s}^{t}\dot{x}^\top(\theta)A^\top(\tfrac{s}{\epsilon})HA(\tfrac{s}{\epsilon})\dot{x}(\theta)\,d\theta\,ds, \tag{9.36}$$

thus obtaining the following inequality

$$\dot{V}_H(t)+2\alpha V_H(t)\leq(\epsilon T)\dot{x}^\top(t)\bar{H}\dot{x}(t)-\frac{2}{\epsilon T}e^{-2\alpha\epsilon T}Y^\top(t)HY(t). \tag{9.37}$$

Moreover, to compensate delayed terms, the differentiation of $V_S(t)$ in (9.27) and $V_W(t)$ in (9.28) yields the following:

$$\begin{aligned}\dot{V}_S(t)+2\alpha V_S(t)=&x^\top(t)Sx(t)-e^{-2\alpha h_M}x^\top(t-h_M)Sx(t-h_M),\\ \dot{V}_W(t)+2\alpha V_W(t)=&h_M\dot{x}^\top(t)W\dot{x}(t)-\int_{t-h_M}^{t}e^{-2\alpha(t-s)}\dot{x}^\top(s)W\dot{x}(s)\,ds\\ &=h_M\dot{x}^\top(t)W\dot{x}(t)-\int_{t-h(t)}^{t}e^{-2\alpha(t-s)}\dot{x}^\top(s)W\dot{x}(s)\,ds\end{aligned}$$

$$- \int_{t-h_M}^{t-h(t)} e^{-2\alpha(t-s)} \dot{x}^\top(s) W \dot{x}(s)\, ds. \tag{9.38}$$

By applying Jensen's inequality to the last two integral terms of (9.38) together with Park inequality (see Lemma 3.4 in [97] and [174]) it yields:

$$\begin{aligned} \dot{V}_W(t)+2\alpha V_W(t) \leq\, & h_M \dot{x}^\top(t) W \dot{x}(t) \\ & - \frac{e^{-2\alpha h_M}}{h_M} \begin{bmatrix} x(t)-x(t-h(t)) \\ x(t-h(t))-x(t-h_M) \end{bmatrix}^\top \begin{bmatrix} W & U \\ \star & W \end{bmatrix} \begin{bmatrix} x(t)-x(t-h(t)) \\ x(t-h(t))-x(t-h_M) \end{bmatrix}, \end{aligned} \tag{9.39}$$

with matrix $U \in \mathbb{R}^{n\times n}$ such that inequality (9.17) holds. Summing-up (9.29)-(9.32)-(9.37)-(9.38)-(9.39) and by applying S-procedure to compensate the terms $\Delta A(\frac{t}{\epsilon})x(t)$ and $\Delta A_d(t)x(t-h(t))$ in (9.29), along (9.15), for $t \geq \epsilon T + h_M$ it yields:

$$\begin{aligned} \dot{V}(t) + 2\alpha V(t) \leq & \dot{V}(t) + 2\alpha V(t) + \lambda[\kappa^2 |x(t)|^2 - |\Delta A(\tfrac{t}{\epsilon})x(t)|^2] \\ & + \lambda_d[\kappa_d^2 |x(t-h(t))|^2 - |\Delta A_d(t)x(t-h(t))|^2], \end{aligned} \tag{9.40}$$

with some constant $\lambda > 0$ and $\lambda_d > 0$. Moreover, under Assumption 11 and Assumption 12, the derivative $\dot{x}(t)$ in (9.37)-(9.38) can be presented as

$$\dot{x}(t) = \sum_{i=1}^{N} \rho_i(\tfrac{t}{\epsilon}) A_i x(t) + (A_d + \Delta A_d(t)) x(t-h(t)) + \sum_{l=1}^{\bar{N}} f_l(\tfrac{t}{\epsilon}) B_l w(t). \tag{9.41}$$

Then, by introducing the following vectors

$$\begin{aligned} \zeta_1(t) &= \mathrm{col}\{x(t),\ G(t),\ Y(t),\ \Delta A(\tfrac{t}{\epsilon})x(t),\ x(t-h(t)),\ x(t-h_M), \\ &\qquad \Delta A_d(t) x(t-h(t))\} \ \in \mathbb{R}^{7n}, \\ \bar{w}(t) &= \mathrm{col}\{w_1(t),\ w_2(t),\ \ldots,\ w_{\bar{N}}(t),\ w(t)\} \ \in \mathbb{R}^{(\bar{N}+1)n_w}, \\ \xi(t) &= \mathrm{col}\{\zeta_1(t),\ \bar{w}(t)\} \ \in \mathbb{R}^{\nu}, \end{aligned} \tag{9.42}$$

with $\nu = 7n + (\bar{N}+1)n_w$, inequality (9.40) can be recast as

$$\dot{V}(t)+2\alpha V(t) - b_0|w(t)|^2 - \sum_{l=1}^{\bar{N}} b_l|w_l(t)|^2 \leq \xi^\top(t)\Omega\xi(t) \\ + \dot{x}^\top(t)\left[(\epsilon^\star T)\bar{H} + h_M W\right]\dot{x}(t) + (\epsilon^\star T)g^\top(t)Rg(t), \quad \forall t \geq \epsilon T, \tag{9.43}$$

where $\Omega \in \mathbb{R}^{\nu\times\nu}$ is the symmetric block matrix whose elements are detailed in (9.20).
Furthermore, by Schur complement, if

$$\begin{bmatrix} \Omega & \Xi_{12} \\ \star & \Xi_{22} \end{bmatrix} < 0, \tag{9.44}$$

with $\Xi_{12} \in \mathbb{R}^{\nu\times 3n}$ and $\Xi_{22} \in \mathbb{R}^{3n\times 3n}$ given as

$$\begin{aligned} \Xi_{12} &= \begin{bmatrix} \sqrt{\epsilon^\star T}\sum_{i=1}^N \rho_i(\frac{t}{\epsilon})A_i^\top R & \sqrt{\epsilon^\star T}\sum_{i=1}^N \rho_i(\frac{t}{\epsilon})A_i^\top \bar{H} & \sqrt{h_M}\sum_{i=1}^N \rho_i(\frac{t}{\epsilon})A_i^\top W \\ 0_{3n\times n} & 0_{3n\times n} & 0_{3n\times n} \\ 0_{n\times n} & \sqrt{\epsilon^\star T}A_d^\top \bar{H} & \sqrt{h_M}A_d^\top W \\ 0 & \begin{matrix} 0_{n\times n} \\ \sqrt{\epsilon^\star T}\bar{H} \\ 0_{\bar{N}\times n} \end{matrix} & \begin{matrix} 0_{n\times n} \\ \sqrt{h_M}W \\ 0_{\bar{N}\times n} \end{matrix} \\ \sqrt{\epsilon^\star T}\sum_{l=1}^{\bar{N}} f_l(\frac{t}{\epsilon})B_l^\top R & \sqrt{\epsilon^\star T}\sum_{l=1}^{\bar{N}} f_l(\frac{t}{\epsilon})B_l^\top \bar{H} & \sqrt{h_M}\sum_{l=1}^{\bar{N}} f_l(\frac{t}{\epsilon})B_l^\top W \end{bmatrix}, \\ \Xi_{22} &= -\,diag\{R, \bar{H}, W\}, \end{aligned} \tag{9.45}$$

for $t \geq \epsilon T + h_M$ it holds:

$$\dot{V}(t) + 2\alpha V(t) - b_0|w(t)|^2 - \sum_{l=1}^{\bar{N}} b_l|w_l(t)|^2 \leq 0. \tag{9.46}$$

Note that, (9.19) implies (9.44) (and thus (9.46)) since (9.44) is affine in $\sum_{i=1}^N \rho_i(\frac{t}{\epsilon})A_i$ and $\sum_{l=1}^{\bar{N}} f_l(\frac{t}{\epsilon})B_l$.
With the aim of proving ISS, it is worth noting that for all $\epsilon \in (0, \epsilon^\star]$, $V(t)$ is positive-definite since, by Jensen's inequality, (9.16) holds. The

comparison principle applied to (9.46) leads to

$$|x(t)|^2 \leq V(t) \leq e^{-2\alpha(t-\epsilon T-h_M)}V(\epsilon T) + \frac{\sum_{l=0}^{\bar{N}} b_l}{2\alpha}\|w[0,t]\|_\infty^2, \tag{9.47}$$

for $t \geq \epsilon T, \epsilon \in (0, \epsilon^\star]$. In addition, by definition of (9.23), for some positive ϵ-independent ν_1, the following holds:

$$V(\epsilon T) \leq \nu_1 \left[\|x_{\epsilon T}\|_W^2 + \int_{-h_M}^{\epsilon T} |\dot{x}(s)|^2 \, ds \right]. \tag{9.48}$$

By denoting $x_t(\theta) = x(t+\theta)$ with $\theta \in [-h_M, 0]$, from (9.1), it follows:

$$x_t(\theta) = \begin{cases} \phi(t+\theta), & t+\theta < 0 \\ \phi(0) + \int_0^{t+\theta} [A(\frac{s}{\epsilon})x(s) + (A_d + \Delta A_d(t))x(s-h(s)) + B(\frac{s}{\epsilon})w(s)] \, ds, & t+\theta \geq 0 \end{cases} \tag{9.49}$$

Due to Assumption 12, there exists $b > 0$ such that $\|B(\tau)\| \geq b$. Then, from (9.49), the following holds:

$$\|x_t\|_W \leq \|\phi\|_W + \int_{-\theta}^{0} \nu_2 \|\phi(s)\|_W \, ds + b(\epsilon T + h_M)\|w[0,t]\|_\infty, \quad t \geq 0, \tag{9.50}$$

for some ϵ-independent $\nu_2 > 0$. By Gronwall's inequality, (9.50) implies

$$\|x_t\|_W \leq e^{\nu_2 h_M}\|\phi\|_W + b(\epsilon T + h_M)\|w[0,t]\|_\infty \quad t \in [0, \epsilon T + h_M]. \tag{9.51}$$

From this latter, it follows that

$$\|x_t\|_W^2 \leq e^{2\nu_2 h_M}\|\phi\|_W + b^2(\epsilon T + h_M)^2\|w[0,t]\|_\infty^2 \quad t \in [0, \epsilon T + h_M]. \tag{9.52}$$

Similarly, (9.1) leads to

$$|\dot{x}(t)|^2 \leq \nu_3\|\phi\|_W^2 + b^2\|w[0,t]\|_\infty^2 \qquad t \in [0, \epsilon T + h_M], \tag{9.53}$$

for some ϵ-independent $\nu_3 > 0$. Substitution of (9.52)-(9.53) into (9.48) leads to

$$V(\epsilon T) \leq \nu_1 \left[e^{2\nu_2 h_M}\|\phi\|_W^2 + b^2(\epsilon T + h_M)^2\|w[0,t]\|_\infty^2 \right]. \tag{9.54}$$

Hence, taking into account (9.47) and (9.54), it is easy to verify that inequality (9.21) holds (and, thus, (9.22)) for some ϵ-independent $\nu > 0$. □

To minimize ellipsoid radius in Equation 9.22, while guaranteeing the fulfillment of Theorem 9, the following constrained optimization problem can be solved:

Let Assumptions 10-12 hold. Given the set of tuning parameters $\{\kappa, \kappa_d, \alpha, \epsilon^\star, T, h_M\}$ and matrices $\{A_{av}, A_i, A_d, B_l\}$ of Theorem 9, find positive definite $n \times n$ matrices P, R, H, S, W, $\bar{H}$, matrix U, scalars $\lambda > 0$, $\lambda_d > 0$ and b_l, $\forall l = 0, \dots, \bar{N}$ such that

$$\begin{aligned} &\min_{b_1, b_2, \dots, b_{\bar{N}}} \sum_{l=0}^{\bar{N}} b_l \Big(\{\kappa, \kappa_d, \alpha, \epsilon^\star, T, h_M\}, \{A_{av}, A_i, A_d, B_l\} \Big) \\ &\qquad \text{subject to } \ (9.16) - (9.19) \end{aligned} \tag{9.55}$$

To solve (9.55), several optimization software tools are available, e.g. MOSEK [175], which has a MATLAB API accessible via the YALMIP parser [213].

Remark 22. *Note that in [40] A_d was supposed to be time-varying with the average $A_{d_{av}}$ and with Hurwitz $A_{av} + A_{d_{av}}$, whereas $G(t)$ was defined by (9.7) with $g(t)$ changed by $\dot{x}$. The latter led to conditions that were feasible for $h_M \sim \mathscr{O}(\epsilon)$. Extension of averaging to non-small delays is important due to non-small delays that appear in feedback controllers or internal dynamics latencies, that require proper compensation in the stability analysis (see [191]). Compared to [40], the change of $g(t)$ (and, thus, of $G(t)$) leads to a novel neutral type transformation in (9.15), where $z(t) = x(t) - G(t)$. Moreover, a novel Lyapunov-Krasovskii candidate in (9.23) with additional terms (9.27)-(9.28) has been exploited to compensate non-small delays.*

Remark 23. *Assume $A_{av} + A_d$ to be Hurwitz. Given $h_M > 0$, let there exist positive constants α, κ and κ_d such that the following standard delay-*

dependent condition

$$\begin{bmatrix} \Omega_0+S & P & PA_d+\frac{1}{h_M}\rho_H(W-U) & \frac{1}{h_M}\rho_H U & P & \sqrt{h_M}A_{av}^\top W \\ \star & -\lambda I_n & 0_{n\times n} & 0_{n\times n} & 0_{n\times n} & 0_{n\times n} \\ \star & \star & -\frac{1}{h_M}\rho_H(2W-U-U^\top)+\lambda_d\kappa_d^2 I_n & -\frac{1}{h_M}\rho_H(W-U) & 0_{n\times n} & \sqrt{h_M}A_d^\top W \\ \star & \star & 0_{n\times n} & -\rho_H(S+\frac{1}{h_M}W) & 0_{n\times n} & 0_{n\times n} \\ \star & \star & \star & \star & -\lambda_d I_n & \sqrt{h_M}W \\ \star & \star & \star & \star & \star & -W \end{bmatrix} < 0 \tag{9.56}$$

and (9.17) *hold with* $\Omega_0 = PA_{av} + A_{av}^\top P + 2\alpha P + \lambda\kappa^2 I_n$. *Then, the averaged system* (9.3) *is exponentially stable with a decay rate* $\alpha > 0$ *for all* $h(t) \leq h_M$ *and for small enough* $\kappa > 0$ *and* $\kappa_d > 0$ *[97]. Therefore, given non-small* ϵ*-independent* $h_M > 0$ *satisfying* (9.56) *and* (9.17)*, LMIs of Theorem 9 are always feasible for small enough* $\epsilon^\star > 0$ *with the same* $\alpha > 0$, $\kappa > 0$ *and* $\kappa_d > 0$ *as in* (9.56) *since, by Schur complements,* (9.19) *is* $\mathcal{O}(\epsilon)$*-perturbation of* (9.56).

9.2.3 Example: Stabilization of the inverted pendulum in the presence of feedback delays and disturbances.

Consider the system consisting of a cart and a planar pendulum apparatus in a reference frame subjected to a periodic amplitude and frequency disturbances along the horizontal axis as in [191]. Note that, these disturbances might arise as the result of attempting control on an unsteady platform. To stabilize the inverted pendulum, a delayed proportional controller for pendulum position has been introduced, where the control delay appears due to sampling, computation or even tele-remote operation. Following the approach of [191] in coordinate changing and by linearizing the model at the upper equilibrium position, i.e. $x_1 = \pi$ and $x_2 = 0$, it results the following dynamical system:

$$\dot{x}(t) = \begin{bmatrix} 0 & 1 \\ \cos^2\frac{t}{\epsilon}-1 & -(c+\Delta c) \end{bmatrix} x(t) + \begin{bmatrix} 0 & 0 \\ K_p & 0 \end{bmatrix} x(t-h(t)) + \begin{bmatrix} \cos^2\frac{t}{\epsilon} \\ \sin\frac{t}{\epsilon} \end{bmatrix} w(t) \tag{9.57}$$

with parameter $c > 0$ and periodic $B(\frac{t}{\epsilon})$ due to attempting control on an unsteady platform. Furthermore, it is reasonable to add uncertanties Δc on this latter arising from the presence of the damping coefficient of the planar joint and such that $|\Delta c| \leq c_1$, with $c_1 > 0$. From $A(\frac{t}{\epsilon})$ in (9.57), Assumptions 1-3 hold with $T = 2\pi$ and

$$A_{av} = \begin{bmatrix} 0 & 1 \\ -0.5 & -c \end{bmatrix}, \quad \Delta A = \begin{bmatrix} 0 & 0 \\ 0 & -\Delta c \end{bmatrix}. \tag{9.58}$$

Note that, to compute matrices in (9.58) it has been used that $\cos\frac{t}{\epsilon} \in [-1, 1]$ and its average is zero, while $\cos^2\frac{t}{\epsilon} \in [0, 1]$ and its average is 0.5. Moreover, $c > 0$ guarantees that $A_{av} + A_d$ is Hurwitz. Hence, it is selected $c = 0.05$. Under above assumptions, $A(\frac{t}{\epsilon})$ and $B(\frac{t}{\epsilon})$ can be expressed as the following convex combination of $N = 4$ and $\bar{N} = 2$ constant matrices, respectively:

$$\begin{aligned} A_i &= \begin{bmatrix} 0 & 1 \\ -0.5 \pm 0.5 & -0.05 + c_1 \end{bmatrix}, \; i = 1, 2, \quad B_1 = \begin{bmatrix} 1 \\ 0 \end{bmatrix}, \\ A_i &= \begin{bmatrix} 0 & 1 \\ -0.5 \pm 0.5 & -0.05 - c_1 \end{bmatrix}, \; i = 3, 4, \quad B_2 = \begin{bmatrix} 0 \\ 0 \end{bmatrix}. \end{aligned} \tag{9.59}$$

In order to prove the feasibility o (9.55), firstly it is required to verify that condition in (9.18) holds. Following the approach of [46], it is assumed $H = hI_2$, with $h > 0$. Then, from (9.18) it follows:

$$\begin{aligned} &\frac{1}{T^2}\int_{\frac{t}{\epsilon}-T}^{\frac{t}{\epsilon}} (\zeta - \tfrac{t}{\epsilon} + T)A^\top(\zeta)HA(\zeta)\,d\zeta \\ &\leq \frac{h}{T^2}\int_{\frac{t}{\epsilon}-T}^{\frac{t}{\epsilon}} (\zeta - \tfrac{t}{\epsilon} + T)A^\top(\zeta)A(\zeta)\,d\zeta \leq \frac{h}{2}\begin{bmatrix} 0 & 0 \\ 0 & 1 \end{bmatrix} \\ &+ \frac{h}{T}\int_{\frac{t}{\epsilon}-T}^{\frac{t}{\epsilon}} \begin{bmatrix} (\cos^2\zeta - 1)^2 & (0.05 + c_1)(1 - \cos^2\zeta) \\ \star & (1 + c_1)^2 \end{bmatrix} d\zeta = h\Lambda = \bar{H}, \end{aligned} \tag{9.60}$$

where Λ has the following form:

$$\Lambda = \begin{bmatrix} 0.3750 & 0.5(0.05 + c_1) \\ \star & (0.05 + c_1)^2 + 0.5 \end{bmatrix}. \tag{9.61}$$

Two cases are considered: i) nominal case, where $c_1 = 0$, meaning that no uncertainties on damping coefficient are imposed, and ii) uncertain case, where $c_1 \neq 0$, with $c_1 = 0.01$. Clearly, in the nominal case, $\kappa = 0$ and the number of vertices in (9.59) are $N = 2$ and $\bar{N} = 2$, respectively, while $\bar{H} = h\Lambda$ with $c_1 = 0$. In the uncertain case, $c_1 = 0.01$ leads to $\kappa = c_1$ and a number of vertices $N = 4$ and $\bar{N} = 2$, while $\bar{H} = h\Lambda$. Both for nominal and uncertain scenarios two different values for the decay rate are considered in order to disclose the impact of the convergence rate on $\epsilon^\star$ and h_M.

Maximum delay bound h_M: Firstly, the aim is to find the upper bound h_M for the time-varying delay $h(t)$ that preserves the ISS by satisfying (9.55) for each set of tuning parameters $\{\kappa_i, \alpha_j, \epsilon^\star, T\}$, $i, j = 1, 2$. This means that the following four sets of tuning parameters are considered: $\mathscr{S}_{1,j} = \{\kappa_1, \alpha_j, \epsilon^\star, T\}$ and $\mathscr{S}_{2,j} = \{\kappa_2, \alpha_j, \epsilon^\star, T\}$, $j = 1, 2$, with $\kappa_1 = 0$, $\kappa_2 = 0.01$, $\alpha_1 = \frac{1}{10\pi}$ and $\alpha_2 = 0.005$. Given $\mathscr{S}_{i,j}$, problem (9.55) is solved by verifying the feasibility of the LMIs of Theorem 9. Specifically, $\epsilon^\star = 0.038$ is fixed and for each set of tuning parameters the value of h_M is iteratively increased in order to find its maximum value till LMIs of Theorem 9 still holds. Results are shown in Table 9.1, where it is possible to observe that for all $\epsilon \in (0, 0.038]$ and for $\alpha = \frac{1}{10\pi}$ the fulfillment of Theorem 9 is guaranteed for $h_M = 0.946$, while in uncertain scenario a lower value is found, i.e. $h_M = 0.913$. A smaller convergence rate (i.e. $\alpha = 0.005$) leads to larger upper bounds for time-varying delays, both in nominal and uncertain scenarios, i.e. $h_M = 0.970$ and $h_M = 0.948$, respectively. The above results confirm that ISS is preserved in the presence of larger delays, whose values are essentially larger than ϵ.

Table 9.1. Example 9.2.3. Upper bound h_M for each set of tuning parameters $\{\sigma_i, \alpha_j, \epsilon^\star, T\}$, with $i, j = 1, 2$ and $\epsilon^\star = 0.038$.

	α	h_M
$\epsilon^\star = 0.038,\quad c_1 = 0$	$\frac{1}{10\pi}$	0.946
	0.005	0.970
$\epsilon^\star = 0.038,\quad c_1 = 0.01$	$\frac{1}{10\pi}$	0.913
	0.005	0.948

Maximum ϵ bound $\epsilon^\star$: Starting from results in Table 9.1, now the value of h_M is fixed and the value of ϵ is iteratively increased so to

find its upper bound $\epsilon^\star$ that preserves the ISS of system (9.57), for all $\epsilon \in (0, \epsilon^\star]$ and $h(t) \in [0, h_M]$. For the four sets of tuning parameters $\mathscr{S}^h_{i,j} = \{\kappa_i, \alpha_j, h_M, T\}$, $i, j = 1, 2$, it is chosen $h_M = 0.8$, while κ_i and α_j are selected as previously. Table 9.2 shows the results of this latter analysis. In particular, it has been found that for the couple $(h_M = 0.8, \alpha = \frac{1}{10\pi})$ ISS is preserved for all $\epsilon \in (0, 0.057]$ in nominal scenario, while this range is restricted in the uncertain scenario, where $\epsilon^\star = 0.051$ due to polytopic uncertainties. Similar results have been obtained for the couple $(h_M = 0.8, \alpha = 0.005)$, even though with larger values for $\epsilon^\star$ due to an improved convergence rate $(\alpha = 0.005)$, i.e. $\epsilon^\star = 0.061$ in nominal scenario and $\epsilon^\star = 0.054$ in uncertain scenario, respectively.
Compared with [191], where both the values of $\epsilon = 0.1$ and $h_M = 0.5$ have been fixed by numerical simulations, firstly the proposed approach leads to larger maximum admissible delays, and also it provides for the first time stability conditions expressed as LMIs whose solution allows quantifying theoretical upper bounds $\epsilon^\star$ and h_M, even if these latter could result smaller with respect to the ones found by simulations.

Moreover, differently from [40] (see Example 5.1 in [40]), Tables 9.1 and 9.2 confirm the feasibility of LMIs in (9.16)-(9.19) for non-small delays

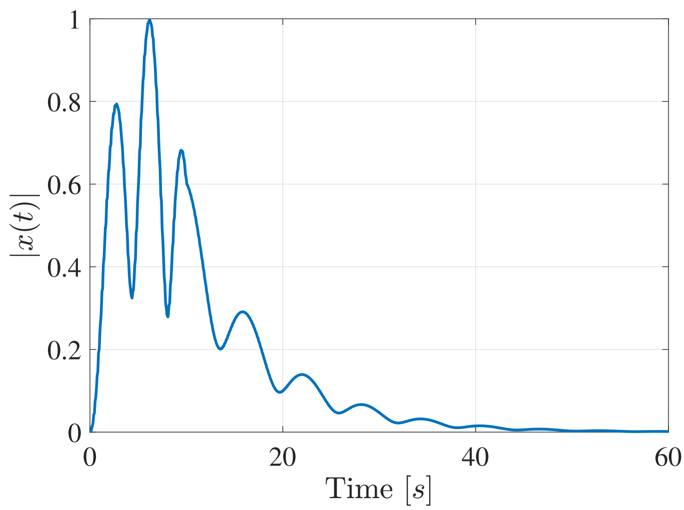

Figure 9.1. Time history of state trajectories of system (9.57) with $\epsilon^\star = 0.054$, $h_M = 0.8$ and $w(t) = \sin(t)$ if $t \leq 10$, $w(t) = 0$ otherwise.

whose upper bound h_M is essentially larger than ϵ. Finally, state tra-

Table 9.2. Example 9.2.3. Upper bound $\epsilon^\star$ for each set of tuning parameters $\{\sigma_i, \alpha_j, \epsilon^\star, T\}$, with $i, j = 1, 2$ and $h_M = 0.8$.

	α	$\epsilon^\star$
$h_M = 0.8,\ \ c_1 = 0$	$\frac{1}{10\pi}$	0.057
	0.005	0.061
$h_M = 0.8,\ \ c_1 = 0.01$	$\frac{1}{10\pi}$	0.051
	0.005	0.054

jectories of system (9.57) can be seen in Figure 9.1, where the external disturbance $w(t)$ has been selected as $w(t) = \sin(t)$ for $t \in [0, 10]$ $[s]$ and $w(t) = 0$ otherwise, thus confirming theoretical derivation.

9.3 Robust stabilization of affine systems by time-dependent switching

In this section it will be applied the averaging via the time-delay approach to switched affine systems with non-small delays

$$\dot{x}(t) = \tilde{A}_{\sigma(t)} x(t) + (A_d + \Delta A_d(t))\, x(t - h(t)) + \tilde{B}_{\sigma(t)}, \tag{9.62}$$

where $x(t) \in \mathbb{R}^n$, $\tilde{A}_{\sigma(t)} = A_{\sigma(t)} + \Delta A_{\sigma(t)}(t)$, $\tilde{B}_{\sigma(t)} = B_{\sigma(t)} + \Delta B_{\sigma(t)}(t)$, $\sigma : \mathbb{R} \to \mathscr{I} = \{1, 2, \ldots, N\}$ is a switching law, $\epsilon > 0$ is a small enough positive constant, $A_d \in \mathbb{R}^{n\times n}$, $A_i \in \mathbb{R}^{n\times n}$, $B_i \in \mathbb{R}^n$ $(i \in \mathscr{I})$ are the nominal matrices, while $\Delta A_d(t) \in \mathbb{R}^{n\times n}$, $\Delta A_i(t) \in \mathbb{R}^{n\times n}$, $\Delta B_i(t) \in \mathbb{R}^n$ $(i \in \mathscr{I})$ are the perturbations with respect to the nominal values satisfying

$$\|\Delta A_d\| \le \kappa_d, \qquad \|\Delta A_i\| \le \kappa, \qquad |\Delta B_i| \le \kappa_b,\ i \in \mathscr{I}.$$

Here κ_d, κ and κ_b are some small enough positive constants. Note that, the study of uncertain switched affine systems as in (9.62) is very challenging due to its own complex dynamics presenting several equilibrium points. Therefore, the design of a proper switching control rule is a pre-requisite for practical stability [204, 205]. For this class of systems, given the simplex

$\Lambda = \left\{\lambda = [\lambda_1, \lambda_2, \ldots, \lambda_N]^{\mathrm{T}} \in \mathbf{R}^N,\ \lambda_i \geq 0,\ \sum_{i=1}^{N} \lambda_i = 1\right\}$, generating the convex combinations

$$\tilde{A}(\lambda) = \sum_{i=1}^{N} \lambda_i A_i + A_d \triangleq A(\lambda) + A_d, \qquad B(\lambda) = \sum_{i=1}^{N} \lambda_i B_i,\ \lambda \in \Lambda,$$

it is assumed that there exists the subset $\Lambda_H \subseteq \Lambda$ such that $\Lambda_H = \{\lambda \in \Lambda : \tilde{A}(\lambda) \text{ is Hurwitz}\}$. In the absence of uncertainties and time-delay, the set of equilibrium points for (9.62) is given by

$$\mathscr{S}_e = \left\{x_e : x_e = -\tilde{A}^{-1}(\lambda)B(\lambda),\ \lambda \in \Lambda_H\right\}.$$

Moreover, any $x_e = -\tilde{A}^{-1}(\lambda)B(\lambda)$ is also an admissible equilibrium point for delayed system (9.62) without uncertainties, since $x(t)$ approaches it for $t \to \infty$ together with $x(t - h(t))$ (see e.g. [208]).

Given an equilibrium point $x_e \neq 0 \in \mathscr{S}_e$ and denote the error $e(t) = x(t) - x_e$, where $x(t)$ is solution of (9.62). It follows that system (9.62) can be presented as

$$\dot{e}(t) = \tilde{A}_{\sigma(t)}e(t) + (A_d + \Delta A_d)e(t - h(t)) + \bar{B}_{\sigma(t)} + \Delta\bar{B}_{\sigma(t)}, \tag{9.63}$$

with $\bar{B}_{\sigma(t)} = B_{\sigma(t)} + (A_{\sigma(t)} + A_d)x_e$ and $\Delta\bar{B}_{\sigma(t)} = \Delta B_\sigma + (\Delta A_{\sigma(t)} + \Delta A_d)x_e$. As $x_e = -\tilde{A}^{-1}(\lambda)B(\lambda)$, $\lambda \in \Lambda_H$, then

$$\sum_{i=1}^{N} \lambda_i \bar{B}_{\sigma(t)} = B(\lambda) + \tilde{A}(\lambda)x_e = 0.$$

Thus, without loss of generality, it is possible to assume that $x_e = 0$ is the equilibrium point of affine system (9.62). Hence, let the following assumption holds.

Assumption 13. *There exists $\lambda \in \Lambda_H$ such that $\tilde{A}(\lambda)$ is Hurwitz and $B(\lambda) = 0$.*

Hence, the time-dependent periodic switching law $\sigma(t)$ can be designed as

$$\sigma(t) = i,\ t \in \left[\left(k + \sum_{j=0}^{i-1} \lambda_j\right)\epsilon, \left(k + \sum_{j=0}^{i} \lambda_j\right)\epsilon\right),\ i \in \mathscr{I} \tag{9.64}$$

with $\lambda \in \Lambda_H$, $\lambda_0 = 0$ and $k = 0, 1, 2, \ldots$. For each time interval in (9.64), we introduce the indicator function $\chi_i(\tau) = \chi_{[(k+\sum_{j=1}^{i-1}\lambda_j)\epsilon,(k+\sum_{j=1}^{i}\lambda_j)\epsilon)}$, with $\tau = \frac{t}{\epsilon} \in [k, k+1]$ and $\sum_{i=1}^{N} \chi_i(\tau) = 1$. Hence, system (9.62) can be presented as

$$\begin{aligned} \dot{x}(t) =& \sum_{i=1}^{N} \chi_i(\tau)(A_i + \Delta A_i(\tau))x(t) + (A_d + \Delta A_d)x(t - h(t)) \\ &+ \sum_{i=1}^{N} \chi_i(\tau)(B_i + \Delta B_i(\tau)), \qquad \forall i \in \mathscr{I}, \end{aligned} \tag{9.65}$$

with $\lambda \in \Lambda_H$, $k = 0, 1, 2...$, $\tau = \frac{t}{\epsilon} \in [k, k+1]$.
Using notations (9.6)-(9.7) and (9.11) and integrating (9.65) $[t-\epsilon, t]$ for $t \geq \epsilon + h_M$, finally it results:

$$\begin{aligned} \dot{z}(t) =& [A_{av} + \Delta A_{\sigma(t)}]x(t) - Y(t) + (A_d + \Delta A_d)\, x(t - h(t)) \\ &+ \Delta B_{\sigma(t)}, \qquad\qquad t \geq \epsilon + h_M. \end{aligned} \tag{9.66}$$

Here $z(t) = x(t) - G(t)$, $A_{av} = A(\lambda)$, $x(t)$ satisfies (9.62), $g(s) = A_{\sigma(s)}x(s) + B_{\sigma(s)}$ and $Y(t)$ as in (9.11) with $A(\frac{s}{\epsilon})$ replaced by $A_{\sigma(s)}$.
Therefore, system (9.62) is practically stable if the time-delay system (9.66) is practically stable. By using arguments of Theorem 9, the following result is obtained for delayed switched affine systems:

Theorem 10. *Consider the switched affine system with time-varying delays (9.62) and let Assumption 13 hold. Given matrices A_{av}, $A_i(i = 1, \ldots, N)$, A_d, ΔA_d, $B_i(i = 1, \ldots, N)$ and positive constants κ, κ_d, κ_b, α, $\epsilon^\star$, $T = 1$ and h_M, let there exist positive-definite matrices P, R, H, W, S and $\bar{H} \in \mathbb{R}^{n\times n}$, a matrix $U \in \mathbb{R}^{n\times n}$ and scalars $\lambda > 0$, λ_d, b_0 and $b > 0$*

that satisfy (9.16),(9.17),(9.18) *and the following LMIs*

$$\begin{bmatrix} \Upsilon & \begin{bmatrix} \sqrt{2}A_i^\top R & \sqrt{2}A_i^\top(\epsilon^\star\bar{H}+h_M W) \\ 0_{2n\times n} & 0_{2n\times n} \\ 0_{n\times n} & \sqrt{2}(\epsilon^\star\bar{H}+h_M W) \\ 0_{n\times n} & \sqrt{2}A_d^\top(\epsilon^\star\bar{H}+h_M W) \\ 0_{n\times n} & 0_{n\times n} \\ 0_{n\times n} & \sqrt{2}(\epsilon^\star\bar{H}+h_M W) \\ 0_{n\times n} & \sqrt{2}(\epsilon^\star\bar{H}+h_M W) \end{bmatrix} \\ \star & \begin{bmatrix} -\frac{1}{\epsilon^\star}R & 0_{n\times n} \\ \star & -(\epsilon^\star\bar{H}+h_M W) \end{bmatrix} \end{bmatrix} < 0, \quad i = 1, \ldots, N, \tag{9.67}$$

$$\begin{bmatrix} b_0(\epsilon^\star + h_M) & B_i^\top[2\epsilon^\star(R+\bar{H}) + 2h_M W] \\ \star & 2\epsilon^\star(R+\bar{H}) + 2h_M W \end{bmatrix} > 0, \tag{9.68}$$

with

$$\Upsilon = \begin{bmatrix} \bar{\Upsilon} & \begin{bmatrix} P \\ -P \\ 0_{5n\times 5n} \end{bmatrix} \\ \star & -b \end{bmatrix}, \tag{9.69}$$

Ξ_{22} *defined in* (9.45) *as* $\Xi_{22} = -diag\{R, \bar{H}, W\}$ *and* $\bar{\Upsilon}$ *obtained from* Ω *in* (9.20) *by removing the last block-column and block-row. Then, the delayed switched affine system* (9.62) *is practically exponentially stable with a decay rate* $\alpha > 0$ *for all* $\epsilon \in (0, \epsilon^\star]$ *and* $h(t) \in [0, h_M]$, *meaning that there exists a positive constant* $\tilde{\nu}$ *such that the solutions of the delayed system* (9.62) *initialized by* $\phi \in W[-h_M, 0]$ *satisfy*

$$\begin{aligned} |x(t)|^2 \leq & \tilde{\nu}e^{-2\alpha(t-\epsilon^\star-h_M)}\|\phi\|_W^2 \\ & + \left[\tilde{\nu}e^{-2\alpha(t-\epsilon^\star-h_M)} + \frac{b_0(\epsilon^\star+h_M)+b\kappa_b^2}{2\alpha}\right], \qquad \forall t \geq 0. \end{aligned} \tag{9.70}$$

Moreover, the ball

$$\mathscr{X}_{\epsilon^\star} = \left\{ x \in \mathbb{R}^n : |x|^2 \leq \frac{b_0(\epsilon^\star+h_M)+b\kappa_b^2}{2\alpha} \right\}, \tag{9.71}$$

is exponentially attractive with decay rate $\alpha > 0$ *for* (9.62) *for all* $\phi \in W[-h_M, 0]$.

Proof. Choose the Lyapunov-Krasovskii functional $V(t)$ as in (9.23), with $A(\frac{s}{\epsilon}) = A_{\sigma(s)}$. Then, following arguments of Theorem 9, for $t \geq \epsilon + h_M$, it follows:

$$\begin{aligned}\dot{V}(t) + 2\alpha V(t) - b|\Delta B_{\sigma(t)}|^2 - b_0(\epsilon^\star + h_M) &\leq \xi_1(t)\Upsilon\xi_1(t)\\ &+ \epsilon^\star(A_{\sigma(t)}x(t) + B_{\sigma(t)})^\top R(A_{\sigma(t)}x(t) + B_{\sigma(t)})\\ &+ \dot{x}^\top(t)(\epsilon^\star\bar{H} + h_M W)\dot{x}(t) - b_0(\epsilon^\star + h_M),\end{aligned} \tag{9.72}$$

with matrix $\bar{H}$ as in (9.18), $\xi_1^\top(t) = [\zeta_1^\top(t),\ \Delta B_{\sigma(t)}^\top]$ and Υ as in (9.69). Substituting (9.62) into (9.72) and applying Young's inequality, it results:

$$\begin{aligned}&\dot{V}(t)+2\alpha V(t) - b|\Delta B_{\sigma(t)}|^2 - b_0(\epsilon^\star + h_M) \leq \xi_1^\top(t)\Upsilon\xi_1(t)\\ &\quad + 2\epsilon^\star x^\top(t)A_{\sigma(t)}^\top RA_{\sigma(t)}x(t) + 2\epsilon^\star B_{\sigma(t)}^\top RB_{\sigma(t)} - b_0(\epsilon^\star + h_M)\\ &+ 2B_{\sigma(t)}^\top(\epsilon^\star\bar{H} + h_M W)B_{\sigma(t)}\\ &+ 2\Big[(A_{\sigma(t)} + \Delta A_{\sigma(t)})x(t) + (A_d + \Delta A_d)x(t-h(t)) + \Delta B_{\sigma(t)}\Big]^\top\\ &\times(\epsilon^\star\bar{H} + h_M W)\Big[(A_{\sigma(t)} + \Delta A_{\sigma(t)})x(t) + (A_d + \Delta A_d)x(t-h(t))\\ &+ \Delta B_{\sigma(t)}\Big] = \xi_1^\top(t)[\Upsilon + \Sigma]\xi_1(t) + 2\epsilon^\star B_{\sigma(t)}^\top RB_{\sigma(t)}\\ &- b_0(\epsilon^\star + h_M) + 2B_{\sigma(t)}^\top(\epsilon^\star\bar{H} + h_M W)B_{\sigma(t)},\end{aligned} \tag{9.73}$$

where Σ is the symmetric block matrix whose elements are

$$\begin{aligned}\Sigma_{11} &= 2\sum_{i=1}^N \chi_i(\tau)A_i^\top(\epsilon^\star\bar{H} + h_M W)\sum_{i=1}^N \chi_i(\tau)A_i\\ &\quad + 2\epsilon^\star\sum_{i=1}^N \chi_i(\tau)A_i^\top R\sum_{i=1}^N \chi_i(\tau)A_i,\\ \Sigma_{14} &= \Sigma_{17} = \Sigma_{18} = 2\sum_{i=1}^N \chi_i(\tau)A_i^\top(\epsilon^\star\bar{H} + h_M W),\\ \Sigma_{15} &= 2\sum_{i=1}^N \chi_i(\tau)A_i^\top(\epsilon^\star\bar{H} + h_M W)A_d, \quad \Sigma_{45} = 2(\epsilon^\star\bar{H} + h_M W)A_d,\\ \Sigma_{44} &= \Sigma_{47} = \Sigma_{48} = \Sigma_{77} = \Sigma_{78} = \Sigma_{88} = 2(\epsilon^\star\bar{H} + h_M W),\\ \Sigma_{55} &= 2A_d^\top(\epsilon^\star\bar{H}+h_M W)A_d, \quad \Sigma_{57} = \Sigma_{58} = 2A_d^\top(\epsilon^\star\bar{H}+h_M W),\end{aligned} \tag{9.74}$$

and other blocks are zero matrices. By applying Schur complement to (9.73) and taking into account that Σ is affine in $\sum_{i=1}^{N} \chi_i(\tau)A_i$, if (9.67)-(9.68) hold, then

$$\dot{V}(t) + 2\alpha V(t) - b|\Delta B_{\sigma(t)}|^2 - b_0(\epsilon^\star + h_M) \leq 0, \quad t \geq \epsilon. \tag{9.75}$$

The rest of the proof is similar to that in Theorem 9. $\square$

Remark 24. *Note that system (9.62) can be presented as (9.1) with* $A(\tau) = \sum_{i=1}^{N} \chi_i(\tau)(A_i + \Delta A_i(\tau))$, $B(\tau) = \sum_{i=1}^{N} \chi_i(\tau)(B_i + \Delta B_i(\tau))$, $\tau = \frac{t}{\epsilon}$. *For* $\Delta A_i = \Delta B_i = 0$, *both* $A(\tau)$ *and* $B(\tau)$ *are* $T = 1$*-periodic. Then,*

$$\Delta A(\tau) = \sum_{i=1}^{N} \int_{\lambda_{i-1}}^{\lambda_i} \Delta A_i(\tau - \theta)\mathrm{d}\theta, \qquad \Delta B(\tau) = \sum_{i=1}^{N} \int_{\lambda_{i-1}}^{\lambda_i} \Delta B_i(\tau - \theta)\mathrm{d}\theta,$$

with $\lambda_0 = 0$ *and*

$$\|\Delta A(\tau)\| \leq \sum_{i=1}^{N} \int_{\lambda_{i-1}}^{\lambda_i} \|\Delta A_i(\tau - \theta)\| \,\mathrm{d}\theta \leq \kappa,$$

$$\|\Delta B(\tau)\| \leq \sum_{i=1}^{N} \int_{\lambda_{i-1}}^{\lambda_i} \|\Delta B_i(\tau - \theta)\| \,\mathrm{d}\theta \leq \kappa_b.$$

Remark 25. *From* (9.70) *and* (9.71)*, it is clear that for* $t \to \infty$*, the trajectories of switched affine system* (9.62) *exponentially approach the attractive ball* $|x|^2 \leq \frac{b_0(\epsilon^\star + h_M) + b\kappa_b^2}{2\alpha}$. *To obtain a smaller ball, firstly it is possible to minimize* b_0 *and* b. *However, this minimization leads to weak performances in terms of convergence rate, which can be improved by increasing the value of decision variables* b_0 *and* b. *Moreover, due to* (9.72)*,* b_0 *is of the order of* $\mathscr{O}(h_M + \epsilon^\star)$. *Hence, larger values of* h_M *and* ϵ *increase the ball radius. Therefore, a good trade-off between non-small delays, frequency switching, convergence rate and attractive ball size has to be also reached.*

Remark 26. *It is worth noting that many recent results on the stabilization of switched affine systems suggest state/output-dependent switching laws (see, e.g. [214],[215],[216],[205]). Although state/output-dependent switching laws may have advantages in robustness to disturbances with respect to time-dependent switching, time-dependent switching law is simpler* *for implementation due to no need of measurements and on-line calculation of the switching law. Moreover, it can be useful to switch from a state-dependent to a time-dependent switching law in some practical applications [217], e.g., when sensor-faults occur.*

9.3.1 Examples: Stabilization of switched affine systems.

Example 1

Consider the delayed version of the switched affine system in [206]:

$$\dot{x}(t) = \begin{cases} A_1x(t) + A_dx(t-h(t)) + B_1, & t \in [k\epsilon, (k+\lambda_1)\epsilon], \\ A_2x(t) + A_dx(t-h(t)) + B_2, & t \in [(k+\lambda_1)\epsilon, (k+\lambda_1+\lambda_2)\epsilon], \\ A_3x(t) + A_dx(t-h(t)) + B_3, & t \in [(k+\lambda_1+\lambda_2)\epsilon, (k+1)\epsilon], \end{cases} \tag{9.76}$$

with $\epsilon > 0$, $k = 0, 1, \dots$ and $\lambda \in (0,1)$. Matrices in (9.76) are given as follows:

$$A_1 = \begin{bmatrix} 0 & 0.5 \\ 0 & -1 \end{bmatrix}, \quad B_1 = \begin{bmatrix} 1 \\ 0.5 \end{bmatrix}, \quad A_2 = \begin{bmatrix} 0.1 & 0 \\ -1 & -1 \end{bmatrix}, \quad B_2 = \begin{bmatrix} -1 \\ -0.5 \end{bmatrix},$$
$$A_3 = \begin{bmatrix} 0 & 1 \\ -1 & 0 \end{bmatrix}, \quad B_3 = \begin{bmatrix} 0 \\ 2 \end{bmatrix}, \quad A_d = \begin{bmatrix} 0.045 & 0.13 \\ -0.5 & -0.8 \end{bmatrix}.$$

Then, (9.76) can be presented as (9.1) with $\Delta A = \Delta A_d = \Delta B = 0$ and

$$A(\tau) = \sum_{i=1}^{N} \chi_i(\tau)A_i, \qquad B(\tau) = \sum_{i=1}^{N} \chi_i(\tau)B_i,$$

with $\chi_i(\tau)$ the indicator function. As in [206], we choose $\lambda = [0.4,\ 0.47,\ 0.13] \in \Lambda_H$ leading to the desired operating point $x_e = [0.1\ \ 0.2]^\top$ and to matrix

$$A_{av} = A(\lambda) + A_d = \sum_{i=1}^{3} \lambda_i A_i + A_d.$$

Table 9.3. Example 9.3.1. Solution of (9.55) for different values of h_M and the corresponding ultimate bound.

	h_M	$b_0^\star$	$UB = \sqrt{\frac{b^\star \kappa_b^2 + b_0^\star(\epsilon^\star + h_M)}{2\alpha}}$
$\epsilon^\star = 0.2,\ \ \alpha_1 = 0.005$	0.1	0.38258	3.3878
	0.3	0.39848	4.4637
	0.5	0.64144	6.7008
	0.7	0.80207	8.4962
	0.9	0.86383	9.7479
$\epsilon^\star = 0.2,\ \ \alpha_2 = 0.5$	0.1	0.3915	0.3427
	0.3	0.41319	0.4545
	0.5	0.68916	0.6946
	0.7	1.0503	0.9723

Table 9.4. Example 9.3.1. Solution of (9.55) for different values of $\epsilon \in (0, \epsilon^\star]$ and corresponding ultimate bound.

	ϵ	$b_0^\star$	$UB = \sqrt{\frac{b^\star \kappa_b^2 + b_0^\star(\epsilon + h_M)}{2\alpha}}$
$h_M = 0.5,\ \ \alpha_1 = 0.005$	0.2	0.64144	6.7008
	0.3	0.7935	7.9674
	0.4	0.79296	8.4479
	0.53	1.2663	11.4207
$h_M = 0.5,\ \ \alpha_2 = 0.5$	0.2	0.68916	0.6946
	0.3	0.85376	0.8264
	0.4	0.85747	0.8785
	0.5	1.2455	1.1160
	0.55	1.3293	1.1814

Moreover, both $A(\tau)$ and $B(\tau)$ are 1-periodic. Hence, for $\tau \geq T = 1$, inequality (9.18) can be easily computed as

$$\int_{\tau-1}^{\tau} (\zeta - \tau + 1) A^\top(\zeta) H A(\zeta)\, d\zeta \leq \int_{\tau-\lambda_1}^{\tau} (\zeta - \tau + 1)\, d\zeta A_1^\top H A_1$$
$$+ \int_{\tau-(\lambda_1+\lambda_2)}^{\tau} (\zeta - \tau + 1)\, d\zeta A_2^\top H A_2 + \int_{\tau-(1-\lambda_1-\lambda_2)}^{\tau} (\zeta - \tau + 1)\, d\zeta A_3^\top H A_3$$
$$= \frac{1 - (1-\lambda_1)^2}{2} A_1^\top H A_1 + \frac{1 - \lambda_3^2}{2} A_2^\top H A_2 + \frac{1 - (\lambda_1 + \lambda_2)^2}{2} A_3^\top H A_3 = \bar{H}.$$

Firstly, two different sets $\{\alpha_i,\ \epsilon^\star,\ T\},\ i = 1, 2$ of tuning parameters are analyzed, which involve different values of decay rate, i.e., $\alpha_1 = 0.005$ and $\alpha_2 = 0.5$ in order to show the impact of this latter on the feasibility of the LMIs of Theorem 10 and the corresponding UB. It is clear that for both sets of tuning parameters, $\kappa = \kappa_d = \kappa_b = 0$ since no system uncertainties

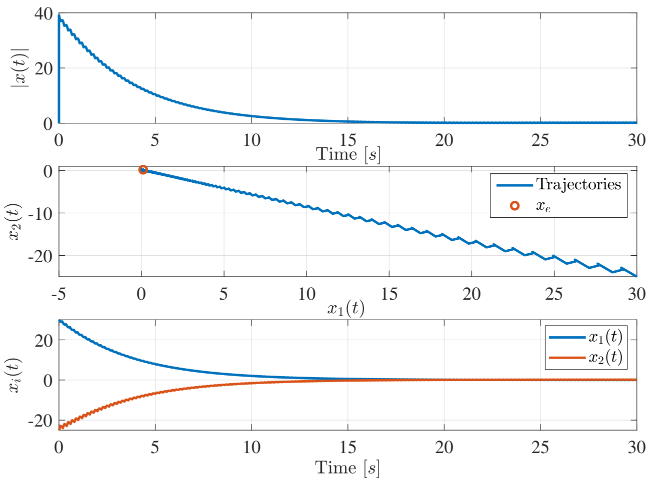

Figure 9.2. Practical stabilization of switched affine systems (9.76) with $\epsilon^\star = 0.2$ and $h_M = 0.8$.

occur, i.e. $\Delta A(\tau) = \Delta A_d = \Delta B(\tau) = 0$.
Maximum delay bound h_M: For each set, here $\epsilon^\star = 0.2$ is fixed and the value of h_M is iteratively increased in order to find its upper bound that guarantees the existence of a solution for (9.55) for all $\epsilon \in (0, \epsilon^\star]$, $h(t) \in [0, h_M]$. Results are reported in Table 9.3, which shows that for all $\epsilon \in (0, 0.2]$ and $\alpha_1 = 0.005$, (9.55) is feasible until $h_M = 0.9$, whereas UB $= 9.7476$. For $\alpha_2 = 0.5$, it is found that for all $\epsilon \in (0, 0.2]$, problem (9.55) holds for $h_M = 0.7$, which leads to an ultimate bound UB $= 0.9723$. As expected, comparing the above results of Table 9.3, for a fixed values of $\epsilon^\star$ and h_M, smaller values of the decay rate lead to a larger attractive ball, thus deteriorating the performances. Hence, a good trade-off between UB size and convergence rate has to be found to satisfy specific control requirements.
Maximum ϵ bound $\epsilon^\star$: Here h_M is fixed, while ϵ has been increased in order to find its upper bound $\epsilon^\star$, whose value preserves the feasibility of (9.55) (and, thus, Theorem 10). Note that, the value of h_M has been fixed as $h_M = 0.5$ according to the results of Table 9.3. The results of the optimization procedure for α_i, $i = 1, 2$ can be seen in Table 9.4, where

it is possible to observe the values of the UB for different values of ϵ. In particular, for $\alpha_1 = 0.005$, practical stability can be guaranteed for all $\epsilon \in (0, \epsilon^\star]$ with $\epsilon^\star = 0.53$, which leads to UB $= 11.4207$. On the other hand, for $\alpha_2 = 0.5$, the LMIs of Theorem 10 are still feasible for all $\epsilon \in (0, 0.55]$, with UB $= 1.1814$. Also in this case, given the value h_M, decay rate α_1 leads to a larger attractive ball with respect to the one obtained with α_2, thus deteriorating performances in terms of ellipsoid radius.

Note that, in [206] state-dependent periodic-time and event-triggered control laws for switched affine systems are proposed, which may be restrictive when state measurements are not available. Moreover, compared with [206], where no state delays have been considered, by verifying the feasibility of Theorem 10 for $h(t) = 0$, $\alpha = 0.005$, it can be found $\epsilon^\star = 1.12$, as well as the result of our optimization procedure leads to UB $= 0.4065$. Finally, numerical simulations shown in Figure 9.2 highlight the stabilization of system (9.76) for all $\epsilon \in (0, \epsilon^\star]$ and $h(t) \in [0, 0.5]$, thus confirming theoretical derivation.

Example 2

Consider the delayed dynamics of flyback power converter from [38],[39], where the model has the form of

$$\begin{aligned} \dot{x}(t) =& A_{\sigma(t)}x(t) + (A_d + \Delta A_d)x(t - h(t)) + B_{\sigma(t)}u(t) \\ &+ D_{\sigma(t)}w(t) + b_{\sigma(t)}, \end{aligned} \tag{9.77}$$

with $u(t) = Kx(t)$ and matrices $\Delta A_1 = \Delta A_2 = 0$,

$$\begin{aligned} &A_1 = \begin{bmatrix} -r/L_m & 0 \\ 0 & -1/R_L C \end{bmatrix},\ b_1 = \begin{bmatrix} E_{in}/L_m \\ 0 \end{bmatrix},\ D_1 = \begin{bmatrix} 0.1 \\ 0.1 \end{bmatrix}, \\ &A_d = \begin{bmatrix} -0.1 & 0.1 \\ 0 & 0.1 \end{bmatrix}, B_1 = \begin{bmatrix} 0 & 0.1 \\ 0.1 & 0.1 \end{bmatrix},\ K_1 = \begin{bmatrix} 19.7287 & -18.9826 \\ -21.1811 & -1.6378 \end{bmatrix}, \\ &\Delta A_d = \begin{bmatrix} -0.1 & 0 \\ 0.2 & -0.2 \end{bmatrix},\ D_2 = \begin{bmatrix} 0.3 \\ 0.3 \end{bmatrix}, A_2 = \begin{bmatrix} -r/L_m & -n/L_m \\ n/C & -1/R_L C \end{bmatrix}, \\ &b_2 = \begin{bmatrix} 0 \\ 0 \end{bmatrix},\ B_2 = \begin{bmatrix} 0 & 0.1 \\ 0.1 & 0.3 \end{bmatrix},\ D_2 = \begin{bmatrix} 0.3 \\ 0.3 \end{bmatrix},\ K_2 = \begin{bmatrix} 58.9652 & -14.0308 \\ -20.4310 & -1.9181 \end{bmatrix}. \end{aligned} \tag{9.78}$$

Note that, controller $u(t)$ has been used as in [38] in order to provide a fair comparison in terms of maximum delay bound h_M and parameter ϵ. However, $u(t)$ can be required in flyback converter due to its non-minimum-phase nature and the presence of a right-half-plane-zero in voltage transfer function in order to guarantee the indirect regulation of the output voltage [218]. Moreover, both non-minimum-phase nature and the presence of a right-half-plane-zero in voltage transfer function may lead to state delay $h(t)$ [39]. The parameters are given as $E_{in} = 6V$, $L_m = 10mH$, $r = 3\Omega$, $C = 2mF$, $R_L = 1.5\Omega$ and the transformer turns ratio $n = 1$. As in [38], it is selected $\lambda = 0.5 \in \Lambda_H$, leading to the desired equilibrium point $x_e = [0.7547 \ 0.7925]$ and to Hurwitz matrix $A_{av} = 0.5(A_1 + B_1K_1) + 0.5(A_2 + B_2K_2) + A_d$. Moreover, in this example $\Delta A = 0$ and $\Delta A_d \neq 0$ brings to $\kappa = 0$ and $\|\Delta A_d\| \leq \kappa_d = 0.2921$ respectively, while it is set $D_{\sigma(t)} = \Delta B_{\sigma(t)}$, which leads to $|\Delta \bar{B}| = |\Delta B_{\sigma_{(t)}}| + |\Delta A_d x_e| \leq \kappa_b = 0.5001$. For all $\tau \geq T = 1$, inequality (9.18) becomes

$$
\begin{aligned}
&\int_{\tau-1}^{\tau} (\zeta - \tau + 1)(A(\zeta) + K(\zeta)B(\zeta))^\top H(A(\zeta) + K(\zeta)B(\zeta))\, d\zeta \\
&\leq \int_{\tau-\lambda}^{\tau} (\zeta - \tau + 1)\, d\zeta (A_1 + B_1K_1)^\top H(A_1 + B_1K_1) \\
&+ \int_{\tau-(1-\lambda)}^{\tau} (\zeta - \tau + 1)\, d\zeta (A_2 + B_2K_2)^\top H(A_2 + B_2K_2) \\
&= \frac{1-(1-\lambda)^2}{2}(A_1 + B_1K_1)^\top H(A_1 + B_1K_1) \\
&+ \frac{1-\lambda^2}{2}(A_2 + B_2K_2)^\top H(A_2 + B_2K_2) = \bar{H}.
\end{aligned}
$$

By verifying the feasibility of (9.16),(9.17),(9.18) and (9.67) with $\alpha = 0.005$, $h_M = 0.4$, the maximum value of ϵ can be found, i.e., $\epsilon^\star = 0.32$ that guarantees the practical stability of (9.77)-(9.78) for all $\epsilon \in (0, \epsilon^\star]$, $h(t) \in [0, h_M]$ and decay rate $\alpha = 0.005$. Moreover, by solving (9.55), it results $b_0^\star = 0.85$, $b^\star = 5.3404$ and, hence, the resulting ball radius UB $= 10.4529$. On the other hand, by solving LMIs (9.16),(9.17),(9.18) and (9.67) with $\alpha = 0.005$, $\epsilon^\star = 0.2$, the resulting maximum delay bound can be obtained as $h_M = 2.2$, which leads to UB $= 23.6443$ provided by $b^\star = 9.3171$ and $b_0^\star = 1.98$.

Therefore, compared with [38], where a state dependent switching rule along with event-triggered control protocol have been implemented with a fixed sampling period $T_{max} = 0.01$ and a delay bound $h_M \approx 0.2$, the proposed strategy allows quantifying the bounds $\epsilon^\star$ and h_M on the small parameter and non-small delay, respectively, without the need of reliable state measurements. Finally, Figure 9.3 shows the practical stabilization of switched affine flyback converter with $\epsilon^\star = 0.32$ and $h_M = 0.4$, thus confirming that the switched system (9.77)-(9.78) exponentially converges to the set $\mathscr{X}_{\epsilon^\star}$ in (9.71).

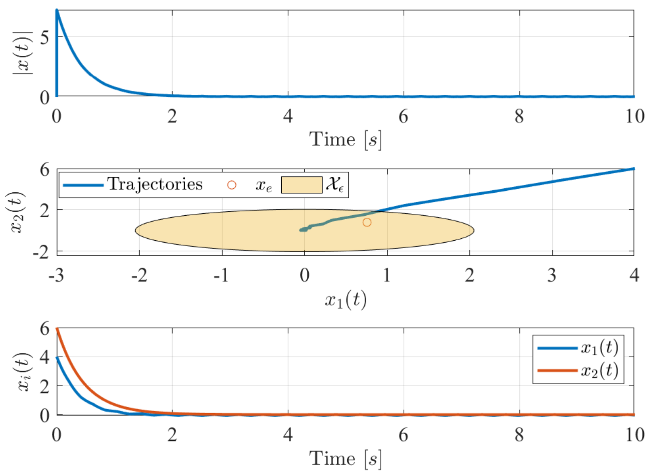

Figure 9.3. Practical stabilization of switched affine system (9.77)-(9.78) with $\epsilon^\star = 0.32$ and $h_M = 0.4$.

9.4 Concluding Remarks

In this chapter the recent time-delay approach to averaging is extended to the class of linear systems with fast-varying coefficients and perturbations in the presence of non-small delays. An appropriate Lyapunov–Krasovskii functional is constructed to prove the ISS of such class of time-delayed systems, thus providing ISS conditions in terms of LMIs, whose solution allows finding upper bounds on both small parameter and non-small delays. The proposed approach is extended to stabilization of uncertain delayed affine systems by periodic time-dependent switching. Numerical examples from the literature illustrate the efficiency of the method.

Chapter 10

Conclusions

The thesis has addressed the problem of designing different distributed control strategies for modern cyber-physical energy systems from a networked control systems perspective. The objective is to promote the current green energy revolution through the deployment of Microgrids (MGs) paradigm, where more reliable, efficient and resilient working operating conditions can be achieved via proper distributed control strategies. The attention has been focused on different open challenges arising in both in MGs applications literature and in the general context of networked control systems, namely:

- designing of distributed control strategies able to cope with time-varying communication delays, while providing a faster convergence rate in order to guarantee a timely adaptation to strongly-varying working environment due to the presence of loads changes, plug-and-play phenomena and nominal set-points variations;
- designing of distributed control strategies resilient with respect to unmodeled dynamics, completely-unknown uncertainties and unbounded disturbances arising from MGs modeling phase, as well as from all the involved complex phenomena;
- design of distributed sampled-data controllers able to facilitate their implementation in digital control platforms, while reducing the communication network workload and saving its limited resources without compromising MGs performance.

To address the above-mentioned issues, the thesis provides a deep excursus of the designing procedures steps of the suggested distributed control laws, strongly supported by an analytical mathematical rigour. Specifically, the stability analysis of these proposed distributed control protocols have been demonstrated by mainly exploiting Lyapunov and Lyapunov-Krasovskii theories, along with a wide range of stability analysis tools. The exploitation of these latter has allowed finding stability criteria for each distributed controllers, usually expressed in the form of linear matrix inequalities, whose feasible solution has provided estimation of crucial control parameters preserving the stability. Furthermore, their effectiveness and robustness have been confirmed via extensive numerical simulations, sometimes carried out even on the well-known benchmarks provided by IEEE 14/30 bus test systems.

Appendix A

Mathematical Review

A.1 Stability of Continuous-Time Systems

Some useful results about stability of linear systems are recalled for the sake of clarity.

Theorem 11. *[113] Let us consider the following n-dimensional LTI system*

$$\begin{aligned} \dot{x}(t) &= Ax(t), \quad t \geq 0 \\ x(0) &= x_0. \end{aligned} \tag{A.1}$$

The following statements are equivalent:

1. *The system (A.1) is globally asymptotically stable.*
2. *The system (A.1) is globally exponentially stable.*
3. *The matrix A is Hurwitz, i.e. $\lambda(A) \in \mathbb{C}_-$.*
4. *There exist matrices P, $Q \in \mathbb{S}^n_{>0}$ such that the Lyapunov equation*

   $$A^\top P + PA + Q = 0$$

   holds.
5. *There exists a matrix $P \in \mathbb{S}^n_{>0}$ such that the Lyapunov inequality*

   $$A^\top P + PA < 0$$

holds.

Proof. The proof of Theorem 11 can be found in [113]. □

Consider now a time-varying linear system in the following form:

$$\dot{x}(t) = A(t)x(t), \tag{A.2}$$

with $A \in \mathbb{R}^{n\times n}$ and $t \in \mathbb{R}$. Without loss of generality, assume $x = 0$ to be an equilibrium point for (A.2). To establish asymptotic stability of this equilibrium point, a standard approach is to seek a quadratic Lyapunov function associated to (A.2). Hence, let $V(x(t)) = x^\top(t)Px(t)$. Then,

$$\dot{V}(x(t)) = x^\top(t)[A^\top(t)P + PA(t)]x(t), \tag{A.3}$$

and thus it is sufficient to seek a matrix $P \in \mathbb{S}_n^+$ which satisfies the continuous-time algebraic Lyapunov equation:

$$A^\top(t)P + PA(t) = -M(t), \tag{A.4}$$

where $M(t) \in \mathbb{S}_n^+$ is given. Here $\mathbb{S}_n^+$ denotes the set of real, $n \times n$ positive definite symmetric matrices.

Theorem 12. *[219] The unique solution of (A.4) is given by:*

$$P = \int_{t_0}^{\infty} \Phi_A^\top(s,t_0)M(t)\Phi_A(s,t_0)\,ds, \tag{A.5}$$

where $\Phi_A(t,t_0)$ is the transition matrix for the system (A.2). Moreover, $P \in \mathbb{S}_n^+$ whenever $M(t) \in \mathbb{S}_n^+$.

On the other hand, suppose we seek a Lyapunov function of the form $V(x(t)) = x^\top(t)P(t)x(t)$, the emphasis being that P is time-varying. Then,

$$\dot{V}(x(t)) = x^\top(t)[A^\top(t)P(t) + P(t)A(t) + \dot{P}(t)]x(t),$$

and so we seek a $P(t) \in \mathbb{S}_n^+$ which satisfies the continuous-time differential Lyapunov equation:

$$A^\top(t)P(t) + P(t)A(t) + \dot{P}(t) = -M(t), \tag{A.6}$$

where $M(t) \in \mathbb{S}_n^+$ is specified.

Theorem 13. *[219] The unique solution of* (A.6) *subject to initial condition $P(t_0) = P_0$ is given by*

$$P(t) = \Phi_A^{-\top}(t,t_0)P(t_0)\Phi_A^{-1}(t,t_0) - \int_{t_0}^{\infty} \Phi_A^{\top}(s,t_0)M(t)\Phi_A(s,t_0)\,ds, \quad \text{(A.7)}$$

where $\Phi_A(t,t_0)$ is the transition matrix for the system (A.2)*. Moreover, $P(t) \in \mathbb{S}_n^+$ whenever $M(t) \in \mathbb{S}_n^+$.*

A.2 Stability Analysis of Time-Delay Systems

Time-delay often appears in many real-world engineering systems either in the state, the control input, or the measurements. Delays are strongly involved in challenging areas of communication and information technologies: in stabilization of NCS and in high-speed communication networks. Time-delay is, in many cases, a source of instability. However, for some systems, the presence of delay can have a stabilizing effect. The stability analysis and robust control of Time-Delay Systems are, therefore, of theoretical and practical importance [97]. Time-Delay Systems (TDSs) belong to the class of functional differential equations, which are infinite-dimensional, as opposed to Ordinary Differential Equations (ODEs). The simple example of such system is

$$\dot{x}(t) = -x(t-h), \quad x(t) \in \mathbb{R},$$

where $h > 0$ is the time-delay [97]. The analysis of TDSs is well-developed field gathering a lot of different techniques. These methods can be categorized to either belong to frequency-domain or time-domain techniques. Frequency-domain approaches are mostly devoted to LTI systems, yet under some circumstances, it is possible to adapt them to address the case of varying delays using, for instance, model transformations. Time-domain approaches can, however, be applied to any type of systems: linear or non-linear, with constant or time-varying delays, etc [113, 220, 221]. As in systems without delay, an efficient method for stability analysis of TDSs is the Lyapunov method. Specifically, for TDSs, there exist two main Lyapunov methods [97]:

- The *Lyapunov-Razumikhin* method that looks for functions which normally allow one to prove stability of systems with bounded but freely fast time-varying delays.

- The *Lyapunov-Krasovskii* method that looks for functionals which only allow one to prove stability of TDSs where delay parameters are bounded both in length and time variation.

Note that, in [222] a discussion about the conservatism between the different methods is given. The main difference among the two approaches relies in the fact that Razumikhin method gives more conservative bound on the maximum allowable delay preserving stability than Lyapunov-Krasovskii approach, as showed in [223].
In order to present general statments about TDSs, let us consider the general form of a Retarded Functional Differential Equation (RFDE):

$$\begin{aligned} \dot{x}(t) &= f(t, x_t), \quad t \geq t_0 \\ x(t_0 + s) &= \phi(s), \quad s \in [-h, 0] \end{aligned} \tag{A.8}$$

where $h > 0$ is the delay and $\phi \in C([-h, 0], \mathbb{R}^n)$ is the functional of initial conditions. The state of the system, denoted by $x_t \in C([-h, 0], \mathbb{R}^n)$ is defined as $x_t(\theta) = x(t + \theta)$. Assume $x_t(t_0, \psi)$ to be the state-value at time t with initial condition $x_{t_0} = \phi$. Moreover, without loss of generality, assume that system (A.8) has as a unique solution $x(t) = 0$, i.e., $f(t, 0) = 0$, generally referred to as the *trivial solution*. The following definitions hold.

Definition 3. *(Uniform Norm [113]) Let $\phi \in C([a, b], \mathbb{R}^n)$ be the set of continuous function mapping the interval $[a, b]$ to $\mathbb{R}^n$, then the uniform norm of ϕ is defined as:*

$$\|\phi\|_C = \max_{a \leq s \leq b} \|\phi(s)\|, \tag{A.9}$$

where $\|\cdot\|$ is any vector-norm, e.g. the vector 2-norm.

Definition 4. *Consider TDSs as in (A.8). The trivial solution is said to be*

- ***stable** if for any $t_0 \geq 0$ and any $\epsilon > 0$, there exists $\delta = \delta(t_0, \epsilon) > 0$*

such that for all $t \geq t_0$

$$\|x_{t_0}\|_C \leq \delta \Longrightarrow \|x(t)\| \leq \epsilon.$$

- ***attractive*** *if for any* $t_0 \geq 0$ *and any* $\epsilon > 0$*, there exists* $\delta_a = \delta_a(t_0, \epsilon) > 0$ *with the property that*

$$\|x_{t_0}\|_C \leq \delta_a \Longrightarrow \lim_{t\to\infty} \|x(t)\| = 0.$$

- ***asymptotically stable*** *(in the sense of Lyapunov), if it is both stable and attractive.*

- ***uniformly stable****, it is is stable and* $\delta(t_0, \epsilon)$ *can be chosen independently of* t_0*.*

- ***exponentially stable*** *if there exist* $\delta, \alpha > 0$ *and* $\beta \geq 1$ *such that*

$$\|x_{t_0}\|_C \leq \delta \Longrightarrow \|x(t)\| \leq \beta e^{-\alpha t}\|x_0\|, \quad \forall t \geq 0.$$

- ***unstable****, if it is not stable in the sense of Lyapunov.*

A.2.1 Lyapunov-Krasovskii Theorem

The idea of Krasovskii was to extend Lyapunov result to account for the infinite-dimensionality of the state through the use of functionals, according to the following theorem.

Theorem 14. *(Lyapunov-Krasovskii Stability Theorem [113, 97]) Suppose that the function* $f : \mathbb{R}_{\geq t_0} \times C([-h, 0], \mathbb{R}^n) \to \mathbb{R}^n$ *in* (A.8) *maps* $\mathbb{R}_{\geq t_0} \times$ *(bounded sets of* $C([-h, 0], \mathbb{R}^n)$*) into bounded sets of* $\mathbb{R}^n$*, and* u*,* v*,* w : $\mathbb{R}_{\geq 0} \to \mathbb{R}_{\geq 0}$ *are continuous nondecreasing functions, where* $u(s)$ *and* $v(s)$ *are positive for* $s > 0$*, and* $u(0) = v(0) = 0$*. Assume further that there exists a continuous differentiable functional* $V : \mathbb{R} \times C([-h, 0], \mathbb{R}^n) \to \mathbb{R}$ *such that*

$$u(\|\phi(0)\|) \leq V(t, \phi) \leq v(\|\phi\|_C) \tag{A.10}$$

and

$$\dot{V}(t,\phi) = \lim \epsilon \to 0^+ \sup \frac{1}{\epsilon}[V(t+\epsilon, x_{t+\epsilon}(t,\phi)) - V(t,\phi)] \leq -w(\|\phi(0)\|). \tag{A.11}$$

Then, the trivial solution of (A.8) *is uniformly stable. Moreover, if* $w(s) > 0$ *for* $s > 0$*, then is is uniformly asymptotically stable. If, in addition,* $\lim_{s\to+\infty} u(s) = +\infty$*, then it is globally uniformly asymptotically stable.*

Proof. The proof of Theorem 14 can be found in [224]. □

Note that, two types of stability results may be distinguished on whether they depend on the delay value. This leads to the concepts of delay-independent and delay-dependent stability according to the following definitions.

Definition 5. *(Delay-Independent Stability [113, 97]) A time-delay system is* ***stable independently of the delay*** *or* ***delay-independent stable*** *if stability does not depend on the delay value, that is, if the system is stable for any delay value in* $[0, \infty]$.

Definition 5 can be applied also to systems with multiple delays and time-varying delays. This concept of stability is quite strong since delays must have no impact on stability. This imposes, in return, strong constraints on the structure of the system. It is therefore expected that TDSs are, most likely, not delay-independent stable.

Definition 6. *(Delay-Dependent Stability [113, 97]) A time-delay system is* ***delay-dependent stable*** *if there exists a (bounded) interval* $\mathscr{I} \subset \mathbb{R}_{\geq 0}$ *for which the system is stable for any delay in* $\mathscr{I}$*, and unstable otherwise.*

The concept of stability in Definition 6 is sensitive to change in the delay values. This is certainly the most realistic notion of stability since delays are, most of the time, influential on the stability of real world systems.

A.2.2 Model Transformations

Model transformation is a very common procedure introduced quite early in the analysis of time-delay systems, but not restricted to. The rationale behind model transformations is to turn a time-delay system into

another system, referred to as a comparison system or comparison model, which may or may not be a time-delay system. Analysis tools are then applied on the comparison system in order to draw conclusions on the stability of the original time-delay system. Model transformations lie at the core of many efficient analysis techniques, such as Lyapunov-Razumikhin and Lyapunov-Krasovskii approaches. The goal of model transformations is to simplify the analysis of TDSs. The compensation for this is that the comparison system may exhibit additional dynamics leading to a possible loss of equivalence, in terms of stability, between the original and the comparison system. Additional dynamics consist of supplementary zeros in the characteristic equation of the comparison model. When at least one of these additional zeros is unstable, the comparison model is unstable and the stability of the original system cannot be inferred from the comparison model. Many different model transformation procedures have been proposed in the technical literature. Now, two model transformations widely used through the thesis will be shown: the first one is referred as *Newton-Leibnitz model transformation*, while the second one is the *descriptor model transformation*, more recently introduced in [225, 226].
Before introducing these latter, consider the LTI TDSs:

$$\begin{aligned} \dot{x}(t) &= Ax(t) + A_h x(t-h) \\ x(\theta) &= \phi(\theta), \quad \theta \in [-h, 0]. \end{aligned} \tag{A.12}$$

Newton-Leibnitz Model Transformation

The Newton-Leibnitz model transformation is based on the following identity:

$$x(t-h) = x(t) - \int_{t-h}^{t} \dot{x}(\theta)\, d\theta \tag{A.13}$$

Model transformation in (A.13) allows to substitute the delayed term $x(t-h)$ in (A.12) by the right-hand sude of the above expression, thus obtaining the following comparison system:

$$\dot{x}(t) = (A + A_h)x(t) - A_h \int_{t-h}^{t} [Ax(s) + A_h x(s-h)]\, ds. \tag{A.14}$$

Note that, different from (A.12), comparison model in (A.14) requires an initial condition in $C([-2h,0],\mathbb{R}^n)$ due to the delayed term in the integral. Not it is possible to analyze (A.14) by exploiting Lyapunov-Krasovskii functionals, Lyapunov-Razumikhin functions or some robust analysis techniques.

Descriptor Model Transformation

Taking into account system (A.12), the descriptor model transformation, introduced more recently in [225, 226], relies on the following equality:

$$\dot{x}(t) = y(t), \quad y(t) = Ax(t) + A_h x(t-h), \tag{A.15}$$

and, hence, the descriptor system (i.e., the comparison model) is:

$$\dot{x}(t) = y(t), \quad 0 = -y(t) + (A + A_h)x(t) - A_h \int_{t-h}^{t} y(s)\, ds, \tag{A.16}$$

or, equivalently,

$$\begin{bmatrix} I & 0 \\ 0 & 0 \end{bmatrix} \begin{bmatrix} \dot{x}(t) \\ \dot{y}(t) \end{bmatrix} = \begin{bmatrix} 0 & I \\ A + A_h & -I \end{bmatrix} \begin{bmatrix} x(t) \\ y(t) \end{bmatrix} + \int_{t-h}^{t} \begin{bmatrix} 0 & 0 \\ 0 & -A_h \end{bmatrix} \begin{bmatrix} x(s) \\ y(s) \end{bmatrix} ds \tag{A.17}$$

Note that, system (A.16) (and, hence, (A.17)) is equivalent to (A.12) in the sense of stability. In the descriptor approach, $\dot{x}(t)$ is not substituted by the right-hand side of the differential equation; instead, it is considered as an additional state variable of the resulting descriptor system (A.16)-(A.17).

A.2.3 Free-Weighting Matrices Technique

The idea of Free-Weighting Matrices Technique is to sum to the differential equation (A.12) the following null-term [97]:

$$0 = C[x(t) - \int_{t-h}^{t} \dot{x}(s)\, ds - x(t-h)],$$

with free matrix parameter C, thus obtaining:

$$\dot{x}(t) = (A + C)x(t) + (A_h - C)x(t-h) - C\int_{t-h}^{t} \dot{x}(s)\,ds.$$

Another way for inserting free-weighting matrices is to add the following null term to $\dot{V}$ through the Lyapunov-based stability analysis:

$$0 = 2[x^\top(t)N_1 + x^\top(t-h)N_2][x(t) - \int_{t-h}^{t} \dot{x}(s)\,ds - x(t-h)]$$

with free matrices N_1 and N_2. The interested reader can refer to [97] and references therein for more details.

A.2.4 Useful Integral Inequalities

Lemma 4. *(Jensen's inequality and Extended Jensen's inequality [97].) For any $n \times n$ matrix $R > 0$, scalars $\alpha \leq \beta$ with $\delta = \beta - \alpha$, functions $f : [\alpha, \beta] \to \mathbb{R}$ and $\phi : [\alpha, \beta] \to \mathbb{R}^n$ such that the the integrations concerned are well defined, the following Jensen's inequality*

$$\int_\alpha^\beta \phi^\top(s)\,ds R \int_\alpha^\beta \phi(s)\,ds \leq (\beta - \alpha)\int_\alpha^\beta \phi^\top(s) R \phi(s)\,ds, \tag{A.18}$$

as well as extended Jensen's inequalities hold

$$\int_\alpha^\beta f(s)\phi^\top(s)\,ds R \int_\alpha^\beta f(s)\phi(s)\,ds \leq \int_\alpha^\beta |f(\theta)|\,d\theta \int_\alpha^\beta |f(s)|\phi^\top(s) R \phi(s)\,ds, \tag{A.19}$$

$$\int_\alpha^\beta \int_\alpha^\beta \phi^\top(\theta)\,d\theta\,ds R \int_\alpha^\beta \int_\alpha^\beta \phi(\theta)\,d\theta\,ds \leq \frac{\delta^2}{2}\int_\alpha^\beta \int_\alpha^\beta \phi^\top(\theta) R \phi(\theta)\,d\theta\,ds. \tag{A.20}$$

Lemma 5 (Exponential Wirtinger's inequality)**.** *Let $f : [a, b] \to \mathbb{R}^n$ be an absolutely continuous function with a square integrable first order derivative such that $f(a) = 0$ or $f(b) = 0$. Then, for any $\alpha \in \mathbb{R}$ and $0 \leq W \in \mathbb{R}^{n\times n}$,*

$$\int_a^b e^{2\alpha t} f^\top(t) W f(t)\,dt \leq e^{2|\alpha|(b-a)} \frac{4(b-a)^2}{\pi^2} \int_a^b e^{2\alpha t} \dot{f}^\top(t) W \dot{f}(t)\,dt.$$

A.2.5 Finite-Time Stability of Time-Delay Systems

Let a delayed system as

$$\dot{x}(t) = Ax(t) + Bx(t - \tau(t)) + Fw(t) \tag{A.21}$$

being $x(t) \in \mathbb{R}^N$ the state vector, $\tau(t)$ the time-varying delay due to the communication network such that $\tau(t) \in [0, \tau^\star]$, $\dot{\tau}(t) \in [0, \mu]$ with $\mu < 1$ [97]; $w(t) \in \mathbb{R}^N$ the bounded disturbances vector; and A, B, F known matrices of appropriate dimensions.

Definition 7 (*Robust Finite-time Stability for time-delay systems* [227, 228])**.** *Given positive scalars T^f, $\tau^\star$, Π, c_1 and c_2 with $c_2 > c_1$ and a matrix $\Psi > 0$, system (A.21) is said to be robust finite-time stable (RFTS) with respect to $(c_1, c_2, \tau^\star, T^f, \Psi, \Pi)$ if*

$$\begin{aligned} &\sup_{-\tau^\star \leq t_0 \leq 0} \{x^\top(t_0)\Psi x(t_0), \dot{x}^\top(t_0)\Psi \dot{x}(t_0)\} \leq c_1 \\ &\qquad \Longrightarrow x^\top(t)\Psi x(t) < c_2 \quad t \in [t_0, t_0 + T^f] \end{aligned}$$

for all the disturbances $w(t)$ satisfying $\int_0^{T^f} w^\top(t)w(t) \leq \Pi$.

A.3 Additional Definitions and Lemmas

Some additional useful definitions and lemmas instrumental through the thesis will be provided.

Lemma 6. *(Halanay Inequality [229]) Let $f(t) > 0$ for $t \in \mathbb{R}$, $\tau^\star \in [0, +\infty)$ and $t_0 \in \mathbb{R}$. Suppose that $\dot{f}(t) \leq -\alpha f(t) + \beta \sup_{t-\tau^\star \leq s \leq t} f(s)$, $\forall t > t_0$. If $\alpha > \beta$, then there exist a value $\delta \in (0, \alpha)$ such that $\delta - \alpha + \beta e^{\delta \tau^\star} = 0$ and*

$$f(t) \leq \sup_{t_0 - \tau^\star \leq s \leq t_0} f(s) e^{-\delta(t - t_0)}, \quad \forall t > t_0. \tag{A.22}$$

Lemma 7 (Barbalat Lemma [144])**.** *If the function $f(t)$ is positive, uniformly continuous and $\int_0^{+\infty} f(t)\, dt < \infty$, then, $\lim_{t \to +\infty} f(t) = 0$.*

Lemma 8. *[147] For any $\phi > 0$ and any $z \in \mathbb{R}$, it holds:*

$$0 \leq |z| - \frac{z^2}{\sqrt{z^2 + \phi^2}} \leq \phi.$$

Lemma 9. *(Rayleigh Inequality [116]) For any symmetric matrix $D \in \mathbb{R}^{n\times n}$, i.e. $D = D^\top$ and a generic vector $x \in \mathbb{R}^{n\times 1}$, the inequality holds:*

$$\underline{\lambda}_D \|x\|^2 \leq x^\top D x \leq \bar{\lambda}_D \|x\|^2,$$

being $\underline{\lambda}_{(\cdot)}$ and $\bar{\lambda}_{(\cdot)}$ the minimum and the maximum eigenvalues, respectively, of the associated matrix into the subscript.

Definition 8. *(Uniform connectivity on average [165]) A graph $\mathscr{G}(t)$, with its corresponding Laplacian $\mathscr{L}(t)$, is said to be uniformly connected on average if*

$$\mathscr{L}_{av} = \lim_{T\to\infty} \frac{1}{T} \int_t^{t+T} \mathscr{L}(\tau)\, d\tau \tag{A.23}$$

is well defined for all $t \geq 0$ and

$$\left\| \frac{1}{T} \int_t^{t+T} \mathscr{L}(\tau)\, d\tau - \mathscr{L}_{av} \right\| \leq \sigma(T), \tag{A.24}$$

being $\sigma(T) : [0, \infty) \to [0, \infty)$ a continuous and decreasing function such that $\lim_{T\to\infty} \sigma(T) = 0$. Moreover, the graph $\mathscr{G}_{av}$ induced from $\mathscr{L}_{av}$ is connected.

A.3.1 Comparison Principle and Gronwall's Inequality

Given the state equation $\dot{x} = f(t, x)$, Comparison lemma and Gronwall's inequality allow computing the bounds on the solution $x(t)$ without computing the solution itself. It applies to a situation where the derivative of a scalar differential function $v(t)$ satisfies inequality of the form $\dot{v}(t) \leq f(t, v(t))$ for all t in a certain time interval. Such inequality is called differential inequality and the function $v(t)$ satisfying the inequality is called solution of the differential inequality. Comparison lemma compares the solution of the differential inequality with the solution of the differential equation $\dot{u}(t) = f(t, u)$, according to the following statement.

Lemma 10. *(Comparison Lemma [144]) Consider the scalar differential equation*

$$\dot{u} = f(t, u), \quad u(t_0) = u_0,$$

where $f(t, u)$ is continuous in t and locally Lipschitz in u, for all $t \geq 0$ and all $u \in J \subset \mathbb{R}$. Let $[t_0, T)$ (T could be infinity) be the maximal interval of existence of the solution $u(t)$, and suppose $u(t) \in J$ for all $t \in [t_0, T)$. Let $v(t)$ be a continuous function whose upper right-hand derivative $D^+v(t)$ satisfies the differential inequality

$$D^+v(t) \leq f(t, v(t)), \quad v(t_0) \leq u_0,$$

with $v(t) \in J$ for all $t \in [t_0, T)$. Then, $v(t) \leq u(t)$ for all $t \in [t_0, T)$.

Lemma 11. *(Gronwall's Inequality [144, 97]) Let $\lambda : [a, b] \to \mathbb{R}$ and $\mu : [a, b] \to \mathbb{R}_+$ be continuous. If a continuous function $y : [a, b] \to \mathbb{R}$ satisfies*

$$y(t) \leq \lambda(t) + \int_a^t \mu(s)y(s)\, ds, \qquad t \in [a, b],$$

then

$$y(t) \leq \lambda(t) + \int_a^t \lambda(s)\mu(s) exp\left[\int_s^t \mu(\xi)\, d\xi\right] ds, \qquad t \in [a, b].$$

If, in addition, $\lambda(t) \equiv \lambda$ and $\mu(t) \equiv \mu \geq 0$ are constant, then

$$y(t) < \lambda e^{\mu(t-a)}, \qquad t \in [a, b].$$

A.3.2 Schur Complement Lemma and S-Procedure

The Schur complement formula is the basic tool for transforming nonlinear matrix inequalities to LMIs.

Lemma 12. *(Schur Complement Lemma [97].) Given matrices A, B, C, the following holds:*

$$M = \begin{bmatrix} A & B \\ B^\top & C \end{bmatrix} > 0 \iff C > 0, \qquad A - BC^{-1}B^\top > 0.$$

Here, $A - BC^{-1}B^\top$ is the Schur complement of the block C of M.

Conversely, S-procedure plays an important role in robust stability theory, according to the following Lemma.

Lemma 13. *(S-Procedure [97].) Let* $F_i \in \mathbb{R}^{n\times n},\ i = 0, 1, \dots, p$. *If there exist real scalars* $\lambda_i \geq 0$ *such that*

$$F_0 - \sum_{i=1}^{p} \lambda_i F_i > 0, \tag{A.25}$$

then,

$$\xi^\top F_0 \xi > 0,\ \text{for any}\ 0 \neq \xi \in \mathbb{R}^n\ \text{satisfying}\ \xi^\top F_i \xi \geq 0,\ \forall i = 1, \dots, p. \tag{A.26}$$

For $p = 1$ *the conditions* (A.25) *and* (A.26) *are equivalent. The proposition is still valid if all the inequalities are non-strict (with* $>$ *changed by* $\geq$*).*

Bibliography

[1] Amjad Anvari-Moghaddam, Hamdi Abdi, Behnam Mohammadi-Ivatloo, and Nikos Hatziargyriou. *Microgrids: Advances in Operation, Control, and Protection*. Springer Nature, 2021.

[2] Naser Mahdavi Tabatabaei, Ersan Kabalci, and Nicu Bizon. *Microgrid architectures, control and protection methods*. Springer, 2019.

[3] Thomas Basso. Ieee 1547 and 2030 standards for distributed energy resources interconnection and interoperability with the electricity grid. Technical report, National Renewable Energy Lab.(NREL), Golden, CO (United States), 2014.

[4] Soma Shekara Sreenadh Reddy Depuru, Lingfeng Wang, Vijay Devabhaktuni, and Nikhil Gudi. Smart meters for power grid—challenges, issues, advantages and status. In *2011 IEEE/PES Power Systems Conference and Exposition*, pages 1–7. IEEE, 2011.

[5] European Commission. Fit for 55, 2020. https://www.consilium.europa.eu/en/policies/green-deal/fit-for-55-the-eu-plan-for-a-green-transition/.

[6] Fei Gao, Ren Kang, Jun Cao, and Tao Yang. Primary and secondary control in dc microgrids: a review. *Journal of Modern Power Systems and Clean Energy*, 7(2):227–242, 2019.

[7] Yousef Khayat, Qobad Shafiee, Rasool Heydari, Mobin Naderi, Tomislav Dragičević, John W Simpson-Porco, Florian Dörfler, Mohammad Fathi, Frede Blaabjerg, Josep M Guerrero, et al. On the secondary control architectures of ac microgrids: An overview. *IEEE Transactions on Power Electronics*, 35(6):6482–6500, 2019.

[8] Ali Bidram, Vahidreza Nasirian, Ali Davoudi, and Frank L Lewis. *Cooperative synchronization in distributed microgrid control*. Springer, 2017.

[9] Xiaoqing Lu and Jingang Lai. Communication constraints for distributed secondary control of heterogenous microgrids: A survey. *IEEE Transactions on Industry Applications*, 2021.

[10] Jiayi Liu, Jiaqi Li, Huihui Song, Arshad Nawaz, and Yanbin Qu. Nonlinear secondary voltage control of islanded microgrid via distributed consistency. *IEEE Transactions on Energy Conversion*, 35(4):1964–1972, 2020.

[11] Mohsen Keshavarz, Aref Doroudi, Mohammad Hossein Kazemi, and Nima Mahdian Dehkordi. A novel adaptive distributed secondary voltage controller with high convergence rate for islanded microgrids. *IEEE Systems Journal*, 15(3):4157–4167, 2020.

[12] Xiaohua Ge, Qing-Long Han, Derui Ding, Xian-Ming Zhang, and Boda Ning. A survey on recent advances in distributed sampled-data cooperative control of multi-agent systems. *Neurocomputing*, 275:1684–1701, 2018.

[13] Fanghong Guo, Changyun Wen, Jianfeng Mao, and Yong-Duan Song. Distributed secondary voltage and frequency restoration control of droop-controlled inverter-based microgrids. *IEEE Transactions on industrial Electronics*, 62(7):4355–4364, 2014.

[14] Bianca Caiazzo, Emilia Fridman, Alberto Petrillo, and Stefania Santini. Distributed sampled-data pid control for voltage regulation in inverter-based islanded microgrids using artificial delays. *IFAC-PapersOnLine*, 54(18):186–191, 2021.

[15] Nur IqtiyaniIlham, M Hasanuzzaman, and M Hosenuzzaman. European smart grid prospects, policies, and challenges. *Renewable and Sustainable Energy Reviews*, 67:776–790, 2017.

[16] Filippo Bovera and Luca Lo Schiavo. From energy communities to sector coupling: a taxonomy for regulatory experimentation in the age of the european green deal. *Energy Policy*, 171:113299, 2022.

[17] European Commission. A european climate law, 2020. https://climate.ec.europa.eu/eu-action/european-green-deal/european-climate-law_en.

[18] Dongming Fan, Yi Ren, Qiang Feng, Yiliu Liu, Zili Wang, and Jing Lin. Restoration of smart grids: Current status, challenges, and opportunities. *Renewable and Sustainable Energy Reviews*, 143:110909, 2021.

[19] Sunetra Chowdhury, Shyama P Chowdhury, and Peter Crossley. *Microgrids and active distribution networks.* 2022.

[20] Antonio Carlos Zambroni de Souza and Miguel Castilla. *Microgrids design and implementation.* Springer, 2019.

[21] Omid Palizban and Kimmo Kauhaniemi. Hierarchical control structure in microgrids with distributed generation: Island and grid-connected mode. *Renewable and Sustainable Energy Reviews*, 44:797–813, 2015.

[22] Yulin Chen, Chaoyong Li, Donglian Qi, Zhenming Li, Zhenyu Wang, and Jianliang Zhang. Distributed event-triggered secondary control for islanded microgrids with proper trigger condition checking period. *IEEE Transactions on Smart Grid*, 13(2):837–848, 2021.

[23] Amedeo Andreotti, Bianca Caiazzo, Alberto Petrillo, Stefania Santini, and Alfredo Vaccaro. Robust finite-time voltage restoration in inverter-based microgrids via distributed cooperative control in presence of communication time-varying delays. In *2020 IEEE International Conference on Environment and Electrical Engineering and 2020 IEEE Industrial and Commercial Power Systems Europe (EEEIC/I&CPS Europe)*, pages 1–6. IEEE, 2020.

[24] Jingang Lai, Xiaoqing Lu, Xinghuo Yu, and Antonello Monti. Stochastic distributed secondary control for ac microgrids via event-triggered communication. *IEEE Transactions on Smart Grid*, 11(4):2746–2759, 2020.

[25] Giovanni Fiengo, Dario Giuseppe Lui, Alberto Petrillo, and Stefania Santini. Distributed robust output consensus for linear multi-agent systems with input time-varying delays and parameter uncertainties. *IET Control Theory & Applications*, 13(2):203–212, 2018.

[26] Guannan Lou, Wei Gu, Jianhui Wang, Wanxing Sheng, and Lijing Sun. Optimal design for distributed secondary voltage control in islanded microgrids: Communication topology and controller. *IEEE Transactions on Power Systems*, 34(2):968–981, 2018.

[27] Xiaoqing Lu, Xinghuo Yu, Jingang Lai, Josep M Guerrero, and Hong Zhou. Distributed secondary voltage and frequency control for islanded microgrids with uncertain communication links. *IEEE Transactions on Industrial Informatics*, 13(2):448–460, 2016.

[28] Jingang Lai, Hong Zhou, Xiaoqing Lu, Xinghuo Yu, and Wenshan Hu. Droop-based distributed cooperative control for microgrids with time-varying delays. *IEEE Transactions on Smart Grid*, 7(4):1775–1789, 2016.

[29] Yinliang Xu and Hongbin Sun. Distributed finite-time convergence control of an islanded low-voltage ac microgrid. *IEEE Transactions on Power Systems*, 33(3):2339–2348, 2017.

[30] Alessandro Pilloni, Alessandro Pisano, and Elio Usai. Robust finite-time frequency and voltage restoration of inverter-based microgrids via sliding-mode cooperative control. *IEEE Transactions on Industrial Electronics*, 65(1):907–917, 2017.

[31] Boda Ning, Qing-Long Han, and Lei Ding. Distributed finite-time secondary frequency and voltage control for islanded microgrids with communication delays and switching topologies. *IEEE Transactions on Cybernetics*, 51(8):3988–3999, 2020.

[32] Ricardo Pérez-Ibacache, Rafael S Castro, Guilherme Araujo Pimentel, and Bruno Salgado Bizzo. Dynamic output-feedback decentralized control synthesis for integration of distributed energy resources in ac microgrids. *IEEE Transactions on Smart Grid*, 13(2):1225–1237, 2021.

[33] Zixiao Ma, Zhaoyu Wang, Yifei Guo, Yuxuan Yuan, and Hao Chen. Nonlinear multiple models adaptive secondary voltage control of microgrids. *IEEE Transactions on Smart Grid*, 12(1):227–238, 2020.

[34] Chun Sha, Ji Luo, and Masoud Taleb Ziabari. A new robust decentralized approach based on adaptive fuzzy backstepping method for microgrid secondary voltage control. *Sustainable Energy, Grids and Networks*, 27:100487, 2021.

[35] Mohamad Abedini, Esmail Mahmodi, MirRahim Mousavi, and Iman Chaharmahali. A novel fuzzy pi controller for improving autonomous network by considering uncertainty. *Sustainable Energy, Grids and Networks*, 18:100200, 2019.

[36] Xian-Ming Zhang, Qing-Long Han, Xiaohua Ge, Derui Ding, Lei Ding, Dong Yue, and Chen Peng. Networked control systems: A survey of trends and techniques. *IEEE/CAA Journal of Automatica Sinica*, 7(1):1–17, 2019.

[37] Jiang Long, Wei Wang, Jiangshuai Huang, Jing Zhou, and Kexin Liu. Distributed adaptive control for asymptotically consensus tracking of uncertain nonlinear systems with intermittent actuator faults and directed communication topology. *IEEE Transactions on Cybernetics*, 51(8):4050–4061, 2019.

[38] Hongzhen Xie, Guangdeng Zong, Wei Bu, Dong Yang, and Kaibo Shi. Input-to-state practical stability of switched affine systems with time-varying delay: an event-triggered mechanism. *International Journal of Systems Science*, pages 1–12, 2022.

[39] Ned Mohan, Tore M Undeland, and William P Robbins. *Power electronics: converters, applications, and design*. John Wiley & sons, 2003.

[40] Emilia Fridman and Jin Zhang. Averaging of linear systems with almost periodic coefficients: A time-delay approach. *Automatica*, 122:109287, 2020.

[41] Bianca Caiazzo, Dario Giuseppe Lui, Alberto Petrillo, and Stefania Santini. On the exponential leader-tracking control for high-order multi-agent systems via distributed pi strategy in the presence of heterogeneous time-varying delays. *IFAC-PapersOnLine*, 54(18):139–144, 2021.

[42] Amedeo Andreotti, Bianca Caiazzo, Alberto Petrillo, and Stefania Santini. Distributed robust finite-time secondary control for stand-alone microgrids with time-varying communication delays. *IEEE Access*, 9:59548–59563, 2021.

[43] Bianca Caiazzo, Dario Giuseppe Lui, Alberto Petrillo, and Stefania Santini. Cooperative adaptive pid-like voltage regulation in inverter-based islanded microgrids under unknown uncertainties. *submitted*, 2022.

[44] Bianca Caiazzo, Emilia Fridman, Alberto Petrillo, and Stefania Santini. Synchronization of multi-agent systems under time-varying network via time-delay approach to averaging. *IFAC-PapersOnLine*, 55(36):133–138, 2022.

[45] Amedeo Andreotti, Bianca Caiazzo, Emilia Fridman, Alberto Petrillo, and Stefania Santini. Distributed dynamic event-triggered control for voltage recovery in islanded microgrids by using artificial delays. *submitted*, 2022.

[46] Jin Zhang and Emilia Fridman. L2-gain analysis via time-delay approach to periodic averaging with stochastic extension. *Automatica*, 137:110126, 2022.

[47] Bianca Caiazzo, Emilia Fridman, and Xuefei Yang. Averaging of systems with fast-varying coefficients and non-small delays with application to stabilization of affine systems via time-dependent switching. *Nonlinear Analysis: Hybrid Systems*, 48:101307, 2023.

[48] Ruofei Ma, Hsiao-Hwa Chen, Yu-Ren Huang, and Weixiao Meng. Smart grid communication: Its challenges and opportunities. *IEEE transactions on Smart Grid*, 4(1):36–46, 2013.

[49] Muhammad Baqer Mollah, Jun Zhao, Dusit Niyato, Kwok-Yan Lam, Xin Zhang, Amer MYM Ghias, Leong Hai Koh, and Lei Yang. Blockchain for future smart grid: A comprehensive survey. *IEEE Internet of Things Journal*, 8(1):18–43, 2020.

[50] Horizon Europe. Horizon europe, the next eu research & innovation investment programme., 2019. 2021-2027. https://ec.europa.eu/info/sites/info/files/research_and_innovation/strategy_on_research_and_innovation/presentations/horizon_europe_en_investing_to_shape_our_future.pdf.

[51] Ying Wu, Yanpeng Wu, Halil Cimen, Juan C Vasquez, and Josep M Guerrero. Towards collective energy community: Potential roles of microgrid and blockchain to go beyond p2p energy trading. *Applied Energy*, 314:119003, 2022.

[52] Chao Deng, Yu Wang, Changyun Wen, Yan Xu, and Pengfeng Lin. Distributed resilient control for energy storage systems in cyber–physical microgrids. *IEEE Transactions on Industrial Informatics*, 17(2):1331–1341, 2020.

[53] Sandeep Kakran and Saurabh Chanana. Smart operations of smart grids integrated with distributed generation: A review. *Renewable and Sustainable Energy Reviews*, 81:524–535, 2018.

[54] Magdi Sadek Mahmoud, S Azher Hussain, and Mohammad A Abido. Modeling and control of microgrid: An overview. *Journal of the Franklin Institute*, 351(5):2822–2859, 2014.

[55] Ye Yan, Yi Qian, Hamid Sharif, and David Tipper. A survey on smart grid communication infrastructures: Motivations, requirements and challenges. *IEEE communications surveys & tutorials*, 15(1):5–20, 2012.

[56] Danielly B Avancini, Joel JPC Rodrigues, Simion GB Martins, Ricardo AL Rabêlo, Jalal Al-Muhtadi, and Petar Solic. Energy meters evolution in smart grids: A review. *Journal of cleaner production*, 217:702–715, 2019.

[57] European Commission. A european green deal, 2019. https://commission.europa.eu/strategy-and-policy/priorities-2019-2024/european-green-deal_en.

[58] Maurizio Delfanti, Enrico Fasciolo, Valeria Olivieri, and Mauro Pozzi. A2a project: A practical implementation of smart grids in the urban area of milan. *Electric Power Systems Research*, 120:2–19, 2015.

[59] Tim Schittekatte, Leonardo Meeus, Tooraj Jamasb, and Manuel Llorca. Regulatory experimentation in energy: Three pioneer countries and lessons for the green transition. *Energy Policy*, 156:112382, 2021.

[60] Osama Majeed Butt, Muhammad Zulqarnain, and Tallal Majeed Butt. Recent advancement in smart grid technology: Future prospects in the

electrical power network. *Ain Shams Engineering Journal*, 12(1):687–695, 2021.

[61] João Crispim, José Braz, Rui Castro, and Jorge Esteves. Smart grids in the eu with smart regulation: Experiences from the uk, italy and portugal. *Utilities Policy*, 31:85–93, 2014.

[62] Autorità per l'Energia Elettrica e GAS (AEEG). A2a reti elettriche, 2014. https://ses.jrc.ec.europa.eu/a2a-reti-elettriche-0.

[63] Maurizio Delfanti, Davide Falabretti, Massimo Fiori, and Marco Merlo. Smart grid on field application in the italian framework: The as se. m. project. *Electric Power Systems Research*, 120:56–69, 2015.

[64] Stefano Bracco, Federico Delfino, Fabio Pampararo, Michela Robba, and Mansueto Rossi. A mathematical model for the optimal operation of the university of genoa smart polygeneration microgrid: Evaluation of technical, economic and environmental performance indicators. *Energy*, 64:912–922, 2014.

[65] Giovanni Messina. The role of the committee of the regions (cor) to implement the green deal at the local level: an overview of italy. *AIMS Geosciences*, 7(4):613–622, 2021.

[66] Ali Bidram and Ali Davoudi. Hierarchical structure of microgrids control system. *IEEE Transactions on Smart Grid*, 3(4):1963–1976, 2012.

[67] Ioan Serban, Sandra Cespedes, Corneliu Marinescu, Cesar A Azurdia-Meza, Juan S Gomez, and Doris Sáez Hueichapan. Communication requirements in microgrids: A practical survey. *IEEE Access*, 8:47694–47712, 2020.

[68] Omid Palizban, Kimmo Kauhaniemi, and Josep M Guerrero. Microgrids in active network management—part i: Hierarchical control, energy storage, virtual power plants, and market participation. *Renewable and Sustainable Energy Reviews*, 36:428–439, 2014.

[69] Sonam Shrivastava and Bidyadhar Subudhi. Comprehensive review on hierarchical control of cyber-physical microgrid system. *IET Generation, Transmission & Distribution*, 14(26):6397–6416, 2020.

[70] John Brewer. Kronecker products and matrix calculus in system theory. *IEEE Transactions on circuits and systems*, 25(9):772–781, 1978.

[71] Frank L Lewis, Hongwei Zhang, Kristian Hengster-Movric, and Abhijit Das. *Cooperative control of multi-agent systems: optimal and adaptive design approaches*. Springer Science & Business Media, 2013.

[72] Miguel Angel Trujillo, Rodrigo Aldana-López, David Gómez-Gutiérrez, Michael Defoort, Javier Ruiz-León, and HM Becerra. Autonomous and non-autonomous fixed-time leader–follower consensus for second-order multi-agent systems. *Nonlinear Dynamics*, 102(4):2669–2686, 2020.

[73] Johannes Schiffer, Daniele Zonetti, Romeo Ortega, Aleksandar M Stanković, Tevfik Sezi, and Jörg Raisch. A survey on modeling of microgrids—from fundamental physics to phasors and voltage sources. *Automatica*, 74:135–150, 2016.

[74] Yelun Peng, Zhikang Shuai, Xuan Liu, Zuyi Li, Josep M Guerrero, and Z John Shen. Modeling and stability analysis of inverter-based microgrid under harmonic conditions. *IEEE Transactions on Smart Grid*, 11(2):1330–1342, 2019.

[75] Ying Wu, Yanpeng Wu, Josep M Guerrero, Juan C Vasquez, and Jiao Li. Ac microgrid small-signal modeling: Hierarchical control structure challenges and solutions. *IEEE Electrification Magazine*, 7(4):81–88, 2019.

[76] Khizir Mahmud, Animesh K Sahoo, Jayashri Ravishankar, and Zhao Yang Dong. Coordinated multilayer control for energy management of grid-connected ac microgrids. *IEEE Transactions on Industry Applications*, 55(6):7071–7081, 2019.

[77] Sonam Shrivastava, Bidyadhar Subudhi, and Susmita Das. Distributed voltage and frequency synchronisation control scheme for islanded inverter-based microgrid. *IET Smart Grid*, 1(2):48–56, 2018.

[78] Karel De Brabandere, Bruno Bolsens, Jeroen Van den Keybus, Achim Woyte, Johan Driesen, and Ronnie Belmans. A voltage and frequency droop control method for parallel inverters. *IEEE Transactions on power electronics*, 22(4):1107–1115, 2007.

[79] Johannes Schiffer, Romeo Ortega, Alessandro Astolfi, Jörg Raisch, and Tevfik Sezi. Conditions for stability of droop-controlled inverter-based microgrids. *Automatica*, 50(10):2457–2469, 2014.

[80] Josep M Guerrero, Mukul Chandorkar, Tzung-Lin Lee, and Poh Chiang Loh. Advanced control architectures for intelligent microgrids—part i: Decentralized and hierarchical control. *IEEE Transactions on Industrial Electronics*, 60(4):1254–1262, 2012.

[81] Johannes Schiffer, Thomas Seel, Jörg Raisch, and Tevfik Sezi. Voltage stability and reactive power sharing in inverter-based microgrids with consensus-based distributed voltage control. *IEEE Transactions on Control Systems Technology*, 24(1):96–109, 2015.

[82] John J Grainger, William D Stevenson, William D Stevenson, et al. *Power system analysis*. 2003.

[83] Md Shakawat Hossan, HM Mesbah Maruf, and Badrul Chowdhury. Comparison of the zip load model and the exponential load model for cvr factor evaluation. In *2017 IEEE Power & Energy Society General Meeting*, pages 1–5. IEEE, 2017.

[84] Nima Mahdian Dehkordi, Nasser Sadati, and Mohsen Hamzeh. Distributed robust finite-time secondary voltage and frequency control of islanded microgrids. *IEEE Transactions on Power Systems*, 32(5):3648–3659, 2016.

[85] Dong Wang and Wei Wang. Necessary and sufficient conditions for containment control of multi-agent systems with time delay. *Automatica*, 103:418–423, 2019.

[86] Dan Ma, Jianqi Chen, Renquan Lu, Jie Chen, and Tianyou Chai. Delay effect on first-order consensus over directed graphs: Optimizing pid protocols for maximal robustness. *SIAM Journal on Control and Optimization*, 60(1):233–258, 2022.

[87] Xianwei Li, Yang Tang, and Hamid Reza Karimi. Consensus of multi-agent systems via fully distributed event-triggered control. *Automatica*, 116:108898, 2020.

[88] Zongyu Zuo, Qing-Long Han, Boda Ning, Xiaohua Ge, and Xian-Ming Zhang. An overview of recent advances in fixed-time cooperative control of multiagent systems. *IEEE Transactions on Industrial Informatics*, 14(6):2322–2334, 2018.

[89] Quan Zhou, Mohammad Shahidehpour, Aleksi Paaso, Shay Bahramirad, Ahmed Alabdulwahab, and Abdullah Abusorrah. Distributed control and communication strategies in networked microgrids. *IEEE Communications Surveys & Tutorials*, 22(4):2586–2633, 2020.

[90] Wenhao Jia and Jinzhi Wang. Distributed disturbance observer based consensus control for linear multi-agent systems with mismatched disturbances. *Journal of the Franklin Institute*, 359(1):578–598, 2022.

[91] Giovanni Fiengo, Dario Giuseppe Lui, Alberto Petrillo, Stefania Santini, and Manuela Tufo. Distributed leader-tracking for autonomous connected vehicles in presence of input time-varying delay. In *2018 26th Mediterranean Conference on Control and Automation (MED)*, pages 1–6. IEEE, 2018.

[92] Chong-Xiao Shi and Guang-Hong Yang. Robust consensus control for a class of multi-agent systems via distributed pid algorithm and weighted edge dynamics. *Applied Mathematics and Computation*, 316:73–88, 2018.

[93] Dario Giuseppe Lui, Alberto Petrillo, and Stefania Santini. An optimal distributed pid-like control for the output containment and leader-following of heterogeneous high-order multi-agent systems. *Information Sciences*, 541:166–184, 2020.

[94] Emma Tegling and Henrik Sandberg. On the coherence of large-scale networks with distributed pi and pd control. *IEEE control systems letters*, 1(1):170–175, 2017.

[95] Gianmaria De Tommasi, Dario Giuseppe Lui, Alberto Petrillo, and Stefania Santini. Al 2-gain robust pid-like protocol for time-varying output formation-containment of multi-agent systems with external disturbance and communication delays. *IET Control Theory & Applications*, 2021.

[96] Haibo Gu, Peng Liu, Jinhu Lü, and Zongli Lin. Pid control for synchronization of complex dynamical networks with directed topologies. *IEEE transactions on cybernetics*, 2019.

[97] Emilia Fridman. *Introduction to time-delay systems: Analysis and control.* Springer, 2014.

[98] Giovanni Fiengo, Dario Giuseppe Lui, Alberto Petrillo, and Stefania Santini. Distributed leader-tracking adaptive control for high-order nonlinear lipschitz multi-agent systems with multiple time-varying communication delays. *International Journal of Control*, pages 1–13, 2019.

[99] Di Zhao, Zidong Wang, Daniel WC Ho, and Guoliang Wei. Observer-based pid security control for discrete time-delay systems under cyber-attacks. *IEEE Transactions on Systems, Man, and Cybernetics: Systems*, 2019.

[100] Yang Han, Ke Zhang, Hong Li, Ernane Antônio Alves Coelho, and Josep M Guerrero. Mas-based distributed coordinated control and optimization in microgrid and microgrid clusters: A comprehensive overview. *IEEE Transactions on Power Electronics*, 33(8):6488–6508, 2017.

[101] Yu Wang, Tung Lam Nguyen, Yan Xu, Zhengmao Li, Quoc-Tuan Tran, and Raphael Caire. Cyber-physical design and implementation of distributed event-triggered secondary control in islanded microgrids. *IEEE Transactions on Industry Applications*, 55(6):5631–5642, 2019.

[102] Zhongwen Li, Zhiping Cheng, Jing Liang, Jikai Si, Lianghui Dong, and Shuhui Li. Distributed event-triggered secondary control for economic dispatch and frequency restoration control of droop-controlled ac microgrids. *IEEE Transactions on Sustainable Energy*, 11(3):1938–1950, 2019.

[103] Nima Mahdian Dehkordi, Hamid Reza Baghaee, Nasser Sadati, and Josep M Guerrero. Distributed noise-resilient secondary voltage and frequency control for islanded microgrids. *IEEE Transactions on Smart Grid*, 10(4):3780–3790, 2018.

[104] Zhiping Cheng, Zhongwen Li, Jing Liang, Jinfeng Gao, Jikai Si, and Shuhui Li. Distributed economic power dispatch and bus voltage control for droop-controlled dc microgrids. *Energies*, 12(7):1400, 2019.

[105] Xiangyu Wu, Laijun Chen, Chen Shen, Yin Xu, Jinghan He, and Chen Fang. Distributed optimal operation of hierarchically controlled microgrids. *IET Generation, Transmission & Distribution*, 12(18):4142–4152, 2018.

[106] Jingang Lai and Xiaoqing Lu. Nonlinear mean-square power sharing control for ac microgrids under distributed event detection. *IEEE Transactions on Industrial Informatics*, 17(1):219–229, 2020.

[107] Jingang Lai, Xiaoqing Lu, Xinghuo Yu, Antonello Monti, and Hong Zhou. Distributed voltage regulation for cyber-physical microgrids with coupling delays and slow switching topologies. *IEEE Transactions on Systems, Man, and Cybernetics: Systems*, 50(1):100–110, 2019.

[108] Alberto Petrillo, Antonio Pescape, and Stefania Santini. A secure adaptive control for cooperative driving of autonomous connected vehicles in the presence of heterogeneous communication delays and cyberattacks. *IEEE transactions on cybernetics*, 2020.

[109] Xingwen Liu and James Lam. Relationships between asymptotic stability and exponential stability of positive delay systems. *International Journal of General Systems*, 42(2):224–238, 2013.

[110] Weisheng Chen, Changyun Wen, and Jian Wu. Global exponential/finite-time stability of nonlinear adaptive switching systems with applications in controlling systems with unknown control direction. *IEEE Transactions on Automatic Control*, 63(8):2738–2744, 2018.

[111] Jingang Lai, Xiaoqing Lu, and Antonello Monti. Distributed secondary voltage control for autonomous microgrids under additive measurement noises and time delays. *IET Generation, Transmission & Distribution*, 13(14):2976–2985, 2019.

[112] Emilia Fridman. Tutorial on lyapunov-based methods for time-delay systems. *European Journal of Control*, 20(6):271–283, 2014.

[113] Corentin Briat. Linear parameter-varying and time-delay systems. *Analysis, observation, filtering & control*, 3:5–7, 2014.

[114] Chien-Hua Lee. Upper and lower matrix bounds of the solution for the discrete lyapunov equation. *IEEE transactions on automatic control*, 41(9):1338–1341, 1996.

[115] Jigui Jian and Wenlin Jiang. Lagrange exponential stability for fuzzy cohen–grossberg neural networks with time-varying delays. *Fuzzy Sets and Systems*, 277:65–80, 2015.

[116] Roger A Horn and Charles R Johnson. *Matrix analysis*. Cambridge university press, 2012.

[117] Waleed Alasmary and Weihua Zhuang. Mobility impact in ieee 802.11 p infrastructureless vehicular networks. *Ad Hoc Networks*, 10(2):222–230, 2012.

[118] Johan Lofberg. Yalmip: A toolbox for modeling and optimization in matlab. In *2004 IEEE international conference on robotics and automation (IEEE Cat. No. 04CH37508)*, pages 284–289. IEEE, 2004.

[119] Alberto Petrillo, Alessandro Salvi, Stefania Santini, and Antonio Saverio Valente. Adaptive synchronization of linear multi-agent systems with time-varying multiple delays. *Journal of the Franklin Institute*, 354(18):8586–8605, 2017.

[120] Stephen Boyd, Laurent El Ghaoui, Eric Feron, and Venkataramanan Balakrishnan. *Linear matrix inequalities in system and control theory*, volume 15. Siam, 1994.

[121] Ping Tong, Shihua Chen, and Lei Wang. Finite-time consensus of multi-agent systems with continuous time-varying interaction topology. *Neurocomputing*, 284:187–193, 2018.

[122] Zhengrong Xiang, Ya-Nan Sun, and Magdi S Mahmoud. Robust finite-time h_∞ control for a class of uncertain switched neutral systems. *Communications in Nonlinear Science and Numerical Simulation*, 17(4):1766–1778, 2012.

[123] Ray D Zimmerman and Carlos E Murillo-Sánchez. Matpower 6.0 user's manual. *Power Systems Engineering Research Center*, 9, 2016.

[124] Amedeo Andreotti, Bianca Caiazzo, Alberto Petrillo, Stefania Santini, and Alfredo Vaccaro. Decentralized smart grid voltage control by synchronization of linear multiagent systems in the presence of time-varying latencies. *Electronics*, 8(12):1470, 2019.

[125] Vahidreza Nasirian, Qobad Shafiee, Josep M Guerrero, Frank L Lewis, and Ali Davoudi. Droop-free distributed control for ac microgrids. *IEEE Transactions on Power Electronics*, 31(2):1600–1617, 2015.

[126] Quan Zhou, Mohammad Shahidehpour, Mingyu Yan, Xi Wu, Ahmed Alabdulwahab, and Abdullah Abusorrah. Distributed secondary control for islanded microgrids with mobile emergency resources. *IEEE Transactions on Power Systems*, 35(2):1389–1399, 2019.

[127] Fazel Mohammadi, Behnam Mohammadi-Ivatloo, Gevork B Gharehpetian, Mohd Hasan Ali, Wei Wei, Ozan Erdinç, and Mohammadamin Shirkhani. Robust control strategies for microgrids: A review. *IEEE Systems Journal*, 2021.

[128] Fazel Mohammadi and Mircea Neagoe. Emerging issues and challenges with the integration of solar power plants into power systems. *Solar Energy Conversion in Communities*, pages 157–173, 2020.

[129] Hongxun Hui, Yulin Chen, Shaohua Yang, Hongcai Zhang, and Tao Jiang. Coordination control of distributed generators and load resources for frequency restoration in isolated urban microgrids. *Applied Energy*, 327:120116, 2022.

[130] Pudong Ge, Yue Zhu, Tim C Green, and Fei Teng. Resilient secondary voltage control of islanded microgrids: An eskbf-based distributed fast terminal sliding mode control approach. *IEEE Transactions on Power Systems*, 36(2):1059–1070, 2020.

[131] Xueqiang Shen, Haiqing Wang, Jian Li, Qingyu Su, and Lan Gao. Distributed secondary voltage control of islanded microgrids based on rbf-neural-network sliding-mode technique. *IEEE Access*, 7:65616–65623, 2019.

[132] Mingmin Zhang, Yong Li, Fang Liu, Wei-Jen Lee, Yanjian Peng, Yuxin Liu, Wenguo Li, and Yijia Cao. A robust distributed secondary voltage control method for islanded microgrids. *International Journal of Electrical Power & Energy Systems*, 121:105938, 2020.

[133] Xueqiang Shen, Haiqing Wang, Dezhen Zhang, Jian Li, Renshu Wang, and Qingyu Su. Distributed finite-time secondary voltage restoration of droop-controlled islanded microgrids. *IEEE Access*, 8:118183–118191, 2020.

[134] Guangliang Liu, Qiuye Sun, Rui Wang, and Xuguang Hu. Nonzero-sum game-based voltage recovery consensus optimal control for nonlinear microgrids system. *IEEE Transactions on Neural Networks and Learning Systems*, 2022.

[135] Dario Giuseppe Lui, Alberto Petrillo, and Stefania Santini. Leader tracking control for heterogeneous uncertain nonlinear multi-agent systems via a distributed robust adaptive pid strategy. *Nonlinear Dynamics*, 108(1):363–378, 2022.

[136] Dario Giuseppe Lui, Alberto Petrillo, and Stefania Santini. h_∞-pid distributed control for output leader-tracking and containment of heterogeneous mass with external disturbances. *Journal of Control and Decision*, pages 1–14, 2021.

[137] Subrata K Sarkar, Md Hassanul K Roni, D Datta, Sajal K Das, and Hemanshu R Pota. Improved design of high-performance controller for voltage control of islanded microgrid. *IEEE Systems Journal*, 13(2):1786–1795, 2018.

[138] Subroto K Sarkar, Faisal R Badal, and Sajal K Das. A comparative study of high performance robust pid controller for grid voltage control of islanded microgrid. *International Journal of Dynamics and Control*, 6(3):1207–1217, 2018.

[139] Alireza Esmaeili Karkevandi, Matin Jamaliyan Daryani, and Omer Usta. Anfis-based intelligent pi controller for secondary frequency and voltage control of microgrid. In *2018 IEEE PES Innovative Smart Grid Technologies Conference Europe (ISGT-Europe)*, pages 1–6. IEEE, 2018.

[140] Mario Russo and Giuseppe Fusco. Robust decentralized pi controllers design for voltage regulation in distribution networks with dg. *Electric Power Systems Research*, 172:129–139, 2019.

[141] Abu Bakar Siddique, Md Shahin Munsi, Subrata K Sarker, Sajal K Das, and Md Rabiul Islam. Voltage and current control augmentation of islanded microgrid using multifunction model reference modified adaptive pid controller. *International Journal of Electrical Power & Energy Systems*, 113:492–501, 2019.

[142] Guangliang Liu, Michael V Basin, Hongjing Liang, and Qi Zhou. Adaptive bipartite tracking control of nonlinear multiagent systems with input quantization. *IEEE Transactions on Cybernetics*, 2020.

[143] Sachidananda Sen and Vishal Kumar. Microgrid control: A comprehensive survey. *Annual Reviews in control*, 45:118–151, 2018.

[144] Hassan K Khalil. Nonlinear systems third edition. *Patience Hall*, 115, 2002.

[145] Yuan-Xin Li and Guang-Hong Yang. Robust adaptive fault-tolerant control for a class of uncertain nonlinear time delay systems. *IEEE Transactions on Systems, Man, and Cybernetics: Systems*, 47(7):1554–1563, 2016.

[146] Zhongkui Li, Guanghui Wen, Zhisheng Duan, and Wei Ren. Designing fully distributed consensus protocols for linear multi-agent systems with directed graphs. *IEEE Transactions on Automatic Control*, 60(4):1152–1157, 2014.

[147] Wei Wang, Changyun Wen, and Jiangshuai Huang. Distributed adaptive asymptotically consensus tracking control of nonlinear multi-agent systems with unknown parameters and uncertain disturbances. *Automatica*, 77:133–142, 2017.

[148] Dongdong Yue, Jinde Cao, Qi Li, and Qingshan Liu. Neural-network-based fully distributed adaptive consensus for a class of uncertain multiagent systems. *IEEE Transactions on Neural Networks and Learning Systems*, 32(7):2965–2977, 2020.

[149] Ghazal Razeghi, Fei Gu, Russell Neal, and Scott Samuelsen. A generic microgrid controller: Concept, testing, and insights. *Applied Energy*, 229:660–671, 2018.

[150] Weihua Li, Huaguang Zhang, Shaoxin Sun, and Juan Zhang. Fully distributed event-triggered consensus protocols for multi-agent systems with physically interconnected network. *Neurocomputing*, 418:191–199, 2020.

[151] Lian-Na Zhao, Hong-Jun Ma, Lin-Xing Xu, and Xin Wang. Observer-based adaptive sampled-data event-triggered distributed control for multi-agent systems. *IEEE Transactions on Circuits and Systems II: Express Briefs*, 67(1):97–101, 2019.

[152] Ge Guo, Lei Ding, and Qing-Long Han. A distributed event-triggered transmission strategy for sampled-data consensus of multi-agent systems. *Automatica*, 50(5):1489–1496, 2014.

[153] Shan Zuo, Tuncay Altun, Frank L Lewis, and Ali Davoudi. Distributed resilient secondary control of dc microgrids against unbounded attacks. *IEEE Transactions on Smart Grid*, 11(5):3850–3859, 2020.

[154] Yijing Xie and Zongli Lin. Distributed event-triggered secondary voltage control for microgrids with time delay. *IEEE Transactions on Systems, Man, and Cybernetics: Systems*, 49(8):1582–1591, 2019.

[155] Xiangyu Wu, Yin Xu, Jinghan He, Chen Shen, Gang Chen, Juan C Vasquez, and Josep M Guerrero. Delay-dependent small-signal stability analysis and compensation method for distributed secondary control of microgrids. *IEEE Access*, 7:170919–170935, 2019.

[156] Bo Yang, Jingbo Wang, Yiyan Sang, Lei Yu, Hongchun Shu, Shengnan Li, Tingyi He, Lei Yang, Xiaoshun Zhang, and Tao Yu. Applications of supercapacitor energy storage systems in microgrid with distributed generators via passive fractional-order sliding-mode control. *Energy*, 187:115905, 2019.

[157] Anton Selivanov and Emilia Fridman. An improved time-delay implementation of derivative-dependent feedback. *Automatica*, 98:269–276, 2018.

[158] Anton Selivanov and Emilia Fridman. Robust sampled-data implementation of pid controller. In *2018 IEEE Conference on Decision and Control (CDC)*, pages 932–936. IEEE, 2018.

[159] Jin Zhang and Emilia Fridman. Digital implementation of derivative-dependent control by using delays for stochastic multi-agents. *IEEE Transactions on Automatic Control*, 2021.

[160] Iasson Karafyllis. Robust global stabilization by means of discrete-delay output feedback. *Systems & Control Letters*, 57(12):987–995, 2008.

[161] Adrián Ramírez, Sabine Mondié, Rubén Garrido, and Rifat Sipahi. Design of proportional-integral-retarded (pir) controllers for second-order lti systems. *IEEE Transactions on Automatic Control*, 61(6):1688–1693, 2015.

[162] Guanghui Wen, Zhisheng Duan, Wei Ren, and Guanrong Chen. Distributed consensus of multi-agent systems with general linear node dynamics and intermittent communications. *International Journal of Robust and Nonlinear Control*, 24(16):2438–2457, 2014.

[163] Haofei Meng, Zhiyong Chen, and Richard Middleton. Consensus of multi-agents in switching networks using input-to-state stability of switched systems. *IEEE Transactions on Automatic Control*, 63(11):3964–3971, 2018.

[164] D Gray Roberson and Daniel J Stilwell. $\mathscr{L}_2$ gain of periodic linear switched systems: Fast switching behavior. *IEEE transactions on automatic control*, 54(7):1632–1637, 2009.

[165] Hongkeun Kim, Hyungbo Shim, Juhoon Back, and Jin Heon Seo. Consensus of output-coupled linear multi-agent systems under fast switching network: Averaging approach. *Automatica*, 49(1):267–272, 2013.

[166] Wei Wang and Dragan Nesic. Input-to-state stability and averaging of linear fast switching systems. *IEEE Transactions on Automatic Control*, 55(5):1274–1279, 2010.

[167] Kairui Chen, Junwei Wang, Yun Zhang, and Zhi Liu. Leader-following consensus for a class of nonlinear strick-feedback multiagent systems with state time-delays. *IEEE Transactions on Systems, Man, and Cybernetics: Systems*, 50(7):2351–2361, 2018.

[168] Fang Qiu and Jinde Cao. Exponential stability and l2-gain analysis for sampled-data control of linear systems. *Journal of the Franklin Institute*, 353(2):462–477, 2016.

[169] David G Feingold, Richard S Varga, et al. Block diagonally dominant matrices and generalizations of the gerschgorin circle theorem. *Pacific Journal of Mathematics*, 12(4):1241–1250, 1962.

[170] Gene F Franklin, J David Powell, Abbas Emami-Naeini, and J David Powell. *Feedback control of dynamic systems*, volume 4. Prentice hall Upper Saddle River, NJ, 2002.

[171] Tao Liu, Jun Zhao, and David J Hill. Exponential synchronization of complex delayed dynamical networks with switching topology. *IEEE Transactions on Circuits and Systems I: Regular Papers*, 57(11):2967–2980, 2010.

[172] Lei Ding and Wei Xing Zheng. Network-based practical consensus of heterogeneous nonlinear multiagent systems. *IEEE Transactions on Cybernetics*, 47(8):1841–1851, 2016.

[173] Jack K Hale and Sjoerd M Verduyn Lunel. *Introduction to functional differential equations*, volume 99. Springer Science & Business Media, 2013.

[174] PooGyeon Park, Jeong Wan Ko, and Changki Jeong. Reciprocally convex approach to stability of systems with time-varying delays. *Automatica*, 47(1):235–238, 2011.

[175] Erling D Andersen and Knud D Andersen. The mosek interior point optimizer for linear programming: an implementation of the homogeneous algorithm. In *High performance optimization*, pages 197–232. Springer, 2000.

[176] Antoine Chaillet, Iasson Karafyllis, Pierdomenico Pepe, and Yuan Wang. The iss framework for time-delay systems: a survey. *Mathematics of Control, Signals, and Systems*, pages 1–70, 2023.

[177] Guopin Liu, Changchun Hua, Peter Xiaoping Liu, and Ju H Park. Input-to-state stability for time-delay systems with large delays. *IEEE Transactions on Cybernetics*, 2021.

[178] Enrique Espina, Jacqueline Llanos, Claudio Burgos-Mellado, Roberto Cardenas-Dobson, Manuel Martinez-Gomez, and Doris Sáez. Distributed control strategies for microgrids: An overview. *IEEE Access*, 8:193412–193448, 2020.

[179] Guanglei Zhao, Lanqing Jin, and Yifeng Wang. Distributed event-triggered secondary control for islanded microgrids with disturbances: A hybrid systems approach. *IEEE Transactions on Power Systems*, 2022.

[180] Tong Qian, Yang Liu, Wenhao Zhang, Wenhu Tang, and Mohammad Shahidehpour. Event-triggered updating method in centralized and distributed secondary controls for islanded microgrid restoration. *IEEE Transactions on Smart Grid*, 11(2):1387–1395, 2019.

[181] Pudong Ge, Boli Chen, and Fei Teng. Event-triggered distributed model predictive control for resilient voltage control of an islanded microgrid. *International Journal of Robust and Nonlinear Control*, 31(6):1979–2000, 2021.

[182] Bo Zhang, Chunxia Dou, Dong Yue, Zhanqiang Zhang, and Tengfei Zhang. A packet loss-dependent event-triggered cyber-physical cooperative control strategy for islanded microgrid. *IEEE Transactions on Cybernetics*, 51(1):267–282, 2019.

[183] Antoine Girard. Dynamic triggering mechanisms for event-triggered control. *IEEE Transactions on Automatic Control*, 60(7):1992–1997, 2014.

[184] Yezheng Wang, Zidong Wang, Lei Zou, and Hongli Dong. Multiloop decentralized h_∞ fuzzy pid-like control for discrete time-delayed fuzzy systems under dynamical event-triggered schemes. *IEEE Transactions on Cybernetics*, 2020.

[185] Fei Han, Xilin Lao, Jiahui Li, Mei Wang, and Hongli Dong. Dynamic event-triggered protocol-based distributed secondary control for islanded microgrids. *International Journal of Electrical Power & Energy Systems*, 137:107723, 2022.

[186] Anton Selivanov and Emilia Fridman. Sampled-data implementation of derivative-dependent control using artificial delays. *IEEE Transactions on Automatic Control*, 63(10):3594–3600, 2018.

[187] Emilia Fridman and Leonid Shaikhet. Stabilization by using artificial delays: An lmi approach. *Automatica*, 81:429–437, 2017.

[188] Chi Huang, Guisheng Zhai, and Gesheng Xu. Necessary and sufficient conditions for consensus in third order multi-agent systems. *IEEE/CAA Journal of Automatica Sinica*, 5(6):1044–1053, 2018.

[189] Francesco Bullo. Averaging and vibrational control of mechanical systems. *SIAM Journal on Control and Optimization*, 41(2):542–562, 2002.

[190] Miroslav Krstić and Hsin-Hsiung Wang. Stability of extremum seeking feedback for general nonlinear dynamic systems. *Automatica*, 36(4):595–601, 2000.

[191] Brad Lehman and Steven P Weibel. Fundamental theorems of averaging for functional differential equations. *Journal of differential equations*, 152(1):160–190, 1999.

[192] Yang Zhu and Emilia Fridman. Extremum seeking via a time-delay approach to averaging. *Automatica*, 135:109965, 2022.

[193] JK Hale and SM Verduyn Lunel. Averaging in infinite dimensions. *The Journal of integral equations and applications*, pages 463–494, 1990.

[194] Brad Lehman and Joseph Bentsman. Vibrational stabilization and calculation formulas for nonlinear time delay systems: linear multiplicative vibrations. *Automatica*, 30(7):1207–1211, 1994.

[195] Hai Lin and Panos J Antsaklis. Stability and stabilizability of switched linear systems: a survey of recent results. *IEEE Transactions on Automatic control*, 54(2):308, 2009.

[196] Mathias Serieye, Carolina Albea, Alexandre Seuret, and Marc Jungers. Synchronization on a limit cycle of multi-agent systems governed by discrete-time switched affine dynamics. *IFAC-PapersOnLine*, 54(5):295–300, 2021.

[197] Damien Koenig, Benoît Marx, and Sébastien Varrier. Filtering and fault estimation of descriptor switched systems. *Automatica*, 63:116–121, 2016.

[198] Grace S Deaecto, José C Geromel, Felipe S Garcia, and José A Pomilio. Switched affine systems control design with application to DC–DC converters. *IET control theory & applications*, 4(7):1201–1210, 2010.

[199] Pascal Hauroigne, Pierre Riedinger, and Claude Iung. Switched affine systems using sampled-data controllers: robust and guaranteed stabilization. *IEEE Transactions on Automatic Control*, 56(12):2929–2935, 2011.

[200] Francesca Parise, Maria Elena Valcher, and John Lygeros. Computing the projected reachable set of stochastic biochemical reaction networks modeled by switched affine systems. *IEEE Transactions on Automatic Control*, 63(11):3719–3734, 2018.

[201] Roman Kuiava, Rodrigo A Ramos, Hemanshu R Pota, and Luis FC Alberto. Practical stability of switched systems without a common equilibria and governed by a time-dependent switching signal. *European Journal of Control*, 19(3):206–213, 2013.

[202] Paolo Bolzern and William Spinelli. Quadratic stabilization of a switched affine system about a nonequilibrium point. In *Proceedings of the 2004 American Control Conference*, volume 5, pages 3890–3895. IEEE, 2004.

[203] Grace S Deaecto and José C Geromel. Stability analysis and control design of discrete-time switched affine systems. *IEEE Transactions on Automatic Control*, 62(8):4058–4065, 2017.

[204] Laurentiu Hetel and Emilia Fridman. Robust sampled–data control of switched affine systems. *IEEE Transactions on Automatic Control*, 58(11):2922–2928, 2013.

[205] Grace S Deaecto. Dynamic output feedback h_∞ control of continuous-time switched affine systems. *Automatica*, 71:44–49, 2016.

[206] Carolina Albea and Alexandre Seuret. Time-triggered and event-triggered control of switched affine systems via a hybrid dynamical approach. *Nonlinear Analysis: Hybrid Systems*, 41:101039, 2021.

[207] Daniel Liberzon. *Switching in systems and control*, volume 190. Springer, 2003.

[208] Tonametl Sanchez, Andrey Polyakov, Emilia Fridman, and Laurenţiu Hetel. A switching controller for a class of mimo bilinear systems with time delay. *IEEE Transactions on Automatic Control*, 65(5):2250–2256, 2020.

[209] Guangdeng Zong, Dong Yang, James Lam, and Xiaoqi Song. Fault-tolerant control of switched LPV systems: A bumpless transfer approach. *IEEE/ASME Transactions on Mechatronics*, 27(3):1436–1446, 2021.

[210] Dong Yang, Guangdeng Zong, Sing Kiong Nguang, and Xudong Zhao. Bumpless transfer H_∞ anti-disturbance control of switching markovian LPV systems under the hybrid switching. *IEEE Transactions on Cybernetics*, 2020.

[211] Guangdeng Zong, Hangli Ren, and Hamid Reza Karimi. Event-triggered communication and annular finite-time h_∞ filtering for networked switched systems. *IEEE Transactions on Cybernetics*, 51(1):309–317, 2020.

[212] Emilia Fridman and Leonid Shaikhet. Delay-induced stability of vector second-order systems via simple Lyapunov functionals. *Automatica*, 74:288–296, 2016.

[213] Marco Ariola, Mele Adriano, Tartaglione Gaetano, et al. On the numerical solution of differential linear matrix inequalities. *Journal of Optimization Theory and Applications*, 185(2):540–553, 2020.

[214] Lucas N Egidio and Grace S Deaecto. Dynamic output feedback control of discrete-time switched affine systems. *IEEE Transactions on Automatic Control*, 66(9):4417–4423, 2021.

[215] Zhuoyu Li, Dan Ma, and Jun Zhao. Dynamic event-triggered l_∞ control for switched affine systems with sampled-data switching. *Nonlinear Analysis: Hybrid Systems*, 39:100978, 2021.

[216] Gaëtan Beneux, Pierre Riedinger, Jamal Daafouz, and Louis Grimaud. Adaptive stabilization of switched affine systems with unknown equilibrium points: Application to power converters. *Automatica*, 99:82–91, 2019.

[217] Xiaozeng Xu, Hongbin Zhang, Qunxian Zheng, and Wei Chen. Global exponential stability and h_∞ control of limit cycle for switched affine systems under time-dependent switching signal. *Applied Mathematics and Computation*, 423:126807, 2022.

[218] Tarakanath Kobaku, R Jeyasenthil, Subham Sahoo, and Tomislav Dragicevic. Experimental verification of robust PID controller under feedforward framework for a nonminimum phase DC–DC boost converter. *IEEE Journal of Emerging and Selected Topics in Power Electronics*, 9(3):3373–3383, 2020.

[219] John M Davis, Ian A Gravagne, Robert J Marks, and Alice A Ramos. Algebraic and dynamic lyapunov equations on time scales. In *2010 42nd Southeastern Symposium on System Theory (SSST)*, pages 329–334. IEEE, 2010.

[220] Silviu-Iulian Niculescu. *Delay effects on stability: a robust control approach*, volume 269. Springer Science & Business Media, 2001.

[221] Wim Michiels and Silviu-Iulian Niculescu. *Stability and stabilization of time-delay systems: an eigenvalue-based approach*. SIAM, 2007.

[222] Emilia Fridman and Uri Shaked. Delay-dependent stability and h_∞ control: constant and time-varying delays. *International journal of control*, 76(1):48–60, 2003.

[223] Keqin Gu and Silviu-Iulian Niculescu. Survey on recent results in the stability and control of time-delay systems. *J. Dyn. Sys., Meas., Control*, 125(2):158–165, 2003.

[224] Keqin Gu, Jie Chen, and Vladimir L Kharitonov. *Stability of time-delay systems*. Springer Science & Business Media, 2003.

[225] Emilia Fridman and Uri Shaked. New bounded real lemma representations for time-delay systems and their applications. *IEEE Transactions on Automatic control*, 46(12):1973–1979, 2001.

[226] Emilia Fridman. New lyapunov–krasovskii functionals for stability of linear retarded and neutral type systems. *Systems & control letters*, 43(4):309–319, 2001.

[227] Xueyan Yang, Xiaodi Li, and Jinde Cao. Robust finite-time stability of singular nonlinear systems with interval time-varying delay. *Journal of the Franklin Institute*, 355(3):1241–1258, 2018.

[228] Shuping He, Jun Song, and Fei Liu. Robust finite-time bounded controller design of time-delay conic nonlinear systems using sliding mode control strategy. *IEEE Transactions on Systems, Man, and Cybernetics: Systems*, 48(11):1863–1873, 2017.

[229] Aristide Halanay and Aristide Halanay. *Differential equations: Stability, oscillations, time lags*, volume 6. Academic press New York, 1966.

Author's Publications

1. Caiazzo, B., Fridman, E., & Yang, X. (2023). Averaging of systems with fast-varying coefficients and non-small delays with application to stabilization of affine systems via time-dependent switching. Nonlinear Analysis: Hybrid Systems, 48, 101307.

2. Petrillo, A., Caiazzo, B., Piccirillo, G., Santini, S., & Murino, T. (2022). An IoT-based and cloud-assisted AI-driven monitoring platform for smart manufacturing: design architecture and experimental validation. Journal of Manufacturing Technology Management.

3. Caiazzo, B., Fridman, E., Petrillo, A., & Santini, S. (2022). Synchronization of Multi-Agent Systems under Time-Varying Network via Time-Delay Approach to Averaging. IFAC-PapersOnLine, 55(36), 133-138.

4. Caiazzo, B., Lui, D. G., Petrillo, A., & Santini, S. (2022). Cooperative Finite-time Control for autonomous vehicles platoons with nonuniform V2V communication delays. IFAC-PapersOnLine, 55(36), 145-150.

5. Caiazzo, B., Di Nardo, M., Murino, T., Petrillo, A., Piccirillo, G., & Santini, S. (2022). Towards Zero Defect Manufacturing paradigm: A review of the state-of-the-art methods and open challenges. Computers in Industry, 134, 103548.

6. Andreotti, A., Caiazzo, B., Di Pasquale, A., & Pagano, M. (2021, October). On Comparing Regressive and Artificial Neural Network Methods for Power System Forecast. In 2021 AEIT International Annual Conference (AEIT) (pp. 1-6). IEEE.

7. Caiazzo, B., Coppola, A., Petrillo, A., & Santini, S. (2021). Distributed nonlinear model predictive control for connected autonomous electric vehicles platoon with distance-dependent air drag formulation. Energies, 14(16), 5122.

8. Caiazzo, B., Lui, D. G., Petrillo, A., & Santini, S. (2021). Distributed Double-Layer Control for Coordination of Multiplatoons Approaching Road

Restriction in the Presence of IoV Communication Delays. IEEE Internet of Things Journal, 9(6), 4090-4109.

9. Caiazzo, B., Lui, D. G., Petrillo, A., & Santini, S. (2021, June). Distributed Robust Finite-Time PID control for the leader-following consensus of uncertain Multi-Agent Systems with communication delay. In 2021 29th Mediterranean Conference on Control and Automation (MED) (pp. 759-764). IEEE.

10. Andreotti, A., Caiazzo, B., Petrillo, A., & Santini, S. (2021). Distributed Robust Finite-Time Secondary Control for Stand-Alone Microgrids With Time-Varying Communication Delays. IEEE Access, 9, 59548-59563.

11. Caiazzo, B., Fridman, E., Petrillo, A., & Santini, S. (2021). Distributed Sampled-data PID Control for Voltage Regulation in Inverter-Based Islanded Microgrids Using Artificial Delays. IFAC-PapersOnLine, 54(18), 186-191.

12. Caiazzo, B., Lui, D. G., Petrillo, A., & Santini, S. (2021). On the exponential leader-tracking control for high-order multi-agent systems via distributed PI strategy in the presence of heterogeneous time-varying delays. IFAC-PapersOnLine, 54(18), 139-144.

13. Caiazzo, B., Coppola, A., Petrillo, A., & Santini, S. (2021). Energy-Oriented Inter-Vehicle Distance Optimization for Heterogeneous E-Platoons. In Optimization and Data Science: Trends and Applications (pp. 113-125). Springer, Cham.

14. Andreotti, A., Caiazzo, B., Petrillo, A., Santini, S., & Vaccaro, A. (2020). Hierarchical two-layer distributed control architecture for voltage regulation in multiple microgrids in the presence of time-varying delays. Energies, 13(24), 6507.

15. Andreotti, A., Caiazzo, B., Petrillo, A., Santini, S., & Vaccaro, A. (2020, June). Robust Finite-time Voltage Restoration in Inverter-Based Microgrids via Distributed Cooperative Control in presence of communication time-varying delays. In 2020 IEEE International Conference on Environment and Electrical Engineering and 2020 IEEE Industrial and Commercial Power Systems Europe (EEEIC/I&CPS Europe) (pp. 1-6). IEEE.

16. Andreotti, A., Caiazzo, B., Petrillo, A., Santini, S., & Vaccaro, A. (2019). Decentralized smart grid voltage control by synchronization of linear multiagent systems in the presence of time-varying latencies. Electronics, 8(12), 1470.

17. Bifulco, G. N., Caiazzo, B., Coppola, A., & Santini, S. (2019, November). Intersection crossing in mixed traffic flow environment leveraging v2x information. In 2019 IEEE International Conference on Connected Vehicles and Expo (ICCVE) (pp. 1-6). IEEE.